Yukon
Exploration & Geology
2018

Yukon Geological Survey staff

Standing (left to right): Scott Casselman, Derek Torgerson, Tiffani Fraser, Patrick Sack, Maurice Colpron, Brett Elliot, Karen MacFarlane, Jeffrey Bond, Kristen Kennedy, Rosie Cobbett, Julie Minor, Olwyn Bruce, Panya Lipovsky, David Moynihan

Kneeling (left to right): Carolyn Relf, Lara Lewis, Leyla Weston, Sydney van Loon, Midori Kirby

Missing from photo: Bailey Staffen, Craig Nicholson

Yukon

Yukon Exploration & Geology 2018

Edited by
K.E. MacFarlane

Yukon Geological Survey
Energy, Mines and Resources
Government of Yukon

Published under the authority of the Department of Energy, Mines and Resources, Government of Yukon http://www.emr.gov.yk.ca.

Printed in Whitehorse, Yukon, 2019.

Publié avec l'autorisation du Ministères de l'Énergie, des Mines et des Ressources du gouvernement du Yukon, http://www.emr.gov.yk.ca.

Imprimé à Whitehorse (Yukon) en 2019.

ISSN 1718-8326

Yukon Geological Survey publications can be obtained from:
Yukon Geological Survey
102-300 Main Street
Box 2703 (K-102)
Whitehorse, Yukon, Canada Y1A 2C6

email geology@gov.yk.ca

Visit the Yukon Geological Survey website at www.geology.gov.yk.ca.

In referring to this publication, please use the following citation:
Yukon Geological Survey, 2019. Yukon Exploration and Geology 2018, K.E. MacFarlane (ed.), 2019. Yukon Geological Survey, 142 p.

Front cover photograph: Heading northeast on Kalzas Range on a smokey morning en route to a forested traverse. Photo by Halley Keevil, Yukon Geological Survey.

Preface

Yukon Exploration and Geology (YEG) papers and the Yukon Exploration and Geology Overview are two of the main publications of the Yukon Geological Survey (Energy, Mines and Resources, Government of Yukon). Individual YEG papers, with colour images, are available in digital format and can be downloaded from our website. The YEG Overview is available in digital format and in a limited colour print run.

YEG 2018 contains up-to-date information on mining and mineral exploration activity, studies by industry and results of recent geological field studies. Information in this volume comes from prospectors, exploration and government geologists, mining companies, and students, all of whom are willing to contribute to public geoscience for the benefit of the scientific community, general public and mineral and petroleum industries of Yukon. Their work is appreciated.

Colleagues at the Yukon Geological Survey are thanked for their involvement in authoring and reviewing YEG papers.

Sherry Tyrner of the Queen's Printer ensured that the printing process went smoothly.

We welcome any input or suggestions that you may have to improve future YEG publications. Please contact me at (867) 667-8519, or by email at karen.macfarlane@gov.yk.ca.

Karen MacFarlane

Yukon Exploration and Geology 2018

Table of Contents

Analyses of regional wetland distribution using predictive ecosystem mapping data sets for west-central Yukon and east-central Alaska

Jeffrey D. Bond
Yukon Geological Survey

Bond, J.D., 2019. Analyses of regional wetland distribution using predictive ecosystem mapping data sets for west-central Yukon and east-central Alaska. *In:* Yukon Exploration and Geology 2018, K.E. MacFarlane (ed.), Yukon Geological Survey, p. 1–18.

Abstract

Predictive ecosystem mapping (PEM) in west-central Yukon and east-central Alaska effectively defines the location of larger, contiguous wetlands; however, it does not provide an accurate estimate of wetland. A quality control comparison between detailed mapping in the Indian River drainage and a regional PEM data set indicates that wetland area is underestimated by approximately two thirds within the PEM data set. Despite this, the PEM is useful at locating areas of wetland abundance from a regional perspective. Within the Tr'ondëk Hwëch'in Traditional Territory, the Ogilvie Mountains and Tintina Trench contain the largest concentrations of wetlands, whereas the Klondike Plateau has approximately 50% less wetland density due to topographic characteristics. When analyzing wetland distribution for the Klondike Plateau ecoregion that spans the border between Yukon and Alaska, the largest wetlands are located distal to the Yukon River in valleys that have not been affected by Pleistocene base level change. Overall average wetland coverage, for all study areas, is estimated to be upwards of 10% of the landscape. Their abundance is attributed to a combination of suitable terrain, Pleistocene aeolian sedimentation, periglacial processes and a climate supporting extensive discontinuous permafrost. Understanding regional wetland distribution through PEM can help frame significance when considering land management decisions that weight the placer mining economy and environment.

* jeff.bond@gov.yk.ca

Introduction

The distribution and character of wetlands in west-central Yukon, and in particular the Indian River drainage, has become a topic of interest in recent years. This was initiated by increasing awareness of placer mining activities in the drainage and concern that with wetland loss, an important part of the environment and its function could not be recovered. Best management practices for placer mining in wetlands continue to evolve, although fundamental differences in opinion remain regarding landscape transformation. This paper sets out to analyze the distribution and abundance of wetlands from the greater landscape perspective. The goal is to help frame the significance of landscape transformation in the Indian River drainage and advise land use planning decisions as they attempt to balance the environment and economy. Previously published predictive ecosystem mapping (PEM) and detailed mapping data sets are utilized to both identify the location of large wetland complexes and quantify their spatial significance within a variety of political and ecological boundaries in west-central Yukon and east-central Alaska.

Background

Location of Study Areas

Analysis of wetlands in west-central Yukon can be assessed from a number of regional perspectives. Politically, there are two important regional boundaries in which to analyze spatial data: the Dawson Land Use Planning area and the Tr'ondëk Hwëch'in Traditional Territory (Fig. 1). A second perspective is by ecoregion boundary, which defines a region based on similar physiography, ecology and climate (Fig. 1). For the purposes of this study, wetland distribution in west-central Yukon will be assessed according to the Tr'ondëk Hwëch'in Traditional Territory (63 983 km^2) and the Klondike Plateau ecoregion (102 490 km^2) that spans the border between Yukon and Alaska.

The distribution of wetlands will also be assessed within the Indian River drainage (2257 km^2), both as a means to evaluate the accuracy of regional data sets and to understand Indian River wetland area within the context of other wetland complexes in the region (Fig. 1).

Placer Mining in the Klondike Plateau and Indian River

Placer mining within the study areas, and in particular the Klondike Plateau, has been on-going since the 1880s. Robert Henderson prospected the Indian River drainage prior to the Klondike gold rush and focused on the tributary Quartz Creek before discovering gold in the Hunker Creek drainage. His efforts and communication with other prospectors led to the discovery of gold in nearby Bonanza Creek that kick-started the Klondike gold rush of 1897–98. During the ensuing years, all of the major gold-bearing creeks in the Klondike district were discovered and partially prospected or mined by hand. This included a number of tributaries to the Indian River including, Dominion, Gold Run, Sulphur, Eureka and Quartz creeks. The main stem of the Indian River was prospected during these early years, but was considered too low grade for early hand-mining methods. Following the hand-mining era, came a period of dredging that lasted from 1901–1966. The modern era of placer gold mining ensued with the introduction of bulldozer and excavator methods. In the late 1970s, prospecting was initiated along the Indian River floodplain. It was realized during this time that while placer gold distribution was erratic, high-grade patches were present that enabled economic production, especially with the rising gold price. In the early 1980s, placer mining along the main stem of the Indian River was initiated below the mouth of Quartz Creek marking the beginning of development in some of the larger wetland complexes in the valley (Debicki, 1983).

Total placer gold production from the Indian River drainage is estimated at more than 2 million crude ounces. Half of this production has occurred since excavator mining was initiated in the early 1980s. This equates to a modern economic value of more than $2.5 billion. To this day, miners in the Indian River drainage cumulatively produce more than 50% of the Yukon's placer gold every year. Approximately 250 people are directly employed by placer mining in the drainage and from an economic perspective, it is the most important placer gold producing watershed in Yukon.

More regionally, creeks and rivers of the Klondike Plateau ecoregion in Yukon such as the Klondike, Bonanza, Hunker, Sixtymile, Blackhills, and Henderson have historically produced more than 13 million crude ounces. Little to no production has been documented north of the Tintina Trench in the study area.

Physiography and Surficial Geology

Environments of west-central Yukon and east-central Alaska include a number of physiographic subdivisions including Klondike Plateau, Tintina Trench, and the southern and northern Ogilvie Mountains (Fig. 1; Smith *et al.*, 2004). The surficial geology is broadly subdivided

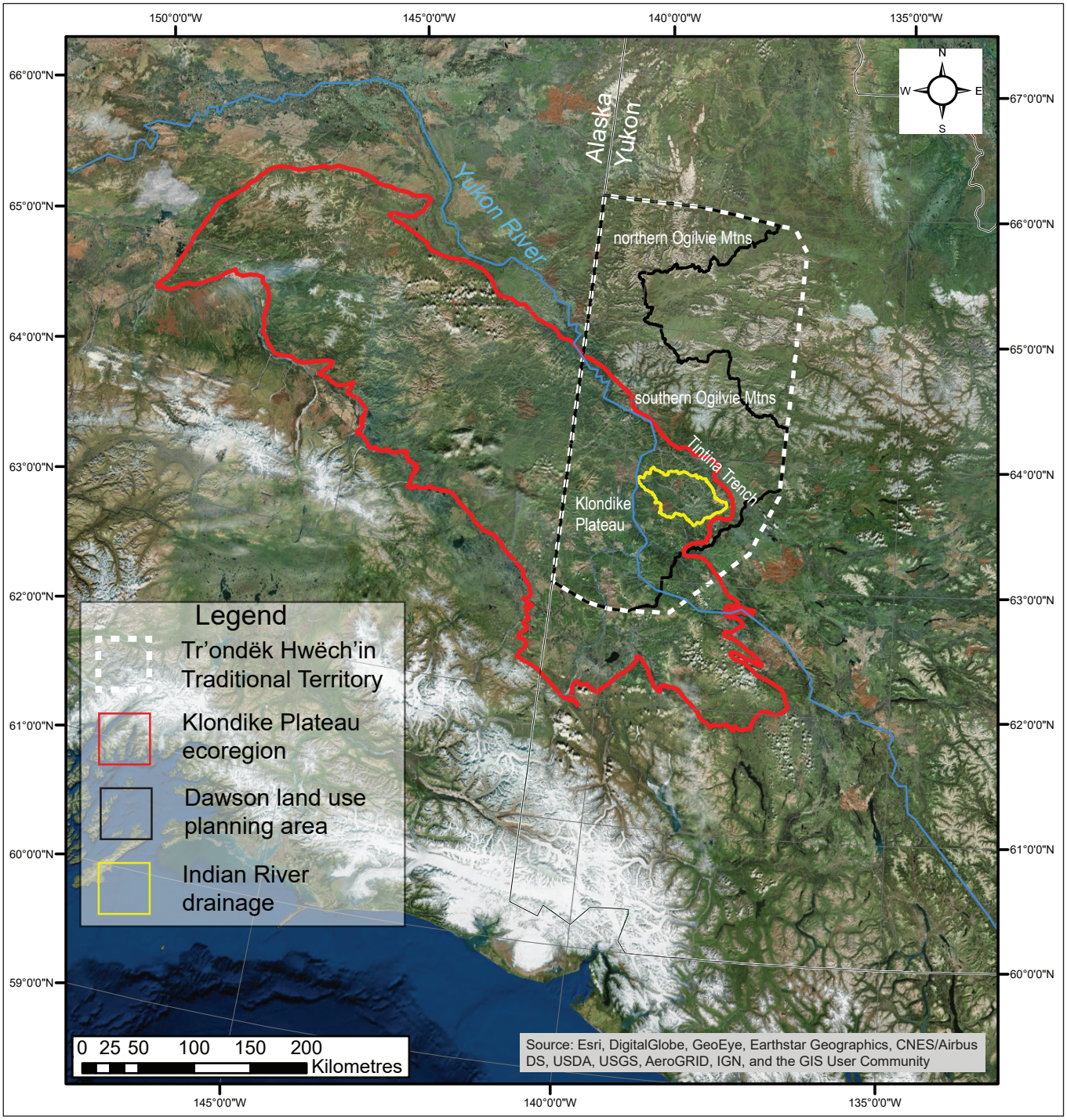

Figure 1. *Location of the study areas located in Yukon and Alaska.*

by the physiography and glacial history of the region. Isolated ice caps formed repeatedly in the Ogilvie Mountains and Tanana Uplands in the Pleistocene and the Cordilleran Ice Sheet flowed into the area from the east along the Stewart River valley and Tintina Trench (Fig. 2). In these glaciated areas, valley bottoms are filled with mixed glacial debris and fluvial sediments. On steeper landscape positions the slopes are overlain by a variable cover of colluviated weathered bedrock and till. Outside of the glacial limits in the Ogilvie Mountains, the surficial deposits consist of colluviated weathered bedrock and fluvial deposits. Silt-rich loess deposits are incorporated into soils. The north slope of the southern Ogilvie Mountains, is a region of more subdued unglaciated foothills and a peneplain that encompasses the headwaters of the Ogilvie River.

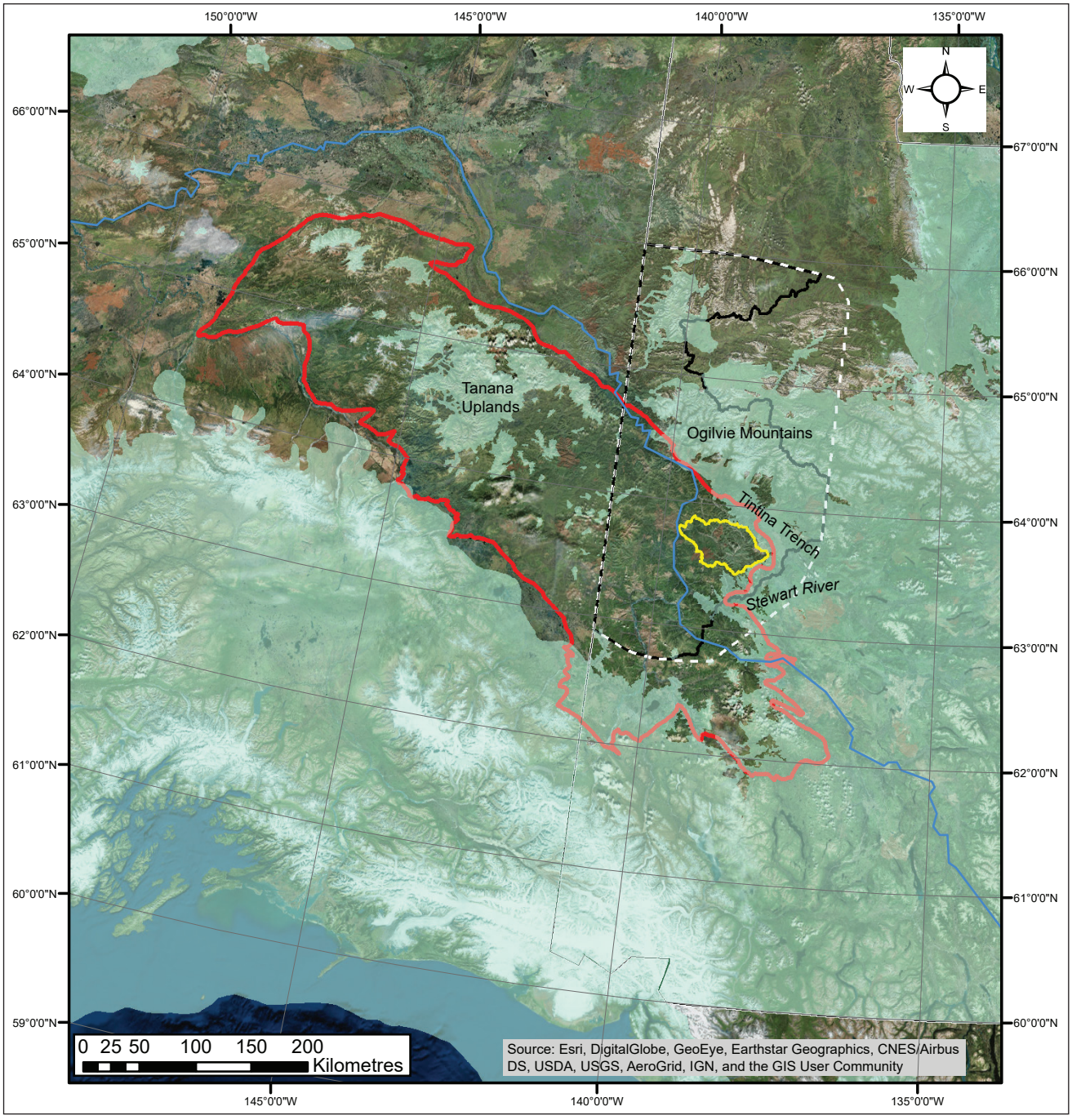

Figure 2. *The all-time limit of glaciation to affect the study areas (Duk-Rodkin, 1999; Manley and Kaufman, 2002).*

The Tintina Trench is a major strike slip fault with a physiographic expression that is characterized by a wide northwest trending valley. Within the study area the trench separates the Ogilvie Mountains from the Klondike Plateau ecoregions (Smith *et al.*, 2004). The trench was a conduit for ice during glaciation that formed low relief and rolling topography. Sediments within the trench consist of dissected, unconsolidated glacial and fluvial sediments originating largely from the Ogilvie Mountains to the north (Duk-Rodkin, 1996).

The Klondike Plateau ecoregion in the southern part of the study areas extends northwest into Alaska and differs from the rugged mountainous terrain to the north (Fig. 1). The dissected plateau exhibits mature landscape characteristics with more subdued topography. With the exception of the Stewart River and Tanana Uplands in Alaska, most of the Klondike Plateau escaped glaciation (Fig. 2). Upland slopes are gentle, however cliff faces form where fluvial processes and base-level change have caused erosion against valley sides. Slopes are covered by weathered-bedrock colluvium. Fluvial deposits are widespread in the valley bottoms and include Pliocene and Pleistocene fluvial terraces that developed in response to early Pleistocene base-level change along the Yukon River.

Loess deposits are widespread on the Klondike Plateau in Yukon and Alaska and are an important soil component for wetlands. Loess was produced largely during glacial climates when interior Yukon and Alaska were drier and less vegetated. Floodplains during these periods were more active and therefore had less vegetation to stabilize surface sediment, making them susceptible to wind erosion. Repeated glacial climates during the Pleistocene have resulted in significant loess accumulations on the landscape. Reworking of loess deposits off hillsides and into valley bottoms by sheetwash and solifluction processes is ongoing. The result is poorly drained, silt-rich, surficial accumulations that are geomorphologically important for establishing terrain characteristics ideal for hosting wetland soils (Figs. 3 and 4).

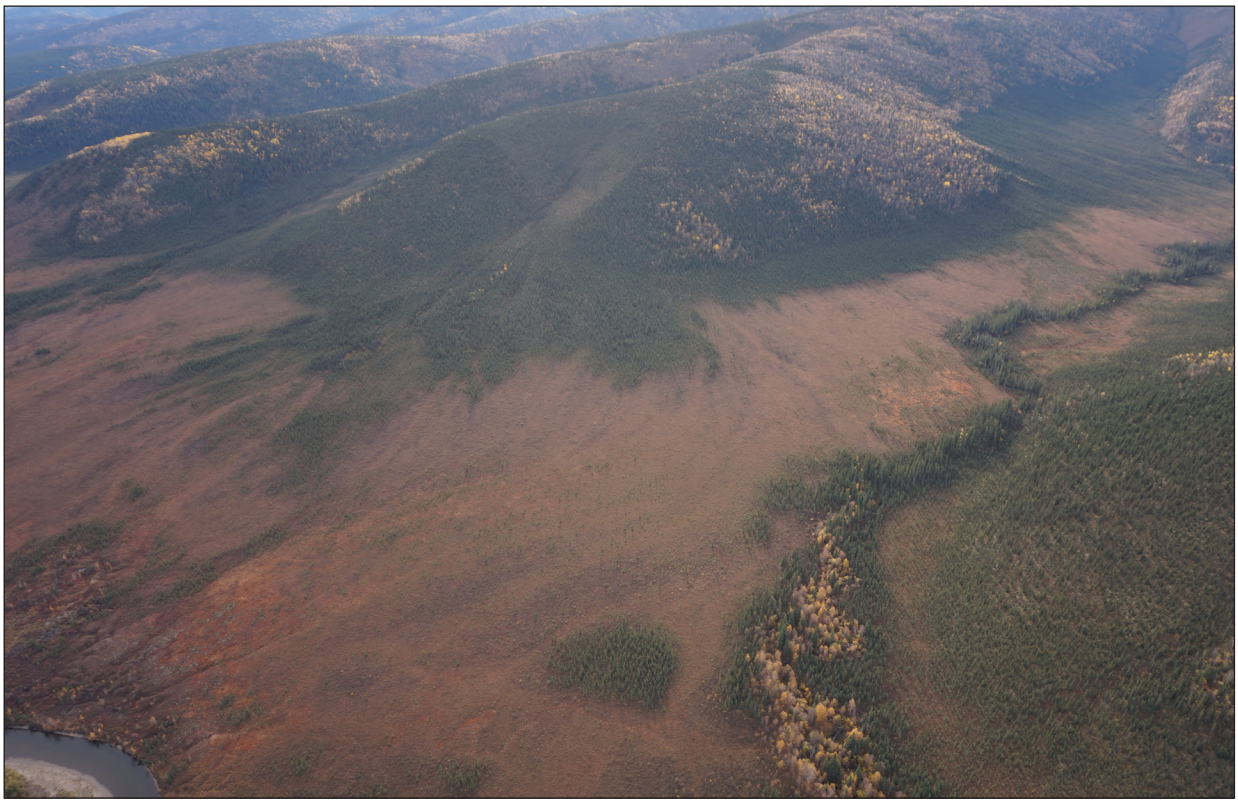

Figure 3. *An example of terrain modified by sheetwash processes in the Klondike Plateau ecoregion near Dip Creek. Subtle lines or streaks within the light-red coloured vegetation highlight the flow of water and sediment (loess) across this landform. This process creates a smooth apron underlain by fine sediment and permafrost. This landform would be considered a fen wetland.*

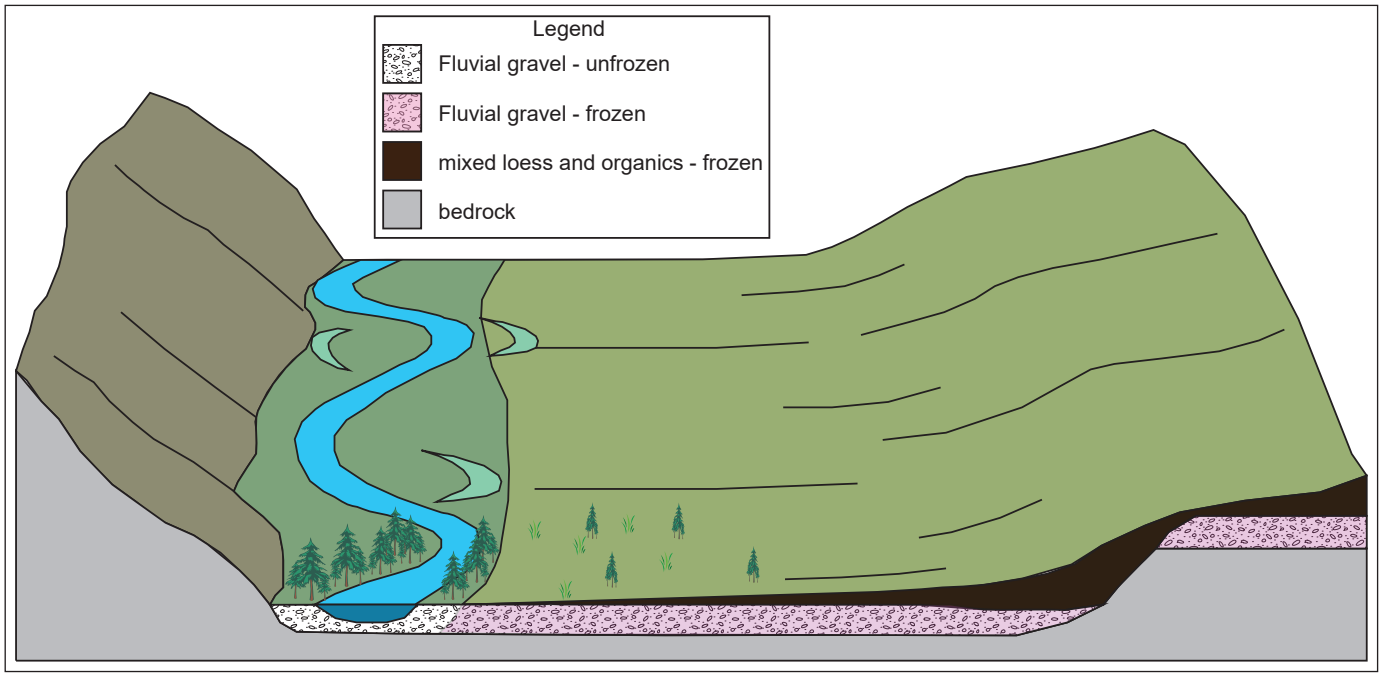

Figure 4. *A block diagram depicting typical sediment stratigraphy in an unglaciated valley in the study areas. Note the mixed loess and organic unit forms a wedge of sediment across the floodplain. This unit traps moisture and provides insulation, which promotes permafrost development.*

Permafrost

The study areas span the zones of extensive discontinuous and continuous permafrost. Its presence and characteristics are further controlled by site topographic position, aspect and surficial geology. Disseminated to massive ice may be present and ice wedge polygons are common, particularly in poorly drained valley bottoms (Fig. 5). Permafrost is an important controlling factor in most wetlands within the study areas.

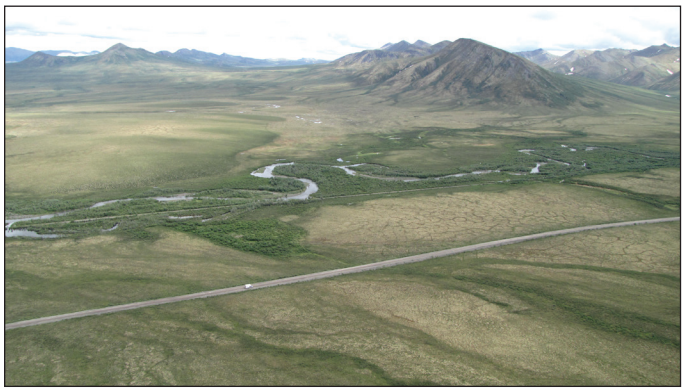

Figure 5. *Ice wedge polygons are visible in the flat-lying terrain near the Dempster Highway in the southern Ogilvie Mountains.*

Wetlands

Detailed wetland classification in the study areas has not occurred outside of the Indian River valley. Therefore, the major classes of wetlands in the Indian River area are assumed to be found across the greater study areas. According to McKenna (2018) the major classes include fens, bogs, marshes, swamps and open water ponds. Fens are by far the most common wetland class, largely due to the prevalence of permafrost-rich sloping terrain (Figs. 6 and 7).

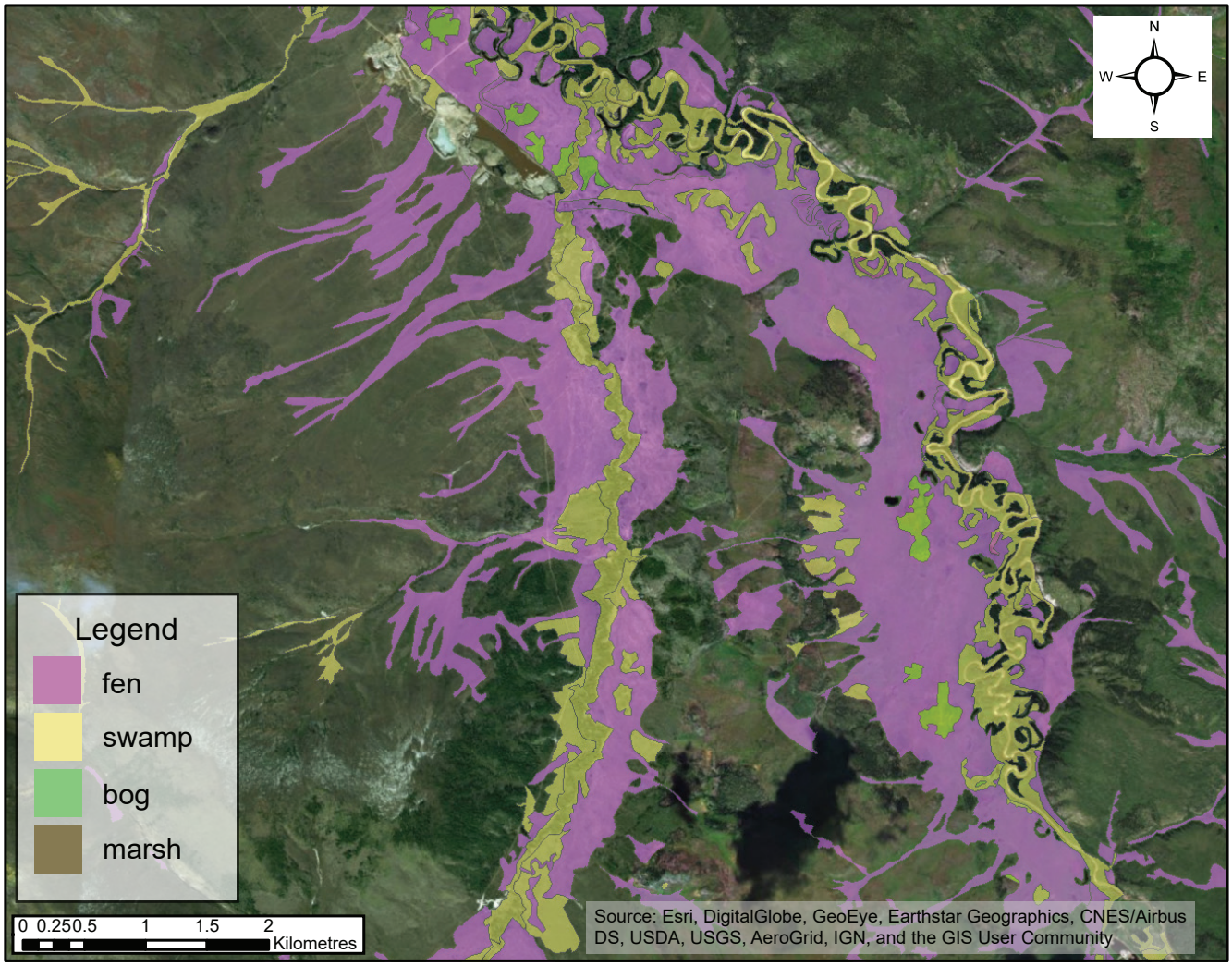

Figure 6. *An excerpt of the mapping completed by McKenna (2018) in the Indian River drainage near the mouth of Montana Creek. Fen wetlands account for the majority of the wetlands in the valley bottom.*

Figure 7. *An aerial view over a typical fen wetland near a placer mine in the Indian River valley. The sparsely treed fen wetland is underlain by a layer of reworked loess that is interbedded with organics that accumulated over the last 6,000 years. Permafrost is prevalent. The relatively flat surface is dipping gently towards the foreground allowing surface waters to drain slowly across that landform.*

Methods

Predictive Ecosystem Mapping (PEM) Data Sets

Two predictive ecosystem mapping data sets were used to evaluate the regional distribution of wetlands within the study areas. For west-central Yukon, the broad ecosystem spatial data was used, and in Alaska, the National Land Cover Database was analyzed (Grods *et al*., 2012a; Homer *et al*., 2015). PEM modeling uses a series of data inputs such as spectral land cover, surficial geology and topography, along with knowledge of ecosystems, to predict ecosystem distribution over large areas (Grods *et al*., 2012b). The final product is a raster data set with a best-fit classification for each cell.

The west-central Yukon broad ecosystem spatial data set established 44 different possible ecosystem phases from 11 broad ecosystem types (Grods *et al*., 2012b; Fig. 8). The modelling generated a raster map with 25 by 25 m resolution of the ecosystem phases. For this study, wetland distribution and abundance analyses included the phases: Wetland–Herb Bryoid (311), Wetland–Shrub (312) and Wetland–Treed (315). Phases excluded from the analyses that may have wetland characteristics, included floodplain ecosystems and wet drainage and depression phases. By only including the "most obvious" wetland phases it allowed spatial identification of the more significant wetland complexes. As a result, the area calculations are considered a minimum, which is discussed further in the Data Accuracy section below. Within Alaska, a similar PEM data set was used that classified the land cover into 20 different units and applied the modeling to a 30 by 30 m resolution raster (Fig. 9; Homer *et al*., 2015). For analyses of wetlands using this data set, the Woody Wetlands (90) and Emergent Herbaceous Wetlands (95) units were utilized. In addition to analyzing the wetland phases, the anthropogenic disturbances are also quantified for discussion purposes.

The distribution and abundance of wetlands within the study areas was assessed using ArcMap software. With the two PEM data sets loaded into ArcMap, various political or physiographic boundaries were used to clip the raster data sets. After the clipping process, the attribute table for the newly created raster data set was extracted to Excel to multiply the attribute "count" field by the area of the raster cells (625 m^2–Yukon data; 900 m^2–Alaska data). The spatial abundance of a particular land cover attribute can then be quantified within the respective study boundary. Identification of concentrated and relatively abundant wetland cells was completed visually by toggling off non-wetland attributes in ArcMap.

The boundaries used for clipping and analyzing the PEM raster data sets included the Tr'ondëk Hwëch'in Traditional Territory (TT), Klondike Plateau ecoregion and the Indian River watershed. Where large wetland complexes were identified (e.g., >30 km^2), an arbitrary shapefile polygon was created around the specific complex and used to clip the PEM raster data to extract the statistics.

Data Accuracy

The accuracy of the PEM data sets was assessed by comparing it to detailed 1:10 000-scale wetland mapping by McKenna (2018) and 1:50 000-scale surficial geology mapping of organic units by Jackson (2005) within the Indian River drainage. Both of these detailed data sets included ground-truthing. While it is recognized that PEM will not be as accurate as manual airphoto and field-based mapping, the comparison was useful to assess and quantify spatial differences and accuracy.

A visual comparison revealed that the PEM data are reasonably effective at identifying the major valley-bottom wetland complexes that occur on relatively flat to gently-sloping surfaces in the Indian River valley bottom and its tributaries (Fig. 10). The PEM method is less accurate at identifying wetlands on sloped topographic positions and in narrow valley bottoms (Fig. 10). In addition, some areas that were identified as 'floodplain' on the PEM classification were mapped as a wetland class in the detailed mapping by McKenna. Table 1 summarizes the wetland area for the Indian River according to the different methodologies. It should be noted that wetland mapping completed by McKenna (2018) did not include most of Dominion Creek, which accounts for 19.4% of the drainage. Approximately 1818 km^2 of the Indian River drainage was mapped during the McKenna study and this value is used when calculating percentage of wetlands as land cover.

Group	Type *		Phase *
DRY	Ecosystems (100)	Rock (700)	Not applicable
		Ridge (110)	Ridge – Herb-Bryoid (111) Ridge – Shrub (112) Ridge – Deciduous (113) Ridge – Mixed wood (114) Ridge – Coniferous (115)
		Steep South-Facing Slope (120)	Steep South-Facing Slope – Herb-Bryoid (121) Steep South-Facing Slope – Shrub (122) Steep South-Facing Slope – Deciduous (123) Steep South-Facing Slope – Mixed wood (124) Steep South-Facing Slope – Coniferous (125)
		Upper Slope (130)	Upper Slope – Herb-Bryoid (131) Upper Slope – Shrub (132) Upper Slope – Deciduous (133) Upper Slope – Mixed wood (134) Upper Slope – Coniferous (135)
MOIST	UPLAND	Gentle Slope and Plain (140)	Gentle Slope – Herb-Bryoid (141) Gentle Slope – Shrub (142) Gentle Slope – Deciduous (143) Gentle Slope – Mixed wood (144) Gentle Slope – Coniferous (145)
		Steep North-Facing Slope (150)	Steep North-Facing Slope – Herb-Bryoid (151) Steep North-Facing Slope – Shrub (152) Steep North-Facing Slope – Deciduous (153) Steep North-Facing Slope – Mixed wood (154) Steep North-Facing Slope – Coniferous (155)
WET	WETLAND Ecosystems (300)	Drainage and Depression (160)	Drainage and Depression – Herb-Bryoid (161) Drainage and Depression – Shrub (162) Drainage and Depression – Deciduous (163) Drainage and Depression – Mixed wood (164) Drainage and Depression – Coniferous (165)
		Wetland (310)	**Wetland – Herb-Bryoid 311)** **Wetland – Shrub (312)** **Wetland – Treed (315)**
		Floodplain (370/380/390)	<u>High Flood Frequency (370)</u>: • Floodplain – Gravel Bar-Herb-Bryoid (371) • Floodplain – Shrub (372) <u>Moderate Flood Frequency (380)</u>: • Floodplain – Deciduous (383) • Floodplain – Mixed wood (384) <u>Low Flood Frequency (390)</u>: • Floodplain – Coniferous (395)
	WATER and ICE (400)		Water (401) Ice (Glacier) (403)
OTHER	**DISTURBANCE (500)**		Natural Disturbances (501) Anthropogenic Disturbances (502) Mine site Disturbances (503)

Figure 8. *The ecosystem phases identified by Grods et al. (2012b) and utilized to produce the west-central Yukon predictive ecosystem map.*

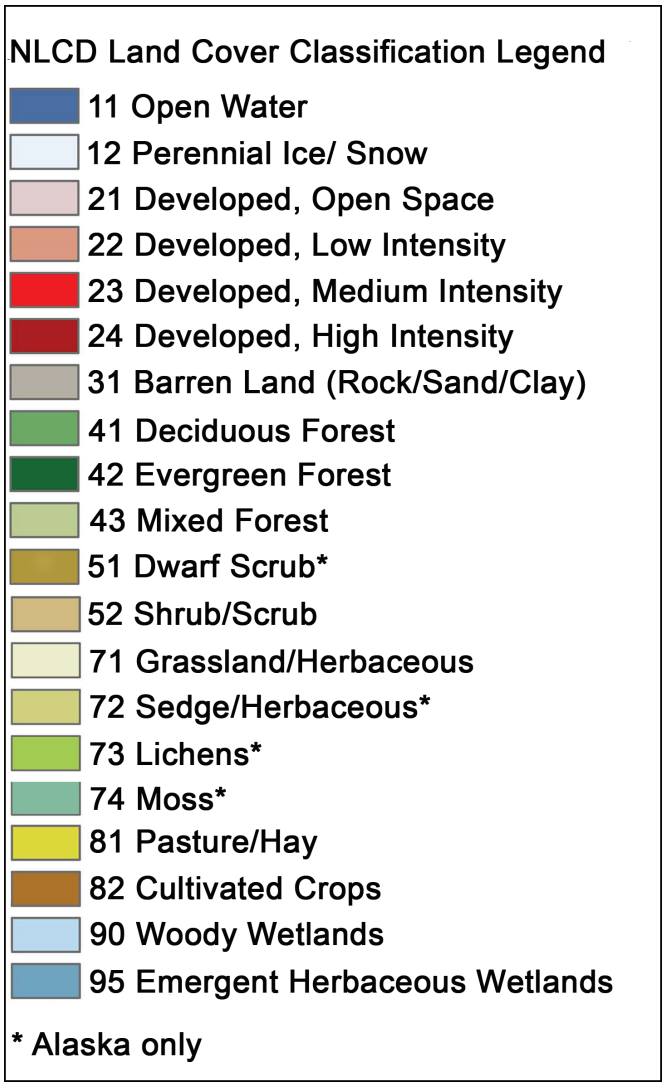

Figure 9. *The land cover classification used to produce the Alaska predictive ecosystem map (Homer, 2015). NLCD = National Land Cover Database.*

The data accuracy results indicate that the west-central Yukon PEM mapping identified areas of contiguous wetlands but does not classify the sloped wetlands and wetlands proximal to the active floodplain environment. The PEM methods mapped 29% of the wetlands that were mapped by McKenna and 19% of the organics mapped by Jackson. For purposes of this study, since the PEM under-estimates the amount of wetlands by about ⅓, a multiplier of 3 is applied to more accurately estimate the true area of wetlands identified using the PEM. The multiplier is not applied to anthropogenic disturbance calculations since these features are spectrally easier to identify. Similarly, a multiplier was not applied to the Alaskan land cover data set because a local case study comparison was not available to evaluate that data set.

Results

The total area of wetlands and anthropogenic disturbance within the respective study area boundaries are presented in Table 2. For the Klondike Plateau ecoregion this includes both Yukon and Alaska data sets. A portion of the Klondike Plateau ecoregion in Yukon was not mapped by the west-central Yukon PEM and therefore the area values are considered minimums.

Within the Tr'ondëk Hwëch'in Traditional Territory the PEM determined there are 2367 km^2 of wetland and possibly as much as 7101 km^2 when considering sloping wetlands and the error adjustment. A number of sizeable wetland complexes were identified during the PEM modeling within the TT (Fig. 11 and Table 3). In the Ogilvie Mountains, extensive wetland complexes are present in the upper Ogilvie River area and along the Blackstone River. Farther south in the Tintina Trench, a considerable wetland area is present northeast of the Indian River drainage. Within the Klondike Plateau portion of the traditional territory, wetland complexes are found in the Indian River, Ladue River, Scottie Creek, and adjacent to the floodplains of the Yukon, White and Stewart rivers. The areas of anthropogenic disturbance include all municipal, transportation and mine-related activities. PEM suggests that 0.29% of the Tr'ondëk Hwëch'in Traditional Territory has been modified by humans.

In the Klondike Plateau, the combined Alaska and Yukon PEM data sets determined that there are >5131 km^2 of wetland covering >5% of the landscape (Fig. 12). These values do not take into account any potential adjustment error. Large wetland complexes are located on the southwestern side of the plateau, in particular, in the upper reaches of the Fortymile River and in the Scottie Creek drainage (Table 4; Fig. 12). On the south side of the Dawson Range, the Dip Creek area, a tributary to the Donjek River also contains a large wetland complex.

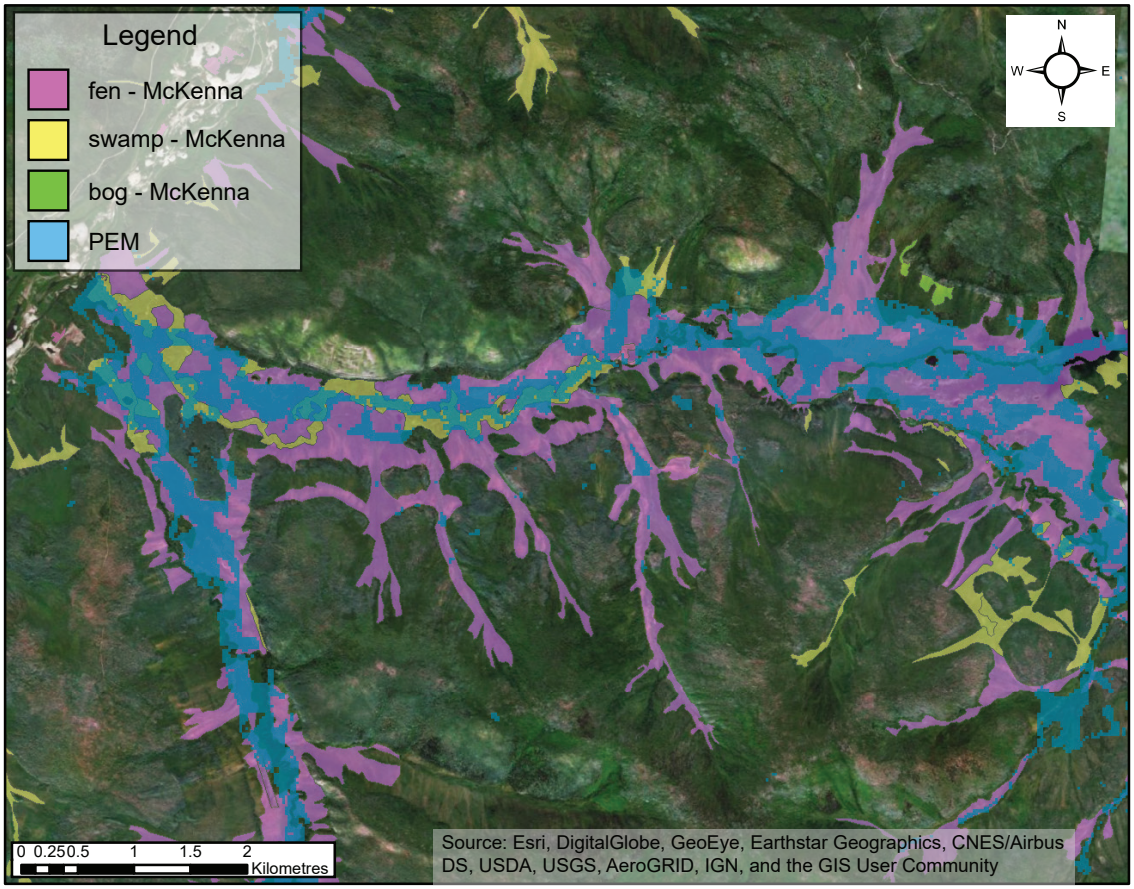

Figure 10. *A comparison of the predictive ecosystem mapping (blue) to detailed mapping completed by McKenna (2018, pink and yellow). PEM identifies wetlands in the flat to gently sloping terrain of the valley bottom but does not map wetlands up the valley slopes.*

Table 1. *Comparison of predictive ecosystem mapping to detailed mapping in the Indian River.*

Wetland Mapping Method	Area (km²)	Percent wetlands as land cover in drainage
PEM (wetlands)	53	2.3
PEM wetlands + floodplain	69	3.0
McKenna	143 (minimum)	7.9 (undisturbed wetlands)
Jackson organic units	278	12

Table 2. *Total area of PEM wetlands and anthropogenic disturbance within study areas.*

Assessment boundary (various)	Phase	Area (km²)	% of land cover	Area with 3× error adjustment (km²)	Adjusted % of land cover
Tr'ondëk Hwëch'in TT	W	2367	3.94	7101	11
Tr'ondëk Hwëch'in TT	A	171	0.29	n/a	n/a
Klondike Plateau	W	>5131	5	n/a	n/a
Klondike Plateau	A	274	0.27	n/a	n/a
Indian River	W	53	2.3	159	7.4
Indian River	A	63	2.8	n/a	n/a

W = wetland, A = anthropogenic disturbance, % of land cover refers to the percent of wetlands relative to the total area within the assessment boundary.

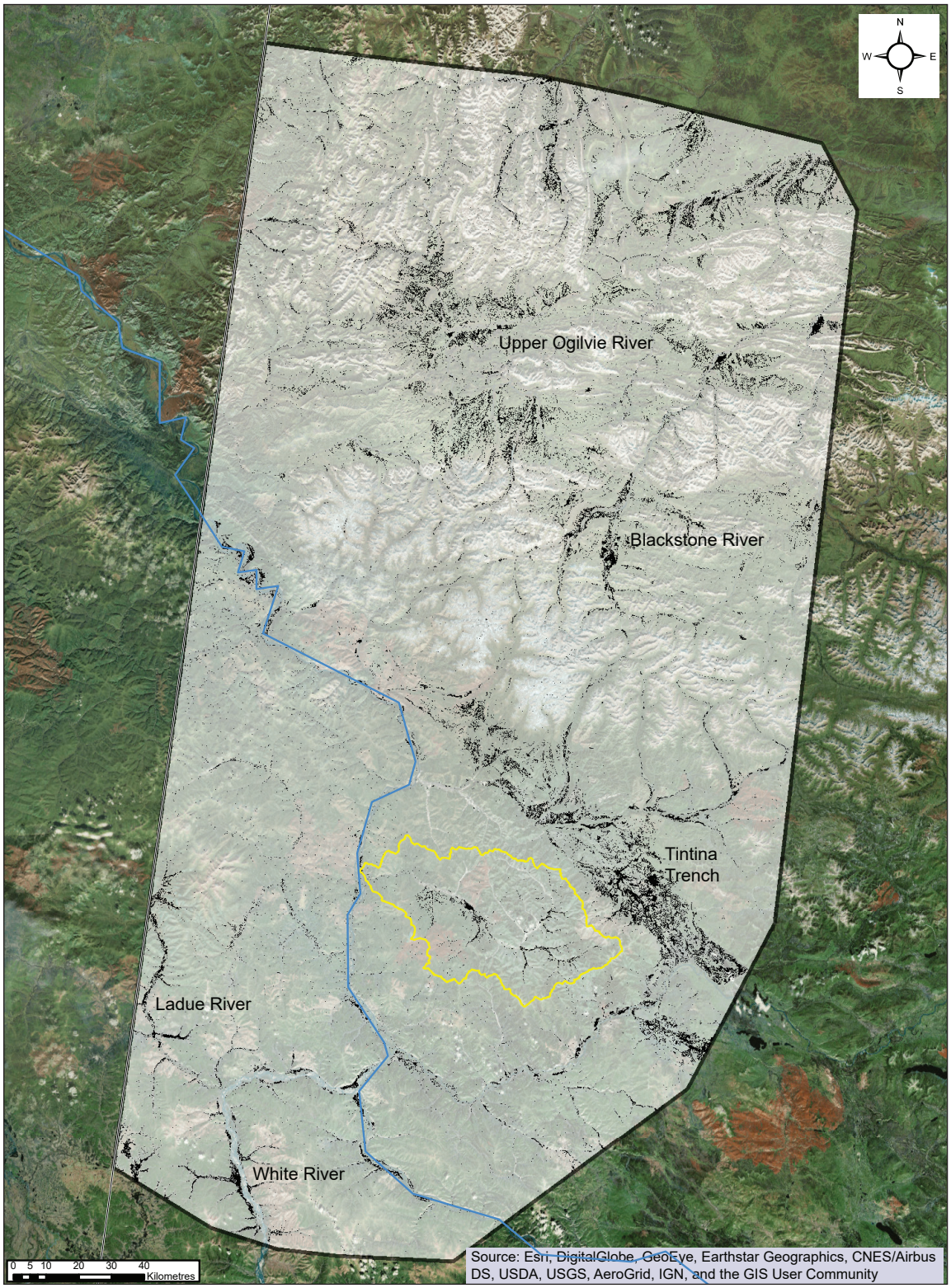

Figure 11. *Wetland distribution map of the Tr'ondëk Hwëch'in Traditional Territory (white shade) from the west-central Yukon PEM (Grods et al., 2012a). Black-coloured pixels correspond to wetlands modeled by Grods, et al., 2012. For reference, the Indian River drainage is highlighted in yellow. Wetland concentration is greater north of the Indian River and Klondike Plateau in the Tintina Trench and Ogilvie Mountains. The Ladue River wetland is the largest wetland in the Klondike Plateau portion of the Traditional Territory.*

Table 3. *Large PEM wetland complexes in the Tr'ondëk Hwëch'in Traditional Territory.*

Wetland Name	Area (km²)	% of land cover	3× error adjustment (km²)	Adjusted % of land cover
Upper Ogilvie River	811	1.3	2433	3.8
Blackstone River	91	0.14	273	0.42
Tintina Trench	491	0.77	1473	2.3
Ladue-White River	73	0.11	219	0.33
Indian River	53	0.08	159	0.25
Sixtymile River	38	0.05	114	0.18

% of land cover refers to the percent of each wetland area relative to the entire Tr'ondëk Hwëch'in Traditional Territory.

Table 4. *Large PEM wetland complexes in the Klondike Plateau ecoregion.*

Wetland Name	Area (km²)	% of land cover	3× error adjustment (km²)	Adjusted % of land cover
Dip Creek	107	0.1	321	0.31
Scottie Creek	204	0.2	612	0.6
Upper Fortymile River	592	0.58	n/a	n/a
Ladue-White River	73	0.07	219	0.21
Indian River	53	0.05	159	0.16
Sixtymile River	38	0.04	114	0.11

% of land cover refers to the percent of each wetland area relative to the entire Klondike Plateau ecoregion.

Discussion

Predictive ecosystem mapping was useful for identifying the location and distribution of large contiguous wetlands within the study areas. However, accurate quantification of wetland areas was problematic and a comparison with detailed mapping in the Indian River drainage suggests PEM captured ~29% of wetlands when analyzing the main wetland phases. In general, PEM does a good job of identifying wetlands on more gently sloping to flat topographic sites, whereas it does not predict wetlands found on moderately sloping topography. Spatial analysis estimates that wetlands cover between 4 and 10% of the total landscape in the study areas. Detailed mapping by McKenna (2018) determined that ~8% of the Indian River drainage contains undisturbed wetlands and 2.8% of the drainage has been modified by humans. Anthropogenically disturbed areas account for 0.29% of the landscape from the regional perspective. Updated disturbance mapping by the Department of Environment, Government of Yukon, indicate that disturbance is closer to 244 km^2 within the Traditional Territory, which amounts to 0.38% of the region (Heynen, *pers. comm.*, 2018).

Wetlands can be found throughout the Tr'ondëk Hwëch'in Traditional Territory largely due to permafrost conditions and the abundance of silt-rich soils. Overall, wetland density is greater north of the Klondike Plateau. The highest concentration of wetlands are found in the Tintina Trench near the Klondike River and in the headwaters of the Ogilvie River (Fig. 11). In the Klondike Plateau portion of the Traditional Territory the largest wetland complexes are found near the valleys of the White, Ladue and Indian rivers (Fig. 11). PEM spatial analysis estimates that the ratio of wetland density in the Ogilvie Mountains and Tintina Trench versus the Klondike Plateau is 2:1. In terms of overall volume inventory within the Tr'ondëk Hwëch'in

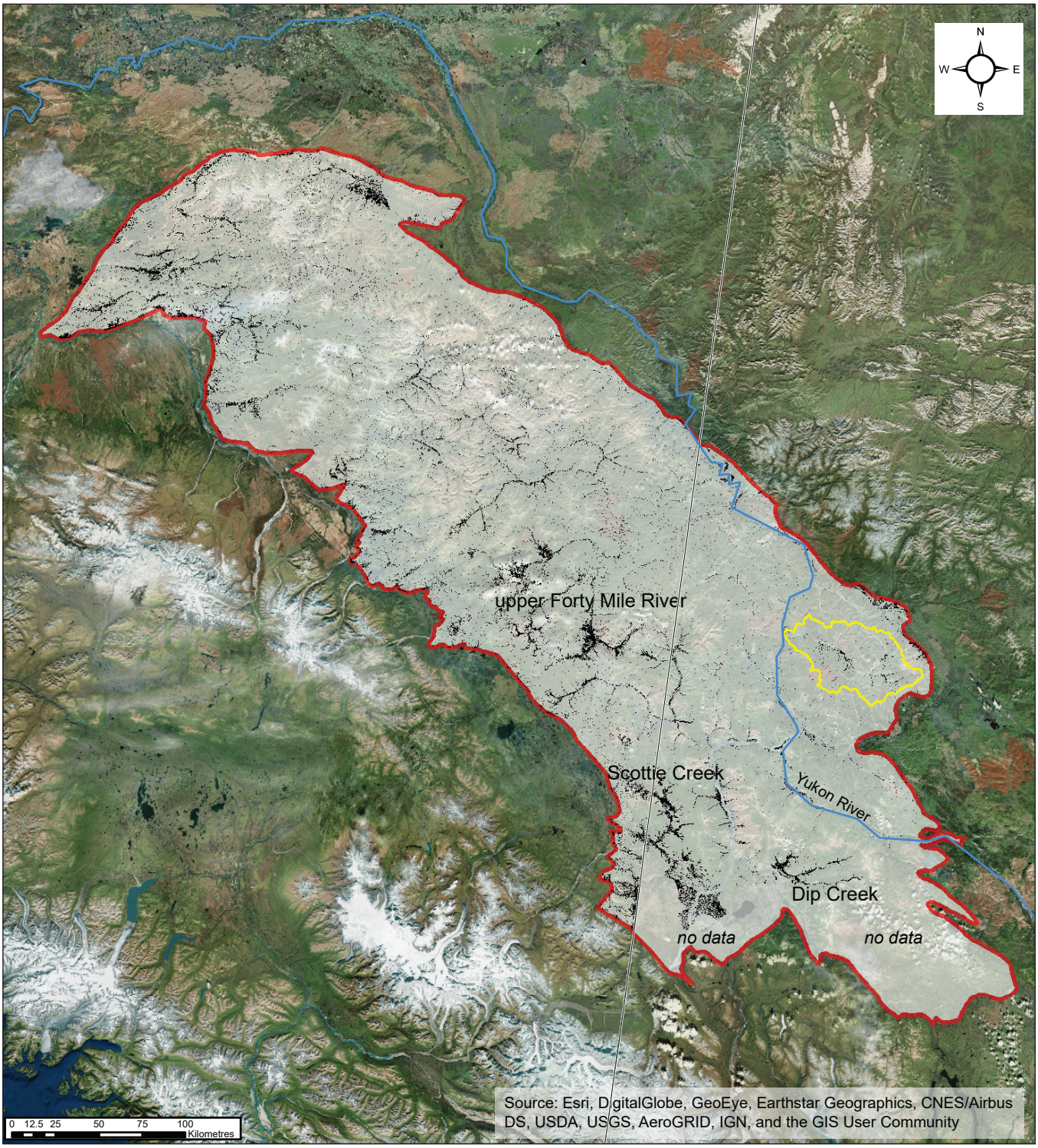

Figure 12. *Distribution of wetlands across the Klondike Plateau ecoregion (white shade) that spans the border between Yukon and Alaska. Black-coloured pixels correspond to wetlands modeled by Grods, et al., 2012 and Homer, et al., 2015. The majority of the wetlands are concentrated in drainage reaches that are distal to the Yukon River such as the upper Fortymile River and Scottie Creek wetlands.*

Traditional Territory, 78% of the wetlands are located in the Ogilvie Mountains and Tintina Trench and the remaining 22% are located in the Klondike Plateau portion of the territory. Conversely, nearly 100% of the placer gold is produced from the Klondike Plateau ecoregion within the Traditional Territory.

A distinct spatial pattern of wetlands was observed in the Klondike Plateau. Drainages proximal to the Yukon River tend to contain fewer contiguous wetlands compared to drainages distal to the Yukon River (Fig. 12). This pattern is caused by the effects of base level change that was initiated when the Yukon River reversal occurred 2.8 million years ago (Hidy et *al.*, 2013 and 2018). The ensuing fluvial erosion had a ripple effect in tributary drainages causing stream incision and creation of a more complex (and less flat) topography in valley bottoms (Fig. 13). On the south side of the Klondike Plateau, drainages are generally more distal to the Yukon River, and as a result contain some of the largest wetland complexes in the ecoregion (Fig. 12). This includes the poorly drained valleys at the headwaters of the Fortymile River in Alaska and tributaries to the Tanana River such as Scottie Creek in Yukon.

Some of the largest placer gold deposits in Yukon remain in the Indian River drainage. This includes the Eureka bench, remaining deposits in Dominion Creek and Indian River, and the largely unexplored prospects of Australia, Wounded Moose and Montana creeks. In addition, opportunities still exist within, or adjacent to, previously mined areas (van Loon, 2017). Finding a balance between placer mining and wetland protection is challenging but possible. To effectively strike this balance, decision makers can benefit from considering both placer and wetland distribution from a more regional perspective. The Klondike Plateau, particularly in vicinity of the Yukon River, is an important placer gold resource area, whereas according to predictive ecosystem mapping, the Tintina Trench, upper Ogilvie River, upper Fortymile River, Ladue River and Scottie Creek have the largest wetland complexes.

While this assessment does not consider specific biological or cultural significance of the various wetlands, it does provide a perspective on the regional inventory and provides context for the Indian River wetlands. Continued improvements in reclamation practices by the placer mining industry are important in wetland environments. The structure of wetlands in the Indian River valley, and across the study areas are governed by geological factors such as permafrost, soil moisture holding capacity and landform. Understanding the natural connectivity and geology of these environments is beneficial for guiding mine planning and reclamation goals.

Conclusions

Wetlands in west-central Yukon and eastern Alaska are largely controlled by loess distribution, topographic position and permafrost. The impermeable soil conditions created by loess, or reworked loess, raises soil moisture conditions and promotes permafrost development, which further compounds water retention. The topography and geomorphology of the study areas varies, which influences the regional distribution of wetlands. Predictive ecosystem mapping is particularly good at identifying large, contiguous wetlands, such as those found on near-level surfaces. PEM is less accurate at predicting the location of sloping wetlands and therefore under estimates total wetland area by approximately two thirds.

Within the Tr'ondëk Hwëch'in Traditional Territory, wetland density is higher in the Tintina Trench and Ogilvie Mountain ecoregions compared with the Klondike Plateau ecoregion. This is largely due to the quantity of flat lying to gently sloping terrain. The Tintina Trench is a sediment-filled fault valley with relatively low-relief terrain and the Ogilvie Mountains have broad valleys and peneplains that are particularly suitable for wetland formation. In the Klondike Plateau ecoregion, the largest wetland complexes are located distally to the Yukon River in drainages that have been less affected by base-level changes. Predictive ecosystem mapping suggests the total volume of wetlands within the various study areas covers between 4 and 10% of the landscape.

In the Indian River drainage, detailed mapping indicates that 8% of the drainage is currently covered by undisturbed wetlands (McKenna, 2018). The total amount of anthropogenic landscape modification due to mining and road building in the drainage is estimated at

Figure 13. *Proximity to the Yukon River has influenced valley bottom morphology in the Klondike Plateau. The upper photo illustrates drainages that are distal to the Yukon River have yet to experience significant base level change and contain broad, relatively flat valley bottoms, which host large wetland complexes. Conversely, the lower photo illustrates drainages that are proximal to the Yukon River have responded to base level change by undergoing a period of incision and terrace development. This creates a more topographically complex landscape in the valley bottom that is less conducive to large wetlands.*

2.8%, with the majority of this located in valley bottoms where wetland and riparian phases are located. From this land area, approximately 2.1 million crude ounces of placer gold have been produced since the gold rush.

Balancing of environmental and economic interests in the Indian River drainage needs to take into account landscape attributes from a regional context. This includes both wetland and placer gold-related attributes. Predictive ecosystem mapping is good at providing a regional inventory of landscape cover, and can help frame significance for local-scale management decisions.

Acknowledgements

This manuscript benefited from reviews by Mitchell Heynen (Ecological Land Classification coordinator, Department of Environment) and Carolyn Relf (Director, Yukon Geological Survey). Technical editing and layout were completed by Karen MacFarlane. Thank you all for your contributions.

References

Debicki, R., 1983. Placer Mining Industry 1978-1982. Indian and Northern Affairs Canada, Whitehorse, Yukon, 203 p.

Duk-Rodkin, A. 1996. Surficial geology, Dawson, Yukon Territory. Geological Survey of Canada, Open File 3288, scale 1:250 000.

Duk-Rodkin, A., 1999. Glacial Limits Map of Yukon. Indian & Northern Affairs Canada/Department of Indian & Northern Development: Exploration & Geological Services Division, Geoscience Map 1999-2.

Grods, J., Francis, S.R., Meikle, J.C. and Lapointe, S., 2012a. Regional Ecosystems of West-Central Yukon, Part 1: Ecosystem descriptions. Report prepared for Environment, Government of Yukon, by Makonis Consulting Ltd. and Associates, West Kelowna, BC.

Grods, J., Francis, S.R., Meikle, J.C. and Lapointe, S., 2012b. West-central broad ecosystems (Version 1.1). Downloaded from Yukon government ftp site on October 16th. Spatial data created for Environment, Government of Yukon, by Makonis Consulting Ltd. and Associates, West Kelowna, BC.

Hidy, A.J., Gosse, J.C., Froese, D.G., Bond, J.D. and Rood, D.H., 2013. A latest Pliocene age for the earliest and most extensive Cordilleran Ice Sheet in northwestern Canada. Quaternary Science Reviews, vol. 61, p. 77–84.

Hidy, A.J., Gosse, J.C., Sanborn, P. and Froese, D.G., 2018. Age-erosion constraints on an Early Pleisticene paleosol in Yukon, Canada, with profiles of ^{10}Be and ^{26}Al: Evidence for a significant loess cover effect on cosmogenic nuclide production rates. Catena, vol. 165, p. 260–271.

Homer, C.G., Dewitz, J.A., Yang, L., Jin, S., Danielson, P., Xian, G., Coulston, J., Herold, N.D., Wickham, J.D. and Megown, K., 2015. Completion of the 2011 National Land Cover Database for the conterminous United States–Representin a decade of land cover change information. Photogrammetric Engineering and Remote Sensing, vol. 81, p. 345–354.

Jackson, L.E. Jr., 2005. Surficial Geology, Stewart River. Geological Survey of Canada, Open File 4583.

Manley, W.F. and Kaufman, D.S., 2002. Alaska PaleoGlacier Atlas. Institute of Arctic and Alpine Research (INSTAAR), University of Colorado, instaar.colorado.edu/QGISL/ak_paleoglacier_atlas, v. 1.

McKenna, K., 2018. Wetland and Adjacent Upland Habitat in the Indian River Valley. CryoGeographic Consulting and Palmer Environmental Consulting Group Inc. Unpublished mapping.

Smith, C.A.S., Meikle, J.C. and Roots, C.F. (editors), 2004. Ecoregions of the Yukon Territory; Biophysical properties of Yukon landscapes. Agriculture and Agri-foods Canada, PARC Technical Bulletin No. 04-01, Summerland, British Columbia, 313 p.

van Loon, S., 2017. Digital analysis of historic drilling data to reconstruct the placer gold distribution in Sulphur Creek and lower Dominion Creek, central Yukon. *In:* Yukon Exploration and Geology 2016, K.E. MacFarlane and L.H. Weston (eds.), Yukon Geological Survey, p. 225–242.

Preliminary observations of the Bouvette Formation at Nadaleen Mountain, Yukon (NTS 106C/2, 3)

J.F. Busch*, J.V. Strauss, M.H. Saylor, T.J. Allen, K. Faehnrich
Dartmouth College, Department of Earth Sciences

J.F. Taylor
Indiana University of Pennsylvania, Department of Geoscience

Busch, J.F., Strauss, J.V., Saylor, M.H., Allen, T.J., Faehnrich, K. and Taylor, J.F., 2019. Preliminary observations of the Bouvette Formation at Nadaleen Mountain, Yukon (NTS 106C/2, 3). *In:* Yukon Exploration and Geology 2018, K.E. MacFarlane (ed.), Yukon Geological Survey, p. 19–42.

Abstract

The Cambrian–Devonian Bouvette Formation outcrops over large parts of central Yukon. Despite its broad lateral and temporal extent, relatively little is known about its age range, facies distribution, depositional history, and significance for early Paleozoic paleogeographic reconstructions of northwestern Laurentia. At Nadaleen Mountain (NTS 106C/2, 3) in east-central Yukon, the Bouvette Formation is remarkably well exposed and provides new insight into the transition between the southeastern Ogilvie platform and northern Selwyn basin. Here, we present preliminary field data collected from this region during 2017 and 2018, including measured stratigraphic sections, biostratigraphy, and detailed imagery acquired from Unmanned Aerial Vehicles (UAVs), in order to test the hypothesis that the Bouvette Formation locally preserves a platform margin reef and forereef succession. These observations not only provide an important new contribution to Yukon's early Paleozoic depositional history, but also identify an exceptional location to study carbonate platform–margin depositional environments.

* james.f.busch.gr@dartmouth.edu

Introduction

In contrast to the many areas located along the Mackenzie platform and Misty Creek embayment of the Northwest Territories, early Paleozoic platform–basin transitional rocks remain largely unstudied in Yukon (Fig. 1; Morrow, 1999). Reconnaissance observations of the Bouvette Formation at Nadaleen Mountain in 2017 noted the existence of well-preserved platform and platform–margin rocks, which are potentially indicative of the Ogilvie platform–Selwyn basin transition. Basinal and slope deposits fringing carbonate platforms can preserve platform-derived sediments, even during periods of relative low sea level, enabling them to record environmental and ecological changes that are locally lost due to erosion in shallow-water settings. Thus, the Bouvette Formation at Nadaleen Mountain could provide a significant opportunity to better understand early Paleozoic paleontology, sequence stratigraphy, paleogeography, and paleoenvironmental change during the Cambrian–Devonian.

In this paper, the platform and platform–margin rocks exposed in the Nadaleen Mountain area are described based upon measured sections and careful mapping carried out in July 2017 (at Nadaleen Mountain) and August 2018 (south of Nadaleen Mountain; Fig. 2). Specifically, the study aims to: (1) understand the depositional environment of the Bouvette Formation in the Nadaleen Mountain area; and (2) collect fossil material to constrain the age and sedimentation history of the Bouvette Formation along the southwestern edge of the Ogilvie platform. In order to accomplish these goals, we measured a number of closely spaced stratigraphic sections along depositional dip and strike, collected trilobite, coral, and brachiopod fossils, and sampled carbonate rocks for carbon isotope chemostratigraphy and conodont biostratigraphy. Lastly, we collected preliminary UAV imagery to generate three-dimensional depositional models of the study area from integrated field observations, elevation data, and structural measurements. Here, we

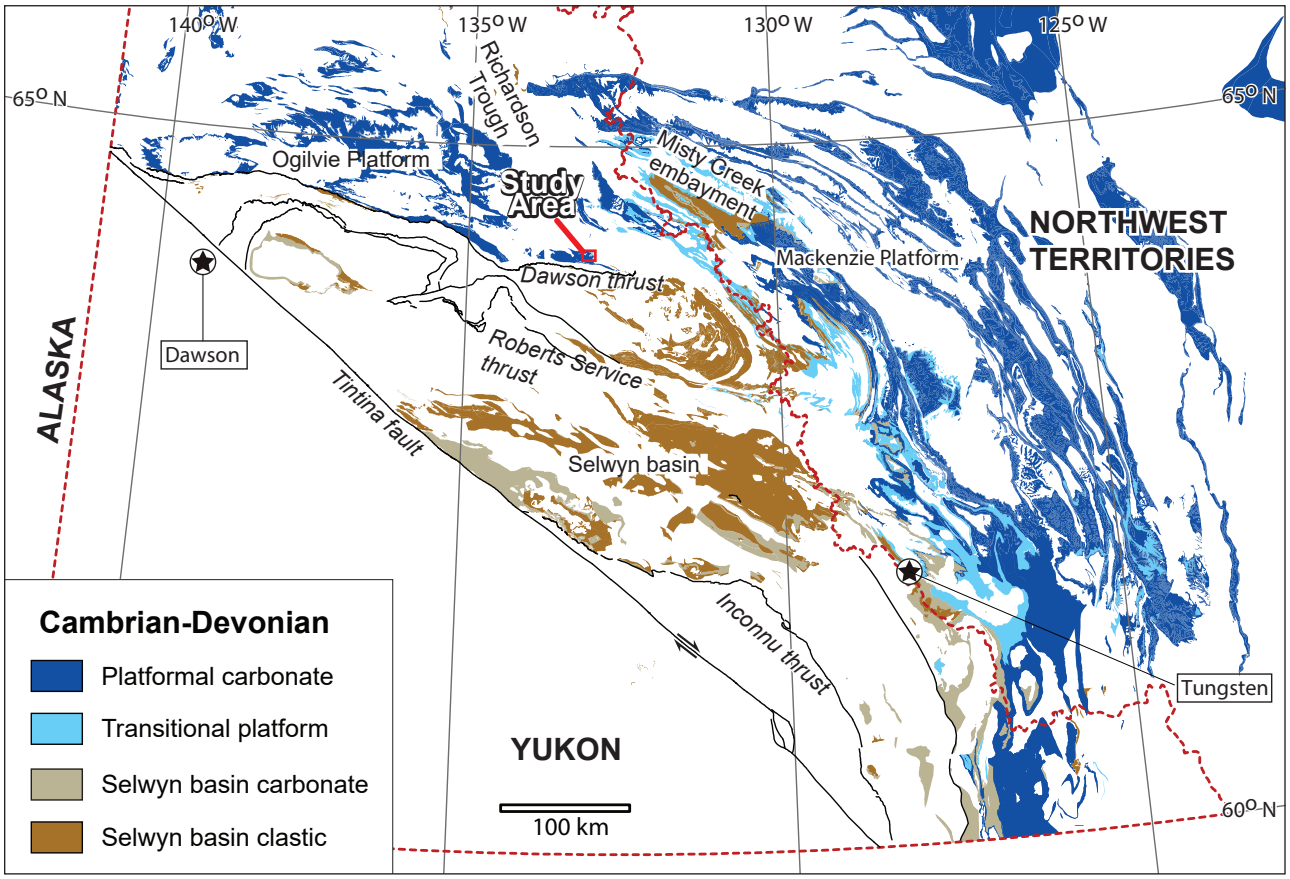

Figure 1. *Simplified geological map of Proterozoic and Paleozoic strata in the northern Canadian Cordillera after Moynihan et al. (accepted). The study area lies north of the Dawson fault, within the Rackla Belt of the Wernecke Mountains and forms part of the arcuate Selwyn–Mackenzie fold-thrust belt.*

present some preliminary field observations and biostratigraphic data from our fieldwork and provide initial interpretations of the depositional history of the Bouvette Formation.

Geological Background

Regional Background

Several major paleogeographic features in northwestern Canada have been identified as important regions of sedimentation during Neoproterozoic–early Paleozoic time. Much of central and western Yukon is underlain by Paleozoic shallow-water carbonate and siliciclastic rocks comprising a region known as the Yukon block (Lenz, 1972). Cambrian–Devonian shallow-water carbonate rocks of the Yukon block comprise an isolated platform, referred to as the Ogilvie platform, that was separated from the main continent-fringing shallow-water depositional system of the Mackenzie-Peel shelf (referred to here as the Mackenzie platform) by the Richardson trough, a narrow N-trending deep-water basin (Fig. 1; Lenz, 1972; Norris, 1985, Cecile, 1982; Cecile *et al.*, 1997; Pyle, 2012). East of the Nadaleen Mountain area, the Ogilvie platform and Mackenzie platform are separated by a deep-water trough called the Misty Creek embayment; to the south exists the much more extensive deep-water Selwyn basin (Fig. 1; Cecile, 1982; Morrow, 1999). Collectively, these shallow-water carbonate rocks of the Ogilvie and Mackenzie platforms form the northwestern edge of the so-called Great American Carbonate Bank (Pyle, 2012).

The Bouvette Formation (Morrow, 1999) comprises an approximately 500 to 1500 m thick Cambrian to Devonian shallow-water carbonate succession that outcrops extensively throughout the Yukon block. The formation was originally considered to be map unit "CDb" during Operation Porcupine (Norris, 1985); it was later formally defined by Morrow (1999). The Bouvette Formation is characteristically very resistant, and often forms steep peaks and spires in linear mountain ranges oriented parallel or subparallel to regional strike in northern Yukon (Morrow, 1999). Despite this resistance to weathering, the Bouvette Formation commonly forms very coarse-grained talus or scree fields throughout these extensive exposures, so it is generally quite challenging to measure detailed stratigraphic sections of these strata.

At its type section in the Ogilvie River map area (NTS 116G; Morrow, 1999), the Bouvette Formation (864 m thick) unconformably overlies unnamed Proterozoic siliciclastic rocks of the Wernecke or Windermere supergroups. Five units are distinguished within the type section, beginning with basal beds of stromatolitic doloboundstone interbedded with intraclast rudstone and grainstone locally containing tepee structures (Morrow, 1999). The second unit consists of thick-bedded finely crystalline or oolitic grey dolograinstone with intervening beds of doloboundstone containing discontinuous lenses of rudstone breccia with localized mudcracks (Morrow, 1999). A rhythmic repetition of shoaling-upward cycles in this unit are marked by thick-bedded oolitic dolograinstone and skeletal dolowackestone grading upwards into doloboundstone. The third unit is similar to the second but contains fewer interbeds of oolitic dolograinstone and rudstone breccia (Morrow, 1999). The fourth unit contains thick intervals of very resistant vuggy sucrosic dolostone with abundant fenestral fabric separated by interbeds of doloboundstone and dolograinstone (Morrow, 1999). The fifth unit is a light grey and resistant massive to thick-bedded coarsely crystalline vuggy dolostone with discontinuous bands of chert. Here, shale of the Road River Group conformably overlie the Bouvette Formation (Morrow, 1999).

Throughout other areas of Yukon, the Bouvette Formation is generally dominated by rubbly exposures of sucrosic dolostone with a notable paucity of well-preserved fossil material (Morrow, 1999). Sparse facies variation includes intervals of fossiliferous pelletal limestone with tentaculitids, brachiopods, colonial corals, and solitary corals in the upper part of the section in the Wind River map area (NTS 106E) near the Knorr Block (Morrow, 1999). Near Royal Mountain (NTS 106E), an incomplete section of the Bouvette Formation is entirely composed of limestone with facies that include abundant stromatolitic boundstone and fossiliferous wackestone that passes laterally into shale of the Road River Group in the Richardson trough (Morrow, 1999).

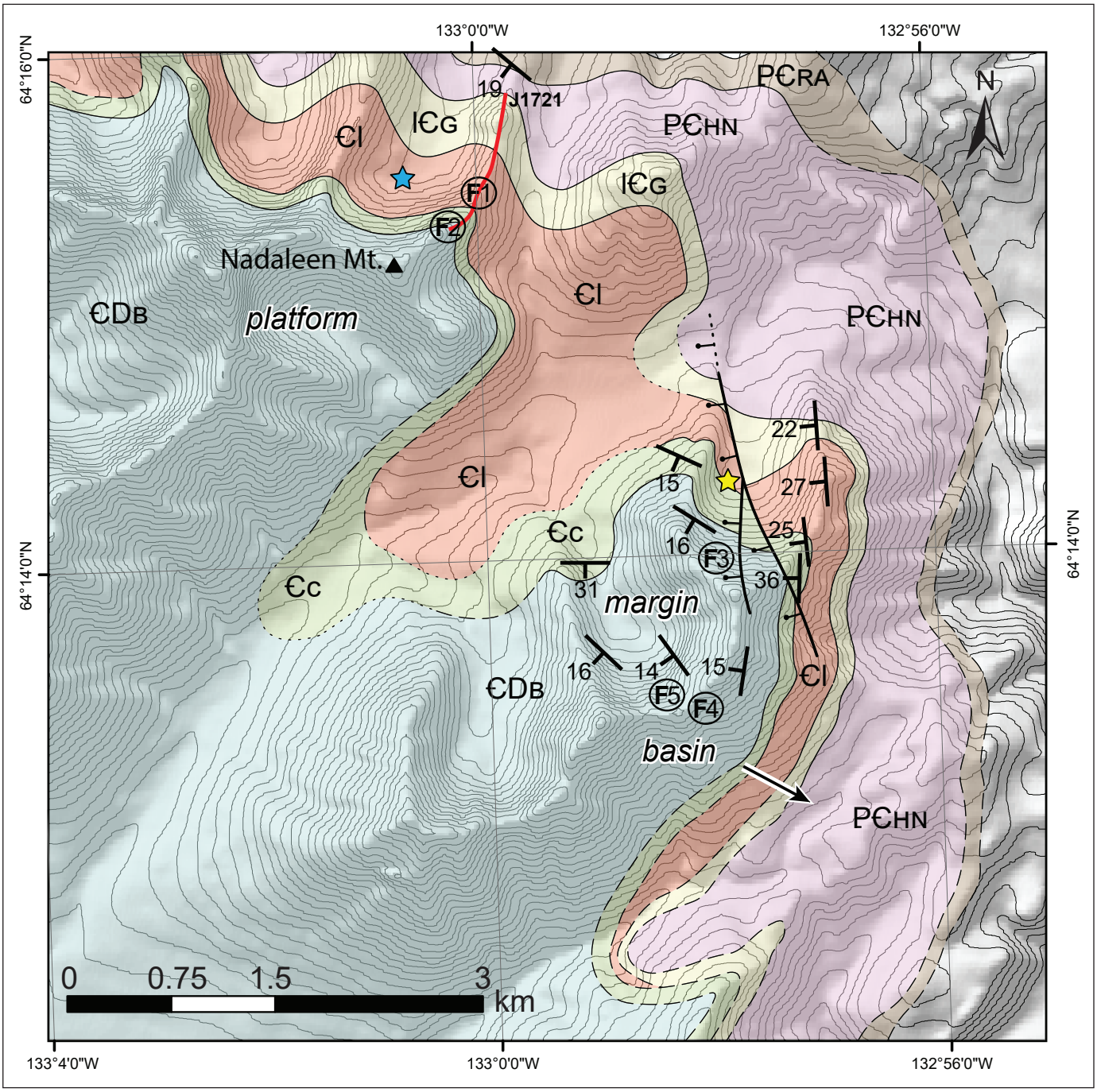

Figure 2. *Preliminary geological map of NTS 106C/2, 3 (scale 1:40 000) based on our field observations and modifications from Colpron (2012a) and Colpron et al. (2013). Elevation contour interval is 20 m. See legend on next page.*

Cambrian–Lower Devonian

Cambrian Furongian to Devonian

ЄDB BOUVETTE FORMATION: *light to dark grey weathering resistant limestone; locally fossiliferous*

Єc UNNAMED CONGLOMERATE: *dark brown to green-weathering clast-supported conglomerate; clasts are locally dominated by mafic volcanic with localized recrystallized limestone and chert; minor intervals of siltstone and sandstone; laterally and vertically transitions to matrix and clast-supported rudstone*

Cambrian Miaolingian–Furongian

Єl UNNAMED LIMESTONE: *dark brown-weathering platy lime mudstone and calcareous shale with rare fossil material; some intervals of carbonate rudstone*

Cambrian Series 2–Miaolingian

lЄG GULL LAKE FORMATION: *dark brown-weathering sandstone, siltstone, shale, and matrix-supported conglomerate; locally heavily bioturbated; upper part of unit is marked by a medium to thick-bedded quartz arenite*

Neoproterozoic–Cambrian Hyland Group

Ediacaran to Lower Cambrian

PЄHN NARCHILLA FORMATION: *dominantly maroon, brown, and olive green shale and slate with local hematite and calcite-cemented quartz arenite and siltstone*

Neoproterozoic Rackla Group

Ediacaran to Lower Cambrian

PЄRA ALGAE FORMATION: *dark to light-grey limestone and dolostone; variably dolomitized with intervals of cross-lamination and sandy/silty limestone*

Symbols

- contact–defined, approximate, covered
- normal fault
- bedding
- F1 fossil locality with interpreted age
- 2017 camp location
- 2018 camp location
- measured section

Fossil Collections

Map #	Age	Map Unit	ID	Date	Fossil Type
F1	Cambrian, Series 2-Miaolingian	Єl	John Taylor	2018	*Bonnia or Kootenia* genus?, trilobite
F1	Cambrian, Miaolingian-Furongian	Єl	John Taylor	2018	*Psuedagnostus*, agnostid arthropod
F1	Cambrian, Furongian (Jianshanian Stage)	Єl	John Taylor	2018	*Loganopeltoides*, trilobite
F1	Cambrian, Furgonian (Paibian-Jianshanian Stage)	Єc	John Taylor	2018	*Irvingella* genus, trilobite
F2	Upper Ordovician	ЄDB	R. Blodgett	2017	*Grewingkia* sp., solitary rugose coral *Septentrionites*? sp., tabulate coral *Paleofavosites*, favositid tabulate coral
F2	Upper Ordovician	ЄDB	R. Blodgett	2017	*Maclurites* sp., gastropod
F3	Late Ordovician-Early Silurian	ЄDB	R. Elias	2018	*Palaeophyllum* sp., colonial rugose coral streptelasmatine, solitary rugose coral
F4	Late Ordovician-Early Silurian	ЄDB	R. Elias	2018	*Catenipora* sp., halysitid tabulate coral *Paleofavosites*, favositid tabulate coral
F5	Late Ordovician-Early Silurian	ЄDB	R. Elias	2018	*Palaeophyllum* sp., colonial rugose coral

Figure 2. *Map legend.*

The Bouvette Formation ranges in age from early Cambrian (Series 2) to early Devonian (Morrow, 1999). The lower Cambrian Series 2 age constraint is based upon the occurrence of poorly preserved archeocyathids in what was originally mapped as unit 8 (Green, 1972) and later assigned to the Bouvette Formation in the Coal Creek inlier, Ogilvie Mountains (Fritz, 1982; Mustard *et al.*, 1988). The uppermost beds of the Bouvette Formation are highly diachronous and range in age from Middle Ordovician to Early Devonian (Morrow, 1999). These upper age constraints are assigned based upon the presence of pre-Devonian undetermined fossil material and Middle or Late Ordovician tabulate corals in the Hart River map area (NTS 116H) and Early Devonian brachiopods, stromatoporoids, and tabulate corals collected in the Wind River map area (NTS 106E; Morrow, 1999). Drill core intersections of the Bouvette Formation recovered from Eagle Plain yielded Late Ordovician echinoderms, rugose corals, brachiopods, and stromatoporoids near its upper contact with the Road River Group (Morrow, 1999).

In the southern Wind River map area and southeastern Hart River map area parts of the Yukon block, Morrow (1999) suggests the Bouvette Formation conformably overlies fine-grained carbonate rocks of the Upper Cambrian Taiga Formation; however, Fritz (1997) reported an erosional unconformity marking the contact between the Bouvette and Taiga formations (Fig. 3). Over large swaths of the central and western Yukon Block, the Bouvette Formation unconformably overlies Proterozoic strata of the Quartet and Gillespie Lakes groups (Morrow, 1999). These relationships indicate the Bouvette Formation onlapped basement paleo-highs while transitioning conformably into deeper water carbonate settings following early to middle Cambrian extension (Morrow, 1999). The Bouvette Formation passes westward into the Cambrian–Ordovician Jones Ridge Formation of east-central Alaska and western Yukon (Fig. 3; Brabb, 1967; Norris, 1982; Taylor *et al.*, 2015). To the north of the study area, the Bouvette Formation of the Ogilvie platform passes into basinal shale of the Road River Group in the Richardson trough; to the east, the Bouvette Formation transitions into argillaceous limestone of the Rabbitkettle Formation in the Misty Creek embayment (Fig. 3; Cecile 1982; Morrow, 1999). On the eastern side of the Misty Creek embayment, the Mackenzie platform equivalent of the Bouvette Formation consists of the Cambrian–Ordovician Franklin Mountain and Ordovician–Silurian Mt. Kindle formations (Cecile, 1982); farther south, the Bouvette Formation is equivalent to the Cambrian–Ordovician Haywire Formation (Fig. 3; Gordey and Anderson, 1993). Throughout most of its extent, the Bouvette Formation is overlain by, and interfingers with, shale of the Road River Group (Morrow, 1999).

Study Area

Paleozoic platformal carbonate rocks of the Nadaleen Mountain study area overlie the Neoproterozoic to Cambrian Rackla Group and Narchilla Formation (Fig. 2) and are locally juxtaposed against Paleozoic slope and basinal rocks assigned to the Road River and Earn groups along the Kathleen Lakes fault (Blusson, 1974; Colpron *et al.*, 2013; Moynihan, 2016). Regionally, this area is known informally as the Rackla belt, referring to a metallogenic trend which closely follows the Dawson thrust at the northern edge of the Selwyn basin (Colpron, 2012b). In the study area, Paleozoic sedimentation commenced with siliciclastic strata of the Narchilla and Gull Lake formations, which are succeeded by an unnamed Cambrian limestone unit and an unnamed Cambrian conglomerate (Fig. 4; Colpron, 2012b; Moynihan, 2016; *this contribution*). The Bouvette Formation, which marks the establishment of a stable carbonate platform in the region, unconformably overlies the unnamed Cambrian conglomerate (Figs. 2 and 4). These strata were examined within two NNE-facing cirques at the base of Nadaleen Mountain (2017), and three NNE-facing cirques ~3 km south of Nadaleen Mountain (2018; Fig. 2). The Bouvette Formation is well-exposed in these cirques and reasonably accessible by foot traverse. The Neoproterozoic to Paleozoic units exposed adjacent to Nadaleen Mountain dip moderately to the west-southwest and are cut by several high-angle normal faults trending NNW (Fig. 2); these strata are generally well-preserved and undeformed. Within the study area, our team measured 27 stratigraphic sections of the Neoproterozoic to Paleozoic units (see Figure 5).

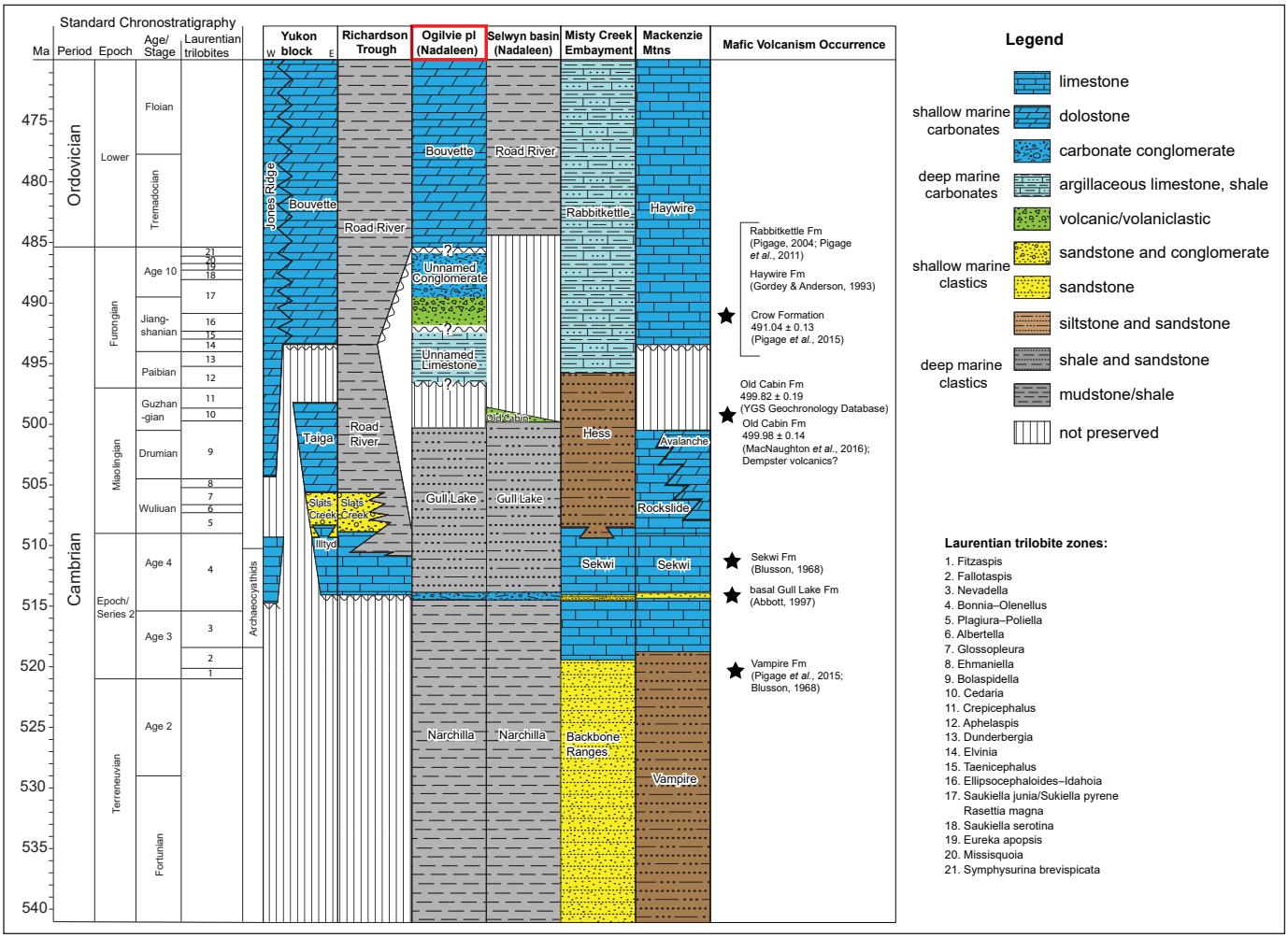

Figure 3. *Correlation of early Paleozoic stratigraphy across NW Canada. Some boundaries are approximate due to limited fossil and geochronological age data. Modified from Moynihan et al. (accepted). The time scale is after Cohen et al. (2013; updated). Data for the Yukon block are after Fritz (1997) and Morrow (1999); for the Richardson trough after Norris (1985) and Fritz (1997); for the Misty Creek embayment after Cecile (1982); for the Ogilvie platform after Mustard et al. (1988) and Colpron et al. (2013); for the Selwyn basin from Cecile (2000), Colpron et al. (2013), and Moynihan (2014); for the Mackenzie Mountains after Gordey and Anderson (1993).*

Stratigraphy of the Nadaleen Mountain Area

Ediacaran–Cambrian Rackla Group

Algae Formation (PCRA)

The Ediacaran–Cambrian(?) Algae Formation (Cecile, 2000) forms a resistant carbonate unit divided into two members. In the type area (NTS 105O/14), the lower member is composed of a flaggy limestone with minor chert and argillite, and an upper member of dolostone and cross-bedded arenaceous dolostone and limestone (Cecile, 2000). Elsewhere in the Nadaleen Mountain area, the Algae Formation consists of lime mudstone and oolitic grainstone, silty to sandy limestone and subordinate intraclast rudstone (Colpron, 2012b; Moynihan, 2014; Moynihan et al., accepted). Regionally, the thickness of the Algae Formation ranges from approximately 80 to 350 m, reaching ~150 m at Nadaleen Mountain. Here, the rocks are exclusively dark to light grey dolostone that are variably recrystallized with fabric-destructive dolomitization. The dominant facies consists of thin to thick-laminated silty to sandy dolomitic grainstone with common ripple cross-lamination. In the intervals that are heavily dolomitized, there is local brecciation, veining, and development of zebra or saddle dolomite textures.

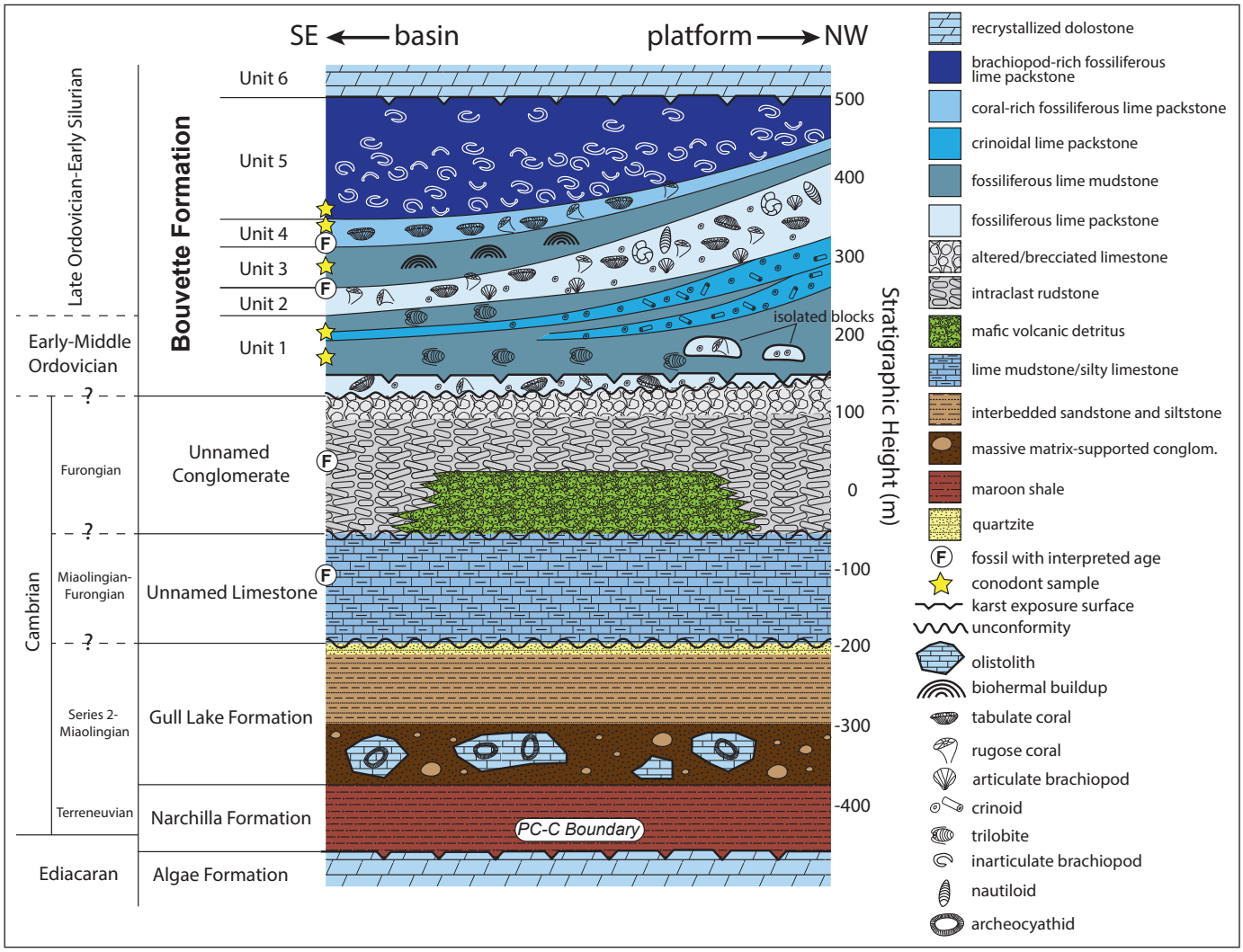

Figure 4. *Schematic stratigraphic column of Neoproterozoic-Paleozoic strata in the Nadaleen Mountain study area. Sedimentary unit geometries and thickness changes are drawn schematically to capture broad trends observed across the study area. Horizontal axis is not drawn to scale.*

Ediacaran–Cambrian Hyland Group

Narchilla Formation (PCHN)

The lower Cambrian Narchilla Formation (Gordey and Anderson, 1993) is a dominantly fine-grained siliciclastic succession that disconformably overlies the Algae Formation in the study area (Colpron, 2012b; Moynihan, 2014; Moynihan *et al.*, *accepted*). At its type section, the contact is interpreted as conformable (Gordey and Anderson, 1993; Cecile, 2000). In the Nadaleen Mountain area, a locally recognized erosional surface separates the Narchilla and Algae formations and is expressed as an approximately 1 to 5 m thick matrix-supported brecciated limestone with varying amounts of brown, sandy matrix. This paleokarst horizon variably possesses characteristic *terra rosa* coloration, dissolution surfaces, and sand-filled grikes that are indicative of subaerial exposure (Moynihan, 2014; Moynihan *et al.*, *accepted*). At the type section near the little Nahanni River (NTS 105O/15), the Narchilla Formation is divided into three members (Gordey and Anderson, 1993); Cecile (2000) later defined two members in the Narchilla Formation in the Niddery Lake map area (NTS 105O). The ~400 m thick lower Senoah Member is composed of brown to tan siltstone and shale with thick interbeds of resistant quartzite. The upper Arrowhead Lake Member (~120 m thick) consists of maroon and olive-green siltstone and

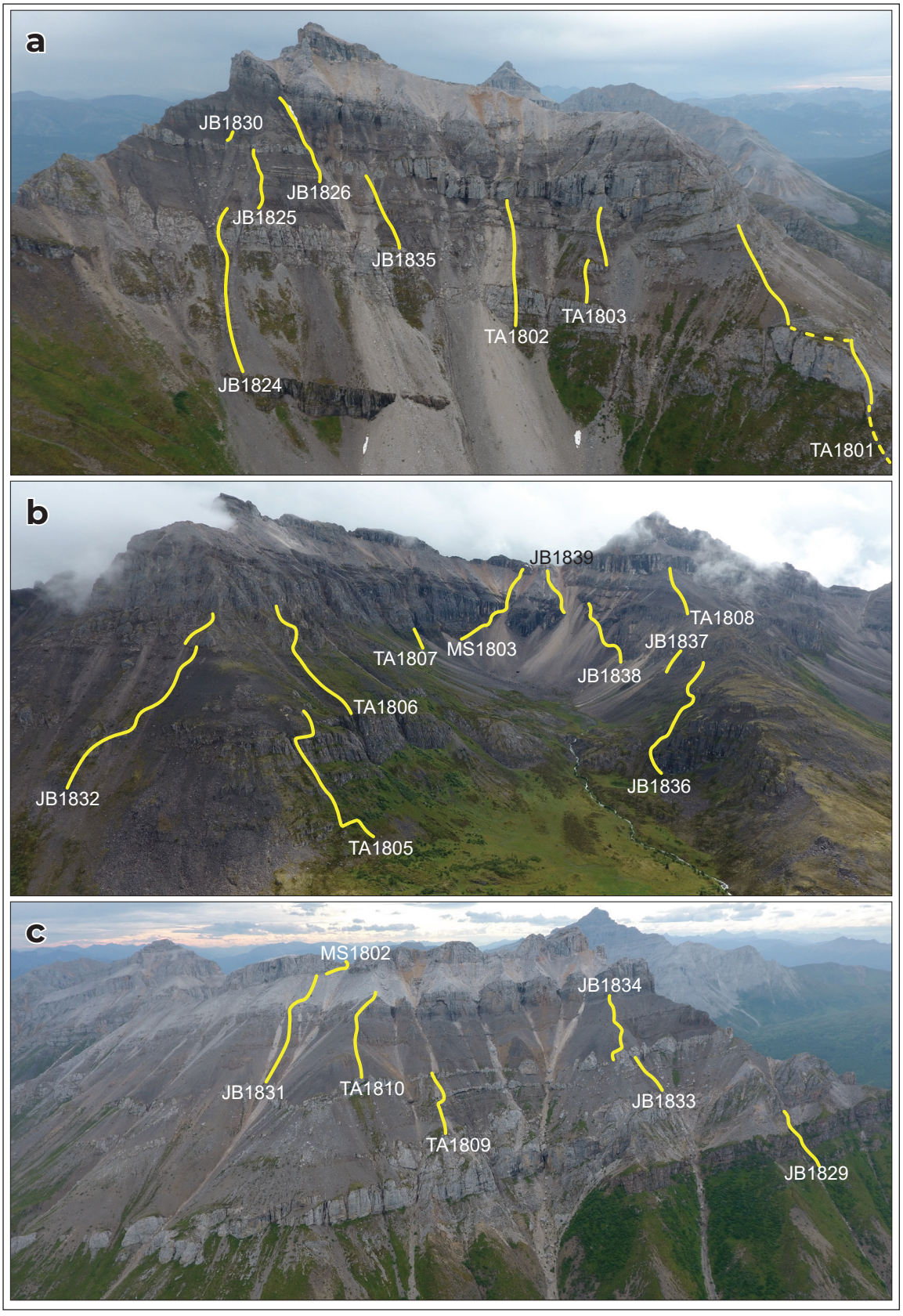

Figure 5. *Locations of measured sections in the study area, southeast of Nadaleen Mountain. Colored lines show routes of the measured sections.*

shale with minor quartzite interbeds. In the Nadaleen Mountain area, the Narchilla Formation is undivided and comprises a basal lithologically variable interval that includes thickly laminated hematite-cemented quartz arenite, dark grey calcite-cemented sandstone and siltstone, and carbonate clast rudstone. This thin basal unit is overlain by a maroon and green siltstone and shale unit that locally contains a penetrative cleavage that obscures primary sedimentary structures. The presence of simple horizontal trace fossils preserved on the soles of sandstone beds within this unit, including *Oldhamia*, likely indicate deposition during the Terreneuvian to Cambrian Stages 2–3 (Hofmann et *al.*, 1994; Moynihan, 2014; MacNaughton et *al.*, 2016; Moynihan et *al.*, *accepted*).

Cambrian-Devonian

Gull Lake Formation (lCG)

The Gull Lake Formation (Gordey and Anderson, 1993) predominantly comprises fine-grained siliciclastic rocks in the Nadaleen Mountain area. The basal strata consist of dark brown poorly sorted matrix-supported conglomerate with granule to boulder-sized clasts of calcite-cemented sandstone, chert, recrystallized limestone, and archeocyathid-bearing boundstone (Moynihan, 2014). This basal unit is overlain by a package of thin to medium-bedded medium to coarse-grained quartz arenite, quartz wacke, and sublitharenite with local carbonate matrix. This unit is pervasively bioturbated and contains minor carbonate rudstone and a variety of different Bouma subdivisions, which broadly suggest deposition by suspension sedimentation and turbidity and sediment-gravity flows. A distinctive 4 to 10 m thick medium to thick-bedded quartz arenite marks the top of the Gull Lake Formation in the Nadaleen Mountain area. The archeocyathid-bearing limestone clasts in the basal unit provide an approximate maximum age constraint of Cambrian Series 2 for the Gull Lake Formation (Moynihan, 2014; Moynihan et *al.*, *accepted*), which is consistent with Abbott's (1997) report of *Bonnia-Ollenelus* Zone trilobites within the Gull Lake Formation in the Hart River area. Occurrences of *Oldhamia* trace fossils in the upper part of the Gull Lake Formation provide a minimum age constraint of Cambrian Stage 5, as *Oldhamia* does not occur above middle Cambrian strata worldwide (Herbosch and Verniers, 2011; Moynihan, 2014; MacNaughton et *al.*, 2016).

Unnamed Cambrian Limestone (Cl)

An unnamed fine-grained carbonate unit conformably overlies the dominantly siliciclastic Gull Lake Formation in the Nadaleen Mountain area (Colpron et *al.*, 2013). This unit was identified by Colpron et *al.* (2013) with its base marked by the first carbonate that overlies siliciclastic rocks of the Gull Lake Formation. The Cambrian limestone unit is approximately 150 m thick and composed predominantly of recessive, thin-bedded and locally fossiliferous grey-brown platy lime mudstone and calcareous shale. Some intervals from this unit contain distinct Bouma CDE alternations with subtle grain-size differences, thin beds of lime mudstone with localized coarse-grained fossiliferous or sandy lags, and zones of soft-sediment deformation and slump folds. There are several 1 to 2 m thick interbeds of dark grey-brown rudstone and orange to dark grey limestone clasts, some of which are fossiliferous. The top of the unit is marked by a sharp contact with either intraclast rudstone or volcaniclastic conglomerate of the overlying unnamed conglomerate map unit.

Unnamed Cambrian Conglomerate (Cc)

In the Nadaleen Mountain area, an unnamed, approximately 200 m thick conglomerate unit disconformably overlies the unnamed limestone unit identified by Moynihan (2016). The contact is marked by a sharp to irregular surface filled with light grey to tan-weathering thick-bedded and poorly sorted conglomerate with pebble to boulder-sized clasts composed of silty lime grainstone, recrystallized limestone, and calcite-cemented sandstone supported by a calcitic quartz sand matrix. Where measured (JB1829; Fig. 5c), there is a lower interval of volcanic detritus in the informal conglomerate unit that is approximately 70 m thick and composed of a basal succession dominated by dark green to light grey volcaniclastic conglomerate. The interval begins with a polymict conglomerate composed of well-rounded to subrounded clasts of recrystallized limestone, sandy dolograinstone, and mafic volcanic rocks in a poorly sorted, medium to coarse subrounded litharenite matrix

with subordinate quartz sand and minor green silt. Above the basal interval, the clasts become exclusively composed of pebble to boulder-sized dark green mafic volcanic rocks that are variably amygdaloidal with void-filling chalcedony. The matrix is dominated by sand and silt-size particles of the same composition and has rare interbeds of volcaniclastic litharenite and siltstone. The lower volcaniclastic strata pass laterally to the northwest and southeast of the study area and vertically into carbonate-clast rudstone, which is locally up to approximately 160 m thick. The carbonate rudstone is very thick bedded to massive and is locally interbedded with matrix and clast-supported rudstone and grainstone (Fig. 6a) dominated by granule to pebble-sized tabular and subrounded clasts of finely crystalline limestone with variable silicification and a sandy/silty lime matrix. Some clasts contain silicified, well-rounded, granule-sized coated grains as well as beautifully preserved trilobites. The basal, approximately 120 m thick rudstone interval is succeeded by a dark grey limestone interval with subangular to subrounded clasts and no observable matrix (Fig. 6b). The upper ~5 m of the unnamed conglomerate unit is fossiliferous in places having abundant tabulate and rugose corals and stromatolites, but it also contains discontinuous lenses and vertical pipes of brecciated limestone with a tan sandy/silty matrix tentatively interpreted as paleokarst breccia. The upper surface of the unnamed conglomerate is highly irregular with up to ~5 m of relief (see Fig. 7a,c); the upper fossiliferous interval is only preserved in the southeastern part of the study area.

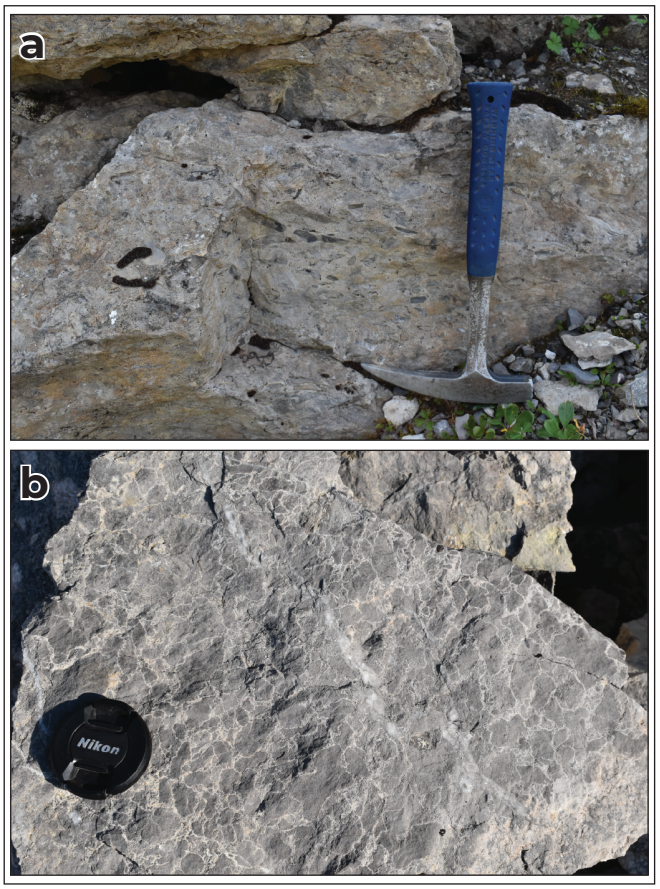

Figure 6. (a) *Medium to thick-bedded rudstone that composes most of the Unnamed Conglomerate; and* ***(b)*** *peculiar altered, brecciated, or microbial limestone facies near the top of the Unnamed Conglomerate.*

The Cambrian volcaniclastic conglomerate map unit, approximately 3 km to the west (Colpron, 2012a), yielded a chemical abrasion-isotope dilution-thermal ionization mass spectrometry (CA-ID-TIMS) U-Pb zircon age of 499.82 ± 0.19 Ma (YGS Geochronology Database, 2018). This map unit shares many lithological similarities to the reworked mafic volcanic detritus interval identified at the base of the unnamed conglomerate unit here. Additionally, Old Cabin Formation mafic volcanic rocks of the northeastern Selwyn basin have been dated to *ca.* 499 Ma (MacNaughton *et al.*, 2016). This could be a likely source of the mafic volcanic detritus given its proximity to the Nadaleen Mountain area, but as the volcanic material in the unnamed conglomerate is reworked, it only suggests a maximum depositional age for the unit.

Bouvette Formation (CDB)

In this preliminary study, 24 closely spaced stratigraphic sections of the Bouvette Formation were measured utilizing a Jacob staff at cm-resolution (Fig. 5). Based on the variation in lithology, sedimentary structures, and fossil assemblages, we identified six distinct stratigraphic units. The thickness of these units varies along depositional dip and is schematically shown in Figure 4, along with a composite stratigraphic column for the Nadaleen Mountain area. Several high-resolution UAV images accompany the measured sections and illustrate the stratigraphic expression of the six units distinguished within the Bouvette Formation (Fig. 7).

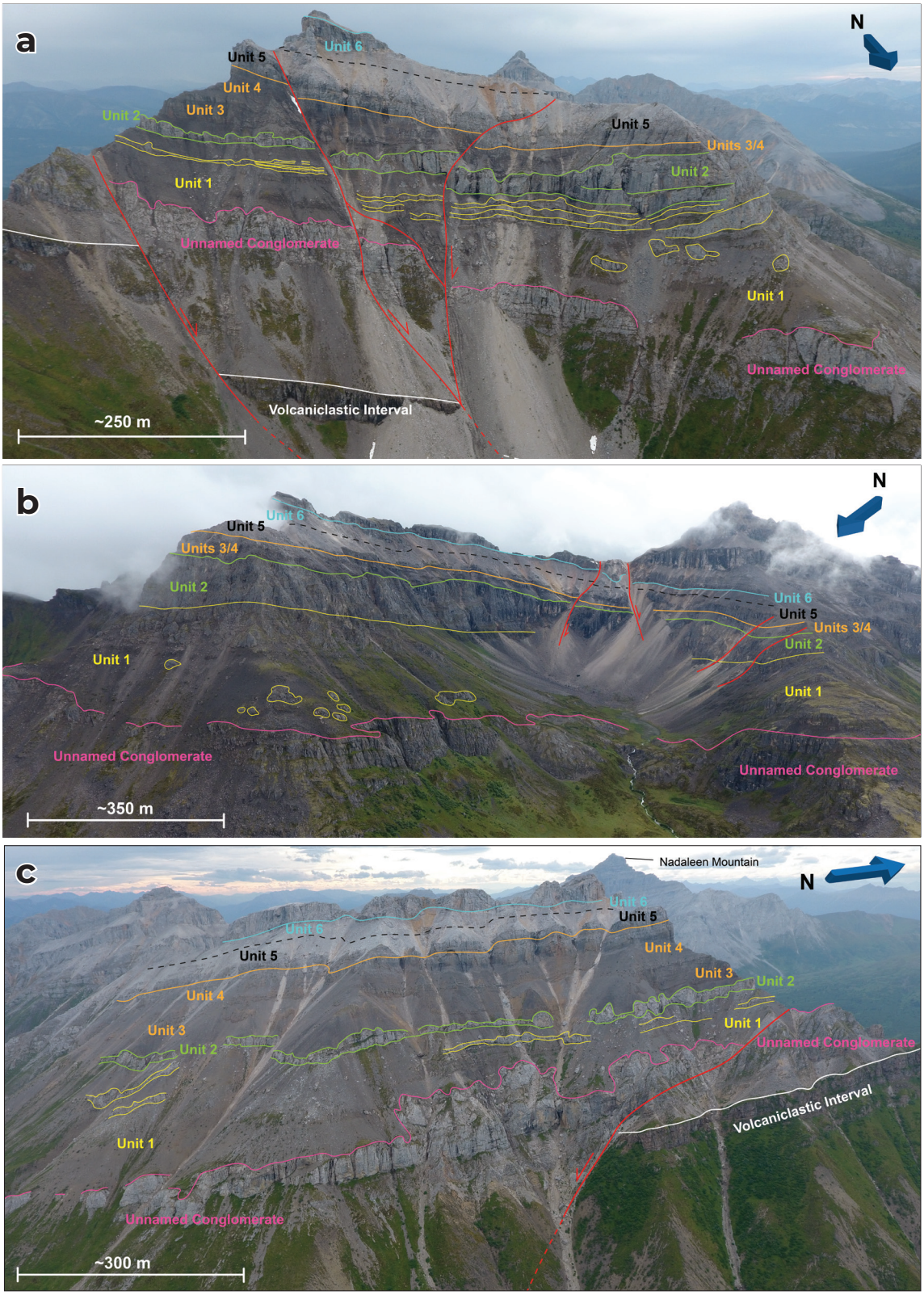

Figure 7. *Interpreted drone photographs illustrating the expression of the six distinct units in the Bouvette Formation across the study area. Unit contacts are drawn based on observations within measured sections and while on traverse (see Fig. 5).*

Unit 1: This approximately 50 to 175 m thick unit consists of fossiliferous lime wackestone and lime mudstone (Fig. 8a) containing trilobites, crinoids, bivalves and brachiopods. Towards the top of the lime mudstone interval at the northwestern end of the study area, there are isolated, recrystallized and fossiliferous limestone bodies (ranging from 5 to 13 m wide by 4 to 11 m tall) containing fragments of stromatolitic boundstone and silicified rugose and tabulate coral. These fossiliferous bodies of limestone are onlapped by the overlying thin-bedded fossiliferous lime packstone (Fig. 8b) and may represent patch reefs due to the lack of evidence for subaerial exposure, no observable deformation in the underlying beds, and the abundance of coral fossils. Alternatively, they could represent allochthonous blocks shed from the edge of the carbonate platform. These limestone bodies are overlain by thin and wavy-bedded fossiliferous echinodermal lime packstone (Fig. 8c) that form more resistant outcrops and comprise resistant wedges that thicken to the northwest from approximately 50 to 175 m in distinct clinoformal geometries (Fig. 7a). This unit is followed by a recessive fossiliferous lime mudstone/wackestone package that contains trilobites and brachiopods.

Unit 2: This unit is approximately 25 to 100 m thick and has an erosive base with several metres of relief that contain ripped-up cobbles of the underlying lime mudstone/wackestone facies and boulders of fossiliferous lime packstone containing abundant coral and reef fossil material. The basal rudstone passes upwards into massive fossiliferous lime packstone containing abundant trilobite, rugose coral, tabulate coral, crinoids, brachiopods, gastropods and nautiloids (Fig. 9a,b). At the top is a highly irregular mound-shaped surface with up to 10 m of relief (Fig. 9d). There are abundant *in situ* rugose and tabulate corals, suggestive of an isolated reefal buildup with no evidence of subaerial exposure (Fig. 9c). This upper reef/mound interval is onlapped by fine-grained facies of Unit 3. Unit 2 thickens to the northwest from ~25 to 100 m where it becomes difficult to discern from the underlying Unit 1 and forms a massive cliff-forming unit composed of fossiliferous lime packstone (Fig. 7a,b).

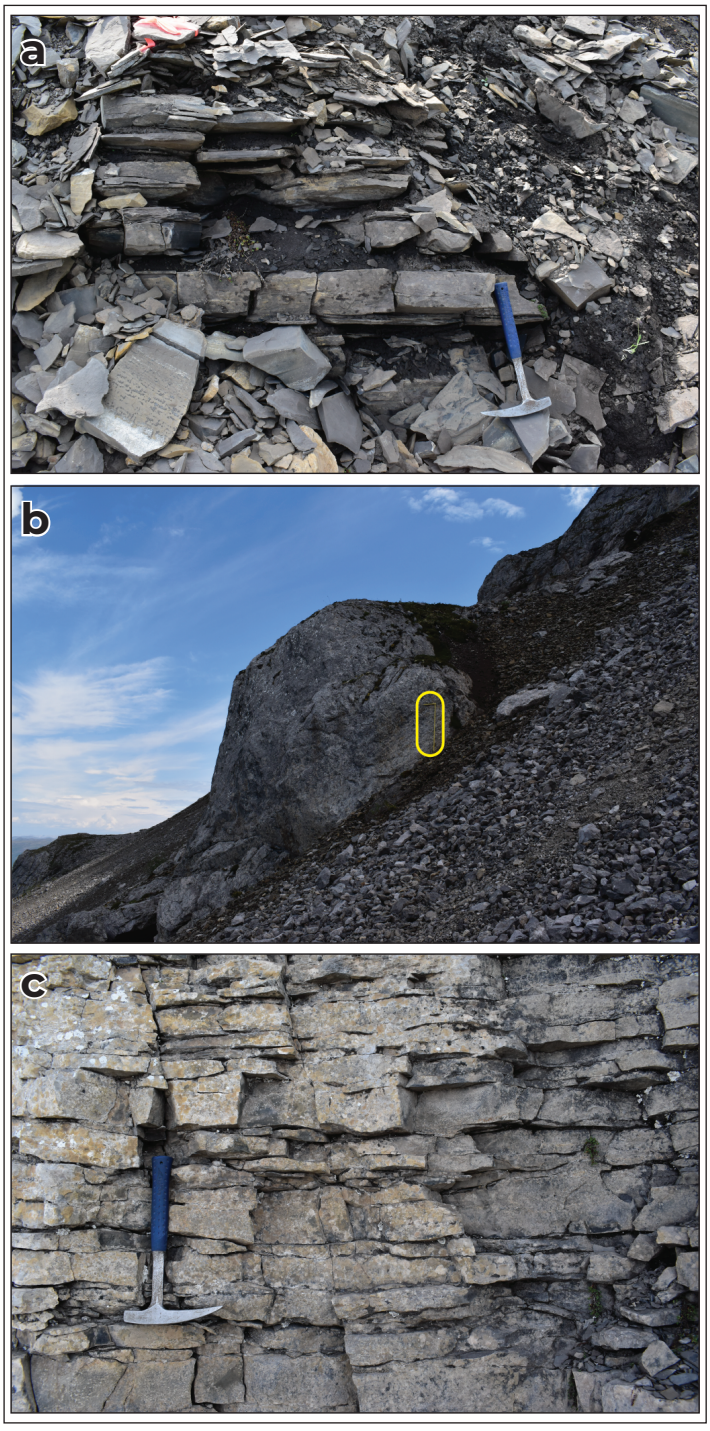

Figure 8. (a) *Thin and planar-bedded fossiliferous lime mudstone at the base of Unit 1;* ***(b)*** *isolated block in Unit 1 composed of recrystallized fossiliferous lime packstone surrounded and overlain by fossiliferous lime wackestone (m stick circled for scale); and* ***(c)*** *thin and wavy-bedded fossiliferous echinodermal lime packstone that comprises one of the clinoformal wedges in Unit 1 (see Fig. 7a).*

Figure 9. ***(a)*** *gastropods and a possible stromatoporoid in a massive outcrop of fossiliferous lime packstone that comprises Unit 2;* ***(b)*** *nautiloid fossils found within the massive fossiliferous lime packstone of Unit 2;* ***(c)*** *in situ corals, including halysitid and favositid tabulate and rugosan corals, found on the uppermost surface of a Unit 2 reef shown in panel (d);* and ***(d)*** *dome-shaped reef buildup with ~10 m of stratigraphic relief and in situ corals at the top of Unit 2, which is onlapped by dark grey fossiliferous lime mudstone of Unit 3.*

Unit 3: This unit is approximately 10 to 75 m thick and comprises dark brown-grey thin to wavy-bedded fossiliferous lime wackestone, packstone, and mudstone that onlaps the top of Unit 2 and transitions laterally into microbial and stromatolitic boundstone. Fossil material includes crinoids, brachiopods, rugose corals and tabulate corals. Fossiliferous packstone intervals are often composed almost entirely of echinodermal debris with minor rugose or tabulate corals. Within intervals of stromatolitic and microbial boundstone, there are approximately 3 to 5 m wide dome-shaped features where bedding changes to nearly vertical (Fig. 10). Strata overlying these dome-shaped features are undeformed, suggesting they could represent large bioherms rather than structural deformation. Unit 3 is thickest in the southeastern part of the study area and thins notably towards the northwest.

Figure 10. *Biohermal buildup (geologist for scale) near the base of Unit 3 within a thin to medium-bedded stromatolitic boundstone facies.*

Unit 4: This approximately 10 to 50 m thick unit consists of light to dark grey thin to wavy-bedded fossiliferous lime wackestone/packstone and boundstone with *in situ* tabulate and less abundant rugose corals (Fig. 11). The tabulate corals are silicified and are upright and in-place, rather than transported and overturned. The Unit 4–5 boundary is marked by an abrupt transition in fossil content from tabulate and rugose corals to disarticulated and whole brachiopods. The first appearance of brachiopods occurs as minor, thin, interbeds of relatively small shells. Within several metres, the corals disappear

Figure 11. *In situ favositid tabulate coral at the base of Unit 4 within a thin and wavy-bedded fossiliferous wackestone.*

entirely, and the brachiopods occur in medium to thick, tabular, cross-stratified beds (Fig. 12a). Similar to Unit 3, it is thickest in the southeastern part of the study area and thins towards the northwest.

Unit 5: This approximately 50 to 100 m thick unit consists of light grey and thick-bedded brachiopod packstone and grainstone containing rare corals (Fig. 12a,b). Beds have tabular geometries and are cross-stratified. At the base, the brachiopod shells are small and grow larger and more abundant up-section. Farther up-section, these strata become entirely recrystallized and dolomitized with vuggy replacement of bioclasts. The brachiopod fossils disappear at the top of the unit, which is poorly exposed. This unit also is thickest in the southeastern part of the of the study area and thins towards the northwest.

Unit 6: This approximately 25 m thick unit consists of light grey and highly recrystallized sucrosic dolostone and limestone. The unit weathers massive and outcrops poorly until its top, where it transitions into a cliff-forming limestone containing no visible fossils (Fig. 7). This unit was not examined in detail due to its general inaccessibility.

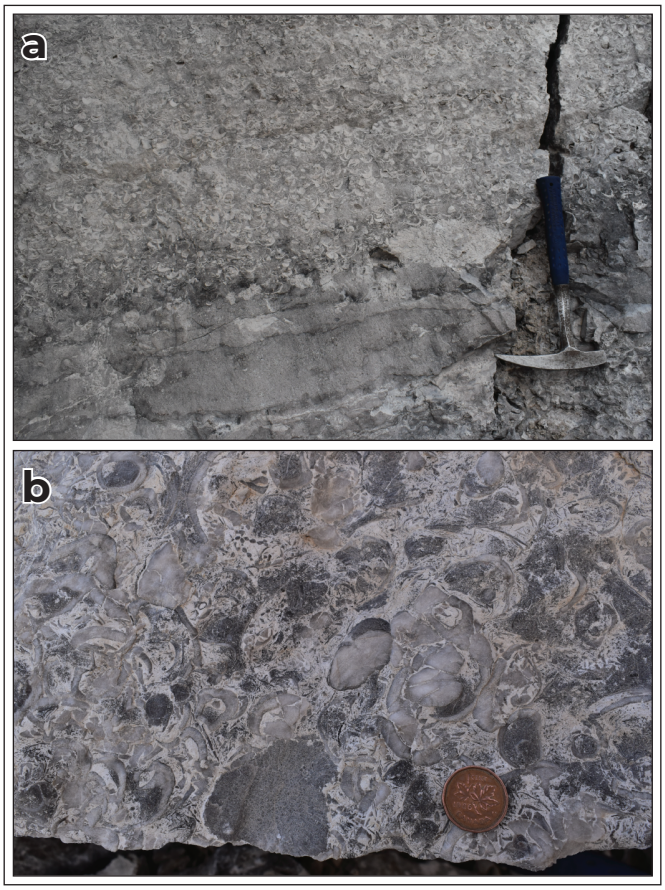

Figure 12. (a) *Medium to thick-bedded fossiliferous lime packstone composed mostly of brachiopod shells within Unit 5; and* ***(b)*** *fossiliferous lime packstone at the base of Unit 5 composed mostly of brachiopod shells with some clasts of halysitid and favositid tabulate corals.*

Fossil Collections

The only previous age constraint on the Bouvette Formation in the Nadaleen Mountain map area was defined by an Early Ordovician gastropod collected approximately 15 km west of the study area (Colpron, 2012a). In 2018, a number of fossils were collected from measured sections south of Nadaleen Mountain (see Fig. 2; fossil locations 3, 4, 5) and preliminary identifications of coral fossils have been made. In 2017, a reconnaissance section was measured at the base of Nadaleen Mountain (J1721; Fig. 2) where several fossils were collected from the unnamed Cambrian limestone unit and the Bouvette Formation (see Fig. 2; fossil locations 1, 2). These fossil collections were recovered approximately 3 km from the detailed measured sections described herein, so future fieldwork in the area will focus on linking these strata more precisely to the units described above.

Sampling of limestone conglomerate beds in the reconnaissance section from Nadaleen Mountain (J1721; Fig. 2) produced arthropod-dominated collections from seven different horizons, all of them Cambrian in age. Completed work has focused on two horizons in the section from which sizeable collections were recovered: one at 241 m, within the unnamed limestone map unit, and the other at 520 m, within the unnamed conglomerate map unit. The collection from 520 m is particularly diverse both taxonomically and morphologically (see Fig. 13), and contains *Irvingella*, a cosmopolitan and biostratigraphically useful Furongian trilobite genus that is known to occur only in Paibian and basal Jiangshanian strata (Hong *et al.*, 2003; Westrop and Adrain, 2016). Like the trilobites and agnostoid arthropods recovered from similar deep marine, gravity flow deposits in the Quebec and Humber Arm allochthons in eastern Canada (e.g. Rasetti, 1944, 1948; Ludvigsen *et al.*, 1989), those extracted from the Nadaleen Mountain rudstone are very well preserved. Although disarticulated, they display little or no evidence of diagenetic degradation or tectonic deformation. Most specimens are testate, and original cuticle and diagnostic surface textures are very well preserved. Although the taxonomic and biostratigraphic evaluation of the collections is at an early stage, identified fossils confirm that at least three distinct fauna (Fig. 13) are represented in the material from the two particularly productive horizons. Accessory components of the fauna include brachiopods (phosphatic and calcitic), hyoliths, and a few problematic taxa.

As is typical of gravity flow deposits, age determinations are complicated by the composite nature of the debrites, whose fossil content can include not only the remains of organisms that lived at the time of deposition, but also older fauna reworked from significantly older deposits exhumed by erosion higher on the slope. The fossils recovered from the limestone rudstone at 241 m (unnamed limestone map unit) illustrate this problem well. Two distinct fauna are present, a younger one (241-Y) in the matrix (and/or nearly syndepositional

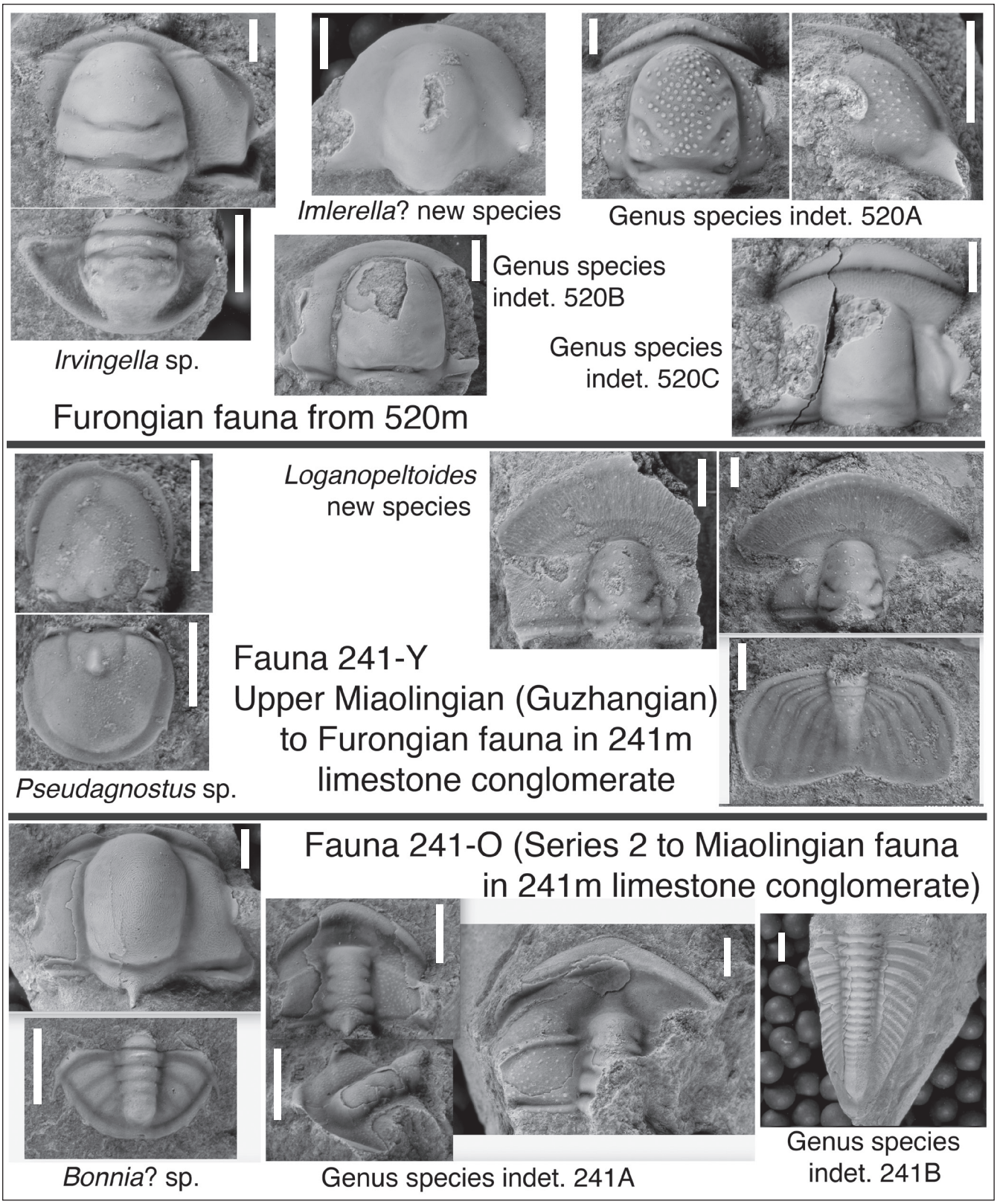

Figure 13. *Trilobites and agnostoid arthropods of the three Cambrian faunas recovered at fossil locality 1 (Fig. 2; section J1721) at Nadaleen Mountain from the unnamed limestone unit (Fauna 241-Y and 241-O) and Unit 1 of the Bouvette Formation (fauna from 520 m). White scale bar in each image is 2 mm long. Delineation of chronostratigraphic units (series and stages) follows Taylor et al. (2012).*

clasts) of light colored grainstone, and an older one (241-O) in well-indurated, darker grainstone clasts within the conglomerate (Fig. 13). These two fauna bracket the age of the unit. The presence of the agnostoid arthropod *Pseudagnostus* in the matrix fauna establishes the time of deposition as no older than late Miaolingian; the oldest documented occurrences of this genus, on multiple continents, lie within the uppermost stage of the Miaolingian, the Guzhangian Stage. The presence of *Loganopeltoides* in collection 241-Y would suggest that deposition occurred in the Jiangshanian, as all known species of that trilobite genus are from the Sunwaptan Stage of Laurentia (Ludvigsen *et al.*, 1989). However, the *Loganopeltoides* in 241-Y is a new species that is most similar to one previously reported from very low within the Sunwaptan. Consequently, a Paibian or even older age for the rudstone at 241 m in the unnamed Cambrian limestone unit is quite possible.

The older fauna (241-O) in the dark clasts is dominated by a species that represents one of several intergrading dorypigid trilobite genera that occur only in sub-Furongian strata (Fig. 13). It most closely resembles species that have been assigned to the "early Cambrian" (Series 2) genus *Bonnia*, but also is similar to many species of *Kootenia*, which occurs in both Series 2 and the "middle Cambrian" (Miaolingian Series). Two other distinctive genera associated with the dorypgid in fauna 241-O have not yet been identified precisely; hopefully when they are identified it will resolve whether that fauna is "early" or "middle" Cambrian in age. Similarly, the age of the 520 m collection (unnamed conglomerate map unit) is likely to be constrained more tightly as a number of distinctive trilobites are identified with greater precision (Fig. 13).

In addition to these arthropod collections from the underlying unnamed limestone and conglomerate units, we also discovered Middle to Upper Ordovician coral and gastropod specimens of *Grewingkia* sp., *Septentrionites* sp., *Paleofavosites*, and *Maclurites* sp. (Fig. 14; identified by Robert Blodgett of Blodgett and Associates LLC) in the Bouvette Formation along the northern edge of Nadaleen Mountain (Fig. 2; fossil location 2). These strata are most likely correlative with Unit 1 described above. Fossils collected in 2018 are from the Bouvette Fromation in the area south of Nadaleen Mountain (Fig. 2; fossil locations 3, 4, 5) and include *in situ* specimens from the upper surface of Unit 2 (see Fig. 9c) and *in situ* specimens from within Unit 4 (see Fig. 11; identified by Robert J. Elias, University of Manitoba). The fossils identified from the top of Unit 2 (JB1825, JB1831, MS1803) include solitary rugose coral, *Streptelasmatine*; colonial rugose coral, *Palaeophyllum* sp., and halysitid tabulate corals, *Catenipora* sp. Fossils identified from within Unit 4 include a favositid tabulate coral, likely *Paleofavosites*. The corals identified above could range from Late Ordovician (Richmondian) to early Silurian (Llandovery).

Discussion

Our preliminary observations from the Bouvette Formation near Nadaleen Mountain are presented as an initial geological map of the study area, biostratigraphic age data from collected fossil material, and sedimentological/stratigraphic data from measured sections and UAV imagery. Throughout the area adjacent to, and south of Nadaleen Mountain, the Guzhangian–Furongian unnamed Cambrian limestone map unit disconformably overlies the Cambrian Series 2–5 Gull Lake Formation (Fig. 2), which represents a significant depositional hiatus that may correlate with the Sauk II–III unconformity (Taylor *et al.*, 2012) and similar hiatal surfaces exposed throughout northwestern Canada (*e.g.*, Gordey and Anderson, 1993; Pigage *et al.*, 2015; Moynihan *et al.*, *accepted*).

Preliminary geological mapping in the Nadaleen Mountain area also facilitates the recognition of a poorly understood conglomeratic unit that was previously mapped as either belonging to the *ca.* 499 Ma Old Cabin volcanic rocks or part of the basal Bouvette Formation (Colpron, 2012a; Moynihan, 2016). The basal portion of the conglomerate unit transitions from carbonate-clast rudstone exposed at the base of Nadaleen Mountain (see 2017 camp location; Fig. 2) into volcaniclastic conglomerate south of Nadaleen Mountain (see 2018 camp location; Fig. 2), potentially highlighting a complex stratigraphic relationship between the unnamed Cambrian limestone unit and the basal Bouvette Formation. Additionally, the upper surface of the unnamed conglomerate is marked by an irregular interval of brecciated limestone with

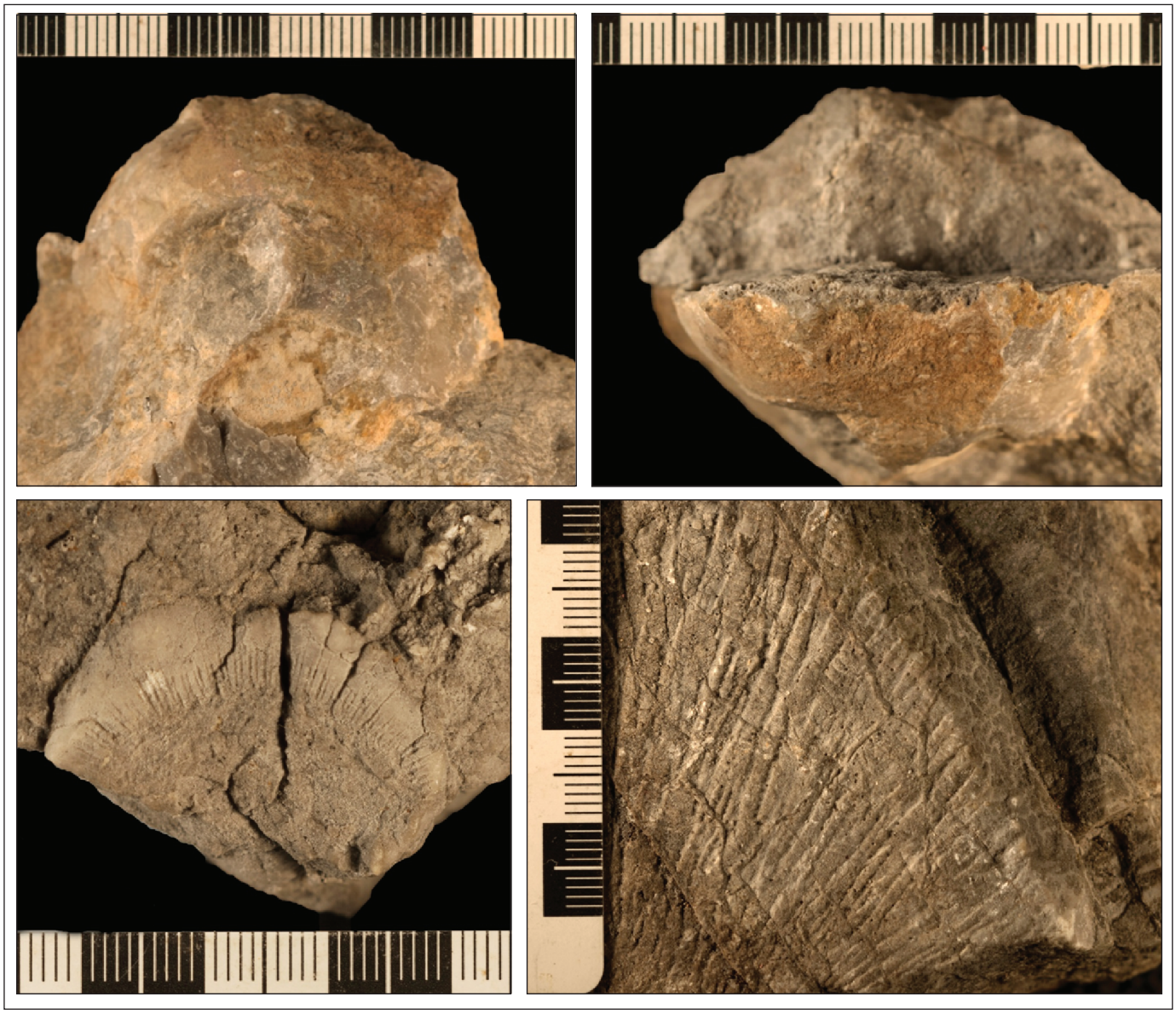

Figure 14. *Fossils collected at locality 2 (Fig. 2): Maclurites sp.* **(a)** *basal view* **(b)** *side view;* **(c)** *Grewingkia sp. solitary rugose coral; and* **(d)** *Septentrionites(?) sp. tabulate coral. Scale bar increments are in mm.*

significant erosional relief and pervasive evidence of subaerial exposure (Figs. 4 and 7). Above this surface, our preliminary biostratigraphic data suggest Middle to Upper Ordovician tabulate and rugose corals and gastropods appear (Fig. 14), implying this unit boundary may represent a significant hiatus during which the platform was exposed to subaerial conditions. This exposure event is potentially correlative with the Sauk–Tippecanoe sequence boundary of Laurentia (Taylor *et al.*, 2012), although future biostratigraphic work is needed to explore this further.

The preliminary measured stratigraphic sections and UAV imagery also reveal several important stratigraphic features, sedimentary facies and fossil assemblages within the Bouvette Formation that are unique to both platform reef margin and forereef depositional environments. Important depositional features in the Nadaleen Mountain area include two approximately 5 to 30 m thick stacked clinoformal wedges of fossiliferous packstone in Unit 1, which thicken to the northwest in the study area and are composed of crinoid, brachiopod and coral fossil debris (Figs. 7a and 8c).

A third massive approximately 15 to 100 m thick wedge in Unit 2 composed entirely of reef fossil debris and topped by domal tabulate and rugose coral reef buildups also thickens to the northwest in a clinoformal geometry (Figs. 7a and 9). The thinning of wedges of reef-derived material to the southeast in the study area, in clinoform-like geometries, strongly suggests a general deepening to the southeast towards the Selwyn basin and away from the Ogilvie platform interior.

Clinoformal wedges of platform reef talus composed of fossiliferous debris are common in fore-reef environments (e.g., Enos and Moore, 1983). Furthermore, the interpreted clinoforms in units 1 and 2 require sufficient accommodation for the deposition of thick wedges of material with significant thickness changes along depositional dip. Collectively, these observations are more consistent with a forereef environment than a reef crest or deep-water basinal environment during the deposition of units 1 and 2. Additionally, the presence of possible allochthonous blocks within Unit 1 (Figs. 6 and 8b) are common in forereef and talus slope environments (Enos and Moore, 1983). The dome-shaped upper surface of Unit 2, containing *in situ* corals, is suggestive of a shallowing-upwards transition between Unit 1 and the top of Unit 2, from the wedge of peri-platform talus onto the lower reef crest. Further stratigraphic analysis is required to validate these initial interpretations of the Bouvette Formation depositional setting.

Another interesting observation within the Bouvette Formation at Nadaleen Mountain is the dramatic shift from coral-dominated fossiliferous packstone of Unit 4 to brachiopod-dominated fossiliferous packstone of Unit 5 (Fig. 12). This shift in the dominant fossil material between units having identical sedimentary facies happens rapidly, with the first appearance of brachiopod fossils being accompanied by complete dominance of this fossil type within several metres of strata. This shift in dominant fossil type within the same sedimentary facies may suggest an important palaeoceanographic or ecological shift at the boundary of units 4 and 5. The significance of this finding will be assessed through future field observations, collection of additional fossil specimens, and chemostratigraphic analyses.

In summary, this study describes, for the first time, the platform edge of the Bouvette Formation as it transitions into the Selwyn basin. The Bouvette Formation in the Nadaleen Mountain area is composed predominately of reef–forereef carbonate facies, making it perhaps the best place to describe the Bouvette Formation due to the excellent preservation of sedimentary facies, fossil material, and depositional features. The Bouvette Formation at Nadaleen Mountain shares similarities to the Royal Mountain area to the northeast (NTS 106E), where the Royal Mountain platform transitions into the Richardson trough, highlighting another area that could elucidate the depositional history of the Yukon block and different tectonic or oceanographic events that affected northwest Laurentia. Finally, there are few examples of well-exposed early Paleozoic reef–forereef successions elsewhere in the world. This study of the margin of the Ogilvie platform will be an excellent contribution to the understanding of early Paleozoic paleontology, sequence stratigraphy, paleogeography, and paleoenvironmental change**.** The extraordinary exposure afforded at Nadaleen Mountain will allow for a complete 3-D reconstruction of the depositional system at the margin of a large, shallow-water carbonate platform and will afford a view into this important, but rarely preserved sedimentary environment.

Future Work

Future work on the Bouvette Formation in the Nadaleen Mountain area will include detailed geological mapping of the study area, additional measured sections of the strata that overlie Unit 6, collection of additional fossil material in the previously measured units 1 through 5, and further collection of UAV imagery. Importantly, the six units described from the Bouvette Formation south of Nadaleen Mountain will be traced to the north into the more massive platformal facies which occur adjacent to Nadaleen Mountain in order to better understand the transitional relationship between reef platform and reef margin facies. Carbonate samples collected for carbon isotope chemostratigraphy and conodont biostratigraphy will also be analyzed to develop a more rigorous chronology to support regional correlations of the Bouvette and underlying stratigraphy. These data will then be combined with three-dimensional elevation

models generated from the UAV imagery to create a complete depositional model of the Bouvette Formation in the Nadaleen Mountain area.

Acknowledgements

We acknowledge the Yukon Geological Survey (YGS) for their generous support of this project. This research was also partially funded by an American Association of Petroleum Geologists (AAPG) Richard W. Beardsley Grant awarded to JFB and a National Science Foundation Grant awarded to JVS (EAR-1624131). Erik Sperling and Tom Boag helped with fieldwork in 2017, and ATAC Resources provided logistical assistance and access to helicopter support with Horizon Helicopters during 2017 and 2018. We would like to thank Julia Lane at ATAC, Karl Marlowe at Barrick, and David Moynihan at the YGS for helpful discussions about the field area. David Moynihan at the YGS provided constructive feedback on a preliminary draft of this manuscript.

References

Abbott, G., 1997. Geology of the upper Hart River area, eastern Ogilvie Mountains, Yukon Territory (116A/10, 116A/11). Whitehorse, Indian and Northern Affairs Canada, Exploration and Geological Services Division, Yukon Region, Bulletin 9, 92 p.

Blusson, S.L., 1974. Five geological maps of northern Selwyn Basin (Operation Stewart), Yukon Territory and District of Mackenzie (105N, O; 106A, B, C). Geological Survey of Canada, Open File 205, scale 1:250 000.

Blusson, S.L., 1968. Geology and Tungsten Deposits near the Headwaters of Flat River, Yukon Territory and southwestern District of Mackenzie, Canada. doi: 10.4095/102251.

Brabb, E.E., 1967. Stratigraphy of the Cambrian and Ordovician rocks of east-central Alaska. United States Geological Survey, Professional Paper 559-A, 30 p.

Cecile, M.P., 1982. The lower Paleozoic Misty Creek Embayment, Selwyn Basin, Yukon and Northwest Territories. Geological Survey of Canada, Bulletin 335, 78 p.

Cecile, M P., 2000. Geology of the northeastern Niddery Lake map area, east-central Yukon and adjacent Northwest Territories. Geological Survey of Canada, Bulletin 553, 120 p.

Cecile, M.P., Morrow, D.W. and Williams, G.K., 1997. Early Paleozoic (Cambrian to Early Devonian) tectonic framework, Canadian Cordillera. Bulletin of Canadian Petroleum Geology, vol. 45, p. 54–74.

Cohen, K.M., Finney, S.C., Gibbard, P.L. and Fan, J.X., 2013; updated. The ICS International Chronostratigraphic Chart. Episodes, vol. 36, p. 199–204.

Colpron, M., 2012a. Preliminary geological map of the Mount Ferrell area (106C/3), central Yukon. Yukon Geological Survey, Open File 2012-11, 1:50 000 scale.

Colpron, M., 2012b. Preliminary observations on the geology of the Rackla belt, Mount Ferrell map area (NTS 106C/3), central Yukon. *In*: Yukon Exploration and Geology 2011, K.E. MacFarlane and P.J. Sack (eds.), Yukon Geological Survey, p. 27–43.

Colpron, M., Moynihan, D., Israel, S. and Abbott, G., 2013. Geological map of the Rackla belt, east-central Yukon (NTS 106C/1-4, 106D/1). Yukon Geological Survey, Open File 2013-13, 1:50 000 scale, 5 maps and legend.

Enos, P. and Moore, C.H., 1983. Fore-reef Slope Environment. *In*: Carbonate Depositional Environments, P.A. Scholle, D.G. Bebout and C.H. Moore (eds.), AAPG Memoir Vol. 33, Chapter 10, p. 507–533.

Fritz, W.H., 1997. Cambrian (Chapter 5); *In*: The Geology, Mineral, and Hydrocarbon potential in Northern Yukon Territory and Northwestern District of Mackenzie, D.K. Norris (ed.), Geological Survey of Canada, Bulletin 422, p. 85–117.

Fritz, W.H., 1982. Report on Two Collections Of Cambrian Fossils From The Ogilvie Mountains, Yukon. Collected by R.I. Thompson, 1982 (NTS: 116C), Geological Survey of Canada, Paleontological Report C-4-WHF-1982, 1 p.

Gordey, S.P. and Anderson, R.G., 1993. Evolution of the Northern Cordilleran Miogeocline, Nahanni Map Area (105I), Yukon and Northwest Territories. Geological Survey of Canada, Memoir 428, 214 p.

Green, L.H., 1972. Geology of Nash Creek, Larsen Creek, and Dawson Map-Areas, Yukon Territory. Geological Survey of Canada, Memoir 364, 157 p.

Herbosch, A. and Verniers, J., 2011. What is the biostratigraphic value of the ichnofossil *Oldhamia* for the Cambrian: a review. Geologica Belgica, vol. 14, p. 229–248.

Hofmann, H. J., Cecile, M. P. and Lane, L. S. 1994. New occurrences of *Oldhamia* and other trace fossils in the Cambrian of the Yukon and Ellesmere Island, Arctic Canada. Canadian Journal of Earth Sciences, vol. 31, p. 767–782.

Hong, P.S., Choi, D.K. and Lee, J.G., 2003. Late Cambrian trilobite *Irvingella* from the Machari Formation, Korea: evolution and correlation. Special Papers in Palaeontology, vol. 70, p. 175–196.

Lenz, A.C., 1972. Ordovician to Devonian history of northern Yukon and adjacent District of Mackenzie. Bulletin of Canadian Petroleum Geology, vol. 20, p. 321–361.

Ludvigsen, R., Westrop, S.R. and Kindle, C.H., 1989. Sunwaptan (Upper Cambrian) trilobites of the Cow Head Group, western Newfoundland, Canada. Palaeontographica Canadiana, vol. 6, 175 p.

MacNaughton, R.B., Moynihan, D.P., Roots, C.F. and Crowley, J.L., 2016. New occurrences of *Oldhamia* in eastern Yukon, Canada: Stratigraphic context and implications for Cambrian deep-marine biostratigraphy. Ichnos, vol. 23, p. 33–52.

Morrow, D.W., 1999. Lower Paleozoic stratigraphy of northern Yukon Territory and northwestern District of Mackenzie. Geological Survey of Canada, Bulletin 538, 202 p.

Moynihan, D., 2014. Bedrock Geology of NTS 106B/04, Eastern Rackla Belt. In: Yukon Exploration and Geology 2013, K.E. MacFarlane, M.G. Nordling and P.J. Sack (eds.), Yukon Geological Survey, p. 147–167.

Moynihan, D., 2016. Bedrock geology compilation of the eastern Rackla belt, NTS 105N/15, 105N/16, 105O/13, 106B/4, 106C/1, 106C/2, east-central Yukon. Yukon Geological Survey, Open File 2016-2, scale 1:75 000, 2 sheets.

Moynihan D., Strauss, J.V., Padget, C.D., Nelson, L.L., *accepted* 2018. Upper part of the Windermere Supergroup in the Nadaleen River area, east-central Yukon: stratigraphy, regional correlations and implications for development of the western Laurentian continental margin. The Geological Society of America Bulletin.

Mustard, P.S., Donaldson, J.A. and Thompson, R.I., 1988. Trace fossils and stratigraphy of the Precambrian-Cambrian boundary sequence upper Harper group, Ogilvie Mountains, Yukon. *In*: Current Research, Part E, Geological Survey of Canada, Paper 88-1E, p. 197–203.

Norris, A.W., 1985. Stratigraphy of Devonian outcrop belts in northern Yukon Territory and northwestern District of Mackenzie (Operation Porcupine area). Geological Survey of Canada, Memoir 410, 81 p.

Norris, D.K., 1982. Geology: Ogilvie River, Yukon Territory. Geological Survey of Canada, Map 1526A, scale 1:250 000.

Pigage, L.C., 2004. Bedrock geology compilation of the Anvil District (parts of NTS 105K/2, 3,5, 7, and 11), Central Yukon. Yukon Geological Survey, Bulletin 15, 103 p.

Pigage, L.C., Abbott, J.G. and Roots, C.F., 2011. Bedrock geology of Coal River map area (NTS 95D), Yukon (1:250 000 scale). Yukon Geological Survey, Open File 2011-1.

Pigage, L.C., Roots, C.F. and Abbott, J.G., 2015. Regional bedrock geology for the Coal River map area (NTS 95D), southeast Yukon. Yukon Geological Survey, Bulletin 17, 155 p.

Pyle, L.J., 2012. Cambrian and Lower Ordovician Sauk megasequence of northwestern Canada, northern Rocky Mountains to the Beaufort Sea. *In*: The great American carbonate bank: The geology and economic resources of the Cambrian – Ordovician Sauk megasequence of Laurentia, J.R. Derby, R.D. Fritz, S.A. Longacre, W.A. Morgan and C.A. Sternbach (eds.), American Association of Petroleum Geologists, AAPG Memoir 98, p. 675–723.

Rasetti, F., 1944. Upper Cambrian trilobites from the Levis Conglomerate. Journal of Paleontology, vol. 18, p. 229–258.

Rasetti, F., 1948. Lower Cambrian trilobites from the conglomerates of Quebec. Journal of Paleontology, vol. 22, p. 1–24.

Taylor, J.F., Allen, T.J., Repetski, J.E., Strauss, J.V. and Irwin, S.J., 2015. Life on the edge in eastern Alaska: Basal Ordovician (Tremadocian), platform-margin faunas of the Jones Ridge Formation. Stratigraphy, vol. 12, p. 71–77.

Taylor, J.F., Repetski, J.E., Loch, J.D. and Leslie, S.A., 2012. Biostratigraphy and chronostratigraphy of the Cambrian – Ordovician great American carbonate bank. *In*: The great American carbonate bank: The geology and economic resources of the Cambrian – Ordovician Sauk megasequence of Laurentia, J.R. Derby, R.D. Fritz, S.A. Longacre, W.A. Morgan and C.A. Sternbach (eds.), American Association of Petroleum Geologists, AAPG Memoir 98, p. 15–35.

Westrop, S.R. and Adrain, J.M., 2016. Revision of *Irvingella tropica* Opik 1963 from Australia and related species from North America: implications for correlation of the base of the Jianghsanian Stage (Cambrian, Furongian). Australasian Palaeontological Memoirs, vol. 49, p. 395–432.

Yukon Geochronology, 2018. Yukon Geochronology – A database of Yukon geochronology sample locations, M. Colpron (compiler). Yukon Geological Survey, http://data.geology.gov.yk.ca/Compilation/22, [accessed November 13, 2018].

Preliminary observations on the geology of northeastern Glenlyon area, central Yukon (parts of NTS 105L/10, 14, 15)

R. Cobbett
Yukon Geological Survey

Cobbett, R., 2019. Preliminary observations on the geology of northeastern Glenlyon area, central Yukon (parts of NTS 105L/10, 14, 15). *In:* Yukon Exploration and Geology 2018, K.E. MacFarlane (ed.), Yukon Geological Survey, p. 43–60.

Abstract

Regional bedrock mapping has revised structural and stratigraphic relationships in the northeastern corner of the Glenlyon map area (NTS 105L). Three structural panels, separated by south and southwest dipping thrust faults, subdivide the area. Cambrian (?) to Ordovician metasedimentary and volcanic rocks underlie the southwestern panel and include all exposures southwest of the Duo fault. Ordovician to Silurian (?) siliciclastic and carbonate strata and phyllite units that are intruded by Late Devonian porphyritic rocks underlie the central panel. Silurian (?) to Triassic siliciclastic and carbonate strata in the northern panel occur to the north, and in the footwall of, the Twopete fault. Mid-Cretaceous granitic rocks that crop out near Kalzas Mountain and occur below the surface near Dromedary Mountain intrude the central and northern panels. Northeast-verging folds and thrust faults deform layered rocks in the northeastern Glenlyon area and are offset by north-south oriented, steeply dipping structures with both normal and strike-slip motion.

Upper Devonian Earn Group strata host layered sulphide bodies and polymetallic veins that contain lead, zinc and silver. This mineralization occurs in the footwall of the Twopete fault, a regional structure that originally developed as a Late Devonian synsedimentary fault.

Ordovician and Silurian (?) quartz-rich clastic rocks are unlike coeval basinal facies rocks mapped elsewhere within the Selwyn basin in Yukon. These rocks represent slope facies deposits that mark a transition from basin to platform that is the northern extension of the McEvoy platform–Selwyn basin boundary.

* rosie.cobbett@gov.yk.ca

Introduction

In 2013 the Yukon Geological Survey initiated a multi-year, regional bedrock mapping project in the western Tay River (NTS 105K) and northeastern Glenlyon (NTS 105L) map areas to better understand the geologic history and mineral potential of the region. This paper describes the structure and stratigraphy of the northeastern Glenlyon area and augments preliminary reports from Anvil Lake and Tay Mountain areas.

Geologic Framework

The area of interest lies within the Selwyn basin of central Yukon, north of, and adjacent to, the Tintina fault (Fig. 1). The Selwyn basin refers to a broad region underlain by predominantly deep-water sedimentary rocks that were deposited along the northwestern edge of Laurentia from the Neoproterozoic to Early Devonian (Gordey and Anderson, 1993; Gabrielse, 1967). The basin is bounded by the Mackenzie platform to the northeast and the Cassiar/McEvoy platform to the southwest (Gordey, 2013; Gabrielse, 1967). During the Late Devonian, widespread extension along the Cordilleran margin resulted in the deposition of quartz-rich siliciclastic rocks on top of Selwyn basin strata. Sediment was mostly derived from northern Yukon, but also locally from uplifted basinal strata that were eroded during local block faulting (Gordey et *al.*, 1987; Gordey, 2013). Following this period of extension, the northwestern margin of Laurentia returned to a continental shelf setting where accumulations of marine shelf sediments continued until Late Triassic (Gordey, 2013).

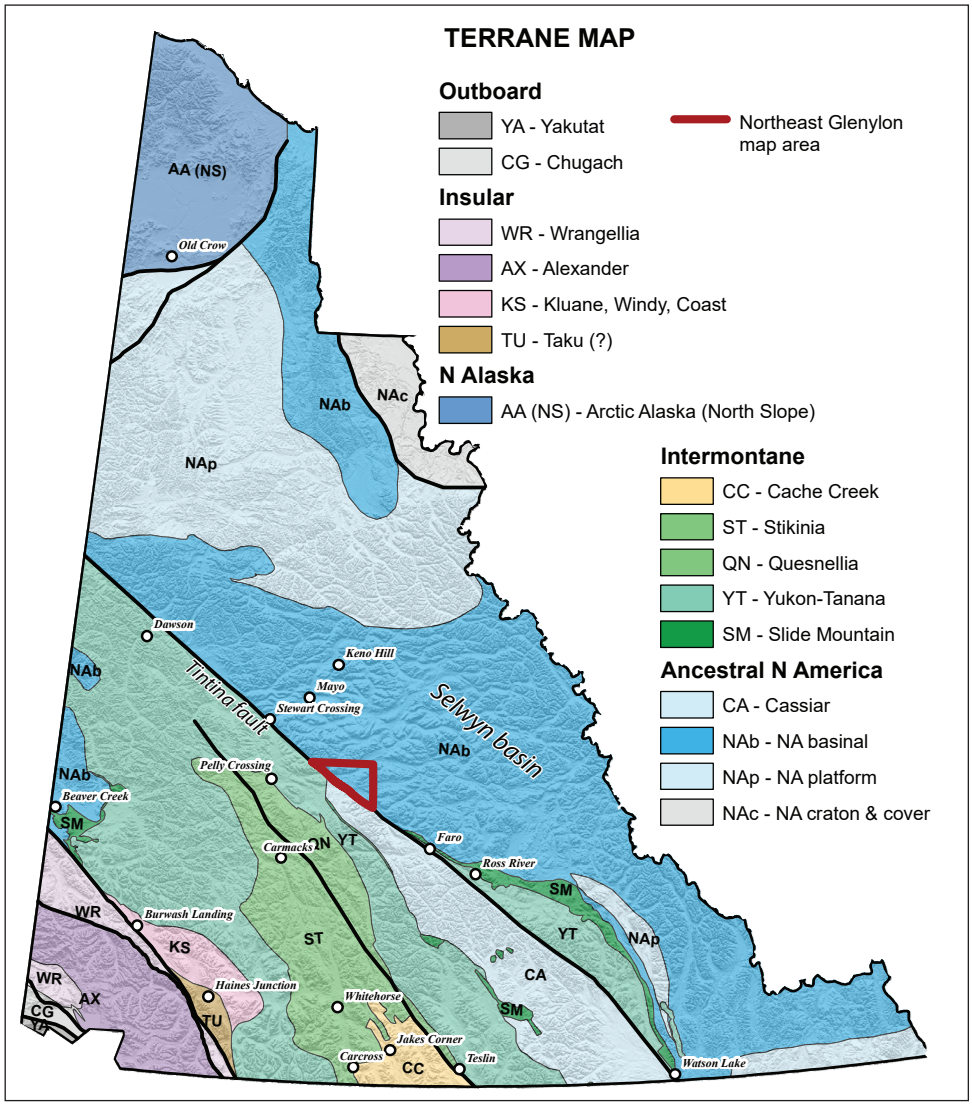

Figure 1. *Geologic terranes of Yukon from (Colpron and Nelson, 2011) showing the outline of the study area (thick red line).*

Northeast-verging folds and thrust faults that comprise the Selwyn fold and thrust belt underlie the map area (referred to as NE Glenlyon area in the rest of the paper). These structures are a result of Middle Jurassic shortening along the northern Cordilleran margin (Colpron *et al.*, 2006; Mair *et al.*, 2006). Mid-Cretaceous post-arc magmatism is widespread throughout the Selwyn basin region (Colpron, 2016b; Rasmussen, 2013). Felsic to intermediate intrusions are generally undeformed and crosscut folds and thrust faults. The Tintina fault, a post-mid-Cretaceous dextral strike-slip fault with 430 km of displacement, cuts off the geology within the NE Glenlyon area to the northwest (Roddick, 1967; Gabrielse *et al.*, 2006).

Stratigraphy

Three structural panels, separated by south and southwest-dipping thrust faults, subdivide the stratigraphy. The Twopete fault is the most prominent structural feature in the area and separates the northern panel of Silurian to Triassic sedimentary rocks from a small, central panel of Ordovician siliciclastic rocks and dark phyllite (Figs. 2 and 3). The Duo fault is subparallel to the Twopete fault and separates these Ordovician siliciclastic rocks from the southern panel of lower Cambrian (?) to Ordovician schist, phyllite and volcanic rocks. Described separately below is the geology of each panel.

Southern Panel – South of Duo fault

Variably exposed volcanic and volcaniclastic rocks and metasedimentary strata that occupy nearly half of the geographic area in NE Glenlyon underlie relatively low-lying terrain north of the Pelly River.

Vangorda formation: calc-silicate schist and amphibolite schist

Schistose calcareous rocks and amphibolite schist of the Vangorda formation crop out in several locations north of the Pelly River and along a moderately exposed ridge south of The Detour river (Fig. 2; Pigage, 2004). Brown weathering, grey-brown, finely foliated calcite-mica schist and light grey marble occur north of the Pelly River. Between the Pelly River and Detour Lakes, dark green and purple, foliated amphibolite schist units are interleaved with the calcite mica schist and calc-silicate schist (Fig. 4a). The map area does not have an exposure of the lower contact, and the upper contact with the Menzie Creek Formation is gradational and drawn at the first occurrence of volcanic rocks. An estimate of minimum thickness is not reported primarily due to limited exposure.

This unit is assigned to the Vangorda formation based on lithological correlations in the Anvil district and its close association with the Menzie Creek Formation (Jennings, 1986; Pigage, 2004). Regionally, the Vangorda formation is interpreted to be a metamorphic equivalent to the Rabbitkettle Formation (Jennings, 1986; Gordey and Anderson, 1993; Pigage, 2004).

Menzie Creek Formation – volcanic facies

Two moderately elevated areas in a broad expanse of subdued topography south of the Duo fault comprise volcanic, tuffaceous and volcaniclastic rocks of the Menzie Creek Formation (Gordey, 2013). Between Horsfall Creek and Duo Creek, dark orange weathering, green, coarse-grained basalt forms crude benches in heavily treed areas. Interbedded with the basalt in this area are volcaniclastic breccia, sandstone and siltstone units. One outcrop from this same region contains clasts of basalt, feldspar crystals and shards of quartz and is likely a crystal-lithic tuff. U-Pb geochronological analysis of a sample of the tuff is being processed in order to determine a crystallization age for this unit. Near Earn River, pyroxene-bearing basalt is interleaved with orange weathering, light green chlorite schist. The NE Glenlyon area does not have exposures of the lower contact of these volcanic piles with the Vangorda formation, but it is inferred to be conformable and gradational based on mapping by Pigage (2004) in the Anvil district.

Menzie Creek Formation – volcanic and sedimentary facies

A large area south of the Duo fault contains amygdaloidal basalt flows, volcaniclastic sandstone and siltstone units that are interbedded with calcareous metasedimentary rocks and grade laterally into volcanic facies of the Menzie Creek Formation. Thick flows to massive bodies of dark orange weathering, green, medium to coarse-grained, pyroxene-bearing basalt

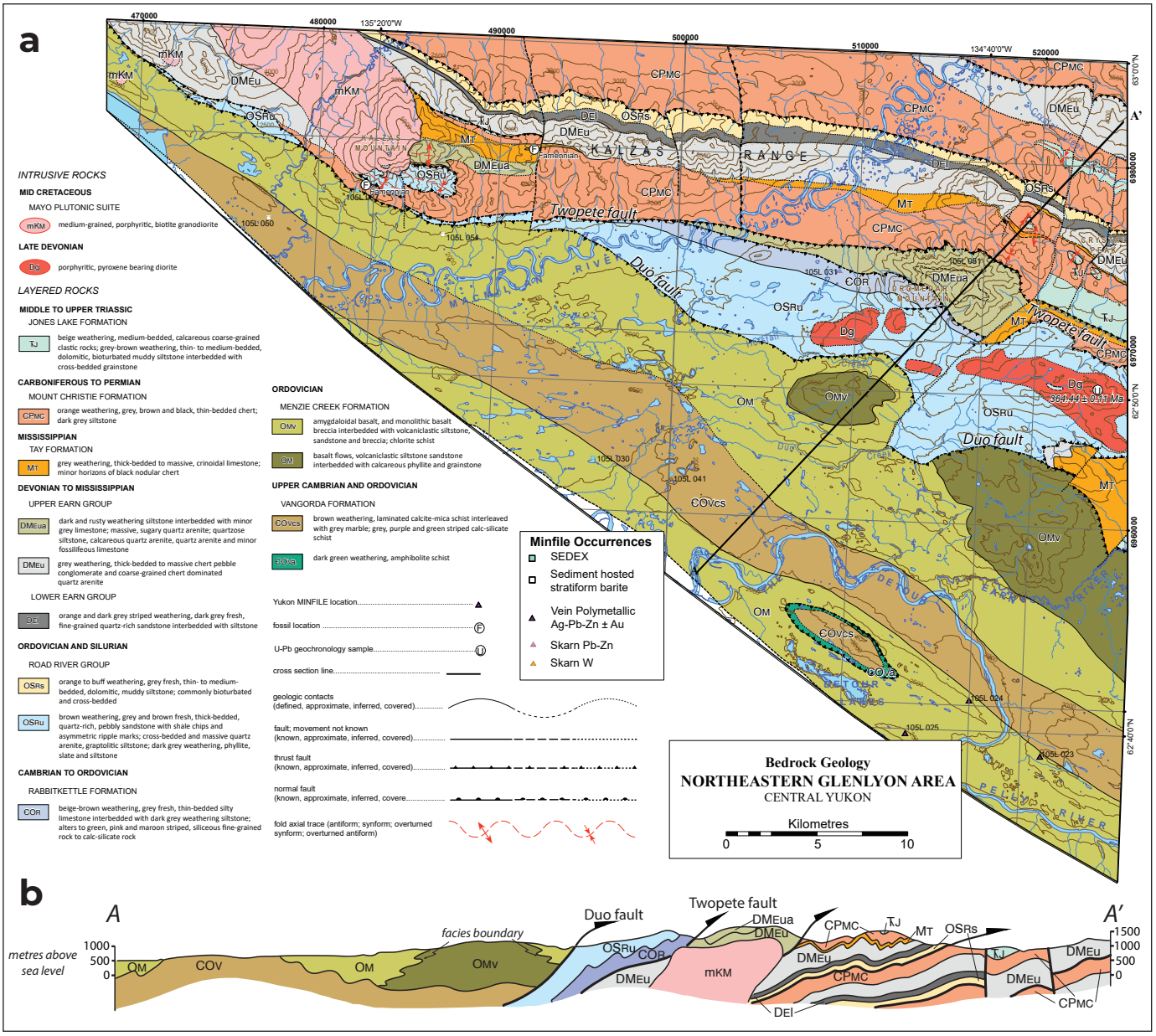

Figure 2. (a) *Bedrock geology of NE Glenlyon area.* ***(b)*** *Cross section A-A'.*

form cliffs throughout this topographically subdued area (Fig. 4b). Flow tops are altered and commonly amygdaloidal, and are typically in contact with laminated fine-grained sedimentary and metasedimentary rocks (Fig. 4c). The sedimentary and metasedimentary rocks include light grey and orange weathering, grey, calcareous phyllite to light grey-brown, thin-bedded, cross-bedded grainstone units that are interleaved with grey-green phyllite. Where primary textures are preserved in the meta-sedimentary rocks the protolith is thin-bedded mudstone to siltstone forming graded beds (Fig. 4d). Calcareous phyllite rarely preserves macrofossils (Fig. 4e). There are no outcrop exposures of the lower contact, but it is inferred to be gradational with the Vangorda formation. Poor exposure and the deformed nature of this succession hinders a thickness estimate for this unit. These rocks are assigned to the Menzie Creek Formation based on lithologic similarities with the type section to the southeast (Gordey, 2013). The depositional environment for this succession is interpreted to be the edge of a platform based primarily on the occurrence of cross-bedded grainstone and graded beds.

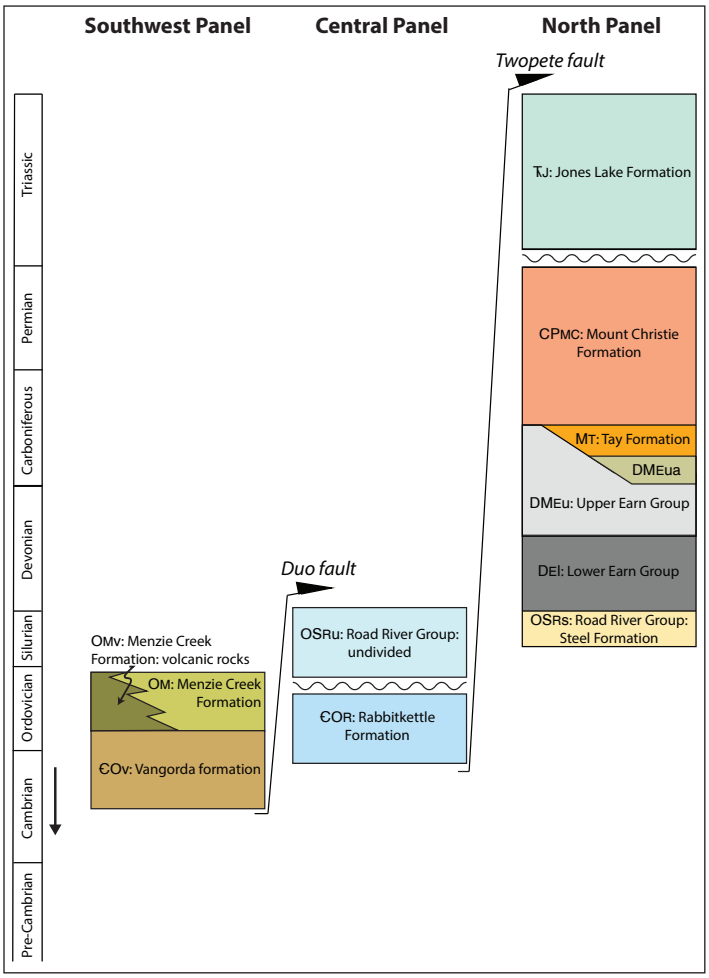

Figure 3. *Stratigraphy of the NE Glenlyon area.*

Central Panel – Between Twopete fault and Duo fault

This fault-bounded panel comprises siliciclastic and carbonate rocks and dark weathering phyllite units that crop out in the central part of the map area. This panel is laterally cut-out where the Duo fault merges with the Twopete fault, both in the northwestern apex of the map area and along its eastern border (Fig. 2).

Rabbitkettle Formation

Variably altered rock units of the Rabbitkettle Formation are well-exposed in the Dromedary Mountain area (Gabrielse *et al.*, 1973). On the southwestern flank of Dromedary Mountain, the Rabbitkettle Formation comprises beige-brown weathering, grey, thin-bedded, silty limestone interbedded with dark grey weathering, maroon-grey siltstone (Fig. 5a). Altered exposures near the top, and along the eastern and southeastern flanks of Dromedary Mountain comprise light pink, green and maroon siliceous siltstone with local limey layers that create a distinctive striped weathering surface. At several localities on Dromedary Mountain light grey weathering, dark grey limestone beds up to 20 cm thick are interbedded with siltstone. The limestone alters to white chalky marble at the peak of Dromedary Mountain.

The contact between the upper Rabbitkettle Formation and younger Earn Group is a fault characterized by rusty weathered scree and several outcrops of ferricrete in the saddle directly north of the Dromedary Mountain peak. The contact between the lower Rabbitkettle Formation and younger Road River Group is exposed on the south side of Dromedary Mountain where it is characterized by black, carbonaceous, highly contorted fault rock. Elsewhere in the map area, between the peak of Dromedary Mountain and Dromedary Creek and between Dromedary Mountain and Macmillan River, the contact is likely unconformable based on previous mapping of the Rabbitkettle/Road River Group contact in Nahanni, Flat River and Glacier Lake areas (Gabrielse *et al.*, 1973; Gordey and Anderson, 1993). A thickness for this succession is not reported because the only exposed contacts are faults.

This unit is assigned to the Rabbitkettle Formation based on lithologic similarities to other parts of the Selwyn basin (Gordey and Anderson, 1993; Gordey, 2013; Gabrielse *et al.*, 1973). The assignment of these rocks to the Rabbitkettle Formation and the interpretation of an unconformable upper contact are subject to change if paleontological reports provide age constraints for this strata.

Road River Group: undivided

Exposed on the south side of Dromedary Mountain, and near Kalzas Mountain, blocky outcrops of quartz-rich clastic rocks containing Ordovician graptolites are interlayered with dark weathering phyllite and siltstone (Gabrielse *et al.*, 1973). Grey to brown, thick-bedded, coarse-grained sandstone with pebble lags and shale chips up to 15 cm-long grade upwards into laminated to massive quartz arenite and graptolitic siltstone on the south side of Dromedary Mountain (Fig. 5b). Exhibited locally in this area are cross-beds and asymmetric

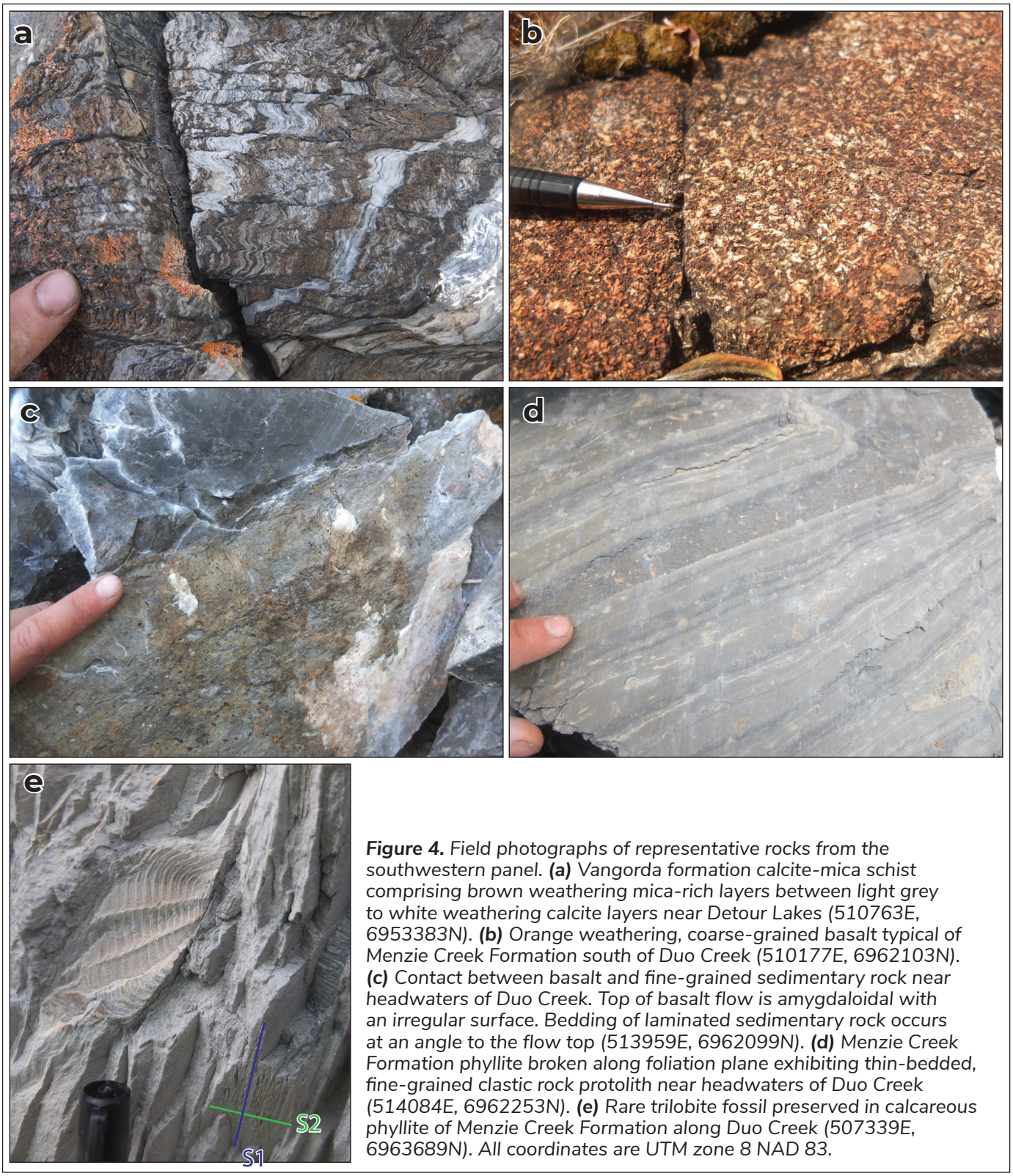

Figure 4. *Field photographs of representative rocks from the southwestern panel.* ***(a)*** *Vangorda formation calcite-mica schist comprising brown weathering mica-rich layers between light grey to white weathering calcite layers near Detour Lakes (510763E, 6953383N).* ***(b)*** *Orange weathering, coarse-grained basalt typical of Menzie Creek Formation south of Duo Creek (510177E, 6962103N).* ***(c)*** *Contact between basalt and fine-grained sedimentary rock near headwaters of Duo Creek. Top of basalt flow is amygdaloidal with an irregular surface. Bedding of laminated sedimentary rock occurs at an angle to the flow top (513959E, 6962099N).* ***(d)*** *Menzie Creek Formation phyllite broken along foliation plane exhibiting thin-bedded, fine-grained clastic rock protolith near headwaters of Duo Creek (514084E, 6962253N).* ***(e)*** *Rare trilobite fossil preserved in calcareous phyllite of Menzie Creek Formation along Duo Creek (507339E, 6963689N). All coordinates are UTM zone 8 NAD 83.*

ripples in the sandstone and fine laminations of sulphide at the base of siltstone beds. Near the headwaters of Duo Creek, orange and grey weathering, grey, rhythmically bedded mudstone to fine-grained sandstone, siltstone with black chert nodules and dark grey siltstone and slate are grouped with this unit. Near Kalzas Mountain, this unit is dominated by dark weathering phyllite and siltstone that commonly exhibit andalusite porphyroblasts. The phyllite is in stratigraphic contact with a variety of interbedded rock types including graptolitic siltstone, quartz-rich sandstone, silty limestone, chert pebble conglomerate and white-weathering marble. The lower contact with the Rabbitkettle Formation is probably unconformable as described above and the upper contact is nowhere exposed. A thickness for this unit is not reported due to the limited exposure, fault-bounded contacts and complicated folding. The occurrence of chert pebble conglomerate within this succession can be confusing due its similarity with analogous Earn Group units. In the absence of exposures of interbedded graptolitic siltstone, this part of the unit could easily be mistaken for the younger group.

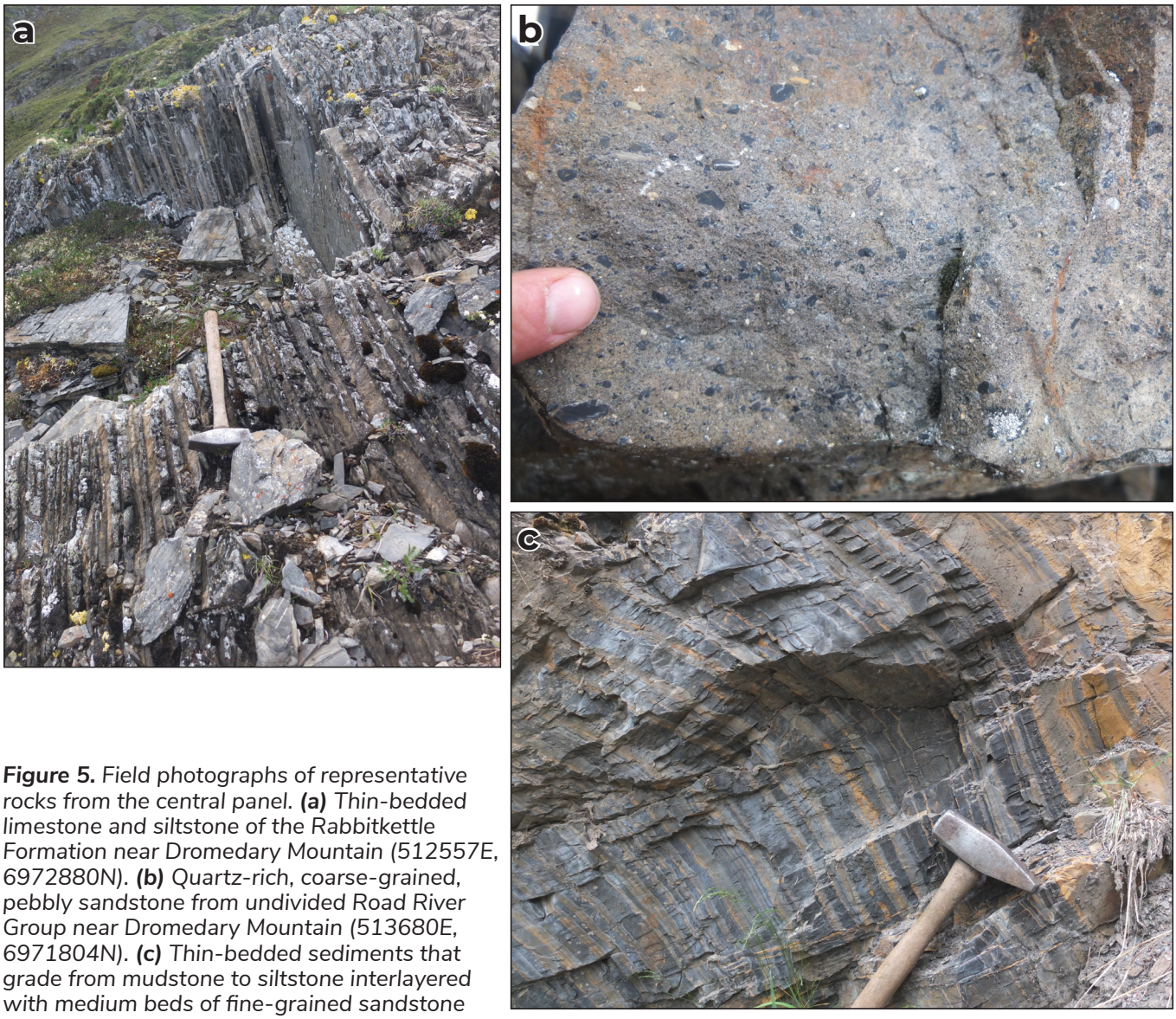

Figure 5. *Field photographs of representative rocks from the central panel.* ***(a)*** *Thin-bedded limestone and siltstone of the Rabbitkettle Formation near Dromedary Mountain (512557E, 6972880N).* ***(b)*** *Quartz-rich, coarse-grained, pebbly sandstone from undivided Road River Group near Dromedary Mountain (513680E, 6971804N).* ***(c)*** *Thin-bedded sediments that grade from mudstone to siltstone interlayered with medium beds of fine-grained sandstone (orange weathering layer in top right corner of photograph). This outcrop is assigned to undivided Road River Group and crops out near the headwaters of Duo Creek (514177E 6964059N). All coordinates are UTM zone 8 NAD 83.*

These rocks are collectively assigned to the Road River Group based primarily on the presence of Ordovician graptolites throughout the succession (Gabrielse et *al.*, 1973). The depositional environment for this unit is interpreted to be above wave-base along a shallow shelf (Gordey and Anderson, 1993).

Northern Panel: Stratigraphy North of the Twopete Fault

Mid to upper Paleozoic siliciclastic rocks, carbonate rocks and chert form a roughly east-west trending belt of strata that crop out north of the Twopete fault (Fig. 2).

Road River Group: Steel Formation

Distinctive orange-brown weathering, grey, thin to medium-bedded, dolomitic siltstone units of the Steel Formation occur as small outcrops within vegetated areas along the northern slopes of the Kalzas Range and Crystal Peak (Fig. 6a; Gordey and Anderson, 1993). The lower contact is nowhere exposed and the upper contact with the lower Earn Group is conformable (Fig. 3). The minimum thickness of the succession is 100 m based on continuous exposure visible on the north slope of Crystal Peak. The lower contact is interpreted to be a thrust fault that places this unit over the Mount Christie Formation. This fault is not well constrained due to lack of outcrop in the area and based on where it has been drawn suggests unit thickness could be up to 200 m (Fig. 2, cross section A-A'). Locally, the siltstone has asymmetric ripples and cross-beds, internal layering characterized by wispy, discontinuous laminations and contains evidence of bioturbation in the form of curvilinear trace fossils approximately 1 cm in width.

This unit is assigned to the Steel Formation based on lithologic similarities elsewhere in the Selwyn basin and its stratigraphic position below the lower Earn Group (Gordey and Anderson, 1993; Gordey, 2013). The depositional age is uncertain, but must be older than Upper Devonian based on fossils in the Earn Group to the southeast (Blodgett, 2015, 2016; Orchard, 2016). A sub-wave base, quiet water environment typical of a continental slope is likely the setting during deposition of the Steel Formation.

Earn Group: lower

Orange and dark-grey weathering, recessive, fine-grained siliciclastic rocks of the lower Earn Group are exposed on the northern slopes of Crystal Peak and Kalzas Range. This unit is well-bedded and forms thin stripes of alternating orange and dark grey weathering beds that correspond to fine-grained, quartz-rich sandstone interbedded with siltstone (Fig. 6b). The percentage of quartz-rich beds and the thickness of these beds both increase up-section. The thickness of this unit is well constrained at 300 m based on a measured section on the northern slope of Crystal Peak. The lower contact with the Steel Formation is conformable and abrupt and the upper contact with the upper Earn Group is gradational and drawn where siltstone is absent (Fig. 3). Near the upper Earn/lower Earn contact, one horizon of quartz arenite has spheres of pyrite up to 2 cm in diameter at the top of the bed.

This succession is assigned to the informal lower Earn Group mainly based on its stratigraphic position between the Steel Formation and the upper Earn Group. In other parts of the Selwyn basin, the Earn Group is divided into the Portrait Lake and Prevost formations, however, the strata mapped in the NE Glenlyon area are not easily correlated with these two units. The age of the lower Earn Group is pre-Upper Devonian based on macro-fossils found in the upper Earn Group (Orchard, 2016, 2017; Blodgett, 2015, 2016). Near Anvil Lake, southeast of the map area, both macro and microfossils indicate the lower Earn Group is Emsian to Givetian (Blodgett unpublished; Blodgett 2015). The depositional setting of the lower Earn Group is interpreted to be a deep-water basin where continent-sourced, quartz-rich detritus was periodically shed between periods of low sedimentation.

Earn Group: upper undivided

Resistant outcrops of upper Earn Group chert pebble conglomerate comprise the central and western parts of the Kalzas Range, prominent peaks north and northeast of Dromedary Mountain and all of Crystal Peak. Light grey to dark grey, very thickly bedded, pebble conglomerate to coarse-grained sandstone describes the majority of this unit (Fig. 6c). Commonly found at the very top of some of the beds

of conglomerate is a cross-bedded, medium-grained quartz arenite unit. The lower contact with the lower Earn Group is gradational and well constrained on both the north slope of Kalzas Range and Crystal Peak. The upper contact with the Tay Formation is conformable and abrupt and well constrained in the eastern-half of the mapped area. Near Kalzas Mountain and on Dromedary Mountain, the upper contact with a unit called the Earn Group upper arenite (described below) is conformable. The thickness of this unit varies across the map area from 600 m on Crystal Peak to 900 m on Kalzas Range, two places where both the upper and lower contacts are well constrained. In areas with limited exposure, the thickness is inferred to be as thin as 250 m. The clasts within the conglomerate consist of multi-coloured chert, including light brown, light and dark grey, black and rare turquoise, and range in size from 0.5 to 5 cm. The conglomerate units are clast-supported with interstitial matrix of quartz and chert sand. Subrounded chert grains along with up to 15% quartz grains and less than 5% shale grains comprise sandstone of the Upper Earn Group.

This succession is assigned to the upper Earn Group based on fossils found southeast of the mapped area that indicate Frasnian to Famennian depositional ages (Blodgett, 2016). The source for the conglomerate is likely high standing fault blocks of Selwyn basin strata such as Neoproterozoic quartz sandstone of the Hyland Group and Road River Group chert (Gordey, 2013; Gordey and Anderson, 1993). Late Devonian to Mississippian chert pebble conglomerate is mapped in many places in the Selwyn basin and is interpreted to be the result of widespread extension throughout the Selwyn basin and bounding platforms (Gordey, 2013; Gordey et *al*., 1987; Gordey and Anderson, 1993).

Earn Group: upper arenite

Variably altered, fine-grained sedimentary rocks of the Earn Group upper arenite formation are found on Dromedary Mountain and near Kalzas Mountain, and include siltstone, calcareous sandstone, quartz arenite and minor limestone. Rusty-orange and dark grey, variably siliceous siltstone comprises most of the outcrops north of the Twopete fault on Dromedary Mountain (Fig. 2). Light grey weathering, white, fine to medium-grained, sugary textured quartz arenite lies stratigraphically above the siltstone. Grey silty limestone forms minor interbeds approximately 2 m thick within the dark siltstone.

Several exposures near Kalzas Mountain include quartzose siltstone, calcareous and non-calcareous quartz arenite and minor fossiliferous siltstone. Rusty to grey weathering, quartz-rich, massive to very thin bedded siltstone is interbedded with beige, sugary, fine and medium-grained quartz arenite. Dark blue-grey, medium to coarse-grained quartz-rich sandstone, comprising grains of chert and distinct rounded grains of vitreous quartz, crop out in a heavily treed area east of the McArthur batholith. Rare exposures of white weathering marble and calcareous quartz-arenite are interbedded with quartz-rich siltstone near the edge of the pluton. Lastly, light grey, recrystallized limestone is interbedded with grey-brown fossiliferous siltstone south of Kalzas Mountain.

The lower contact with the Earn Group chert pebble conglomerate is not exposed, but is assumed to be conformable. The upper contact in most places is conformable with the Tay Formation. This unit is approximately 1200 m thick on Dromedary Mountain. This estimate is a minimum thickness because the succession is bounded by thrust faults. Near Kalzas Mountain this unit is thinner, with an estimated thickness of 300 m. Disseminated pyrite and pyrrhotite are common in siltstone and occur as parallel stringers that make the rock look layered. Exposures on Dromedary Mountain have abundant quartz veins cutting the quartz sandstone and tremolite is a common alteration product in limestone. Here, much of the rock is altered by silica and associated hydrothermal minerals that have not been identified. Pelitic rocks on Kalzas Mountain commonly display porphyroblasts of andalusite.

This unit has been assigned to the Earn Group and been given an informal formation name ‘upper arenite’ (Campbell, 1967). This name was introduced during this multi-year study to describe this distinct package of rocks that crop out from Anvil Lake to Kalzas Mountain (Cobbett, 2016b). Two Late Devonian (Famennian) macrofossils confirm the age of this unit to Late Devonian (preliminary report by Blodgett). The age is further constrained by the overlying Tay Formation that has been dated as Tournaisian (Blodgett, 2016; Gordey, 2013).

Figure 6. *Field photographs of representative rocks from the north panel.* ***(a)*** *Orange and brown weathering, dolomitic siltstone of the Steel Formation on north side of Kalzas Range. Centre of the photograph shows ripple marks on a bedding surface (490616E, 6981968N).* ***(b)*** *Orange and dark grey weathering, thin and medium-bedded siltstone and sandstone from the lower Earn Group on the north slope of Kalzas Range (501427E, 6980985N).* ***(c)*** *Upper Earn Group chert pebble conglomerate from Crystal Peak (524872E, 6976014N).* *Continued on next page.*

Tay Formation

Light grey, resistant outcrops of fossiliferous limestone of the Tay Formation form small prominent peaks in areas of heavy vegetation throughout the area (Gordey, 2013). Grey, massive to thick-bedded, fossiliferous limestone with black chert horizons that forms semi-continuous lozenges describes most of the outcrops in the region (Fig. 6d). Near Kalzas Mountain, this succession is a dark grey silty limestone interbedded with a variably fossiliferous siltstone that alters to white weathering marble and slate within a contact aureole of the McArthur batholith. The lower contact with the Earn Group is conformable and abrupt. The upper contact is interpreted to be conformable, however there is one section of the map area where the Tay Formation limestone was not found. This missing stratigraphy is interpreted to represent a small area that did not see the build-up of carbonate and instead accumulated fine-grained siliciclastic rocks indistinguishable from those of the overlying Mount Christie Formation. The tightly folded nature of this unit hinders accurate thickness estimates in many places. Based on areas where the Tay Formation is well constrained and not

folded, such as Crystal Peak, the maximum thickness is approximately 100 m. Crinoid fossils are very common in the limestone.

Mount Christie Formation

Patchy exposures of orange weathering chert scree of the Mount Christie Formation occur along subdued, heavily vegetated ridges and within incised gullies on the southern slopes of Kalzas Range and northeast of Dromedary Mountain (Gordey and Anderson, 1993). Orange and grey weathering, black to grey and grey-brown, thin-bedded chert is interbedded with grey siltstone and silty chert (Fig. 6e). Grouped with the Mount Christie Formation are dark grey and black shale and siltstone that comprise many small mossy outcrops within the northern half of the mapped area (Fig. 2). The upper and the lower contacts are not exposed in the NE Glenlyon area. The lower contact is inferred to be conformable and the upper contact is inferred to be unconformable (Fig. 3). Limited exposure of this unit hinders accurate thickness estimates, but inferred values range from 175 m near the western end of Kalzas Range to 800 m in the northeast corner of the map area. Many sections probably fall somewhere between these two extreme values.

This succession of rocks has been assigned to the Carboniferous to Permian Mount Christie Formation based on lithologic similarities with exposures of this unit to the southeast where it has been well dated with conodonts and radiolarians (Gordey and Anderson, 1993; Cordey, 2016, 2017; Orchard, 2017; Gordey, 2013).

Jones Lake Formation

Beige and grey-brown weathering, well-bedded, calcareous siliciclastic rocks of the Jones Lake Formation comprise isolated outcrops across the area (Gordey and Anderson, 1993).

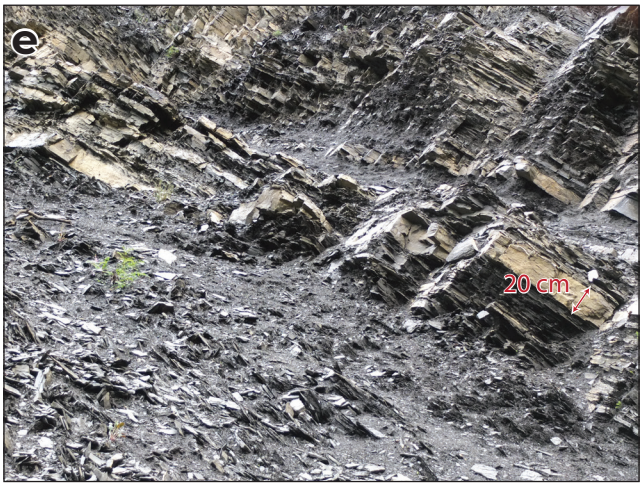

***Figure 6** continued. **(d)** Medium-bedded chert from the Mount Christie Formation on south slope of Kalzas Range (500069E, 6979014N). **(e)** Beige and grey weathering, thin and medium-bedded calcareous siltstone and fine-grained sandstone of the Jones Lake Formation from the south slope of Kalzas Range (502155E, 6978277N). **(f)** Tay Formation limestone with bed of black chert (hammer partly covers chert bed; 491649E, 6979598N). All coordinates are UTM zone 8 NAD 83.*

Grey-brown, medium-bedded siltstone, calcareous fine-grained, quartz sandstone, packstone and calcareous pebbly conglomerate comprise one single outcrop along the western end of Kalzas Range. Similarly, one outcrop on the south slope of the eastern end of the Kalzas Range contains brown weathering, grey, thin to medium-bedded, dolomitic, bioturbated, muddy siltstone that is interbedded with cross-bedded grainstone (Fig. 6f). Northeast of Dromedary Mountain, this unit consists of beige weathering, medium-bedded, silty limestone interbedded with calcareous siltstone. The lower contact with the Mount Christie Formation is not exposed in the NE Glenlyon area, but is well constrained at the western end of Kalzas Range and on the south slope of Crystal Peak where it is inferred to be unconformable. An erosional top to this unit makes a full thickness estimate impossible. An inferred minimum thickness is 150 m.

This unit is assigned to the Jones Lake Formation based on lithologic similarities to this unit in the Tay River area where it has been dated by Middle to Late Triassic micro and macrofossils (Gordey, 2013; Orchard, 2016, 2017; Gordey and Anderson, 1993). These rocks look very similar to the Steel Formation and without fossil and/or stratigraphic constraints could easily be confused with this unit.

Intrusive Rocks

Late Devonian Intrusive Rocks

Several intermediate porphyritic intrusions were mapped south and east of Dromedary Mountain. At outcrop-scale these intrusions are orange and grey weathering, green-grey, fine and medium-grained pyroxene diorite. Thin section analysis shows variably altered mafic minerals (augite and amphibole (?)) in a groundmass with feldspar and minor quartz.

This suite is Late Devonian (*ca.* 364 Ma) based on a preliminary U-Pb zircon age from east of Dromedary Mountain (Yukon Geochronology, 2018). Other intrusions of this age have been discovered southeast of this area during previous mapping (YGS Geochron, 2018).

McArthur batholith

The southeastern tip of the McArthur batholith crops out on Kalzas Mountain. Light grey weathering, salt and pepper, medium and coarse-grained biotite granodiorite to tonalite at this location has phenocrysts of plagioclase up to 5 cm long. A metamorphic contact aureole is mapped along the end of the batholith and ranges in size from 800 m to 2 km.

This body is part of the Mayo plutonic suite (98–93 Ma) based on two U-Pb zircon ages collected 30 km to the northwest, near Grey Hunter Peak (Colpron *et al.*, 2016a).

Structure

Three structural domains divide the area and correspond to the three panels used to subdivide the stratigraphy. The northern domain includes areas north of the Twopete fault, the central domain represents the area between Twopete and Duo faults, and the southwestern domain includes areas southwest of the Duo fault. In general, the NE Glenlyon area is deformed by a northwest-trending fold and thrust belt that affects Triassic and older rocks. Thrust faults are offset by steeply dipping, north-south oriented faults that have both strike-slip and dip-slip displacement.

Northern Domain

Silurian (?) to Triassic strata north of the Twopete fault are deformed by northeast-verging, open to closed folds that are primarily interpreted from changes in bedding orientation across the region. Outcrop-scale folds exhibited locally in carbonate stratigraphy of Jones Lake and Tay formations confirm this interpretation (Fig. 7a). On Kalzas Mountain, Tay Formation marble and slate are isoclinally folded multiple times creating a structurally thickened section within the contact aureole of the McArthur batholith.

On the northern slope of Dromedary Mountain, a sliver of upper Earn Group is thrust over the Mount Christie Formation to the northeast. This thrust fault joins the Twopete fault west of Dromedary Mountain and is not mapped crossing a steep fault east of Dromedary Mountain. North of the Twopete fault, the Steel Formation is thrust over Mount Christie Formation

along a south-dipping thrust fault that continues to the southeast (Cobbett, 2016a). In the northwestern corner of the map area, the upper Earn Group is thrust over the Mount Christie Formation along a south-dipping thrust fault (Fig. 2).

A series of steeply-dipping, north-trending faults offset strata, folds and thrusts within this domain. East-side down normal motion is interpreted as the dominant movement along one of these structures in the middle of the domain. All other faults are likely a combination of dip-slip and strike-slip movement. The small north-trending fault near Kalzas Mountain offsets a klippe of the Twopete fault and is crosscut by the McArthur pluton constraining the age of movement to post-Triassic and pre-mid-Cretaceous (Fig. 2).

Central Domain

This structural domain is a fault-bounded panel of Cambrian (?) to Ordovician strata intruded by Late Devonian granitic rocks. Near the Twopete fault, close folds in thin-bedded limestone of Rabbitkettle Formation have well-developed axial planar cleavage. The high angle, bedding-cleavage intersection in the hinges breaks the rock into small cube-shaped pieces that were subsequently altered and rotated (?) creating brecciated hinge zones (Fig. 7b). East of Dromedary Mountain, laminated siltstone and fine-grained sandstone units of Road River Group are deformed into cm-scale folds with well-developed axial planar cleavage. In both these areas, axial planar cleavage dips moderately to steeply to the southwest.

In one locality on the southwestern flank of Dromedary Mountain, cross-beds and asymmetric ripples indicate an overturned bed is folded into an upright antiform (Fig. 7c). Vergence indicators are absent in this particular outcrop, likely because the thick beds comprising coarse-grained strata are not easily cleaved or folded, making it difficult to fully interpret these rocks. One interpretation of this configuration is that the outcrop preserves the bottom limb of an anticline or the top limb of a syncline of a northwest-verging recumbent fold pair that was subsequently folded into an upright anticline.

Included in the central domain near Kalzas Mountain, a klippe of the Twopete fault places Road River Group strata over upper Paleozoic rocks. Fine-grained clastic rocks are recrystallized into phyllite and slate within the hanging wall of the klippe. More competent rocks, such as chert pebble conglomerate, exhibit a well-developed foliation defined by stretched and slightly flattened chert clasts (Fig. 7d). The McArthur batholith plugs the thrust fault klippe. Axial planar foliation dips moderately to nearly vertically east-southeast and defines the main layering in phyllite and slate.

Southwest Domain

The region south of the Duo fault encompasses the structurally most complex and mostly poorly exposed part of the area. Rocks within this domain range from undeformed (massive basalt) to polydeformed (folded calcite-mica schist) in large part due to the competency of the host lithology, but also with distance away from the Duo fault (rocks are more deformed farther from the fault to the southwest). Near the fault, fine-grained sedimentary rocks have a well-developed slatey cleavage and bedding is typically preserved. Volcanic and volcaniclastic rocks are undeformed and only rarely is there a secondary fabric developed. Between 2 and 7 km from the Duo fault, for example near Earn River and along the upper parts of Duo Creek, layered rocks are typically recrystallized to phyllite. Local preservation of bedding occurs near thick sections of basalt and in areas where layered rocks are non-calcareous. Rare exposures of calcareous phyllite exhibit a crenulation cleavage that overprints the dominant foliation (Fig. 7e). Foliations dip moderately to steeply to the southwest. Exposures south of Kalzas Mountain show similar structural grade despite their close proximity (0–2 km) to the Twopete/Duo faults. The dominant foliation near Kalzas Mountain dips steeply north-northeast. Layered rocks become fully recrystallized into schist more than 7 km from the Duo fault. Near Detour Lakes, layered rocks exhibit an early dominant foliation tightly folded to form a secondary foliation (Fig. 4a). In this area, volcanic and volcaniclastic rocks exhibit weakly to moderately developed foliation. Both early and late foliations are variably oriented with no discernible pattern. Near Detour Lakes a southwest-dipping klippe places Vangorda formation over the Menzie Creek Formation (Fig. 2).

Figure 7. *Field photographs of structural features from northeastern Glenlyon area.* ***(a)*** *Close folding of Triassic Jones Lake Formation from north panel. Cross-beds indicate both limbs of this fold are upright (502155E, 6978277N).* ***(b)*** *Tight folding of Ordovician Rabbitkettle strata showing well-developed axial planar cleavage from central panel. Intersection between bedding and cleavage creates brecciated hinge zones (512557E, 6972880N).* ***(c)*** *Tight folding of thick-bedded sandstone of undivided Road River Group from central panel. Cross-bedding and asymmetric ripple marks suggest both limbs of the anticline are overturned (yellow arrows point in younging direction; 513532E, 6971568N).* ***(d)*** *Foliated chert pebble conglomerate of undivided Road River Group from central panel (485784E, 6977384N). Calcareous phyllite of Menzie Creek Formation from southwestern panel. This outcrop exhibits a dominant foliation (S1) crenulated into a secondary foliation (S2). Bedding (S0) is weakly preserved as a linear feature visible on S1 planes (507339E, 6963689N). All coordinates are UTM zone 8 NAD 83.*

Mineralization

A variety of mineralization types occur within the mapped area including SEDEX (Yukon MINFILE 105L 030, 037, 041), sediment-hosted stratiform barite (Yukon MINFILE 105L 050, 054), polymetallic vein Ag-Pb-Zn ± Au (Yukon MINFILE 105L 023, 024, 025) and skarn (Yukon MINFILE 105L 031, 035).

Historical exploration efforts focused on mineralization discovered in and around the Dromedary Mountain area and on the south side of Kalzas Mountain. Late Devonian strata host pyrite and pyrrhotite dominated layered sulphide bodies that contain minor lead, zinc and silver (Caulfield and Weber, 1997; Carlson, 1981). Previous workers have proposed a syngenetic origin for this mineralization. Late Devonian strata also hosts polymetallic veins with lead, zinc and silver. Both types of mineralization occur in the direct footwall of the Twopete fault.

Discussion

Coarse siliciclastic rocks of the undivided Road River Group that crop out in the central panel are unlike coeval deep-water strata elsewhere in the Selwyn basin (Gordey, 2013; Gordey and Anderson, 1993). We propose these coarse siliciclastic rocks were deposited along a shallow shelf adjacent to a platform located to the southwest in present day coordinates. The Duo fault (Twopete fault to the southeast) likely coincides with the platform-basin boundary that links up with the McEvoy platform–Selwyn basin boundary in the southern part of the Sheldon Lake map area (105J) and into the Frances Lake map area (105H; Fig. 8; e.g., Gordey, 2013). The McEvoy platform in these regions includes Silurian to Devonian siltstone, sandstone and carbonate (Gordey, 2013). If the central panel strata mapped in the NE Glenlyon area are genetically linked to platformal rocks, it suggests parts of the McEvoy platform may be as old as Ordovician. In the NE Glenlyon area, thick carbonate rocks typical of a platform have been eroded away south of the Twopete and Duo faults.

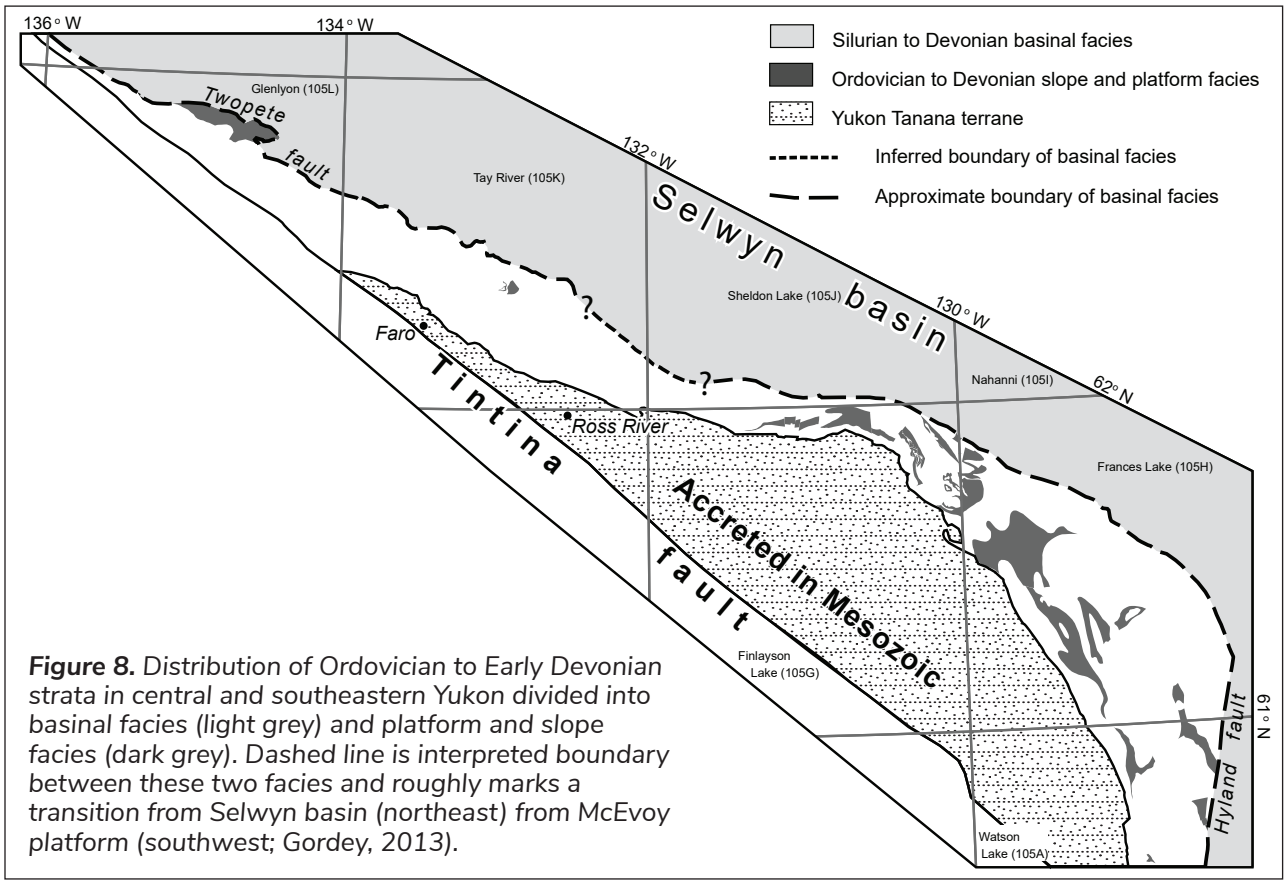

Figure 8. *Distribution of Ordovician to Early Devonian strata in central and southeastern Yukon divided into basinal facies (light grey) and platform and slope facies (dark grey). Dashed line is interpreted boundary between these two facies and roughly marks a transition from Selwyn basin (northeast) from McEvoy platform (southwest; Gordey, 2013).*

We propose heat from a buried pluton caused the alteration and hornfelsing of rocks on Dromedary Mountain. The regional aeromagnetic map delineates a magnetic high surrounding a circular magnetic low centred roughly on Dromedary Mountain (Fig. 9). The magnetic low is delineating a granitic body similar to the magnetic low that is coincident with the McArthur pluton. The magnetic high is delineating a pyrrhotite-rich contact aureole that leaks into the Twopete fault creating the eye-shaped magnetic high. The pluton is the source for hydrothermal fluids that silicify and alter rocks on both sides of the Twopete fault on Dromedary Mountain.

A syngenetic origin for the layered sulphide bodies hosted in Upper Devonian strata near Kalzas and Dromedary mountains is proposed. Several faults mapped southeast of the Glenlyon area, including the Twopete fault, were active in the Late Devonian and controlled the deposition of the upper Earn Group, which includes volcanic rocks in southeastern areas (Cobbett, 2016b). The Twopete fault in the NE Glenlyon area was a synsedimentary structure in the Devonian that facilitated the migration of mineralizing fluids to the surface where sulphide was deposited or replaced as stratabound layers. The timing and style of mineralization is comparable to the Tom and Jason deposits near Macmillan Pass in eastern Yukon where Late Devonian to Mississippian strata host significant syngenetic base metal mineralization (Yukon MINFILE, 2018). Late Devonian synsedimentary faults controlled the deposition of the Earn Group near Macmillan Pass and are spatially coincident with the Tom and Jason deposits (Abbott *et al.*, 1990; Abbott, 2013)

Summary

The main results from mapping in the NE Glenlyon area are:

1. The recognition and accurate mapping of the Twopete fault in the NE Glenlyon area, a major structural boundary that continues for approximately 100 km to the southeast (Cobbett, 2016b, 2014).

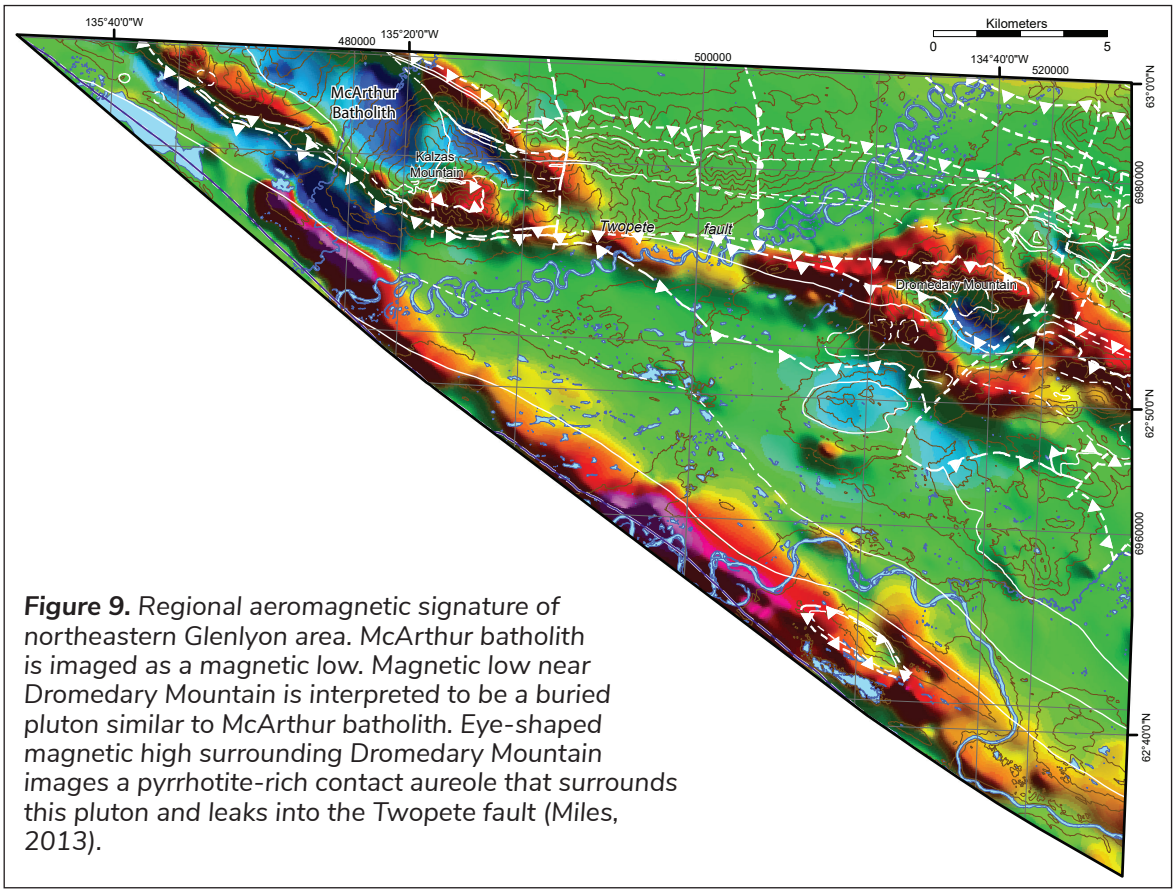

Figure 9. *Regional aeromagnetic signature of northeastern Glenlyon area. McArthur batholith is imaged as a magnetic low. Magnetic low near Dromedary Mountain is interpreted to be a buried pluton similar to McArthur batholith. Eye-shaped magnetic high surrounding Dromedary Mountain images a pyrrhotite-rich contact aureole that surrounds this pluton and leaks into the Twopete fault (Miles, 2013).*

2. Discovery of Ordovician to Silurian (?) coarse siliciclastic rocks, dark weathering phyllite and graptolitic siltstone that represent slope facies representing a platform to basin transition similar to the McEvoy platform–Selwyn basin transition in southeastern Yukon.
3. Upper Devonian strata hosts syngenetic mineralization discovered near Kalzas Mountain and Dromedary Mountain in the direct footwall to the Twopete fault.

Reference

Abbott, G., 2013. Bedrock Geology of the Macmillan Pass area, Yukon and adjacent Nortwest Territories (NTS 105O/1, 2 and parts of 105O/7, 8 and 105P/4, 5). Yukon Geological Survey, Geoscience Map 2013-1.

Abbott, J., Gordey, S. and Tempelman-Kluit, D., 1990. Setting of stratiform, sedimenthosted lead-zinc deposits in Yukon and northeastern British Columbia. *In:* Mineral Deposits of the Northern Canadian Cordillera, Yukon-Eastern British Columbia, J.G. Abbott and R.J.W. Turner (eds.), Geological Survey of Canada, Open File 2169, p. 69–98.

Blodgett, R.B., 2015. Fossil Report to the Yukon Geological Survey, 2015. Anchorage, USA.

Blodgett, R.B., 2016. Report on fossil fauna collected by Rosie Cobbett (Yukon Geological Survey) during 2016 summer field season. Anchorage, USA.

Campbell, R.B., 1967. Geology of Glenlyon map-area, Yukon Territory (105 L). Geological Survey of Canada, Memoir 352, 92 p.

Carlson, G.G., 1981. 1981 Dromedary Project, Yukon Territory NTS 105L/15. Yukon Energy, Mines and Resources, Assessment Report 090888.

Caulfield, D.A. and Weber, J., 1997. 1996 Exploration Program on the Dromedary Mountain Property. Yukon Energy, Mines and Resources, Assessment Report 96–056.

Cobbett, R., 2016a. Geological map of the Earn Lake area, central Yukon, parts of NTS 105L/09, 15 and 16. Yukon Geological Survey, Open File 2016-40, scale 1:50 000.

Cobbett, R.N., 2014. Preliminary observations on the geology of the Anvil Lake area (parts of NTS 105K/11 and 12), central Yukon. *In:* Yukon Exploration and Geology 2013, K.E. MacFarlane and M.G. Nordling and P.J. Sack (eds.), Yukon Geological Survey, p. 33–51.

Cobbett, R.N., 2016b. Preliminary observations on the geology of the Tay Mountain area (parts of NTS 105K/12 and 13, 105/09 and 16), central Yukon. *In:* Yukon Exploration and Geology 2015, K.E. MacFarlane and M.G. Nordling (eds.), Yukon Geological Survey, p. 79–98.

Colpron, M. and Nelson, J., 2011. A digital atlas of terranes for the Northern Cordillera. BC GeoFile 2011-11.

Colpron, M., Mortensen, J.K., Gehrels, G.E. and Villeneuve, M.E., 2006. Basement complex, Carboniferous magmatic arcs and Paleozoic deformation in Yukon-Tanana terrane of central Yukon: Field, geochemical and geochronological constraints from Glenlyon map area. *In:* Paleozoic evolution and metallogeny of pericratonic terranes at the ancient Pacific margin of North America, Canadian and Alaskan Cordillera, M. Colpron and J.L. Nelson (eds.), Geological Association of Canada, Special Paper 45, p. 131–151.

Colpron, M., Israel, S., Murphy, D., Pigage, L. and Moynihan, D., 2016a. Yukon bedrock geology map. Yukon Geological Survey, Open File 2016-1, scale 1:5 000 000.

Colpron, M., Israel, S. and Friend, M., 2016b. Yukon Plutonic Suites. Yukon Geological Survey, Open File 2016-37, scale 1:750 000.

Cordey, F., 2014. Report on Radiolarians No. YGS2014-6. Laboratoire de géologie de Lyon: Terre, Planete, Environnement, Universite Claude Bernard, France.

Cordey, F., 2016. Report on Microfossils No. YGS2016-1. Laboratoire de géologie de Lyon: Terre, Planete, Environnement, Universite Claude Bernard, France.

Cordey, F., 2017. Report on Microfossils No. YGS2017-1. Laboratoire de géologie de Lyon: Terre, Planete, Environnement, Universite Claude Bernard, France.

Gabrielse, H., 1967. Tectonic Evolution of the Northern Canadian Cordillera. Canadian Journal of Earth Sciences, vol. 4, p. 271–298, doi:10.1139/e67-013.

Gabrielse, H., Blusson, S.L. and Roddick, J., 1973. Geology of Flat River, Glacier Lake, and Wrigley Lake Map-areas, District of Mackenzie and Yukon Territory, Part 1: General Geology, Structural Geology and Economic Geography Geological Survey of Canada, Memoir 366, 153 p.

Gabrielse, H., Murphy, D.C. and Mortensen, J.K., 2006. Cretaceous and Cenozoic dextral orogen-parallel displacements, magmatism, and paleogeography, north-central Canadian Cordillera. *In:* Paleogeography of the North American Cordillera: Evidence For and Against Large-Scale Displacements, J.W. Haggart, R.J. Enkin and J.W.H. Monger (eds.), Geological Association of Canada, Special Paper, vol. 46, p. 255–276.

Gordey, S.P., 2013. Evolution of the Selwyn Basin region, Sheldon Lake (105J) and Tay River (105K) map areas, central Yukon Territory. Geological Survey of Canada, Bulletin 599, 176 p. doi: 10.4095/293034.

Gordey, S.P. and Anderson, R.G., 1993. Evolution of the northern Cordilleran miogeocline, Nahanni map area (105I), Yukon and Northwest Territories. Geological Survey of Canada, Memoir 428, 214 p.

Gordey, S.P., Abbott, J.G., Tempelman-Kluit, D.J. and Gabrielse, H., 1987. "Antler" clastics in the Canadian Cordillera. Geology, vol. 15, p. 103–107.

Jennings, D.S.and Jilson, G.A., 1986. Geology and Sulphide deposits of Anvil Range, Yukon. *In*: Mineral Deposits of Northern Cordillera, J.A. Morin (ed.). Canadian Institute of Mining and Metallurgy, Special Volume 37, p. 319–361.

Mair, J.L., Hart, C.J.R. and Stephens, J.R., 2006. Deformation history of the northwestern Selwyn Basin, Yukon, Canada: Implications for orogen evolution and mid-Cretaceous magmatism. Geological Society of America Bulletin, vol. 118, p. 304–323.

Miles, W. (compiler), 2013. Aeromagnetic map compilation. Geological Survey of Canada, ftp://ftp.agg.nrcan.gc.ca/public/gdc/YUKON, [accessed June 2014].

Orchard, M.J., 2016. Paleontological Report MJO-MS-2016-3. Submitted to Yukon Geological Survey.

Orchard, M.J., 2017. Paleontological Report MJO-MS-2017-1. Submitted to Yukon Geological Survey.

Pigage, L.C., 2004. Bedrock geology compilation of the Anvil District (parts of 105K/2, 3, 5, 6, 7 and 11), central Yukon. Yukon Geological Survey, Bulletin 15, 103 p.

Rasmussen, K.L., 2013. The timing, composition, and petrogenesis of syn- to post-accretionary magmatism in the northern Cordilleran miogeocline, eastern Yukon and southwestern Northwest Territories. Unpublished PhD thesis, University of British Columbia,

Roddick, J.A., 1967. Tintina Trench. Journal of Geology, vol. 75, p. 23–33.

Yukon Geochronology, 2018. Yukon Geochronology – A database of Yukon geochronology sample locations, M. Colpron (compiler). Yukon Geological Survey, http://yukon2.maps.arcgis.com/home/item.html?id=0fa83ba4a4794b9d8432d4d1b44da967 [accessed December, 2018].

Yukon MINFILE, 2018. Yukon MINFILE – A database of mineral occurrences. Yukon Geological Survey, http://data.geology.gov.yk.ca [accessed December 2018].

Constraints on the evolution of placer gold deposits at Gladstone Creek, Yukon (NTS 115G/7, 8)

Derek C. Cronmiller and Brent C. Ward
Earth Sciences, Simon Fraser University

Jeffrey D. Bond
Yukon Geological Survey

Daniel Layton-Matthews
Geological Sciences and Geological Engineering, Queens University

Cronmiller, D.C., Ward, B.C., Bond, J.D. and Layton-Matthews, D., 2019. Constraints on the evolution of placer deposits at Gladstone Creek, Yukon (NTS 115G/7, 8). *In:* Yukon Exploration and Geology 2018, K.E. MacFarlane (ed.), Yukon Geological Survey, p. 61–74.

Abstract

Gladstone Creek hosts a productive placer mine and has been glaciated at least three times. Glaciations eroded bedrock and reworked surficial materials, depositing thick sequences of sediment in Gladstone valley, which were subsequently fluvially incised during deglaciation and non-glacial intervals. Fluvial incision and reworking concentrated detrital gold in coarse gravel units that commonly overly bedrock or false-bedrock surfaces. Identifying false-bedrock units in stratigraphy may help placer miners target economical gold deposits perched above the valley bottom.

Gold grain samples were collected from four gravel units. Characterization of gold grain morphology and laser ablation ICP-MS analysis indicate multiple sources of lode mineralization. Based on regional ice flow directions and the stratigraphic and geographic locations of the gold samples, gold is likely sourced from epithermal and gold-rich porphyry deposits associated with the Ruby Range batholith, and orogenic mineralization in the Kluane schist.

* derek.cronmiller@sfu.ca

Introduction

Gladstone Creek is located in the central Ruby Range, southwestern Yukon. The Ruby Range has a long history of placer mining and mineral exploration; placer mining in Gladstone Creek began in the 1910s (Cairnes, 1915). Active and historic placer mines along this creek are well within the most recent glaciation to affect Yukon, and thus are in a much different setting than placer mines in the unglaciated Klondike. Stratigraphy and morphology of gold grains in Gladstone Creek were previously examined by Madsen (2001); however, no morphological or geochemical analysis of gold grains has been used to link placer gold to lode gold sources in the Gladstone area. In this paper we present the sedimentological characteristics and commonalities of economically auriferous gravels within Gladstone Creek and how glaciation has affected the development and distribution of placer deposits in Gladstone Creek. We also examine gold grain morphology and geochemistry to determine the likely sources of lode gold based on the style of mineralization in local lithological units. Understanding the mechanisms controlling the distribution of economic placer deposits will help placer miners locate economic gravels in glaciated regions. Determining the provenance of placer gold in Gladstone Creek may also inform future hard rock mineral exploration in the region. The objectives of this paper are to characterize placer gold grain chemistry and morphology to determine potential bedrock sources and how glaciation has affected the distribution and preservation of placer deposits.

Setting

The central Ruby Range is characterized by rugged peaks greater than 2100 m high, and broad undulating plateaus above 1500 m. The peaks and plateaus are drained by deep, U-shaped valleys, such as Gladstone Creek, that drain westward into the east side of Kluane Lake (Fig. 1). Cronmiller et *al.* (2018) mapped surficial materials throughout the study area. Upland surficial materials are heavily modified by periglacial processes and comprise colluvium derived from weathered bedrock and thin veneers of till below all-time glacial limits (Cronmiller et *al.*, 2018). Valley bottoms are filled with thick, stratigraphically complex Quaternary deposits comprising glacial and interglacial sediment. In Gladstone Creek these deposits are more than 115 m thick.

Glacial History

Early mapping in southwestern Yukon by Hughes et *al.* (1969) found evidence of two Cordilleran ice-sheet

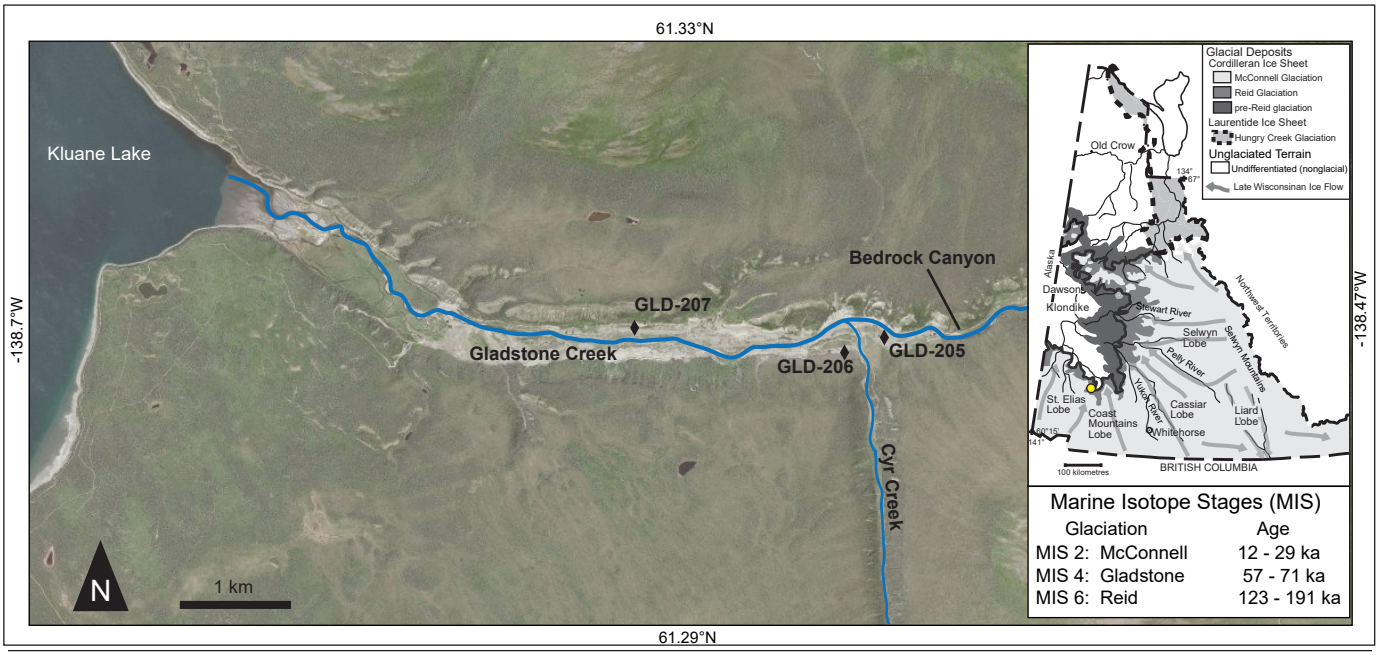

Figure 1. *Lower Gladstone Creek and Cyr Creek. Sample sites are indicated by diamonds. Location of study area shown by yellow dot on inset map.*

advances into the Ruby Range, as well as local ice cap formation on the plateau surfaces above 1500 m (Hughes, 1990). Glacial advances were initially suspected to correlate to what we now know are marine oxygen isotope stages (MIS) 2 and 6; however, recent ^{10}Be dating of erratics above Gladstone Creek suggest the local all-time limit may have occurred during MIS 4 (Fig. 1; Ward *et al.*, 2007). New field and desktop mapping (Cronmiller *et al.*, 2018) confirmed the presence of ice caps on plateau surfaces based on the orientation of moraines and meltwater channels as well as descending U-shaped valleys; all of which suggest ice growth extended beyond the high plateaus and into local trunk valleys including Gladstone Creek. In addition, many well-developed cirques are found on high, northerly aspects. Moraines descending from these cirques suggest significant local alpine glaciation coalesced with the up-valley ice from the St Elias lobe of the Cordilleran Ice Sheet (CIS; Fig. 1). Generalized St Elias lobe ice-flow directions are shown in Figure 2. Ice caps and cirques may have contributed substantially to the local extent of late Pleistocene limits and could account for the local all-time limit corresponding to MIS 4 advance. Till suspected to have been deposited by westward flowing ice from Ruby Range cirques is observed in sections as far down Gladstone Creek

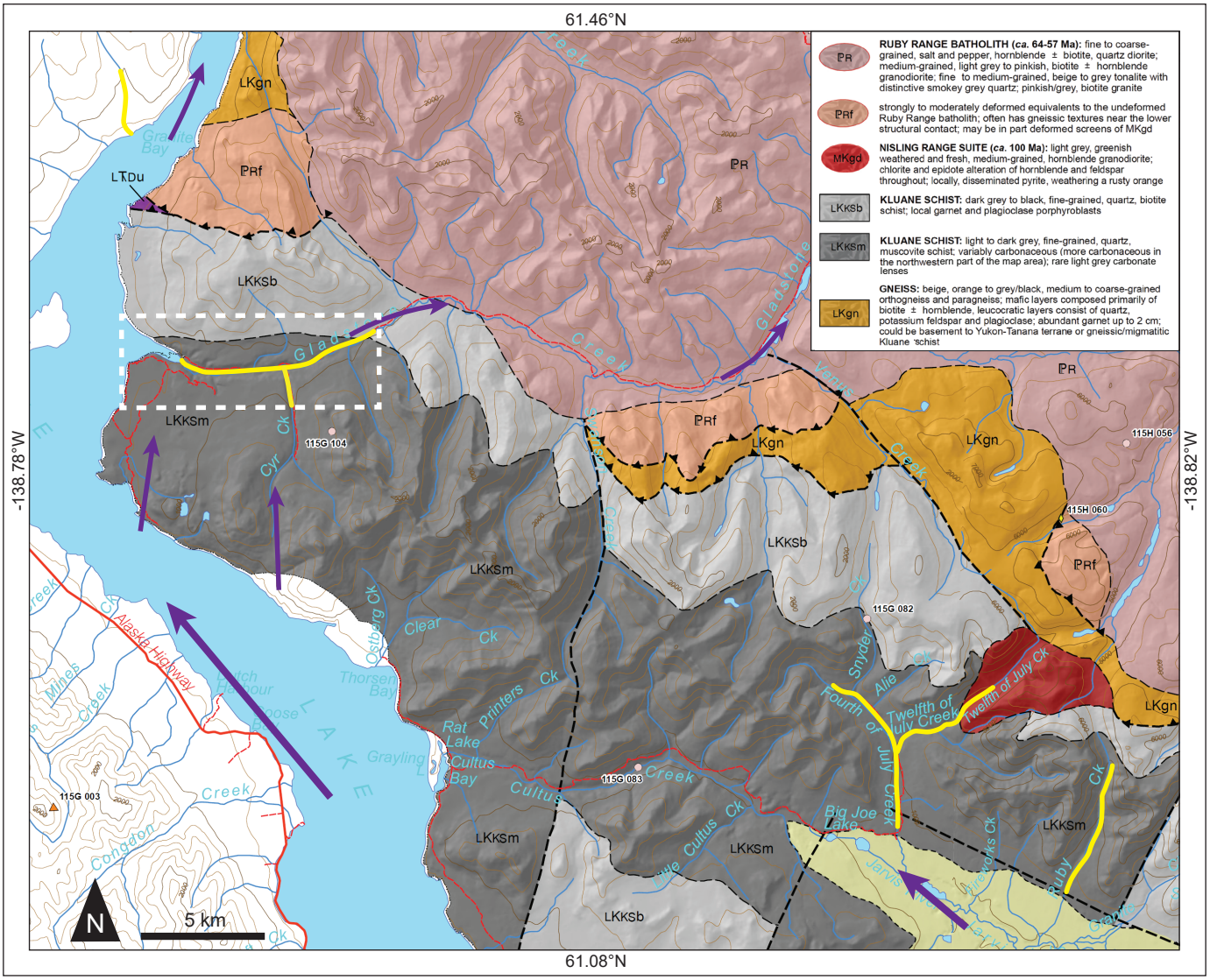

Figure 2. *Bedrock geology of the west-central Ruby Range (modified from Israel et al. 2011b). The location of Figure 1 is shown by dashed white lines. Actively mined placer creeks are shown by yellow lines. Local indicators of St Elias lobe ice flow direction (Hughes et al., 1969) shown by arrows.*

as GLD-205 (Fig. 1). The presence of till in the lower reaches of Gladstone Creek suggests that both east and west-flowing ice could have introduced distal–intrabasinal and extrabasinal auriferous material into Gladstone valley during glaciations.

Geology and Mineralization

Gladstone Creek is underlain by two main lithological units: The Ruby Range batholith, and Kluane schist (Fig. 2). Uncorrelated ortho and paragneiss are commonly found at the boundary of these two units that are thought to be gneissic or migmatitic equivalents of Kluane schist or the basement rock of the Yukon-Tanana terrane (Israel *et al.*, 2011a). Minor outcrops of ultramafic rock occur in association with the Kluane schist.

Ruby Range batholith

The Ruby Range batholith is a large multiphase plutonic complex comprising quartz-diorite, tonalite, granodiorite, with minor diorite, gabbro, and granite (Israel *et al.*, 2011a). The batholith contains porphyry Cu-Mo-Au mineralization (Yukon MINFILE 115G 070, 071) and epithermal Au-Ag mineralization, primarily in the upper crustal part of the batholith. The Ruby Range batholith underlies most of the upper reaches of Gladstone Creek. The main phases of the Ruby Range batholith intrusion occurred between 64 and 57 Ma.

Kluane schist

The Kluane schist occurs between the Denali fault on the west side the Shakwak trench, and the Ruby Range batholith in the east (Fig. 2). It comprises a metamorphic assemblage of metapelitic quartz-mica schist, rare ultramafic and carbonate bodies, and numerous quartz veins systems (Israel *et al.*, 2011a). Kluane schist contains muscovite-rich and biotite-rich units. The characteristics of gold in Kluane schist suggest orogenic mineralization (Israel *et al.*, 2011a). Deposition of the Kluane schist occurred between 95 Ma and 82 Ma—the onset of metamorphism.

Mining and Exploration

Gladstone Creek was first mined in the 1910s below the mouth of Cyr Creek (Cairnes, 1915). The first large-scale operation began with the Kluane Dredge Company, which extracted 5770 ounces of gold from below the confluence of Cyr Creek between 1952 and 1956 (Muller, 1967). The lower reaches of Gladstone Creek and Cyr Creek are now mined by TIC Exploration Inc. Numerous other placer mines are currently operating on the west slopes of the Ruby Range, all of which are located in Kluane schist (Fig. 2). Hard rock exploration has noted similarities between the orogenic mineralization in Kluane schist and the Juneau gold belt (Israel *et al.*, 2011a; Yukon MINFILE 115H 055, 047).

Methods

Sites were visited in summer 2017, as part of a larger program to map surficial geology and log stratigraphy of Gladstone Creek and the central Ruby Range. Thirteen sections were described on Gladstone Creek and two at Cyr Creek; three of these are described herein. Sections were divided into stratigraphic units based on sediment type and general sedimentary characteristics. Gold grain samples were collected from two sections on Gladstone Creek (GLD-205 and GLD-207) and one section at the mouth of Cyr Creek (GLD-206). The samples were obtained from gravel units identified by TIC Exploration as being economically auriferous. Gravel was screened using a 4-mesh sieve and sluiced using a portable sluice box (Fig. 3) to obtain heavy-mineral concentrate. The concentrate was panned to isolate the gold. This process was repeated until a minimum of 25 grains were collected for each sample.

Morphological and chemical analysis of the gold grains was conducted by the geochemistry lab at Queens University. High-resolution electron backscatter images were produced for each sample using a scanning electron microscope. Gold grain morphology was characterized from the backscatter images using Image Metrology's SPIP™ image recognition software. Laser ablation ICP-MS was used to determine major, minor, and trace element composition of the gold grains.

Figure 3. *Collecting auriferous gravel at site GLD-207 and sluicing the fine fraction of sieved gravels to obtain gold grain samples.*

Results

Stratigraphy

GLD-205

Section GLD-205 (Fig. 4) is a mine cut located on the left limit of Gladstone Creek, approximately 200 m downstream of a bedrock canyon (Fig. 1). A description of lithostratigraphic units is provided in Table 1. This section contains two economic gravels, Units 2 and 5. Both gravel units overlie consolidated diamicton interpreted to be tills, corresponding to MIS 4 (Unit 4) and MIS 6 (Unit 1) advances of the St Elias lobe. This interpretation is based on their dense over-consolidated nature, the presence of extrabasinal, striated clasts, and strong unidirectional clast fabrics. A radiocarbon age of 26,720 ± 170 ^{14}C yr BP (UCIAMS-197773) and Dawson tephra (*cf.* Froese et *al.*, 2002) in Unit 6 constrains the tills to pre-MIS 3. A radiocarbon age within Unit 3 of 45,600 ± 2200 ^{14}C yr BP (UCIAMS-197774) is suspected to be non-finite, due to the age being near the useful limit of the technique. Unit 2 is strongly oxidized and contains highly weathered and cryoturbated clasts. Stratigraphy and geochronology indicate Unit 4 is from a MIS 4 advance, suggesting an age of at least MIS 4 for Unit 2. Both economic gravels overlie diamicton which act as false bedrock, where gold is concentrated on an erosionally resistant surface.

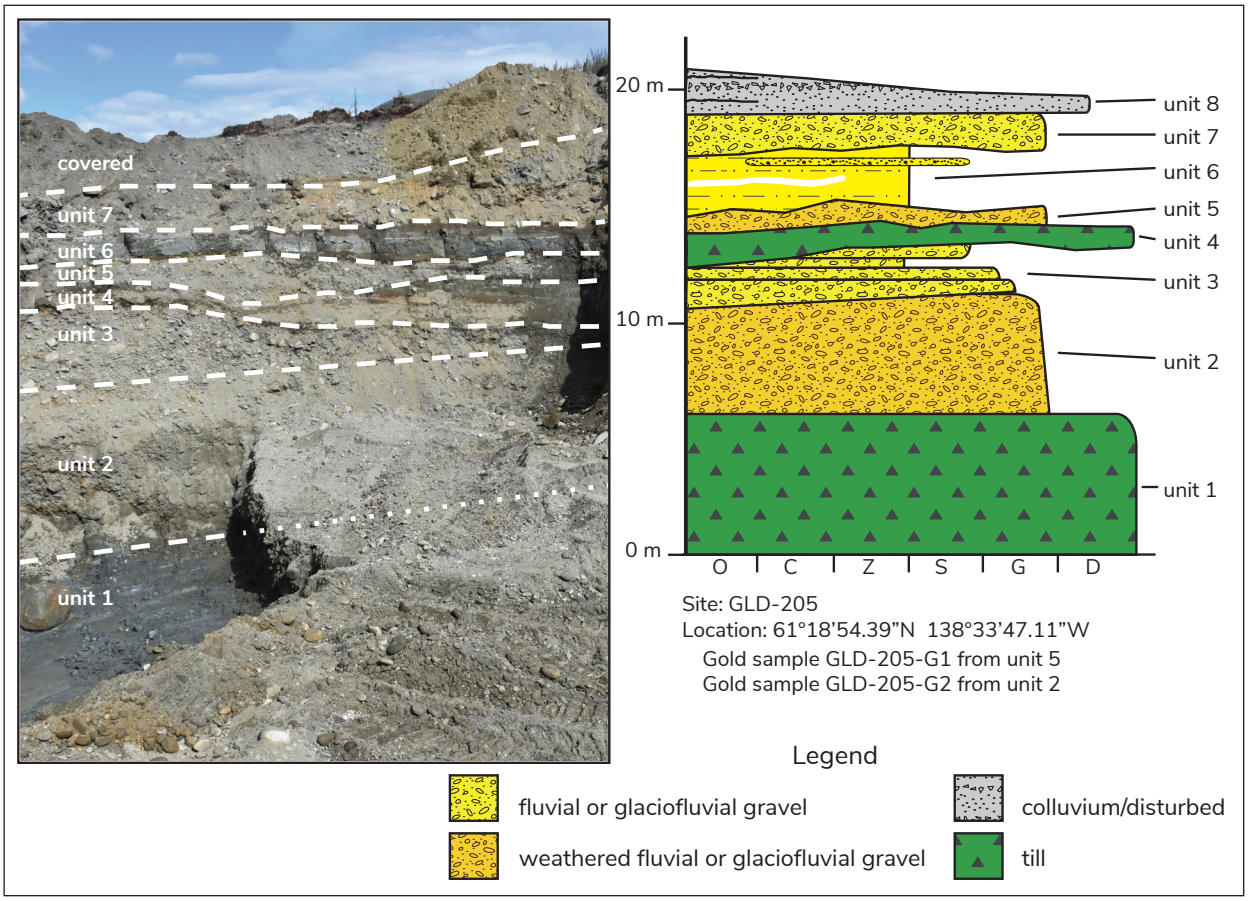

Figure 4. *Stratigraphy in mine cut on left limit of Gladstone Creek, GLD-205.*

Table 1. *GLD-205 unit descriptions.*

GLD-205 - Unit and interpretation	Description
unit 8 – Colluvium	Stratified pebbly sandy diamict with organic layers; 1 m thick; White River tephra at 7 cm depth
unit 7 – Fluvial gravel	Poorly sorted chaotic boulder gravel; 1.25 m thick, laterally variable; 10% boulders, 40% cobbles, 50% pebble; silty sand matrix
unit 6 – Fluvial silts	Fine sandy silt; 2.5 m thick; finely bedded, rare granule lenses; 10 cm thick Dawson tephra at 1.6 m above base of unit; GLD-205-M1: weevil (*Lepidophorus sp.*) macrofossils 26720 ± 170 ^{14}C yr BP (UCIAMS-197773)
unit 5 – Weathered gravel	Weathered, oxidized, auriferous, sandy boulder gravel; 15% boulder, 40% cobble, 45% pebble; silty sand matrix; 1 m thick, laterally variable in thickness and texture; economically auriferous; Gold sample GLD-205-G1
unit 4 – MIS 4 Ruby Range till	Blue grey/grey diamicton; 1.1 m thick, laterally variable; massive; 10% clasts; 90% matrix: 35% silt, 65% clay; upward increase in clast content
unit 3 – Fluvial gravel	Fining upwards silts sands and gravel; 1.9 m thick; 30% cobble, 70% pebble; rare sand lenses and silt rip-up clasts; GLD-205-M5: beetle (*Pterostichus sp.*) macro fossils 45,600 ± 2200 ^{14}C yr BP (UCIAMS-197774; assumed non-finite)
unit 2 – Weathered gravel	Weathered, oxidized, poorly sorted, chaotically-bedded, boulder gravel; 4–5 m thick; 10% boulder, 40% cobble, 50% pebble; 50% sandy silt matrix; vertically oriented clasts (cryoturbation); economically auriferous, gold sample GLD-205-G2
unit 1 – MIS 6 till, unknown source	Blue-grey diamict; >3 m thick, lower contact not exposed; 10% subangular to subrounded clasts: 90% pebble, 10% cobble; 90% matrix: 20% clay, 75% silt, 5% sand; consolidated

GLD-206

Section GLD-206 is a mine cut on the left limit of the Cyr Creek fan at the confluence with Gladstone Creek (Fig. 5). The characteristics of stratigraphic units exposed in this section are summarized in Table 2. Bedrock is exposed on both sides of the Cyr Creek valley immediately above this section that constrain lateral migration and downcutting of the channel.

GLD-207

Section GLD-207 (Fig. 6) is a mine cut on the right limit of Gladstone Creek, approximately 2.7 km downstream from the bedrock canyon. Characteristics of stratigraphic units are summarized in Table 3. Units 1 to 4 are gravels. Unit 3 contains economic concentrations of gold. This unit overlies a consolidated, poorly-sorted, matrix supported gravel (Unit 2), which was likely a paleo-floodplain surface, the age of which is not constrained. Many vertically aligned (Fig. 6 inset) and frost shattered clasts suggest Unit 2 was exposed to strong periglacial conditions. These conditions may have occurred during a glacial stage, prior to ice arrival in lower Gladstone Creek. The high silt content of Unit 2 may be from loess inputs. Like the diamicton units in GLD-205, this unit appears to act as a false-bedrock that limits downcutting due to its consolidation. Unit 5 is modern colluvium from mass wasting of the adjacent valley side.

Gold Grain Morphology

The roundness of gold grains is commonly used as a proxy for travel distance from lode source (Knight *et al.*, 1999). Well-rounded grains are considered to be more travelled than those exhibiting an angular morphology.

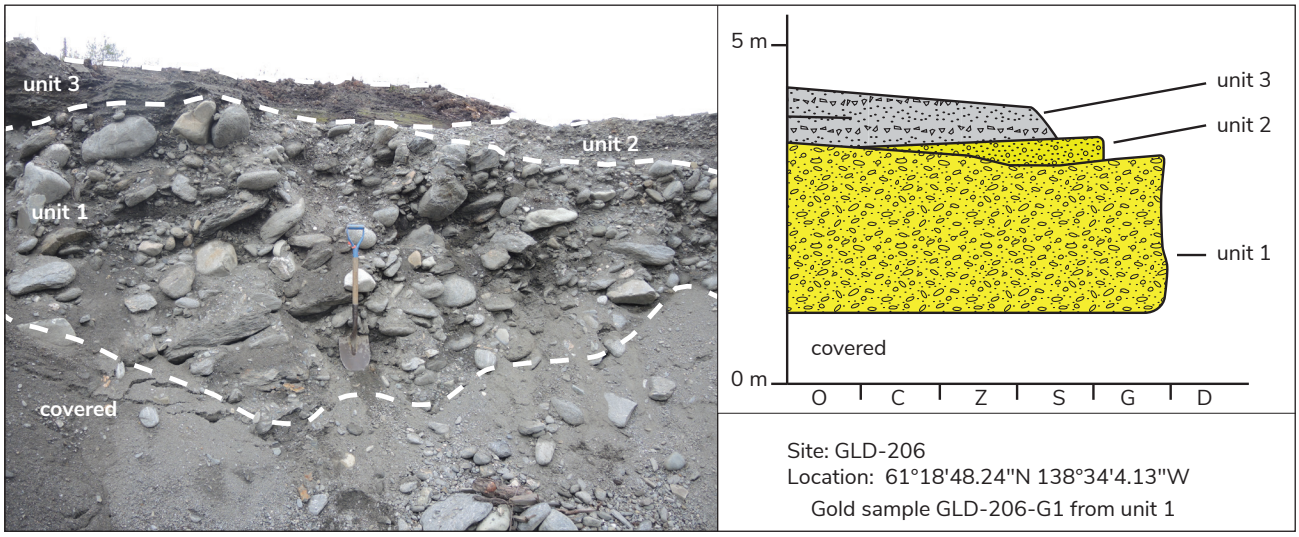

Figure 5. *Stratigraphy in mine cut on left limit of Cyr Creek, GLD-206, near confluence with Gladstone Creek. Section legend in Figure 4.*

Table 2. *GLD-206 unit descriptions.*

GLD-206 - Unit and interpretation	Description
unit 3 – Colluvium	Weakly stratified, pebbly sandy diamict with organic layers; 0.6 m thick
unit 2 – Fluvial pebble gravel	Moderately well-sorted pebble gravel; 0.4 m thick, laterally discontinuous; 75% clasts: 10% cobble, 90% pebble; 10% coarse sand matrix
unit 1 – Fluvial boulder gravel	Poorly-sorted auriferous boulder gravel; >2.3 m thick, lower contact not exposed; 90% clasts: 40% boulder, 40% cobble, 20% pebble; 10% sand matrix; economically auriferous; gold sample GLD-206-G1

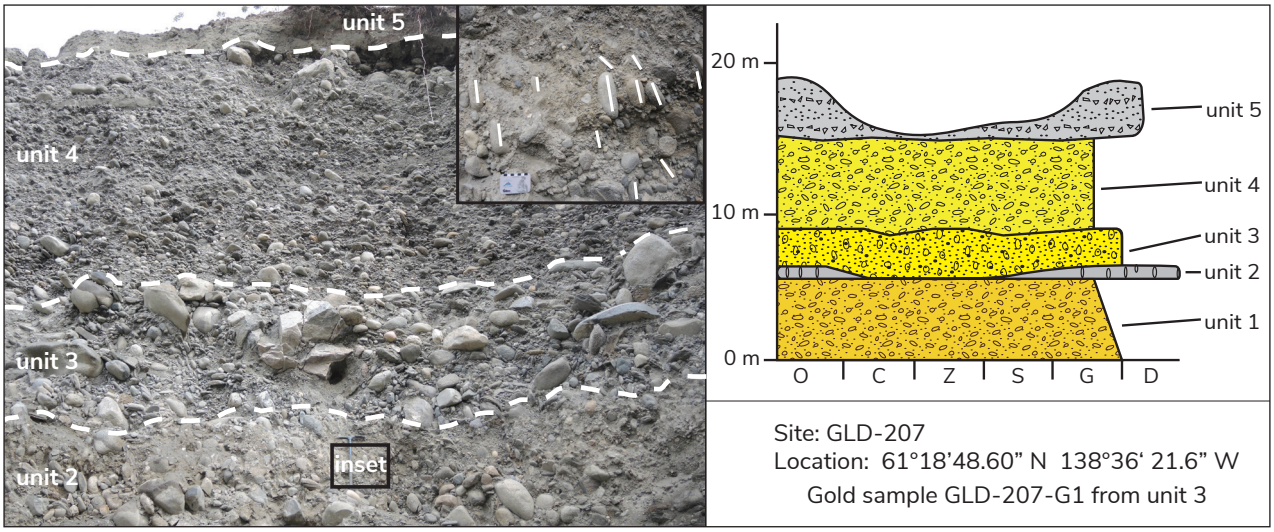

Figure 6. *Stratigraphy in mine cut on right limit of Gladstone Creek, GLD-207. Section legend in Figure 4.*

Table 3. *GLD-207 unit descriptions.*

GLD-207 - Unit and interpretation	Description
unit 5 – Colluvium	Stratified sandy silt with pebbles; 3 m thick, laterally variable; 90% sandy silt, with 5% pebbles and rare cobbles; 4 weakly-developed buried soils with organics; White River tephra 15 cm from top of unit.
unit 4 – Cobble gravel	Well-sorted cobble gravel; 4.5–5 m thick; 90% clasts: 1% boulder, 40% cobble, 59% pebble; matrix coarse to medium sand.
unit 3 – Boulder gravel	Chaotic boulder gravel; 1.9 m thick; 98% clasts; 10% boulder, 60% cobble, 30% pebble; 2% sandy silt matrix; down-valley imbrication; economically auriferous; gold sample GLD-207-G1
unit 2 – Cryoturbated cobble gravel	Cryoturbated diamictic gravel; 0.7 m thick, laterally variable; 70% clasts: common vertically oriented and frost shattered; 30% sandy silt matrix; highly consolidated
unit 1 –Cobble gravel	Oxidized, bouldery cobble gravel; >4.3 m thick, lower contact not exposed; 90% clasts, 10% sand matrix; many clasts highly weathered; crudely to well-sorted; strong down-valley imbrication;

Due to their malleability, gold grains round rapidly in the first three km of fluvial transport, and then more slowly as a stable morphology is achieved (Fig. 7).

The mean roundness of all samples from the Gladstone area is between 0.54 and 0.60; however, considerable variability in roundness is present within each sample (Fig. 8). Sample GLD-06-G1 appears to have a weak bimodal distribution, which may indicate two lode sources have contributed to the deposit. GLD-06-G1 also has the lowest average roundness, with a mode of 0.4–0.5, correlating to approximately 1 km of fluvial transport. This suggests a gold source is located within the lower reaches of Cyr Creek. Based on an empirically derived relationship between transport distance and roundness (Knight *et al.*, 1999), gold grain transport distances in GLD-205-G1 range from 2 km to more than 10 km (Fig. 7). No correlation was found between particle roundness and fineness, %Ag, or %Cu. If gold populations were sourced from discrete zones of mineralization and had simple fluvial transport histories, gold grains within a geochemical population should have a similar degree of rounding.

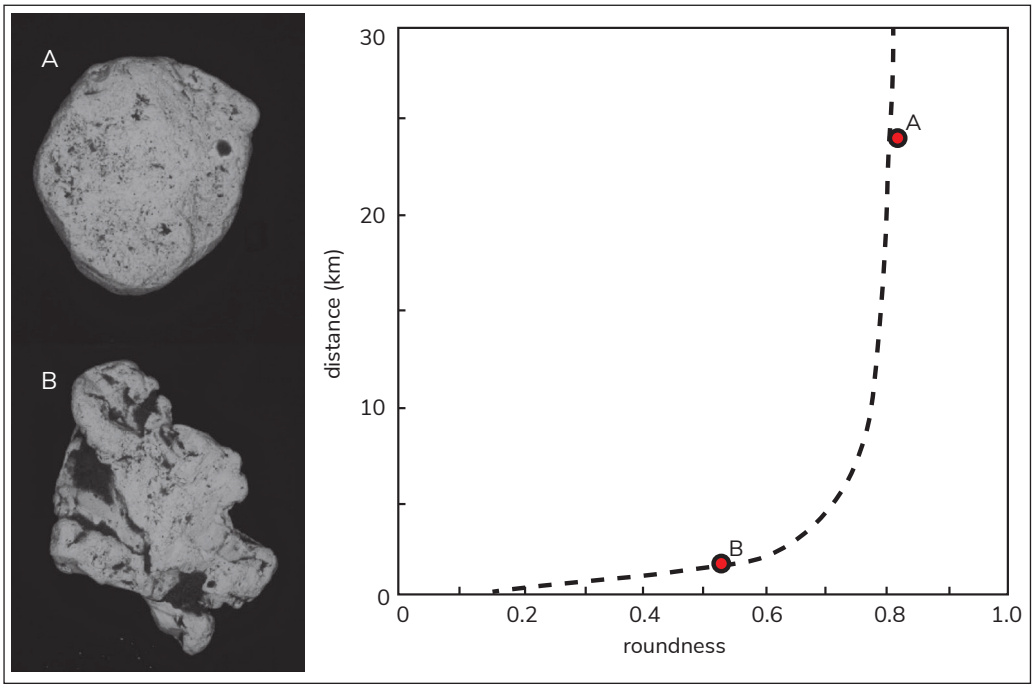

Figure 7. *Electron backscatter image of high-roundness, well-travelled (top) and low-roundness, less-travelled (bottom) gold grains from GLD-205-G1. The more rounded gold grain (0.80) has an estimated travel distance of >10 km, while the less rounded grain (0.53) has travelled approximately 2 km. The roundness-distance curve was empirically determined by analysis of gold grains in the Klondike district (Knight et al., 1999).*

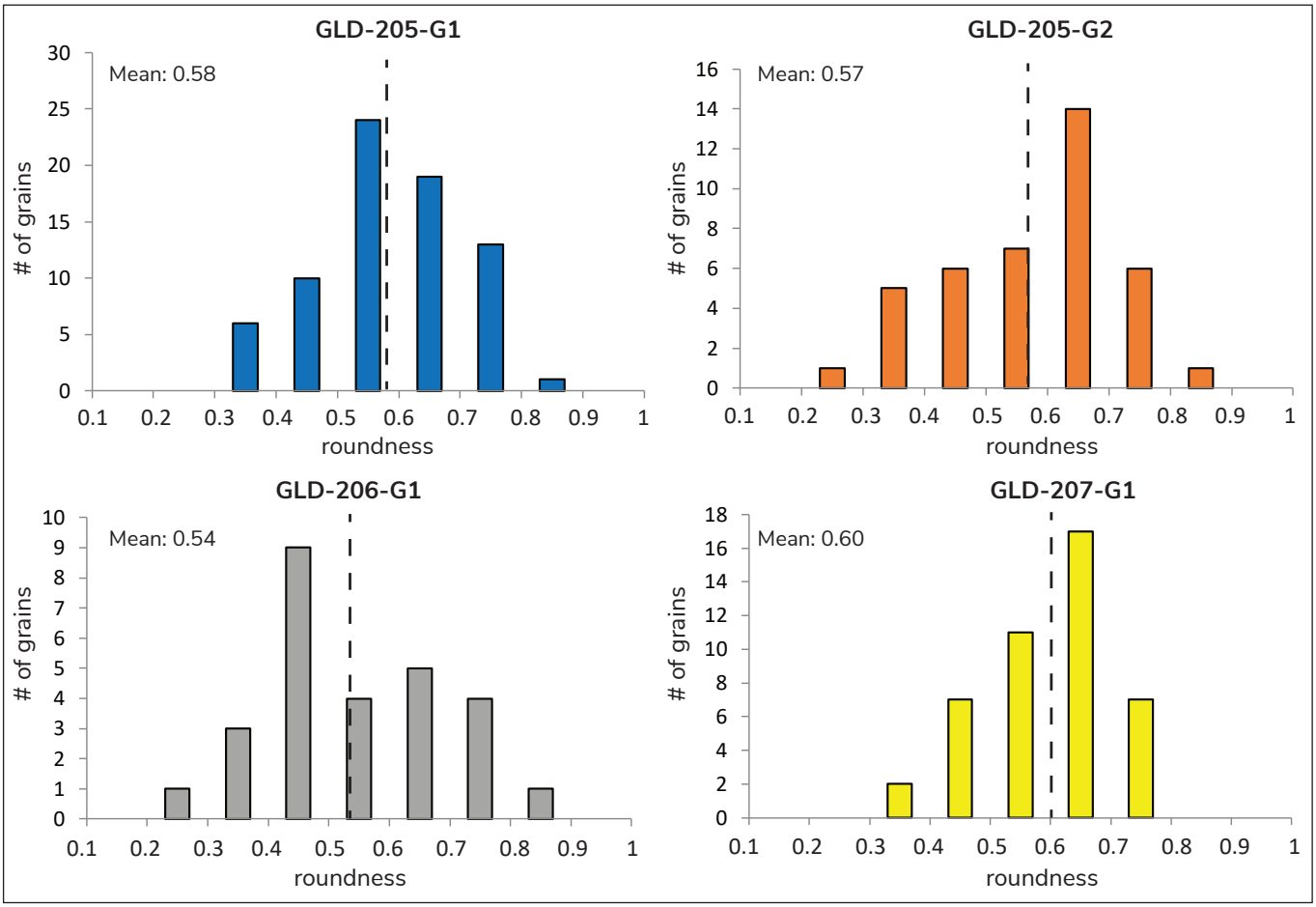

Figure 8. *Comparison of gold grain roundness at sample sites on Gladstone Creek. Dashed lines show the mean roundness of each sample.*

Mineral Chemistry

The proportion of gold, silver, and copper varies greatly within, and between samples (Fig. 9). The fineness of analyzed grains ranges from 22 to 947. Three distinct populations are identified: 950–835, 825–690, and 450–350. GLD-205-G2 contains only a single grain from the highest fineness population.

There are three distinct populations also identified in the distribution of silver content; 3–12% Ag, 38–48% Ag, and 57–60% Ag. Samples GLD-206-G1 and GLD-207-G1 have two high-silver content populations not measured in the samples from GLD-205. This may be due to high silver content in grains sourced from Cyr Creek, downstream of site GLD-205.

Copper content is below detection limits for most gold grains in samples GLD-206-G1 and GLD-207-G1. GLD-205-G1 and GLD-205-G2 have a relatively large range in copper content, between 0.02 and 0.13%, and a few outliers in GLD-205-G1 having approximately 0.25–0.3% Cu.

Chapman et *al.* (2011) used previously established gold alloy compositions from lode gold sources (Townley et *al.*, 2003) to differentiate between epithermal, gold-rich porphyry and gold-rich porphyry copper deposits. Using this method (Fig. 10), we find that epithermal mineralization is the dominant source of gold grains containing <10% Ag, and lesser amounts are derived from gold-rich porphyry mineralization. Gold grains from GLD-206 are not entirely classified in Figure 10 due to high Ag content (>10%) in more than half of the analyzed grains. Multiple grains contain more than 50% Ag. One grain in GLD-205-G2 was predominantly composed of Pb and S, suggesting galena is present from at least one of the sources.

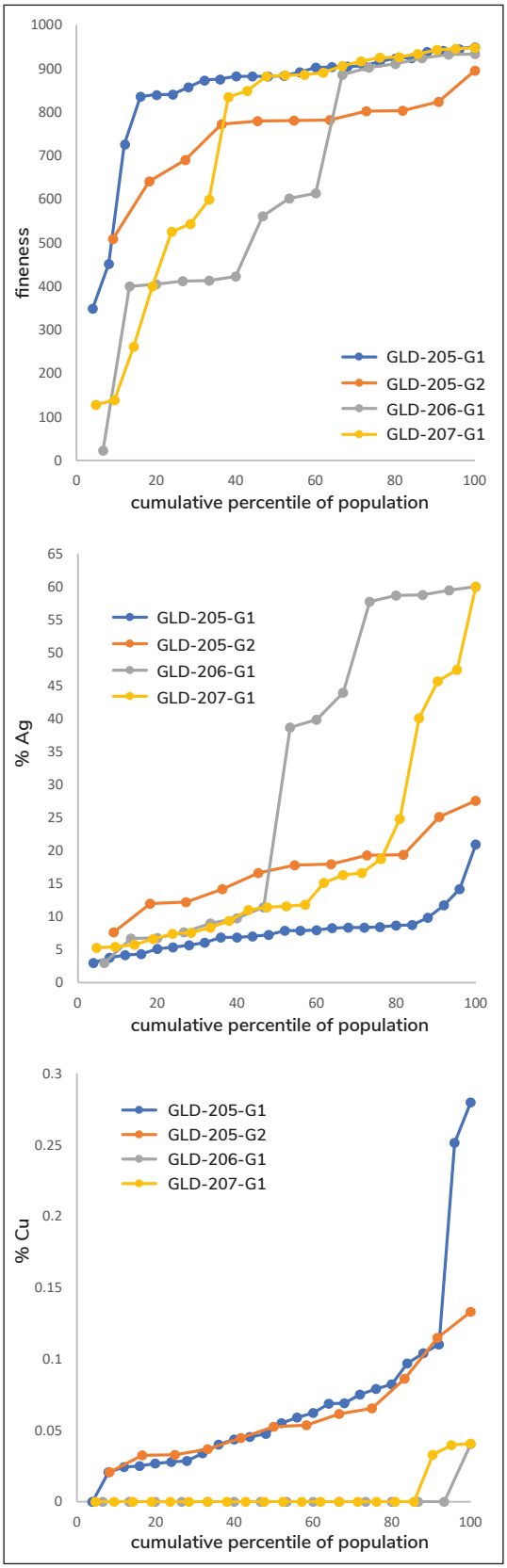

Figure 9. *Composition of major elements in sampled gold grains.*

Discussion

Source Mineralization

Most placer mines in the Ruby Range are underlain by Kluane schist, making it the most prospective source of placer gold. Figure 10 illustrates that most of the gold grains having <10% Ag appear to be derived from epithermal or gold-rich porphyry mineralization, though this requires further confirmation. The gold

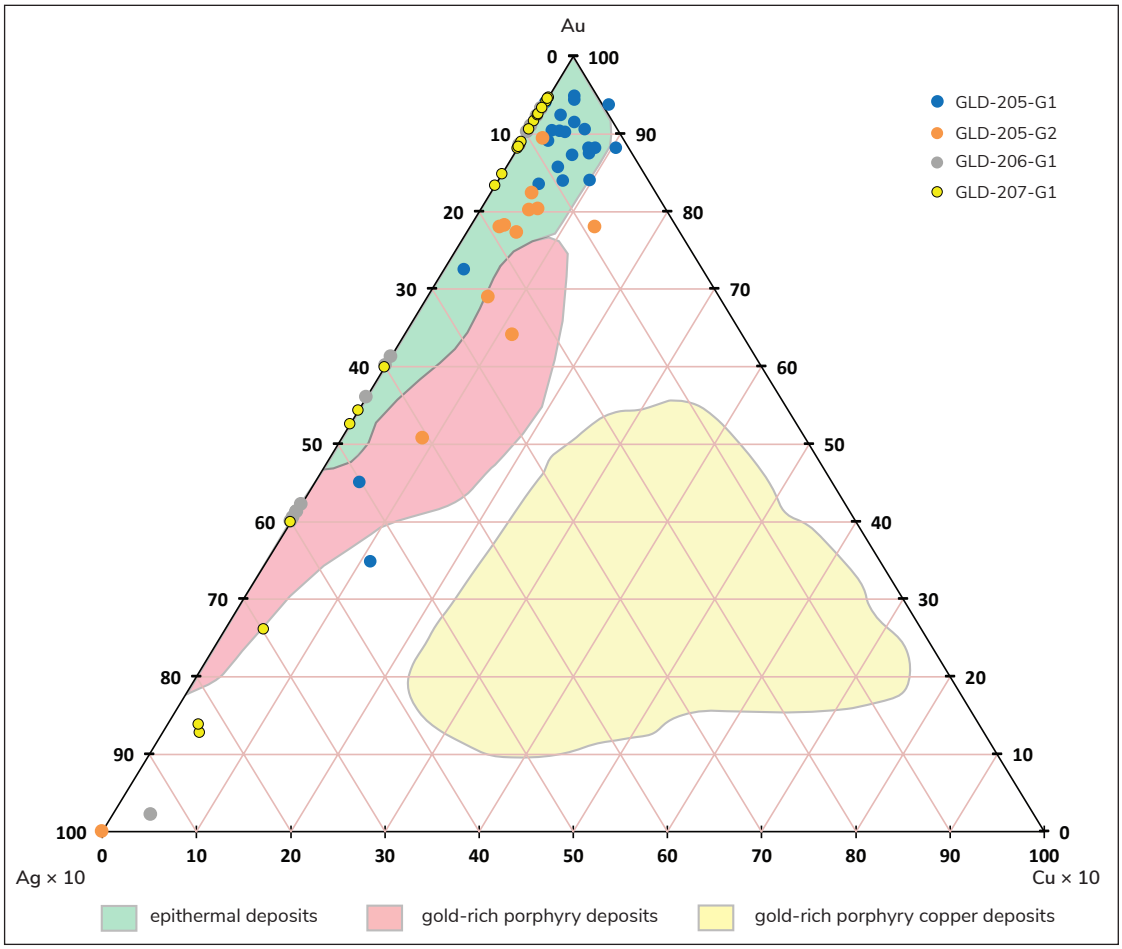

Figure 10. *Au, Ag, and Cu plotted against composition ranges of epithermal, gold-rich porphyry, gold-rich copper porphyry deposits from Townley et al. (2003). Epithermal mineralization appears to be the dominant contributor to placer gold within Gladstone Creek, with minor contributions from gold-rich porphyry; however, many gold grains do not fit on this diagram due to >10% Ag content.*

grains having >10% Ag do not appear on this diagram and make up more than 50% of sampled gold grains, are likely orogenic gold from the Kluane schist. Stream sediment geochemistry in tributaries on the south side of lower Gladstone Creek have gold anomalies as high as 1315.5 ppb, with Swanson Creek having the highest values (Berdahl, 2013). These tributaries are therefore likely contributors to placer gold in Gladstone Creek.

Identifying gold particles derived from orogenic mineralization is commonly not possible based on Au, Ag, and Cu alone. Chapman *et al.* (2018) suggest that analysis of mineral inclusions may allow for differentiation, based on the presence of Bi-Pb-Te-S in the inclusions. Analysis of the geochemical signatures of inclusions is a logical next-step for further work to confirm the suspected contribution of orogenic gold from Kluane schist.

Gold from porphyry and related epithermal systems is typically above 800 fineness (Sillitoe, 2000). Native gold particles coarse enough to be sorted into placer deposits are rare in the main porphyry, therefore, placer gold is typically sourced from later-stage epithermal mineralization (Chapman *et al.*, 2018). This epithermal mineralization may be related to Cu-Mo-Au porphyries (Yukon MINFILE 115G 070, 071) in the drainages north of Gladstone Creek. One active placer mine on Bliss Creek, 10 km north of Gladstone Creek, overlies Ruby Range batholith (Bond and van Loon, 2018), supporting the possibility of the batholith hosting other gold deposits.

Placer in a Glaciated Landscape

The stratigraphy exposed on Gladstone Creek records at least three glacial advances, represented by till units and associated glaciofluvial and glaciolacustrine deposits, and intervening non-glacial stages. The three tills in section likely correlate to MIS 2, 4 and 6. Radiocarbon ages and tephra constrain the MIS 2 and 4 tills. The lowest till, GLD-205 Unit 1, has no lower age constraint. This till is suspected to be MIS 6; pre-Reid glaciation in southwestern Yukon was much less extensive than MIS 6 and has only been observed in sections on the west side of the Shakwak trench, much closer to source areas (Turner *et al.*, 2016). If this interpretation of the stratigraphy is correct, the GLD-205-G2 placer deposit would have accumulated during the MIS 5 interglacial. GLD-205 Unit 4 is a till not bracketed by glaciolacustrine sediment, diagnostic of up-valley ice from the St Elias lobe, suggesting down-valley ice from the Ruby Range preceded arrival of the CIS. GLD-205-G1 accumulated during MIS 3, an interstadial period, and GLD-206-G1 accumulated during the Holocene (MIS 1). GLD-207-G1 is suspected to have accumulated on an erosion- resistive glacial-stage floodplain surface.

The placer deposits examined in this study all appear to have accumulated during interglacial periods, or during later phases of deglaciation when valleys are ice-free, providing lower base levels and allowing incision through glacial sediments. It is likely that pre-glacial deposits exist in paleochannels somewhere under the thick stratigraphy of Gladstone Creek, but have not yet been uncovered. Bedrock crops out at one location on lower Gladstone Creek, approximately 400 m above GLD-205. It is likely that most of the pre-glacial placer accumulation would have occurred on this bedrock surface.

Placers sampled at GLD-205 and GLD-207 accumulated on clay-rich glacial sediment (GLD-205 Unit 1 and Unit 4) and paleosurfaces (GLD-207 Unit 2). Clay-rich glaciolacustrine units found elsewhere in Gladstone Creek may also limit downcutting (*cf.* Levson and Blyth, 1994) and should be explored for placer accumulation.

Gold grain populations defined by fineness (Fig. 9) are morphologically heterogeneous (Fig. 8). This could be due to widespread mineralization in the vein systems in the Kluane schist resulting in wide-ranging transport distances. In Gladstone Creek, some of the gold would have been transported by ice and subsequently subject to fluvial transport, thus transport distance curves may not apply as morphological modification may occur at different rates during glacial transport. This is a possible explanation for the indistinct rounding signatures of the samples, despite large differences in chemical composition. Based on transport distances suggested by gold grain roundness, gold sourced from mineralization in the Ruby Range batholith must have been transported in part by down-valley ice.

Conclusions

Economic placer deposits accumulate where bedrock, or resistant false-bedrock materials such as till or other relatively impervious surfaces, limit downcutting. Regional studies of glacial history and ice flow directions suggest the possibility of distal-intrabasinal and extrabasinal gold sources; however, in Gladstone Creek the most likely sources of mineralization are local Kluane schist and the Ruby Range batholith. Geochemical analysis suggests three populations of gold are present in Gladstone Creek. A high fineness population may be derived from epithermal mineralization, the other appears to be derived from gold-rich porphyry mineralization, both of which are likely hosted by the Ruby Range batholith. More than half of the gold grains sampled are not well constrained by Au-Ag-Cu analysis and are suspected of being derived from orogenic mineralization within Kluane schist. Further analyses, including gold grain microchemistry and inclusion mineralogy, are required to confirm these results.

Acknowledgements

This project took place in the Traditional Territory of the Kluane First Nation. The authors would like to thank Alan Dendys and the TIC Exploration crew for their hospitality and for sharing their local knowledge and enthusiasm for placer mining with us. We thank Megan Simao for

providing capable field assistance and never refusing a till fabric or pebble lithology count. Radiocarbon sample preparation was completed by Alice Telka of Paleotec Services. Britta Jensen, University of Alberta, identified the Dawson tephra. This study was supported by the Yukon Geological Survey and the Canadian Northern Economic Development Agency's Strategic Investments in Northern Economic Development (SINED).

References

Berdhal, S. 2013. Geochemical Assessment Report for Work Performed on the Gladstone Property. Yukon Energy, Mines and Resources Assessment Report 096163, 46 p.

Bond, J.D. and van Loon, S., 2018. Yukon Placer Mining Industry 2015 to 2017. Yukon Geological Survey, 284 p.

Cairnes, D.D. 1915. Exploration in southwestern Yukon. Summary Report of the Geological Survey Department of Mines for the calendar year 1914.

Chapman, R.J., Allan, M.M., Mortensen, J.K., Wrighton, T.M. and Grimshaw, M.R., 2018. A new indicator mineral methodology based on a generic Bi-Pb-Te-S mineral inclusion signature in detrital gold from porphyry and low/intermediate sulfidation epithermal environments in Yukon Territory, Canada. Mineralium Deposita, vol. 53, p. 815–834.

Chapman R.J., Mortensen J.K. and LeBarge W.P., 2011. Styles of lode gold mineralization contributing to the placers of the Indian River and Black Hills Creek, Yukon Territory, Canada as deduced from microchemical characterization of placer gold grains. Mineral Deposita, vol. 46, p. 881–903.

Cronmiller, D.C., Ward, B.C. and Bond, J.D., 2018. Surficial Geology of Gladstone Creek (115G/08), Yukon (1:50 000 scale). Yukon Geological Survey, Open File 2018-20.

Froese, D.G., Westgate, J.A., Preece, S.J. and Storer, J., 2002. Age and significance of the late Pleistocene Dawson tephra in eastern Beringia. Quaternary Science Reviews, vol. 21, p. 2137–2142.

Hughes, O.L., Campbell, R.B., Muller, J. and Wheeler, J.D., 1969. Glacial limits and flow patterns, Yukon Territory south of 65° N latitude. Geological Survey of Canada, Paper 68–34.

Hughes, O.L., 1990. Surficial geology and geomorphology, Aishihik Lake, Yukon Territory. Geological Survey of Canada, Paper 87-29, 23 p. and maps.

Israel, S., Murphy, D., Bennett, V., Mortensen, J. and Crowley, J., 2011a. New insights into the geology and mineral potential of the Coast Belt in southwestern Yukon. In: Yukon Exploration and Geology 2010, K.E. MacFarlane, L.H. Weston and C. Relf (eds.), Yukon Geological Survey, p. 101–123.

Israel, S., Cobbett, R., Westberg, E., Stanley, B. and Hayward, N. 2011b. Preliminary bedrock geology of the Ruby Ranges, southwest Yukon (Parts of NTS 115G, 115H, 115A and 115B) (scale 1:150 000). Yukon Geological Survey, Open File 2011-2.

Knight, J.B., Morrison, S.R. and Mortensen, J.K., 1999. The Relationship between Placer Gold Particle Shape Rimming and Distance of Fluvial Transport as Exemplified by Gold from the Klondike District Yukon Territory, Canada. Economic Geology, vol. 94, p. 635–648.

Levson, V.M. and Blyth, H. 1994. Applications of Quaternary geology to placer deposit investigations in glaciated areas; a case study, Atlin, British Columbia. Quaternary International, vol. 20, p. 93–105.

Madsen, J., 2001. The Quaternary History and Placer Deposits of Gladstone Creek, Southwest Yukon. Unpublished BSc Honours Thesis, University of Victoria.

Muller, J.E., 1967. Kluane Lake map area, Yukon Territory. Geological Survey of Canada, Memoir 340, 137 p.

Sillitoe, R.H., 2000. Gold-rich porphyry deposits: descriptive and genetic models and their role in exploration and discovery. Reviews in Economic Geology, vol. 13, p. 315–345.

Townley, B.K., Herail, G., Maksaev, V., Palacios, C., de Parseval, P., Sepuldeva, F., Orellana, R., Rivas P. and Ulloa, C., 2003. Gold grain morphology and composition as an exploration tool: application to gold exploration in covered areas. Geochemistry: Exploration, Environment, Analysis, vol. 3, p. 29–38.

Turner, D.G., Ward, B.C., Froese, D.G., Lamothe, M., Bond, J.D. and Bigelow, N.H., 2016. Stratigraphy of Pleistocene glaciations in the St Elias Mountains, southwest Yukon, Canada. Boreas, vol. 45, p. 521–536.

Ward, B.C., Bond, J.D. and Gosse, J.C., 2007. Evidence for a 55-50 ka (early Wisconsin) glaciation of the Cordilleran ice sheet, Yukon Territory, Canada. Quaternary Research, vol. 68, p. 141–150.

Yukon MINFILE, 2009. Yukon MINFILE – A database of mineral occurrences. Yukon Geological Survey, http://www.geology.gov.yk.ca/databases_gis.html, [accessed November, 2018].

Evaluating geothermal potential in Yukon through temperature gradient drilling

T. Fraser, M. Colpron, C. Relf
Yukon Geological Survey

Fraser, T., Colpron, M. and Relf, C., 2019. Evaluating geothermal potential in Yukon through temperature gradient drilling. *In:* Yukon Exploration and Geology 2018, K.E. MacFarlane (ed.), Yukon Geological Survey, p. 75–90.

Abstract

As part of the Canadian government's commitment to establishing clean energy in the North, the Yukon Geological Survey is collecting subsurface temperature data near communities in the southern part of the territory. The research is a collaborative effort among federal and territorial geoscientists, universities, First Nation governments, and geothermal consultants. A major goal of the project is to determine whether ground temperatures warrant further geothermal exploration in the territory. The study also presents an opportunity for Yukon Geological Survey to educate the public about geothermal energy. This paper summarizes the methods and results of the drilling of two ~500 m geothermal temperature gradient wells. The first was drilled in the fall of 2017 in the Whitehorse area, near Takhini Hot Springs, where a surface water seep measures 46°C. The second well was drilled in winter 2018 in the Tintina fault system, near Ross River. Results to date suggest warm fluids and possible permeable rocks in the Takhini well between 450 and 500 m from surface, and a higher than average geothermal gradient of ~31°C/km in the Tintina Trench near Ross River. The results do not indicate temperatures for power generation at economic depths, however, they are encouraging enough to warrant further geothermal studies in southern Yukon.

* tiffani.fraser@gov.yk.ca

Introduction

Adjacent to the 'Pacific Ring of Fire', the Yukon Territory in northwestern Canada is a prime candidate for geothermal energy. Major geological features, such as the Tintina and Denali faults (Fig. 1), abundant plutonic rocks, extensive sedimentary rock cover, and numerous seeps and hot springs (Fig. 1) all suggest the possibility of elevated geothermal heat. Previous studies of heat flow and geothermal potential in Yukon relied primarily on sparse and incomplete geoscience data. In 2016, the Yukon Geological Survey initiated a geothermal research project that aims to model areas of high heat flow using existing geological, geochemical and geophysical data, and enhance existing subsurface temperature data by drilling targeted, slimhole temperature gradient (TG) wells in specific geological settings. Primary funding for the project is from the Government of Canada (Canadian Northern Economic Development Agency's Strategic Initiatives in Northern Economic Development (SINED) Fund) and Yukon government. Research partners include the Geological Survey of Canada, University of Alberta, Innovate Geothermal Ltd., Ta'an Kwäch'än Council (TKC), and Ross River Dena Council (RRDC). This paper describes one element of the study, specifically the selection of drill locations and results from two TG wells in southern Yukon near the communities of Whitehorse and Ross River. The study aligns with Canada's interest in reducing remote northern communities' reliance on hydrocarbons for power and heat. Providing baseline geothermal data, and targeting areas of higher heat flow, will reduce geothermal exploration risk in Yukon and potentially drive a shift to development of local clean energy supplies to support remote northern communities.

Background

Energy Supply

In contrast to the United States, which is the world's biggest producer of geothermal power, Canada generates no electricity from geothermal energy, although there is some direct use for district heating applications (Raymond *et al.*, 2015). In Yukon ~94% of the territory's power is currently produced by hydro-generating stations and distributed to most communities (Yukon Energy Corp., 2018), making Yukon one of Canada's leaders in "green" energy. However, Yukon's population is growing rapidly and there are several advanced mineral exploration programs, with a few likely to develop into mines, which will put pressure on the existing electrical grid, or require on-site electrical generation in areas not connected by transmission lines. Diesel and liquefied natural gas are used for back-up on Yukon's grid, particularly in cold winter months or during peak usage times, and four Yukon communities rely solely on diesel-power generation. As no operating pipeline connects Yukon to southern Canada, diesel must be trucked up to the territory along the Alaska Highway and distributed to communities on the local road network. Old Crow, as a fly-in community that uses diesel for electrical production, requires all petroleum products to be flown in at a large expense. Direct usage of geothermal energy in Yukon is limited to low-grade systems to keep water systems from freezing (*e.g.*, Mayo and Haines Junction), and the Takhini Hot Springs resort north of Whitehorse which uses the water for bathing. It is estimated that 74% of space heating in 2016 used fossils fuels (oil and propane), supplemented by 26% renewable sources (wood and wood pellets, and electricity; Yukon Government Energy Branch, 2018). While geothermal power production is not currently top-of-mind for Yukoners, district heating represents a significant opportunity that could see immediate reduction in greenhouse gas emissions.

Previous Geothermal Research in Yukon

In addition to traditional knowledge of hot spring or seep locations from Yukon First Nations (D. Irvine, *pers. comm.*, 2017) our modern understanding of heat flow and geothermal potential in the territory began with the Government of Canada's Geothermal Energy Program (CGEP; see Jessop, 2008a,b; Grasby *et al.*, 2012) which existed between 1976 and 1986. Several Yukon-specific publications resulted from this program including thermal and mineral spring studies (Crandall and Sadlier-Brown, 1978); and temperature profile, heat flow, thermal conductivity, geothermal gradient and depth-temperature maps derived from petroleum and mineral exploration wells (*e.g.*, Geotech Ltd., 1984; Burgess *et al.*, 1982; Majorowicz and Morrow, 1998; Jessop *et al.*, 1984, 2005; Majorowicz

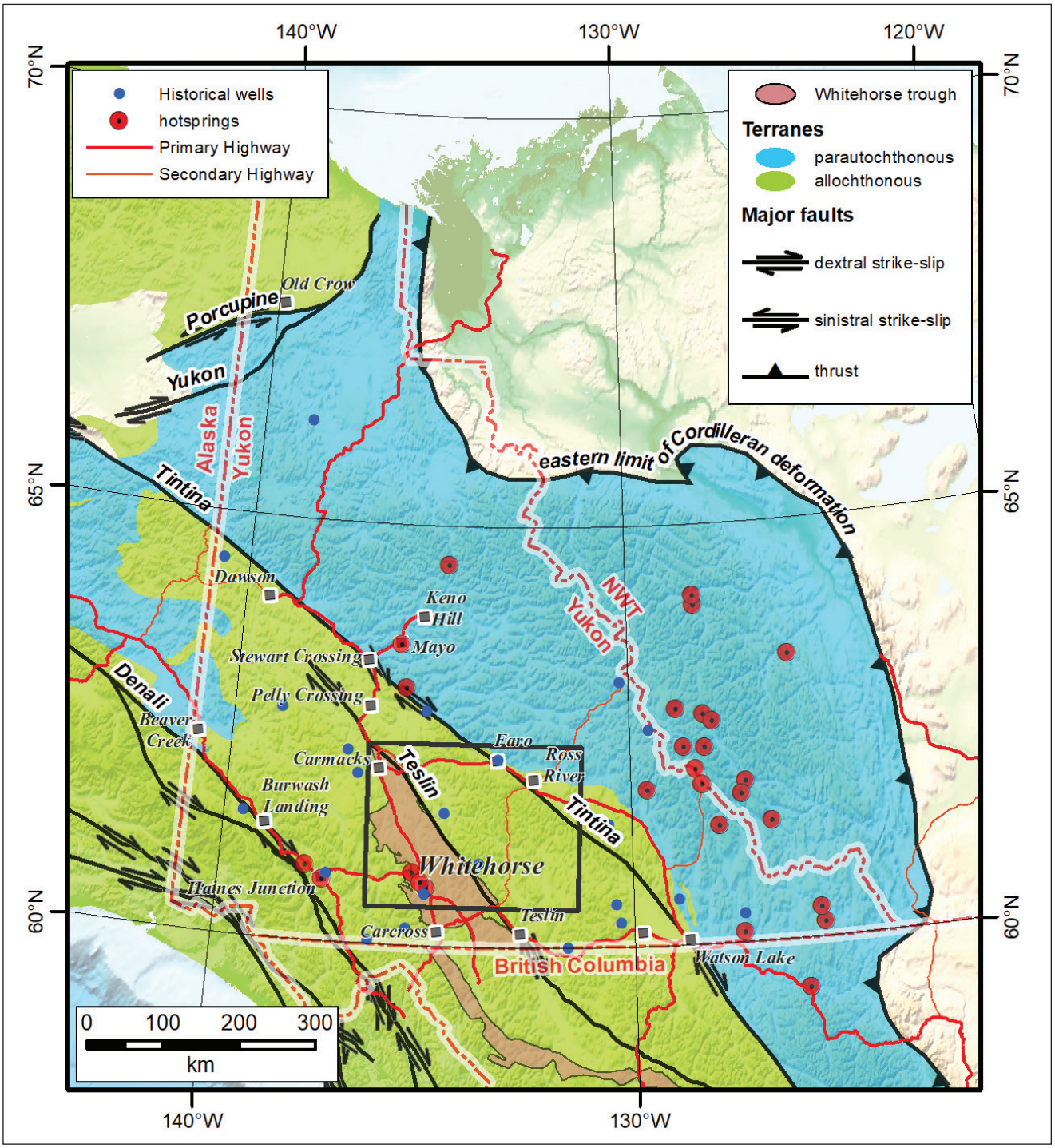

Figure 1. *Simplified terrane map of Yukon showing the distribution of parautochthonous rocks of the Ancestral North American margin, allochthonous terranes of island arc and oceanic affinities, and major crustal faults. The Jurassic Whitehorse trough is shown in brown. Also indicated are the locations of known thermal springs and historical wells from which bottom temperatures were obtained. The black box indicates the area of Figure 2.*

and Dietrich, 1989; Fig. 1). However, these data are sparsely distributed, mostly distal to population centres, are at variable depths, and typically only have one temperature data point (basal temperature only), which can give misleading geothermal gradients. Further, none of these wells were specifically drilled for geothermal exploration, and borehole temperatures likely do not reflect stabilized temperature conditions.

Since the end of CGEP, there have been additional geothermal-related studies. Grasby *et al.* (2000) published an analysis of thermal spring chemistry and geothermometry at Takhini Hot Springs, north of Whitehorse, as part of a larger project looking at the geochemistry of thermal springs in western Canada. Lewis *et al.* (2003) republished some of the heat flow measurements from a number of exploration wells from the CGEP program, and also added seven new measurements from Yukon mineral exploration holes. These data were used to model crustal temperatures in the Cordillera and indicate that heat flow and generation in the Canadian Cordillera north of 59°N (*i.e.*, northern BC and Yukon) is very high (105 ± 22 mW/m^2). A series of confidential studies were commissioned for Yukon Energy Corporation (YEC; a publicly-owned electrical utility) between 2009 and 2013 to collect baseline technical data on potential geothermal sites near a series of hot/warm springs in the territory for the purpose of electricity generation. A published geothermal economic resource analysis by KGS Group (2016) for YEC, based on these confidential studies, concluded that there is a modest geothermal resource available for development in Yukon, with relatively low (<150°C) inferred temperatures, requiring the use of a binary geothermal power plant. However, the study recommended further geological information to adequately evaluate the resources, including drilling TG wells.

In 2012, EBA Engineering Consultants Ltd., drilled a 387 m deep water well for Government of Yukon on behalf of the Kluane First Nation. The well was drilled in the community of Burwash Landing (Fig. 1) to determine the potential of future geoexchange applications. Although the report was never published, the results indicated an elevated geothermal gradient, with the well yielding 16°C water.

In 2014, the Dena Nezziddi Development Corporation of RRDC commissioned a geothermal exploration program of the Tintina fault zone near Ross River (Figs. 1 and 2) to explore options for community heat. This study represents the most comprehensive geothermal exploration program to date in Yukon and presents integrated field-based structural analysis and mapping, with acquisition and interpretation of aeromagnetic and magnetotelluric geophysical data (Mira Geoscience, 2017). This study identified ten drilling targets, one of which was drilled as part of this current study.

In 2016, the Canadian Geothermal Energy Association (CanGEA) published geothermal favourability maps of Yukon based on compilation of existing qualitative and quantitative information about local temperature profiles, geothermal gradient, estimated conductivity, heat flow and technical and theoretical potential (CanGEA, 2016).

Geological Setting

On a regional scale, the rocks in Yukon can be divided into two main domains: rocks that developed on the continental margin of ancestral North American (Laurentia) mainly during the Paleozoic, and those that accreted to the western margin of North America, mainly during the Mesozoic. For the most part, the dividing line between Laurentian or parautochthonous rocks to the northeast and accreted or allochthonous terranes to the southwest is the northwest-striking Tintina fault: one of the most prominent physiographic and geologic features in Yukon (Figs. 1 and 2). The fault is a steeply northeast-dipping dextral strike-slip fault that has ~430 km of early Cenozoic displacement (Gabrielse *et al.*, 2006) with mild activity still recorded today (Leonard *et al.*, 2008). In the corridor between Ross River and Faro, the location of one of the TG wells described in this study, the fault zone is approximately 4 to 10 km wide and consists of six prominent subparallel fault strands linked by a series of high-angle extensional faults (Fig. 3; Mira Geoscience, 2017; Yukon Geological Survey, 2018). Mapped bedrock geology in the fault zone is dominantly Carboniferous sedimentary and volcanic rocks, and Eocene volcanic, volcaniclastic and minor sedimentary rocks, in many areas covered by Pleistocene glaciofluvial and moraine deposits (Mira Geoscience, 2017; Turner, 2014).

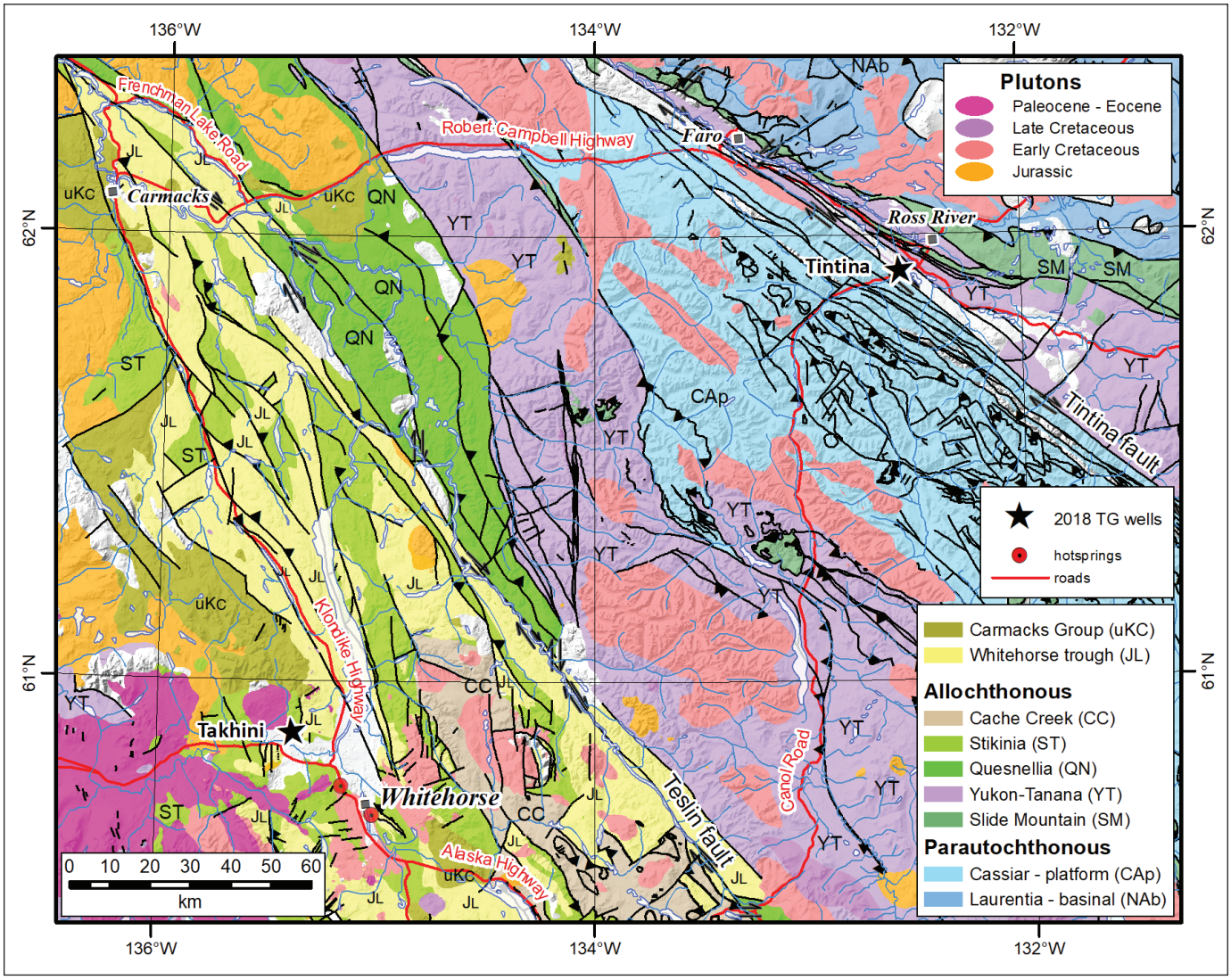

Figure 2. *Simplified geological map of part of southern Yukon showing locations of the two TG wells drilled as part of this study. Geology from Yukon Geological Survey (2018).*

Southwest of the Tintina fault, the Whitehorse trough is a Mesozoic marine sedimentary basin that occupies an elongated belt stretching from north of Carmacks, and extending 650 km south through Whitehorse and into northern British Columbia (Figs. 1 and 2). The basin comprises Lower to Middle Jurassic sedimentary and volcanic rocks that were deposited in a synorogenic basin developed during accretion of allochthonous island arc and oceanic terranes (Colpron et *al.*, 2015). Near Whitehorse, and the Takhini TG well location in this study, Jurassic sedimentary rocks of Whitehorse trough overlie Upper Triassic marine sedimentary, volcanic and volcaniclastic rocks of island arc affinity (Hart, 1997; Fig. 4). Approximately 2 km west of the drill location, an Eocene (54 Ma; Hart, 1997) granitoid pluton intrudes Whitehorse trough and older rocks, including Upper Triassic thick-bedded limestone (Figs. 2 and 4; Yukon Geological Survey, 2018).

Regional ground temperature data for Yukon is sparse. Geothermal gradients compiled for Canada are shown in Figure 5, sourced mainly from bottom-hole temperatures in exploration wells (Grasby et *al.*, 2012; see Fig. 1 for Yukon well locations). This sparse data set indicates that southern Yukon has a geothermal gradient

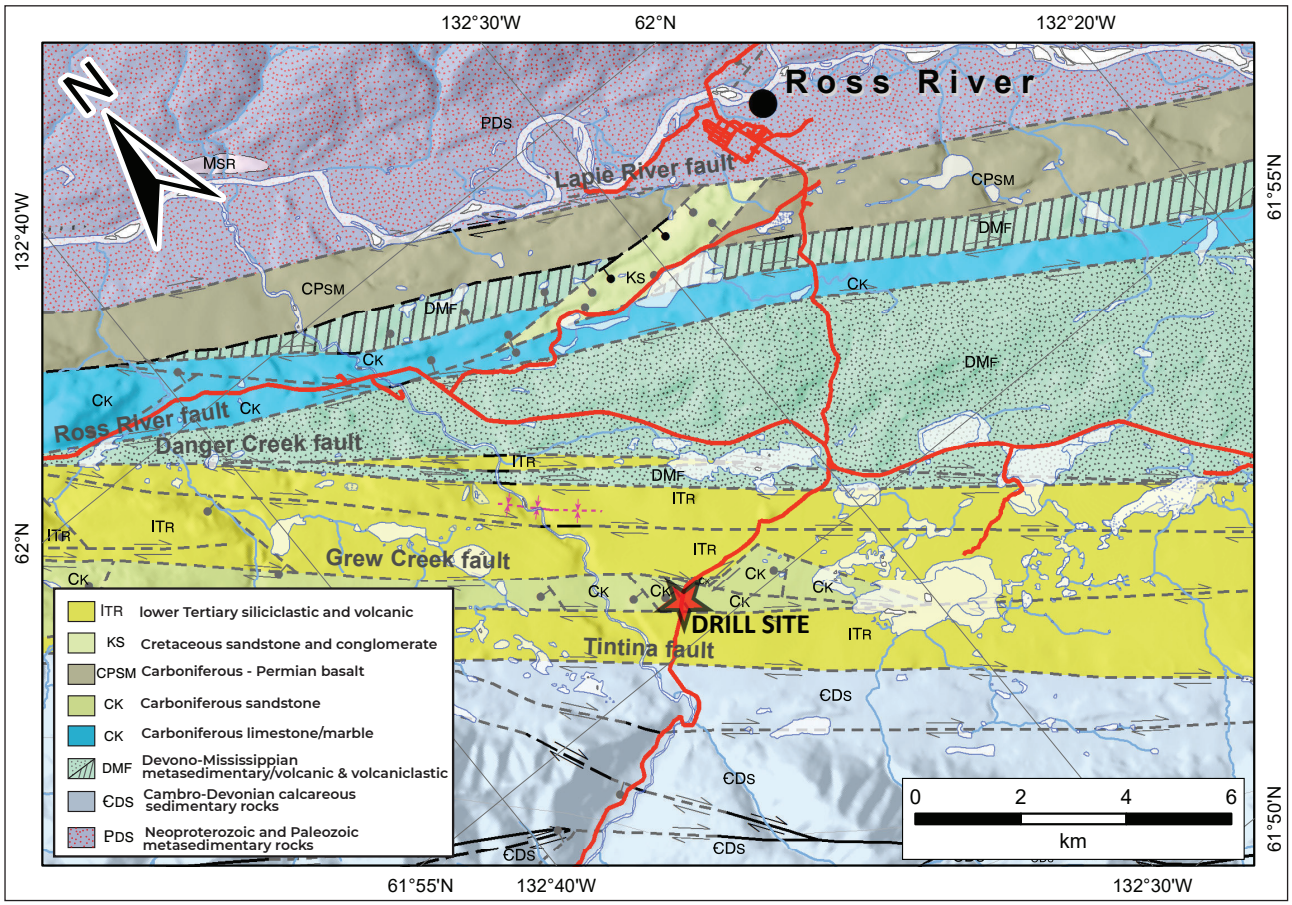

Figure 3. *Geology in vicinity of Tintina Trench TG well southwest of Ross River (geology after Mira Geoscience, 2017).*

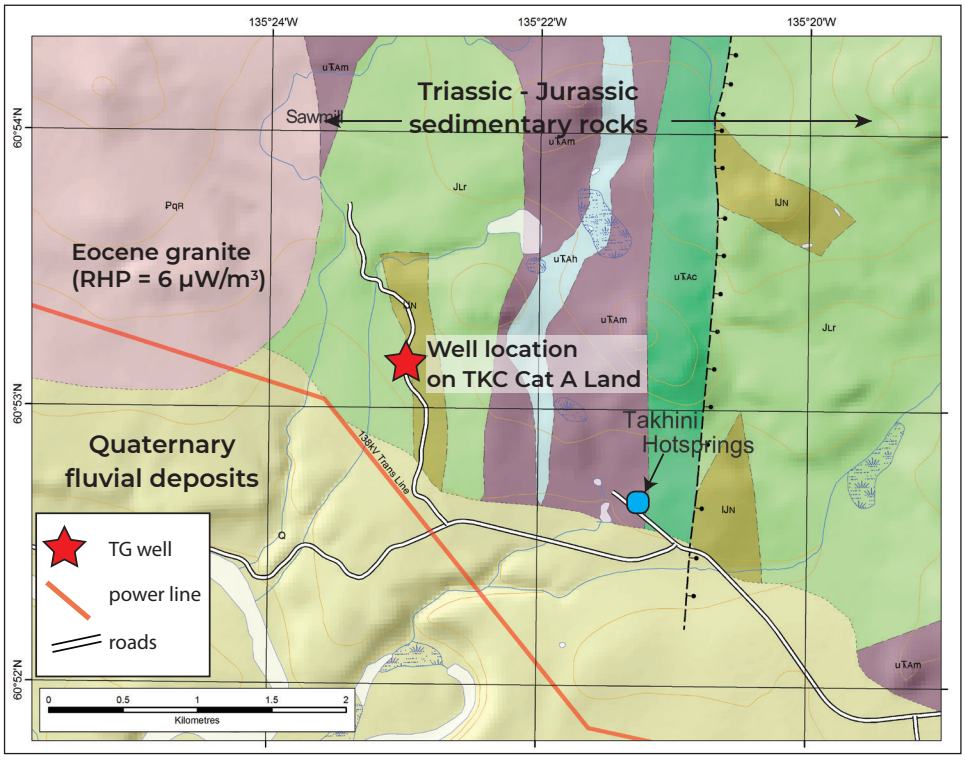

Figure 4. *Geology in vicinity of Takhini TG well (geology from Yukon Geological Survey, 2018). RHP stands for radiogenic heat potential; TKC Cat A Land stands for Ta'an Kwäch'än Council Category A Settlement Land.*

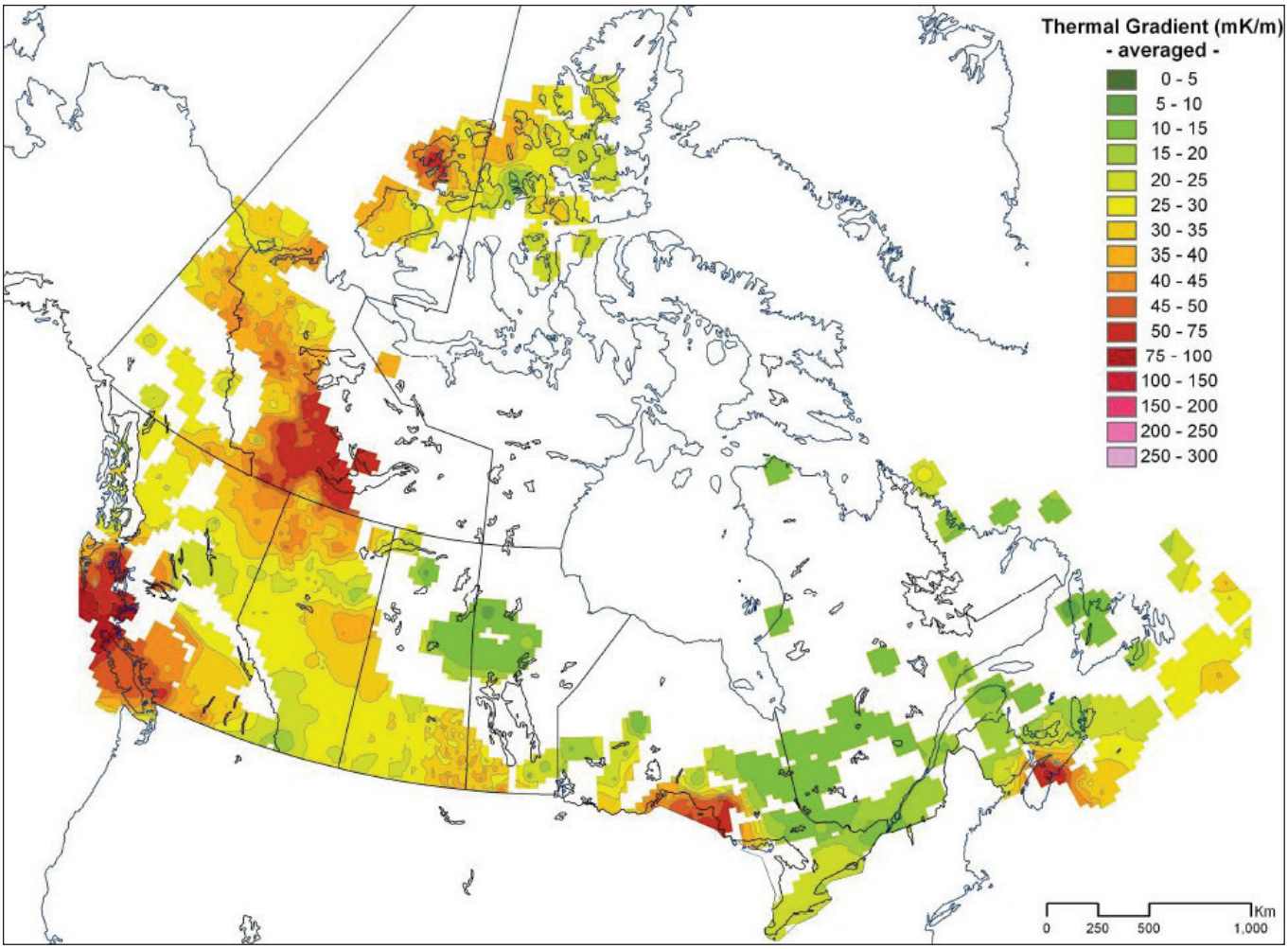

Figure 5. *Contour map of the geothermal gradient in Canada (Grasby et al., 2012). Note that mK/m units are equivalent to °C/km.*

of ~25°C/km which is equivalent to the global average for the upper crust, with slightly higher values of up to 40°C/km in the north. However, it is clear that there is a distinct lack of data overall, particularly in southern Yukon. Based on the regional geological setting, Yukon has geothermal potential for high temperature power generation from volcanic and hot sedimentary basin settings in the south, and potential for direct heat/exchange systems from either cool sedimentary basin settings or fractured rock throughout the territory (Fig. 6). A goal of this study is to fill in some of the gaps in the regional ground temperature data set.

Methods

Prior to drilling, YGS undertook a series of desktop studies to identify potential drill sites including geological evaluation, Curie Point Depth Mapping (CPD) and calculation the radiogenic heat potential of Cretaceous and younger granitoid rocks. Methods and results of the CPD can be found in Witter and Miller (2017) and Witter et *al.* (2018), and the distribution of radiogenic granitic rocks in Friend and Colpron (2017). The CPD mapping suggests that the greatest heat flow to surface in the territory is in south-central and southwestern Yukon, results that are corroborated by the global study of CPD by Li et *al.* (2017). The areas of highest radiogenic heat potential from granitic

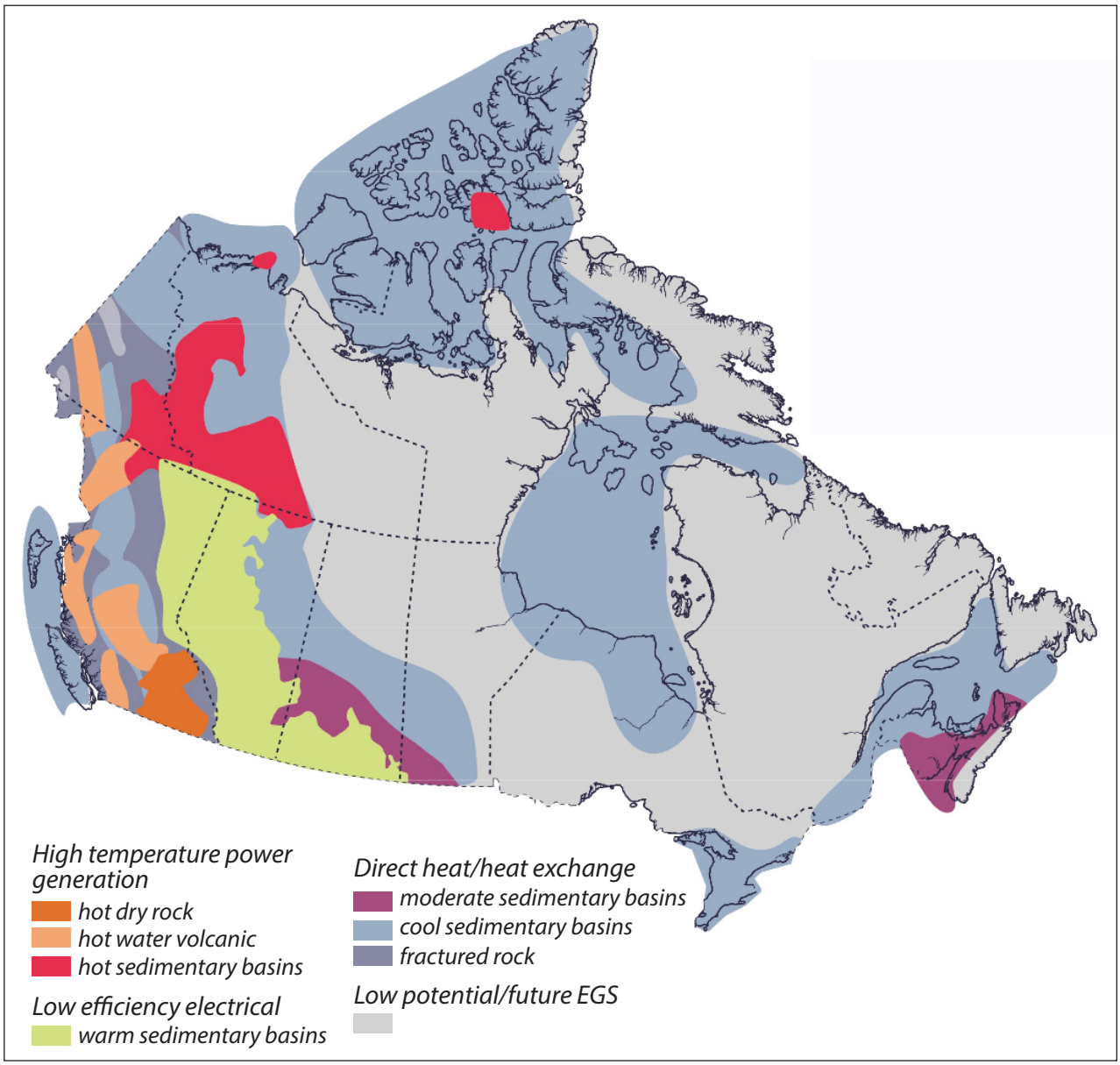

Figure 6. Geothermal potential map of Canada based on end use (Grasby et al., 2012).

rocks are associated with Cretaceous (not younger) granite, particularly northeast of Tintina fault and in a belt between the Teslin and Tintina faults. An additional exercise was conducted to identify potential drill targets based on non-geological factors such as road access, distance to power lines and population centres. Although several targets were identified as good candidates, adequate funds were available to drill two 500 m wells only. After considerable discussion, a decision was made to drill one hole close to Takhini Hot Springs, near Whitehorse, and the other hole near Ross River, in the Tintina Trench. These two locations allowed for the testing of two potential geothermal settings in southern Yukon.

The first site, near Takhini Hot Springs, approximately 30 km northwest of Whitehorse (Takhini on Fig. 2), was chosen to test a hypothesis that the hot water at the springs is the result of the radiogenic heating of meteoric water hosted in a permeable carbonate host rock. The drill location is about halfway between the hot

springs and exposures of a radiogenic granitoid pluton (~6 μW/m^3) ~2 km to the west (Fig. 4). Limestone is observed in the area as well. The well site is located on Settlement Lands of the TKC First Nation who granted permission to locate the well here. TKC's development corporation (Da Daghay Development Corporation) was hired to manage contracts for drilling, support services and thermistor installation. Access to the site was *via* an unserviced, former logging road that required minimal grading for equipment mobilization. Drilling to 500 m took 27 days between October 30 and November 26, 2017, with an average daily temperature of -12°C during this period. The first 50 m was drilled using a reverse circulation (RC) drill with a 241 mm (9.5 inch) bit. Bedrock was encountered within one metre of the surface. This section of the hole was cased and cemented to ensure isolation of any potential aquifers. The bottom 450 m was drilled using a diamond drill coring rig with an HQ (63.5 mm or 2.5 inch) core barrel and a blow-out-preventer to control any pressurized fluids. Within a few days of drilling, a thermistor cable was lowered into the hole using the hoisting system of the drill rig. The thermistor string was custom designed with nodes spaced at 50 m intervals for most of the well, and closer spacing (10 m intervals between 10 and 50 m depth; 3 m intervals from surface to 10 m) to document the thickness and temperature of permafrost, if present. The thermistor was connected to a multimeter at surface which required periodic manual readings. The thermistor was removed from the hole in the spring of 2018, and the site remediated.

The Tintina well target near Ross River was chosen to test a geothermal model of meteoric water circulation in a deep crustal fault zone. The location was identified from an analysis of 10 potential sites initially proposed in a technical study by Mira Geoscience (2017) for the Dena Nezziddi Development Corporation. The TG well location is in the right-of-way of the South Canol road (km 216; Figs. 1, 3 and 7), in an area of complex faulting, and near a buried igneous body inferred from geophysical models (Mira Geoscience, 2017). The drilling of this well was done in partnership with the Ross River Dena Council and the University of Alberta, with YGS as project manager. Drilling began on February 23 and continued intermittently until March 29 (34 days). Temperatures in nearby Faro averaged -14°C during the drilling period, but were as low as -40°C at the drill site, causing delays and equipment problems. The original intent was to drill with an RC rig to consolidated bedrock, which was anticipated from surficial studies to be within 35 m of surface. At 140 m the RC rig had exceeded its depth limit and was replaced by a diamond drill. One hundred metres of PW casing

Figure 7. *Photograph of Tintina Trench drill site looking west towards the Pelly Mountains.*

(140 mm/5.5 inch outside diameter) was left in the hole for stability. HQ core was drilled from 140 m to a total depth of 497 m, with competent rock attained at a depth of 207 m. Approximately 3 weeks after completing the hole, a 5 KΩ thermistor string with 20 m node spacing was installed, and a data logger was taking hourly readings. The string was removed from the hole in September 2018, after stabilized temperatures had been reached. Drill core from the hole is being logged by the YGS. The University of Alberta has sampled the core and will be conducting a variety of rock property studies (porosity, permeability, XRD mineralogy) as part of a larger study of the geothermal potential of Tintina Trench and the Rocky Mountain thrust system.

Results

Temperature Gradient Well at Takhini Hot Springs

The Takhini well encountered mostly sandstone, shale and tuffaceous strata of the Whitehorse trough. Approximately two months after installation of the thermistor string, temperatures at depths between 100 and 500 m were stable (with variations ≤0.1°C), while temperatures at depths in the 20–100 m range were stable within three months. After six months, the upper 10 m still exhibited temperature fluctuations which can be attributed to changes in surface air temperature, and it would be expected that shallow depth temperatures would continue to fluctuate year-round. There is no permafrost at this location, as temperatures in the near subsurface are not consistently below 0°C.

The temperature gradient shows a subtle inversion (decrease in temperature with depth) to a depth of ~50 m (Fig. 8). Temperature inversions are common in wells in the north, and are considered a signal of climate warming, whereby a heat pulse is propagating downward and disrupting the near surface temperature field (Majorowicz et *al.*, 2005). Using data below the inversion, ground temperatures increase from 7.0 to 12.8°C to a depth of 450 m, which results in a geothermal gradient of 16.5°C/km, less than the average upper crust of ~25°C/km, and less than the average crustal temperature gradient predicted by the CPD data of Li et *al.* (2017) of ~39°C/km for the Takhini/Whitehorse area. Between 400 and 450 m, the temperature gradient appears to be nearly vertical. Vertical gradients may indicate a permeable aquifer, as temperature stabilization within the permeable zone can be attained through heat convection within fluids. In impermeable zones we would expect to see an increase in heat as heat is transferred by conduction.

Most notable about the temperature profile is the marked temperature increase from 12.8 to 25.3°C at depths between 450 and 500 m. This temperature increase may represent a temperature increase across a fault plane, separating two separate circulation systems with different thermal gradients. It may also represent a fault plane or permeable rock interval hosting warm fluid. What happens to the gradient below the well is speculative: it could settle back to the gradient above 450 m, *i.e.*, 16.5°C/ km, which would put ground temperatures at ~34°C at a depth of 1000 m (Fig. 8); or it could return to the predicted values for the region from the CPD study, *i.e.*, ~39°C/km, where the temperature at 1000 m would be 45°C; or any number of options not presented here. The temperature spike

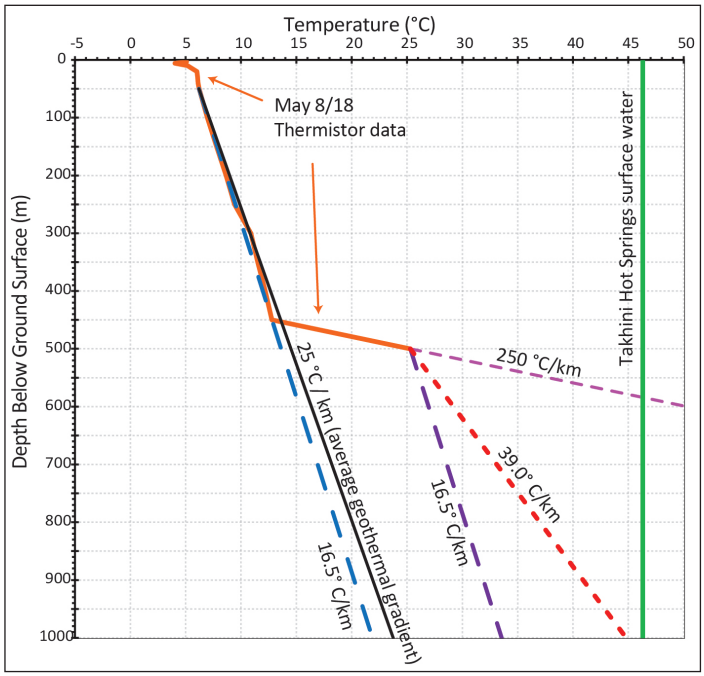

Figure 8. *Stabilized downhole temperature data for the Takhini well, including interpretive geothermal gradients discussed in the text, average geothermal gradient, and the surface water temperature at Takhini Hot Springs.*

could also represent an isolated interruption in the temperature profile caused by warm fluid flow at this depth, for example along a permeable horizon or fault plane, below which the temperature reverts back to the shallower temperature profile with the same geothermal gradient. In this case, ground temperatures at a depth of 1000 m would be in the range of 23°C. Alternatively, the distinct increase in temperature could reflect an impermeable zone of conductive heat transfer from a deeper aquifer. To confirm any of these hypotheses, deeper drilling would be required. An unlikely scenario is that the gradient continues at the rate observed at the bottom of the hole, *i.e.*, 250°C/km, as these values are most commonly seen in tectonically active areas such as volcanic rift zones (Iceland; e.g., Hjartarson, 2015) or volcanic hot spots (Hawaii; e.g., Fowler et *al.*, 1980).

Temperature Gradient Well in Tintina Trench

Cenozoic unconsolidated sediments were encountered in the Tintina well to a depth of 207 m. Preliminary inspection of the core suggests glacial sediments overlying older glaciofluvial and fluvial sediments. Competent sedimentary rock was encountered between 207 and 497 m, including siltstone, sandstone, and pebble conglomerate, however, the age and stratigraphic affinity of these rocks are currently under review. Substantial faulting was encountered in the core, which made drilling and core recovery challenging.

Thermistor readings from 258 m and below were stable (variation was ≤0.1°C) immediately upon thermistor installation (*i.e.*, 3 weeks after drilling ceased). The top 38 m were stable within a few days. These values record temperatures ≤0°C which gives a record of permafrost to at least a depth of 38.4 m (Fig. 9). Intervening thermistor beads were stable 5 weeks post-drilling. The 0 m reading is at ground surface and fluctuates with ambient air temperature. A thermal inversion can be observed to a depth of ~38 m. Below this depth, the temperature gradient is linear at 30.6°C/km (Fig. 9) which is higher than the average crustal gradient and aligns with the predicted average crustal temperature gradient from Li et *al.* (2017) CPD data. The linearity of the data suggests that the subsurface comprises relatively homogenous, low permeability rock that facilitates conductive heat transfer. There is no evidence of permeable zones in the temperature data (*i.e.*, vertical gradient intervals) or temperature spikes that might suggest intervals of hot fluids.

Discussion

The two TG wells drilled for this study represent the first drilled to a depth of 500 m in Yukon that were rigorously investigated for temperature specifically for the purpose of geothermal exploration. The Takhini well does not indicate the presence of permafrost in the near subsurface, but has a thermal inversion to a depth of ~50 m, below which values are believed to represent true geothermal gradient. The data indicate warm water at a depth of 500 m below the surface, however, the well is not deep enough to effectively interpret this reading, and it is unknown whether this is related to the hot water observed at Takhini Hot Springs. It is also difficult to say whether the temperature gradient is higher than average. Further drilling near this location will be necessary to resolve these issues.

Below a thermal inversion of up to ~38 m, with permafrost to at least this same depth, the Tintina well shows a consistent, higher than average geothermal gradient of 30.6°C/km, however, not high enough at

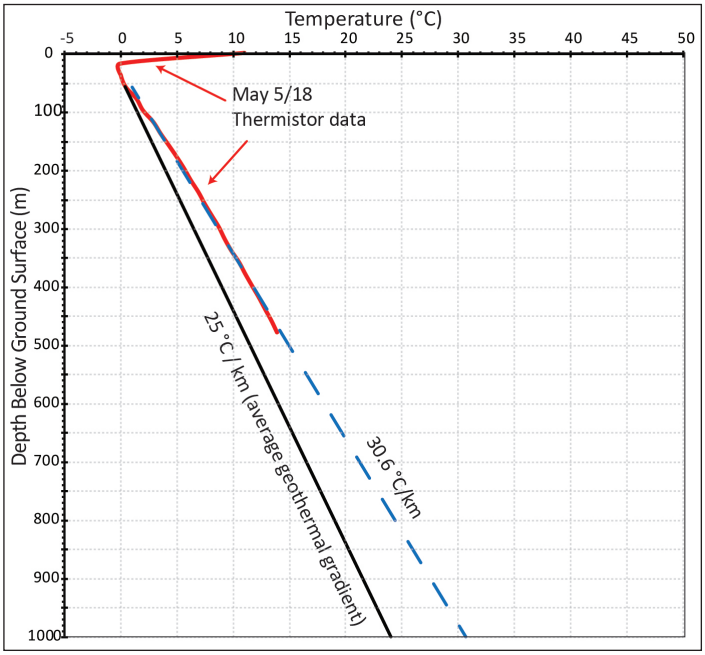

Figure 9. *Stabilized downhole temperature data for the Tintina well, including the interpreted geothermal gradient.*

this location for power generation at an economic depth. The location along an extension fault does not appear to provide a high permeability vertical pathway delivering hot crustal fluids to the near surface, nor were intrusive rocks intercepted in the borehole, which were hypothesized at depth from the previous geophysical study by Mira Geoscience (2017).

This study also highlights some of the challenges involved in designing and undertaking temperature gradient drill programs in frontier areas. For example, the presence of permafrost and thermal inversions caused by ambient air temperature and climate change require drilling to adequate depths to access true geothermal gradient readings. These phenomena are well known in the Canadian north, and their depth of propagation increases northward (e.g., Fraser et al., 2018; Majorowicz et al., 2005). Further, it was the original intention to drill several wells at each location, but costs and time constraints ended up being limiting factors in this study. Drilling costs were substantially higher than anticipated as a result of numerous delays. Cold weather challenged all parts of the field program, particularly for the Tintina well, where -40°C temperatures slowed the drill operations substantially. For example, water for diamond drilling was sourced from a local lake that repeatedly froze over (Fig. 10).

Conclusion

This collaborative project created a new data set of subsurface geology and temperature measurements in two areas of suspected high geothermal energy potential: Takhini Hot Springs and Tintina Trench. New TG well data are inconclusive from the Takhini Hot Springs area, where a spike in temperatures to 25.6°C at 500 m depth may indicate the upper limit of a larger geothermal gradient across a fault plane, and/or warmer fluid flow within a permeable horizon, or any number of interpretations not discussed here. Further drilling is required to resolve this question, and whether this is hydrodynamically-related to the 46.3°C water observed at Takhini Hot Springs, ~2 km to the east. The Tintina well indicates a higher than average geothermal gradient of 30°C/km, however,

Figure 10. *Photograph of truck sourcing water for Tintina well, ~6 km from the drill site. The lake lies in the Tintina Trench and the Pelly Mountains are observed in the distance.*

the location does not indicate the presence of hot fluid flow from depth, nor a source of heat for power production at an economic depth from surface. Despite these findings, the project has significantly advanced our understanding of baseline heat production and geothermal gradients in Yukon.

Continued short-term work on this project includes logging the drill core from the Tintina and Takhini wells, and assessment of rock properties and thermal conductivity being carried out at the University of Alberta; further compilation of heat-generating potential of radiogenic granitoid rocks; and incorporation and interpretation of the Tintina well results into the larger geothermal study focused on the Tintina-Northern Rocky Mountain Trench. Longer term initiatives include assessment of ground temperature along the Denali fault, where CPD results and previous drilling by EBA Engineering Consultants Ltd. show high heat flow potential, and identifying drill targets near heat producing radiogenic granites in southern Yukon.

Acknowledgements

The bulk of funding for this project was provided by CanNor through their Strategic Investments in Northern Economic Development Fund. Jeff Witter (Innovate Geothermal Ltd.) and Steve Grasby (Geological Survey of Canada) area acknowledged for academic guidance and support on many aspects of the geothermal project.

References

Burgess, M.M., Judge, A.S. and Taylor, A.S., 1982. Yukon ground temperature data collection – 1966 to August 1981. Earth Physics Branch Open File 82-1, Department Energy, Mines and Resources Canada, Government of Canada.

CanGEA (Canadian Geothermal Energy Association), 2016. The Yukon geothermal opportunities and applications report. http://www.energy.gov.yk.ca/pdf/Yukon-Geothermal-Opportunities-and-Applications-Report.pdf, 376 p [accessed December, 2018].

Colpron, M., Crowley, J.L., Gehrels, G.E., Long, D.G.F., Murphy, D.C., Beranek, L.P. and Bickerton, L., 2015. Birth of the northern Cordilleran orogen, as recorded by detrital zircons in Jurassic synorogenic strata and regional exhumation in Yukon. Lithosphere, vol. 7, p. 541–562.

Crandall, J.T. and Sadlier-Brown, T.L., 1978. Data on geothermal areas Cordilleran Yukon, Northwest Territories, and adjacent British Columbia Canada. Earth Physics Branch Open File No. 78-1, Department Energy, Mines and Resources Canada, Government of Canada.

Fraser, T.A., Grasby, S.E., Witter, J.B., Colpron, M. and Relf, C., 2018. Geothermal studies in Yukon – collaborative efforts to understand ground temperature in the Canadian North. Geothermal Resources Council Transactions, vol. 42, p. 1451–1470.

Fowler, N., Thomas, D. and Yen, Winifred, 1980. Geothermal Energy. Department of Planning and Economic Development, Honolulu, Hawaii, https://scholarspace.manoa.hawaii.edu/bitstream/handle/10125/21066/geothermal_energy.pdf, 66 p. [accessed May 31, 2018].

Friend, M. and Colpron, M., 2017. Potential radiogenic heat production from Cretaceous and younger granitoid plutons in southern Yukon. Yukon Geological Survey, Open File 2017-60, scale 1:1 000 000.

Gabrielse, H., Murphy, D.C. and Mortensen, J.K., 2006. Cretaceous and Cenozoic dextral orogeny parallel displacements, magmatism and paleogeography, north-central Canadian Cordillera. *In:* Paleogeography of the North American Cordillera: Evidence For and Against Large-Scale Displacements, J.W. Haggart, J.W.H. Monger and R.J. Enkin (eds.), Geological Association of Canada, Special Paper 46, p. 255–276.

Geotech Ltd., 1984. Subsurface temperature data from wells north of sixty Yukon – Northwest Territories. Earth Physics Branch Open File 84-28, Department Energy, Mines and Resources Canada, Government of Canada.

Grasby, S.E., Hutcheon, I. and Krouse, H.R., 2000. The influence of water-rock interaction on the chemistry of thermal springs in western Canada. Applied Geochemistry, vol. 15, p. 439–454.

Grasby, S.E., Allen, D.M., Bell, S., Chen, Z., Ferguson, G., Jessop, A., Kelman, M., Ko, M., Majorowicz, J., Moore, M., Raymond, J. and Therrien, R., 2012. Geothermal energy resources potential of Canada. Geological Survey of Canada, Open File 6914, 322 p.

Hart, C.J.R., 1997. A transect across northern Stikinia: Geology of the northern Whitehorse map area, southern Yukon Territory (105D/13-16). Yukon Geological Survey, Bulletin 8, 112 p.

Hjartarson, A., 2015. Heat Flow in Iceland. Proceedings World Geothermal Congress, 2015, Melbourne, Australia, 4 p.

Jessop, A.M., Souther, J.G., Lewis, T.J. and Judge, A.S., 1984. Geothermal measurements in northern British Columbia and southern Yukon Territory. Canadian Journal of Earth Sciences, vol. 21, p. 599–608.

Jessop A.M., Allen V.S., Bentkowski W., Burgess M., Drury M., Judge A.A., Lewis T., Majorowicz J., Mareschal J.C. and Taylor A.E., 2005. The Canadian geothermal data compilation. Geological Survey of Canada, Open File 4887.

Jessop A.M., 2008a. Review of National Geothermal Energy Program Phase 1 – Geothermal Potential of Sedimentary Basins. Geological Survey of Canada, Open File 5690, 146 p.

Jessop, A.M., 2008b. Review of National Geothermal Energy Program Phase 1 – Geothermal Potential of the Cordillera. Geological Survey of Canada, Open File 5906, 86 p.

KGS Group, 2016. Geothermal Review and Site Inventory. Final Report #16-1404-001, prepared for Yukon Energy, 39 p.

Lewis, T.J., Hyndman, R.D. and Flück, P., 2003. Heat flow, heat generation, and crustal temperatures in the northern Cordillera: Thermal controls of tectonics. Journal of Geophysical Research, vol. 108, no. B6, 2316.

Long, D.G.F., 2015. Depositional and tectonic framework of braided and meandering gravel-bed river deposits and associated coal deposits in active intermontane basins: The Upper Jurassic to mid-Cretaceous Tantalus Formation, Whitehorse trough, Yukon, Canada. Yukon Geological Survey, Open File 2015-23, 80 p.

Leonard, L.J., Mazzotti, S. and Hyndman, R.D., 2008. Deformation rates estimated from earthquakes in the northern Cordillera of Canada and eastern Alaska. Journal of Geophysical Research, vol. 113, B08406.

Li, C.-F., Lu, Y. and Wang, J. A., 2017. Global reference model of Curie-point depths based on EMAG2. Scientific Reports, vol. 7, doi: 10.1038/srep45129.

Majorowicz, J.A. and Dietrich, J.R., 1989. Comparison of the geothermal and organic maturation gradients of the central and southwestern Beaufort – Mackenzie Basin, Yukon and Northwest Territories. Current Research, Part G, Geological Survey of Canada, Paper 89-1G, p. 63–67.

Majorowicz, J.A. and Morrow, D.W., 1998. Subsurface temperature and heat flow. Geological Survey of Canada, Open File 3626.

Majorowicz, J., Grasby, S., Ferguson, G., Safanda, J. and Skinner, W., 2005. Paleoclimatic reconstructions in Western Canada from subsurface temperatures: consideration of groundwater flow. Climate of the Past Discussions, European Geosciences Union, Vienna, vol. 1, p. 93–120.

Mira Geoscience, 2017. Ross River geothermal exploration project: Review of the 2014 work program. Yukon Geological Survey, Miscellaneous Report, MR 18, 141 p. and 1 map (scale 1:50 000).

Raymond, J., Malo, M., Tanguay, D., Grasby, S.E. and Bakhteyar, F., 2015. Direct utilization of geothermal energy from coast to coast: a review of current applications and research in Canada. Proceedings of the World Geothermal Congress.

Turner, D.G., 2014. Surficial geology, Ross River Region, Yukon, parts of NTS 105K/1, 2 and 105F/15, 16. Yukon Geological Survey, Open File 2014-13, 1:25 000 scale.

Witter, J.B. and Miller, C., 2017. Curie point depth mapping in Yukon. Yukon Geological Survey, Open File 2017-3, 38 p.

Witter, J.B., Miller, C.A., Friend, M. and Colpron, M., 2018. Curie Point Depths and Heat Production in Yukon, Canada. Proceedings of the 43rd Workshop on Geothermal Reservoir Engineering, Stanford University, Stanford, California, February 12–14, 11 p.

Yukon Energy Corporation. "Quick Facts." https://yukonenergy.ca/energy-in-yukon/electricity-101/quick-facts [accessed on December 31, 2018].

Yukon Government Energy Branch, 2018. Yukon's Energy Context. Department of Energy, Mines and Resources, pamphlet 9 p. Yukon Energy Branch, http://www.energy.gov.yk.ca/pdf/emr-yukon-energy-context.pdf [accessed December 12, 2018].

Yukon Geological Survey, 2018. Yukon Digital Bedrock Geology. Yukon Geological Survey, http://www.geology.gov.yk.ca/update_yukon_bedrock_geology_map.html [accessed May 31, 2018].

Geochemistry of Devono–Mississippian volcanic and intrusive rocks of the Finlayson Lake district, Yukon-Tanana terrane, Yukon

M.J. Manor and S.J. Piercey
Department of Earth Sciences, Memorial University of Newfoundland

Manor, M.J. and Piercey, S.J., 2019. Geochemistry of Devono–Mississippian volcanic and intrusive rocks of the Finlayson Lake district, Yukon-Tanana terrane, Yukon. *In:* Yukon Exploration and Geology 2018, K.E. MacFarlane (ed.), Yukon Geological Survey, p. 91–110.

Abstract

The Finlayson Lake district in southeastern Yukon is a remnant of a Late Paleozoic arc–back-arc system that consists of metamorphosed volcanic, plutonic, and sedimentary rocks of the Yukon-Tanana and Slide Mountain terranes. These rocks host more than 40 Mt of polymetallic resources in numerous occurrences and styles of volcanogenic massive sulphide (VMS) mineralization. Geochemical data from these rocks support previous interpretations that volcanism and plutonism occurred in arc–marginal arc (e.g., Fire Lake formation) and continental back-arc basin environments (e.g., Kudz Ze Kayah formation, Wind Lake formation, and Wolverine Lake group) where felsic magmatism formed from varying mixtures of crust and mantle-derived material. The rocks have elevated high field strength element (HFSE) and rare earth element (REE) concentrations in VMS-proximal stratigraphy relative to VMS-barren assemblages, suggesting that the petrogenetic conditions that generated felsic rocks likely played a role in the localization of VMS mineralization. Future work aims to constrain magmatic processes and outline prospectivity criteria for delineating productive VMS assemblages within the district, and in similar geodynamic settings globally.

* mjmanor@mun.ca

Introduction

The Finlayson Lake district occurs in one of the Canada's best exposed ancient convergent continental margin systems and contains more than 40 Mt of polymetallic (Zn-Pb-Cu-Co-Au-Ag) volcanogenic massive sulphide (VMS) mineralization (Galley *et al.*, 2007; Peter *et al.*, 2007). Exploration and development in the area are currently focused on the Kudz Ze Kayah Zn-Pb-Cu-Ag-Au deposit which has an indicated mineral resource of 18.3 Mt at 6.3% Zn, 1.9% Pb, 0.9% Cu, 148 g/t Ag, and 1.4 g/t Au, and an additional inferred resource of 0.9 Mt at 6.9% Zn, 1.6% Pb, 1.1% Cu, 138 g/t Ag, and 1.1 g/t Au (BMC Minerals Ltd., 2017). Past geochemical studies have defined the tectonic setting of the Finlayson Lake district as an evolving Late Paleozoic continental arc to evolving back-arc basin assemblage. In this paper, we report new major and trace element lithogeochemical results for mafic to felsic volcanic and intrusive rocks of the Grass Lakes group—Fire Lake, Kudz Ze Kayah, and Wind Lake formations, and Grass Lakes plutonic suite—and the Wolverine Lake group. Our new high-precision data add to existing databases (Piercey, 2001; Piercey *et al.*, 2001, 2002a,b,c, 2003, 2004, 2008, 2012) and are part of a larger, ongoing initiative to evaluate prospectivity of felsic-hosted VMS deposits and their host assemblages in the Finlayson Lake district using lithogeochemistry as well as detailed regional-scale geochronology, radiogenic isotopic geochemistry, and mineral chemistry. Furthermore, we conclude that our new lithogeochemical results overlap with analyses completed 15+ years ago, and support previous geodynamic interpretations for the genesis of the Yukon-Tanana terrane in the mid-Paleozoic.

Geological Setting

The Finlayson Lake district of southeastern Yukon is found within a fault-bounded portion of the peri-Laurentian Yukon-Tanana and Slide Mountain terranes, which are made up of assemblages that were deposited or intruded from the Devonian to Permian (Fig. 1; Tempelman-Kluit, 1979; Mortensen and Jilson, 1985; Murphy *et al.*, 2006). Yukon-Tanana terrane arc and back-arc assemblages are composed of variably deformed and metamorphosed volcanic, plutonic, and sedimentary rocks that locally retain primary geological and geochemical features; these rocks were deposited or intruded above a pre to Late Devonian basement (Colpron *et al.*, 2006; Murphy *et al.*, 2006; Piercey *et al.*, 2006; Piercey and Colpron, 2009). The Jules Creek transform fault juxtaposes the Yukon-Tanana terrane and ophiolitic rocks of the Slide Mountain terrane (Murphy *et al.*, 2006); both terranes were together thrust onto the North American craton along the Inconnu thrust in the Late Jurassic (Murphy *et al.*, 2002). The present-day location of the Finlayson Lake district was achieved during the Eocene with its displacement from the main segment of the Yukon-Tanana terrane in central Yukon by ~430 km along the Tintina strike-slip dextral fault system (Figs. 1 and 2; Gabrielse *et al.*, 2006).

Yukon-Tanana terrane rocks within the Finlayson Lake district are hosted in three thrust sheets: the Big Campbell, Money Creek, and Cleaver Lake thrust sheets (Fig. 2; Murphy *et al.*, 2006). Pre-Upper Devonian metasedimentary rocks of the North River formation make up the basement to the Big Campbell and Money Creek thrust sheets. The Big Campbell thrust sheet is structurally deepest and is bounded below by the post-Late Triassic Big Campbell thrust fault and above by the Early Permian Money Creek thrust fault (Fig. 2). Rocks in the Big Campbell thrust sheet are primarily Middle to Upper Devonian, lower to middle greenschist facies mafic and felsic metavolcanic and metasedimentary rocks of the Grass Lakes group, which includes the basal pre-Upper Devonian North River formation and overlying Fire Lake, Kudz Ze Kayah, and Wind Lake formations (Fig. 2). Late Devonian granitic intrusions of the Grass Lakes plutonic suite cut the Grass Lakes group and then both are unconformably overlain by Lower Mississippian metaclastic and mafic to felsic metavolcanic rocks of the Wolverine Lake group (Fig. 2). The Grass Lakes group contains VMS mineralization at the Kudz Ze Kayah, GP4F, and Fyre Lake deposits, and the Wolverine Lake group contains the Wolverine deposit (Piercey *et al.*, 2001; Sebert *et al.*, 2004; Peter *et al.*, 2007; Bradshaw *et al.*, 2008; Piercey *et al.*, 2016); together, these deposits are interpreted to have formed in an evolving continental arc to back-arc basin tectonic setting (Piercey *et al.*, 2001, 2002b, 2004, 2006; Murphy *et al.*, 2006). The Money Creek thrust sheet comprises the pre-Upper

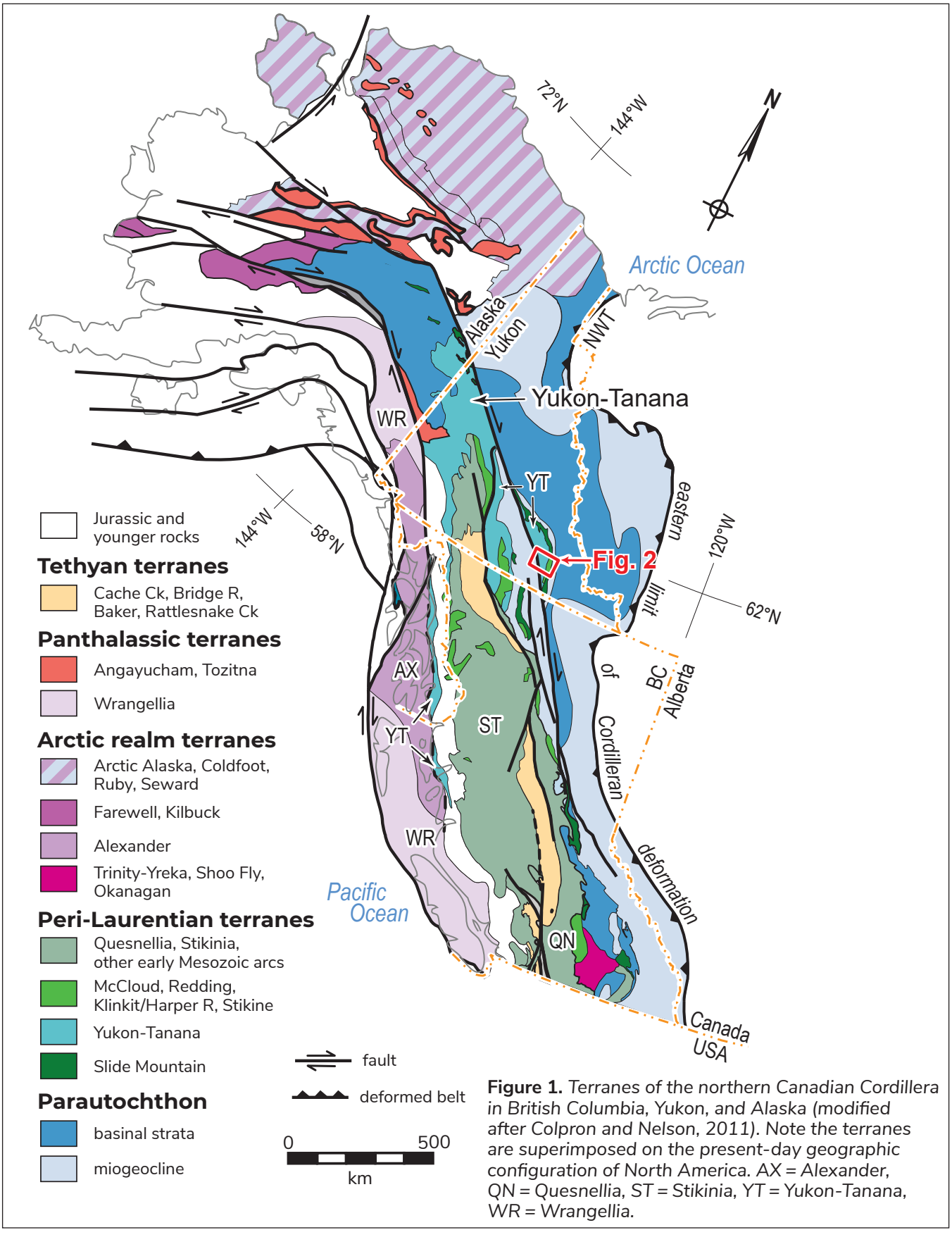

Figure 1. *Terranes of the northern Canadian Cordillera in British Columbia, Yukon, and Alaska (modified after Colpron and Nelson, 2011). Note the terranes are superimposed on the present-day geographic configuration of North America. AX = Alexander, QN = Quesnellia, ST = Stikinia, YT = Yukon-Tanana, WR = Wrangellia.*

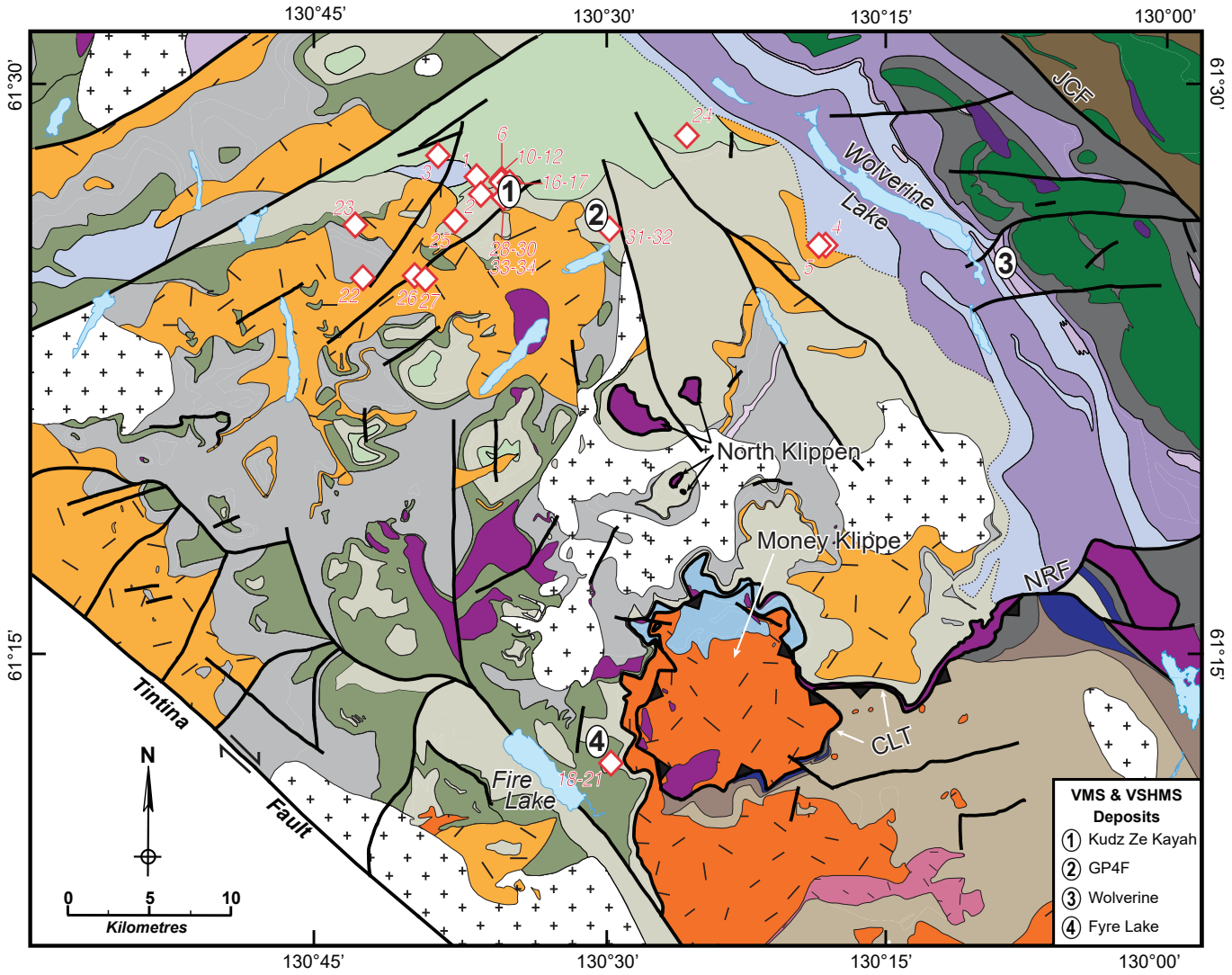

Figure 2. *Regional geologic setting of the south-central Finlayson Lake region, Yukon-Tanana terrane (modified after Piercey et al., 2003, and Yukon Geological Survey, 2018). The Money Creek thrust fault crops out south of the extent of the figure. Diamonds and numbers correspond to sample locations and lithogeochemical results in Table 1. Numbers indicate locations of prospective VMS deposits in the region. VMS = volcanogenic massive sulphide; VSHMS = volcanic sediment-hosted massive sulphide. See legend on next page.*

Devonian North River formation and overlying Upper Devonian to Lower Mississippian felsic-intermediate metavolcanic and metasedimentary rocks (Waters Creek and Tuchitua River formations). These formations are intruded by granitic rocks of the Late Devonian to Early Mississippian Simpson Range plutonic suite, then capped by Mississippian to Lower Permian limestone, mafic metavolcanic and metaclastic rocks (Fig. 2; Mortensen, 1992; Grant, 1997; Murphy *et al.*, 2006). The Money Creek thrust sheet is structurally overlain by the Cleaver Lake thrust sheet, an assemblage of relatively undeformed and unmetamorphosed Late Devonian mafic and felsic volcanic rocks (Cleaver Lake formation) that overlie mafic and ultramafic rocks and are intruded by Early Mississippian granitoid rocks of the Simpson Range plutonic suite (Tempelman-Kluit, 1979; Piercey and Murphy, 2000; Murphy *et al.*, 2006). The Cleaver Lake thrust sheet was thrust above the Money Creek thrust sheet along the Early Permian Cleaver Lake thrust fault after the Early Permian (Murphy *et al.*, 2006). The rocks in the Money Creek and Cleaver Lake thrust sheets were generated in a continental arc setting to the southwest of the Big Campbell thrust sheets and are not associated with any known VMS mineralization (Grant, 1997; Piercey *et al.*, 2001, 2003, 2006; Murphy *et al.*, 2006).

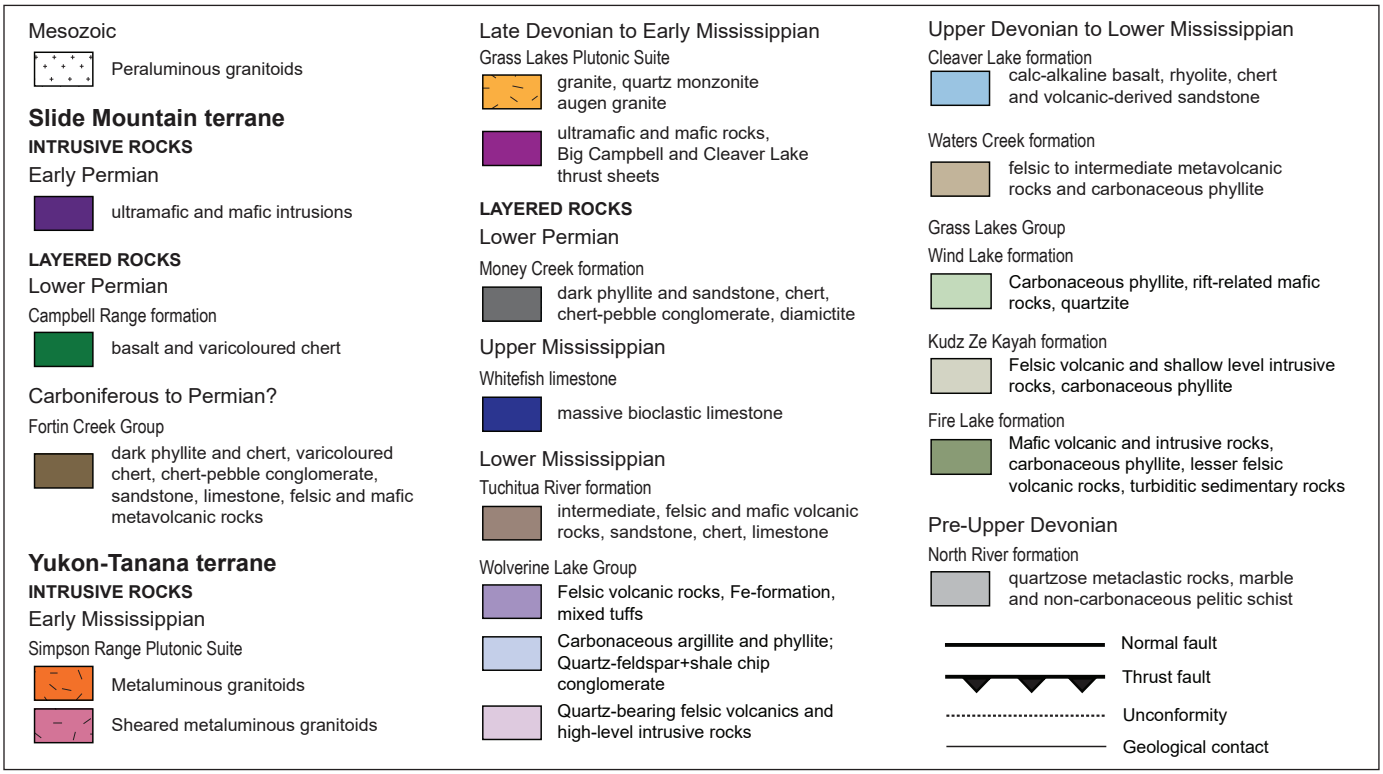

***Figure 2**. Map legend.*

Previous Work

The first integrated geological mapping and lithogeochemical characterization for rocks in the Finlayson Lake district was addressed by Piercey (2001). Mafic volcanic rocks of the Fire Lake formation in the Big Campbell thrust sheet have enriched mid-ocean ridge basalt (E-MORB), back-arc basin basalt (BABB), alkalic ocean island basalt (OIB), and low-Ti tholeiite to boninite affinities (Piercey et *al*., 2002a,b, 2004, 2006). The variation in geochemical affinities—especially the presence of boninite—suggests that the Fire Lake formation was formed due to the initiation of spreading in an arc built above a composite continental–oceanic basement domain (Piercey et *al*., 2002b, 2004). Subsequent work on the overlying felsic volcanic rocks of the Kudz Ze Kayah formation and granitic rocks of the Grass Lakes plutonic suite show overlapping HFSE-REE-enriched, A-type back-arc signatures (Piercey et *al*., 2001, 2003). Both rock packages contain significant crustal contamination from Precambrian continental basement and are inferred to have formed from extensive crustal melting in a continental back-arc inboard of the Fire Lake arc (Mortensen, 1992; Grant, 1997; Piercey et *al*., 2001, 2003). Continued spreading and increased asthenospheric mantle contributions to the crust facilitated the transition from felsic-dominated to alkalic mafic volcanism of the Wind Lake formation (Piercey et *al*., 2002a). The deposition of the Grass Lakes group (ca. 358 Ma; Murphy et *al*., 2006) was followed by a period of deformation and erosion, and then by unconformable deposition of the Wolverine Lake group. Volcanism in the lower Wolverine Lake group footwall subsequently produced rocks with HFSE-REE contents similar to the Kudz Ze Kayah formation and Grass Lakes plutonic suite (Piercey et *al*., 2001). A geochemical shift is observed in higher stratigraphic levels of the Wolverine Lake group, notably to rocks less enriched in HFSE and REE (Piercey et *al*., 2001); at its highest levels, strata are composed of enriched and normal mid-ocean ridge basalt (E-, N-MORB) and back-arc basin basalts (BABB; Piercey et *al*., 2002c).

Sampling and Analytical Methods

During the 2017 field season, 28 samples of felsic and mafic volcanic, plutonic, and sedimentary rocks were taken from outcrops and drill core at different stratigraphic levels of the Grass Lake group and deepest levels of the Wolverine Lake group (Fig. 3; Table 1). Samples were taken from the Kudz Ze Kayah formation (n = 10), Wind Lake formation (n = 6), Fire Lake formation (n = 6), Grass Lakes plutonic suite (n=5), and Wolverine Lake group (n = 1). Mafic volcanic and sedimentary rocks were taken from the Fire Lake and Wind Lake formations to confirm the geodynamic variations set forth by earlier workers (e.g., Piercey et al., 2001, 2002a,b,c, 2003, 2004, 2008, 2012) and to set the groundwork for future isotopic studies. Drilling into the Kudz Ze Kayah formation allowed for sampling of core from previously inaccessible deeper parts of the formation and provided the means to evaluate its lithological and lithogeochemical character. At the Kudz Ze Kayah and GP4F VMS deposits, felsic rocks were sampled from the immediate footwall and hanging wall of mineralization to help identify additional geochemical prospectivity criteria in ancient, felsic-hosted VMS systems.

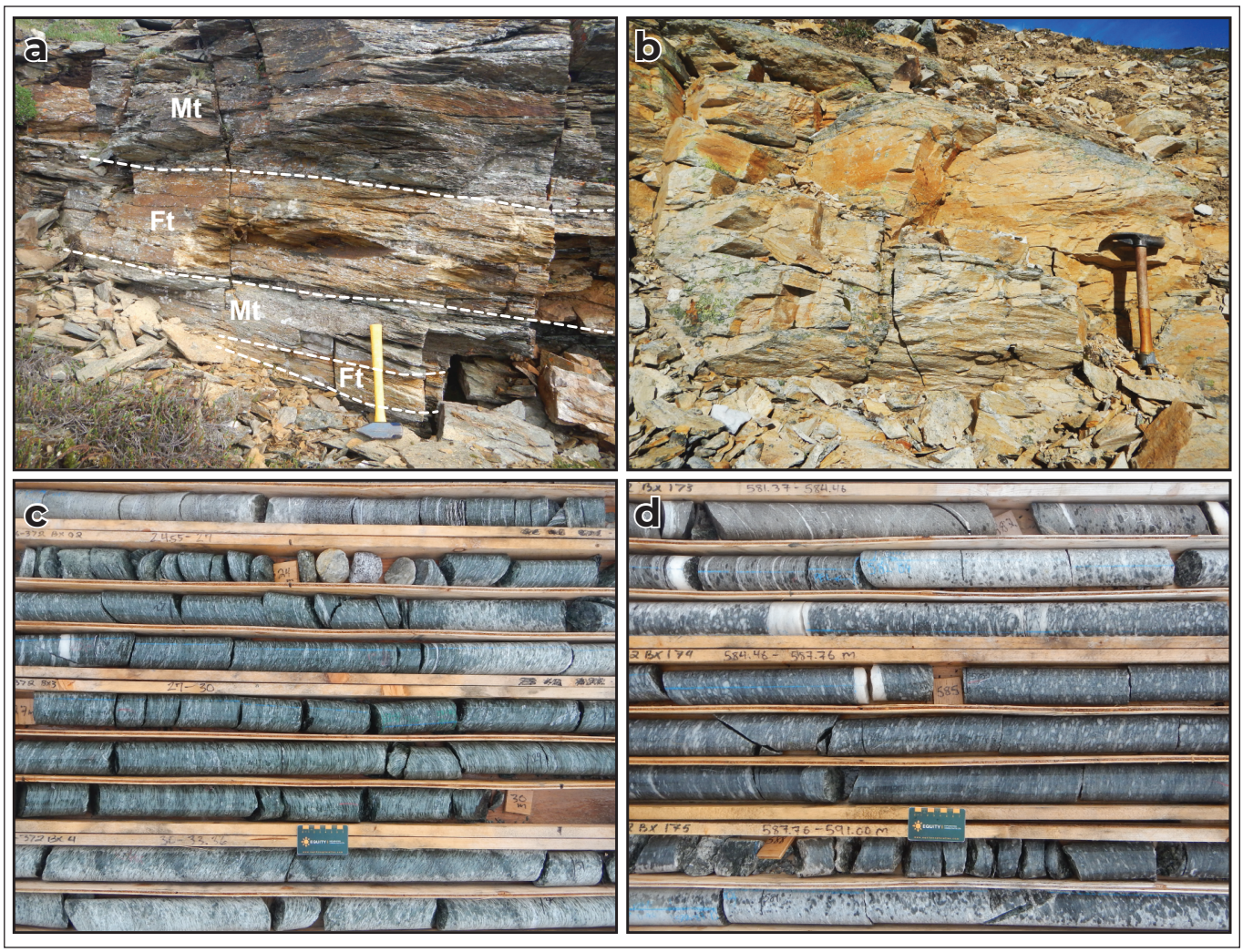

Figure 3. *Field photographs of 2017 sampling locations in the Finlayson Lake region. Sample location coordinates reported as UTM Zone 9N and NAD 83.* **(a)** *17MM-001: Wind Lake formation, felsic tuff (Ft) interbedded with mafic tuff (Mt) ~300 m above the contact with Kudz Ze Kayah formation (413749 E, 6815933 N);* **(b)** *17MM-055: Kudz Ze Kayah formation, massive aphyric rhyolite (413086 E, 6813844 N);* **(c)** *17MM-060: Wind Lake formation (?), biotite-chlorite altered mafic dike that crosscuts KZK stratigraphy (415122 E, 6814798 N);* **(d)** *17MM-062: Grass Lakes plutonic suite, quartz-feldspar porphyry immediately below the deepest known KZK volcanic rocks (~580 m depth; 415122 E, 6814798 N); (e) and (f) on next page.*

***Figure 3** continued.* **(e)** *17MM-074: Kudz Ze Kayah footwall, feldspar-blue quartz eye crystal tuff in the GP4F footwall; and* **(f)** *17MM-004: Wolverine Lake group, massive and foliated quartz-feldspar grit (429446 E, 6812106 N). Hammer (35 cm) for scale in panels* **a,b**.

Sample preparation and measurement of major and trace element data were performed at ALS Laboratories, North Vancouver, British Columbia. Rock samples were crushed and pulverized using steel plates and agate mills, respectively. Sample powders (~0.2 g) were fused with a lithium metaborate flux (0.9 g) at 1000°C. The fused bead was cooled and digested using 100 mL of a 4% HNO_3–2% HCl mixture. Analyses of the sample solutions were completed using inductively coupled plasma-atomic emission spectrometry (ICP-AES) for major elements and inductively coupled plasma-mass spectrometry (ICP-MS) for trace elements.

Two in-house reference materials, two blind duplicates, and one lab duplicate were measured throughout the run to monitor analytical accuracy and reproducibility (Table 1). The SLV-MC basalt and WP-1 dacite (Watts Point, Coast Plutonic Complex) in-house reference materials yielded values generally within 8% of unpublished SLV-MC data and 12% of published WP-1 values (Piercey *et al.*, 2001). The analyses were reproducible to <3% for major elements and <5% for most trace elements (<8% for Nd, Lu [SLV-MC], and Zr [WP-1]; <35% for Cs, Ta, and U [WP-1]; and undetectable W; Appendix 1). The two blind duplicates (17MM-031, 17MM-062) show relatively larger RSD values presumably due to the natural heterogeneity of the rocks. For 17MM-031, the reproducibility of analyses is better than 10% for major elements (17% for CaO) and <20% for trace elements. Results for 17MM-062 gave RSD values better than 5% for major elements (except for <17% for MgO and Fe_2O_3, and 30% for CaO), and <12% for most trace elements except for Cs and U (<22%; Appendix 1). The lab duplicate chosen at ALS (17MM-066) yielded a good reproducibility of <3% for major and trace elements, and <8% for MnO, Tm, and V (Appendix 1).

Geochemical Results

We follow the methodology of Piercey et *al.* (2001) and use immobile elements and ratios that contain Al_2O_3, TiO_2, high field strength elements (HFSE; Zr, Hf, Nb, Ta, Y, Th), and rare earth elements (REE; La to Lu) to evaluate the primary geochemical characteristics of the rocks (Fig. 4). The alkali elements (e.g., Na, K, and Ca) and large ion lithophile elements (LILE; e.g., Cs, Ba, Rb, K, Sr, U) can be significantly affected by hydrothermal alteration and metamorphism (e.g., Fig. 4e); alteration of least-altered felsic rocks resulted in sericite, chlorite-pyrite, and alkali feldspar assemblages, while mafic rocks typically exhibit more abundant carbonate, epidote, and chlorite-pyrite alteration (Fig. 4e; Ishikawa et *al.*, 1976; Lentz, 1999; Large et *al.*, 2001).

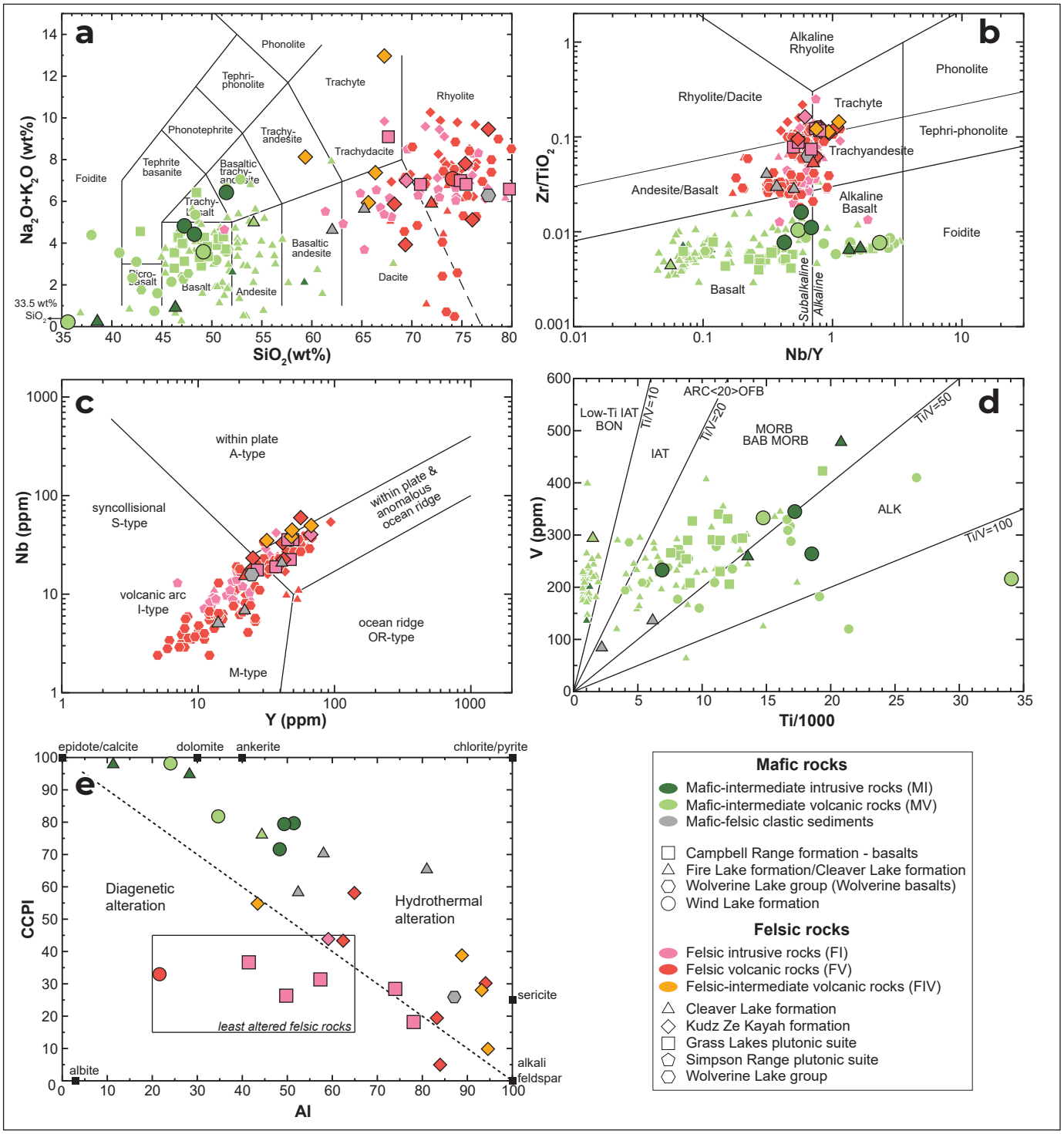

Figure 4. *Major and trace element discrimination diagrams for felsic and mafic rocks in the Finlayson Lake region. Samples from this study are shown as the largest symbols with black outlines; archival data are smaller symbols with white outlines (Piercey, 2001; Piercey et al., 2001, 2002a,b,c, 2003, 2004, 2008, 2012).* **(a)** *SiO_2 vs. $Na_2O + K_2O$, analyses from the Wolverine deposit hanging wall have SiO_2 contents above 80 wt% and are not included;* **(b)** *Nb/Y vs. Zr/TiO_2 (Pearce, 1996 after Winchester and Floyd, 1977);* **(c)** *Y vs. Nb (Pearce et al., 1984);* **(d)** *Ti/1000 vs. V (Shervais, 1982); and* **(e)** *CCPI (chlorite-carbonate-pyrite index) vs. Al (Ishikawa alteration index; Ishikawa et al., 1976) from Large (2001). IAT = island arc tholeiite; BON = boninite; OFB = ocean floor basalt; MORB = mid-ocean ridge basalt; BAB = back-arc basin; ALK = alkaline.*

Grass Lakes group

Fire Lake formation

Samples from the Fire Lake formation comprise ultramafic rocks (metapyroxenite?), a single mafic tuff, and intermediate–felsic clastic sedimentary rocks (Figs. 4–6; Table 1). The ultramafic rocks contain between 38 and 46 wt% SiO_2 and show Nb/Y, Zr/Nb, Ti/V, and Zr/Y ratios indicative of an alkalic affinity, whereas the mafic tuff is relatively more intermediate (SiO_2 = 54.2 wt%) with lower Ti/V and Zr/Y and has an island-arc tholeiitic to boninitic signature (Figs. 4 and 5; e.g., Piercey et *al.*, 2002b, 2004). The ultramafic rocks have steep primitive mantle-normalized patterns with elevated LREE relative to HREE ratios (La/Yb_{PM} = 5–34; La/Sm_{PM} = 1.5–9.1; Gd/Lu_{PM} = 2.7-3.2) similar to Nb-enriched basalts (NEB; Piercey et *al.*, 2004), whereas the mafic tuff has a relatively flatter pattern (La/Yb_{PM} = 0.4; La/Sm_{PM} = 1.2; Gd/Lu_{PM} = 0.4) and overlaps with the boninite field (Fig. 6f). The intermediate–felsic clastic sediments are primarily siltstone (SiO_2 = 62–65 wt%) and rare Si-rich clastic sediments (SiO_2 = 84 wt%) that occur proximal to massive sulphide mineralization at the Fyre Lake VMS deposit (Sebert et *al.*, 2004). Trace element ratios (Nb/Y and Zr/Y) distinguish these sediments as derivatives of calc-alkaline arc rocks (Figs. 4 and 5) and have similar upper continental crustal-normalized patterns (La/Yb_{UCN} = 0.65–0.91) and neutral to weakly negative Eu anomalies (Eu/Eu* = 0.75–1.0; Fig. 6c).

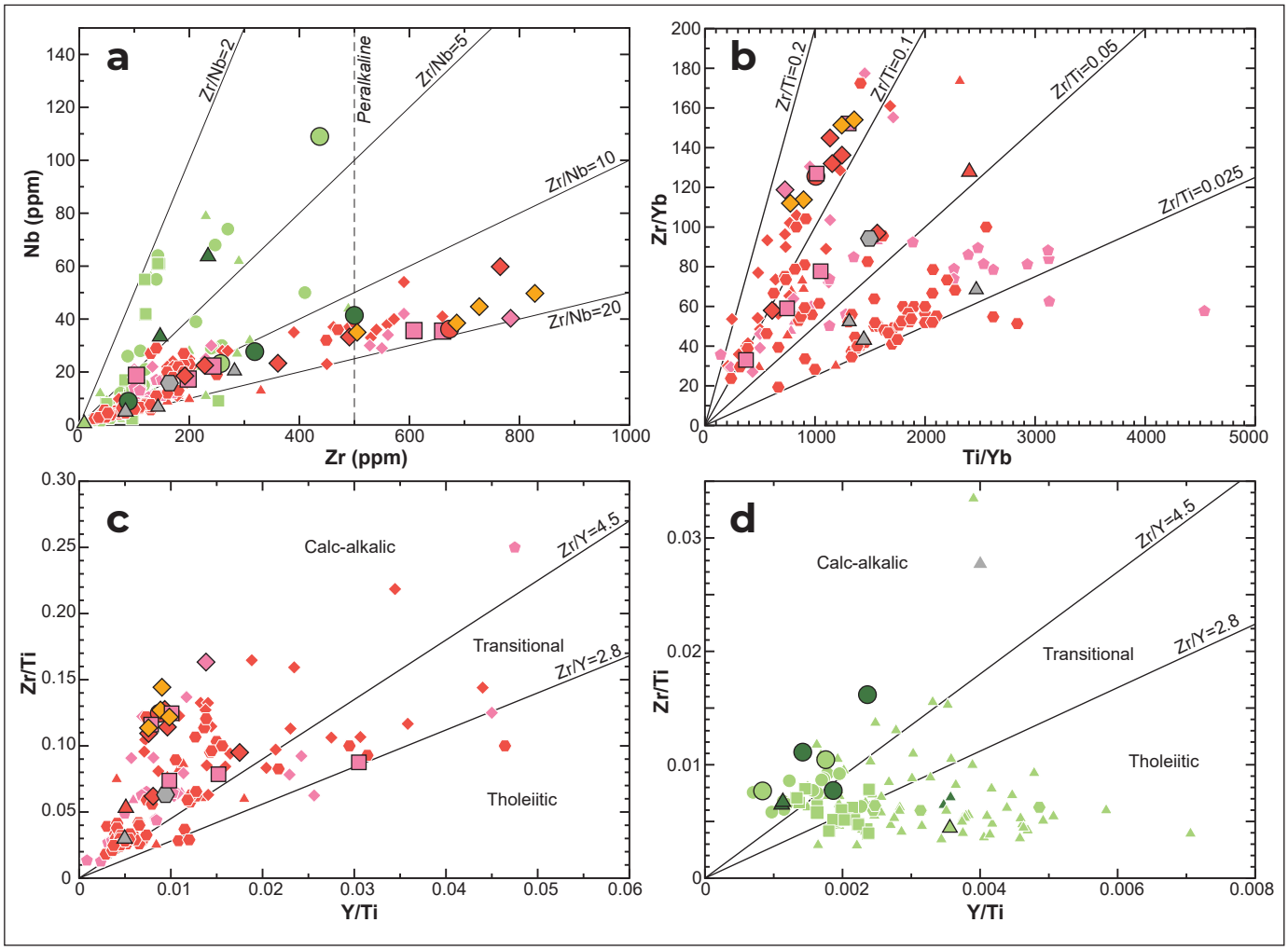

Figure 5. *High field strength element diagrams for felsic and mafic rocks in the Finlayson Lake region.* **(a)** *Zr vs. Nb (Leat et al., 1986);* **(b)** *Ti/Yb vs. Zr/Yb;* **(c)** *Y/Ti vs. Zr/Ti for felsic rocks; and* **(d)** *Y/Ti vs. Zr/Ti for mafic rocks. Panels c and d are modified after (Lentz, 1998, 1999); Zr/Y values defining magmatic affinity classes from Ross and Bédard (2009). Symbol styles as in Figure 4.*

Kudz Ze Kayah formation

Felsic tuffs and coherent rhyolite flows of the Kudz Ze Kayah formation reveal broadly similar geochemical compositions in the hanging wall and footwall of the Kudz Ze Kayah VMS deposits (Figs. 4–6; Table 1). The rocks display a range of SiO_2 contents (59–78 wt%) and have variable alkali concentrations due to hydrothermal alteration (Fig. 4a). The lithofacies have dacite, rhyolite, and trachyte compositions with calc-alkalic to alkalic, within-plate affinities (Nb/Y = 0.74–1.1; Zr/Y = 7.7–16; Ross and Bédard, 2009) except for two samples from the immediate hanging wall and footwall of GP4F mineralization (17MM-066 and 17MM-074, respectively) that have subalkaline affinities (Nb/Y = 0.54–0.61; Zr/Y = 5.4–12; Figs. 4 and 5). Upper continental crust-normalized immobile elements reveal relatively flat patterns with near-neutral LREE (La/Sm_{UCN} = 0.83–1.1) and relatively more abundant HREE (Gd/Lu_{UCN} = 0.57–1.9), and variably negative Eu (Eu/Eu* = 0.39–1.1) and Ti (Ti/Ti* = 0.32–1.0) anomalies (Fig. 6a) that directly overlap with A-type volcanic signatures from Piercey *et al.* (2001).

Wind Lake formation

The Wind Lake formation is composed primarily of carbonaceous argillite; geochemically similar mafic volcaniclastic, volcanic, and intrusive rocks; and lesser felsic volcaniclastic units that are geochemically similar to the underlying Kudz Ze Kayah formation (Figs. 4–6; Table 1). The mafic rocks have low SiO_2 (34–51 wt%) and correspond to basalt and alkaline basalt to basaltic trachyandesite compositions (Fig. 4a,b). They have back-arc basin MORB to alkalic geochemical affinities (Ti/V = 30–160; Fig. 4d; Shervais, 1982) and straddle the subalkaline to alkaline boundary with Nb/Y = 0.42–2.3 (Fig. 4b). Primitive mantle-normalized diagrams show steep patterns with LREE enrichment relative to HREE (La/Yb_{PM} = 3.9–22) and elevated Eu and Ti (Eu/Eu* = 1.9–4.5; Ti/Ti* = 5.9–32) similar to non-arc, ocean island basalt rift-related alkalic basalts (Fig. 6e; Piercey *et al.*, 2002a). The felsic tuff sample has significantly higher SiO_2 (74 wt%) and displays nearly identical trace element compositions to the intermediate–felsic volcanic and volcaniclastic rocks from the Kudz Ze Kayah formation (Figs. 4–6). The sample exhibits a trachytic composition (Fig. 4b) and has an alkalic and peralkaline, within-plate geochemical affinity (Nb/Y = 0.76; Zr/Y = 14.2; Zr/Nb = 125; Figs. 4 and 5). The upper continental crust-normalized pattern is relatively flat (La/Yb_{UCN} = 0.86) and overlaps directly with patterns from the Kudz Ze Kayah formation (Fig. 6a).

Grass Lakes plutonic suite

Most samples of the Grass Lakes plutonic suite come from a laterally extensive batholith-sized intrusion lying south of and stratigraphically beneath the Kudz Ze Kayah VMS deposit (Fig. 2). It is composed of high-silica, peraluminous alkali feldspar augen to megacrystic granitic rocks with apophyses of feldspar-porphyritic granitic rocks that are geochemically similar to, and contemporaneous with, the Kudz Ze Kayah strata (Figs. 4–6; *e.g.*, Piercey *et al.*, 2003; Murphy *et al.*, 2006). Samples from the pluton contain between 68 and 79 wt% SiO_2 and abundant HFSE concentrations which correspond to calc-alkalic, within-plate affinities (Zr/Y = 2.9–14; Nb/Y = 0.52–0.80; Figs. 4c and 5c). The upper continental crust-normalized diagrams show distinct trends for the pluton (La/Yb_{UCN} = 0.64–0.92) and feldspar porphyry dikes (La/Yb_{UCN} = 1.1–1.8); the dikes contain higher concentrations of HFSE and REE compared to the pluton (*e.g.*, Eu/Eu* = ~0.91 *vs.* 0.45; Zr/Zr* = ~1.4 *vs.* 0.55; Fig. 6b). These new results overlap with A-type, within-plate Grass Lakes granitic rocks documented by Piercey *et al.* (2003) and calc-alkalic to alkalic Kudz Ze Kayah volcanic rocks (Piercey *et al.*, 2001; Fig. 6a).

Wolverine Lake group

The Wolverine Lake group overlies the Grass Lakes group above a marked angular unconformity (Murphy *et al.*, 2002). One sample of quartz-feldspar grit (17MM-004) from immediately above the unconformity was analyzed. The grit displays high SiO_2 (78 wt%) and HFSE and REE compositions (Nb/Y = 0.65; Zr/Y = 6.7) comparable to the underlying calc-alkalic, arc to intraplate rocks of the underlying Kudz Ze Kayah formation and Grass Lakes plutonic suite (Piercey *et al.*, 2001; Figs. 4c, 5c, and 6). This sample

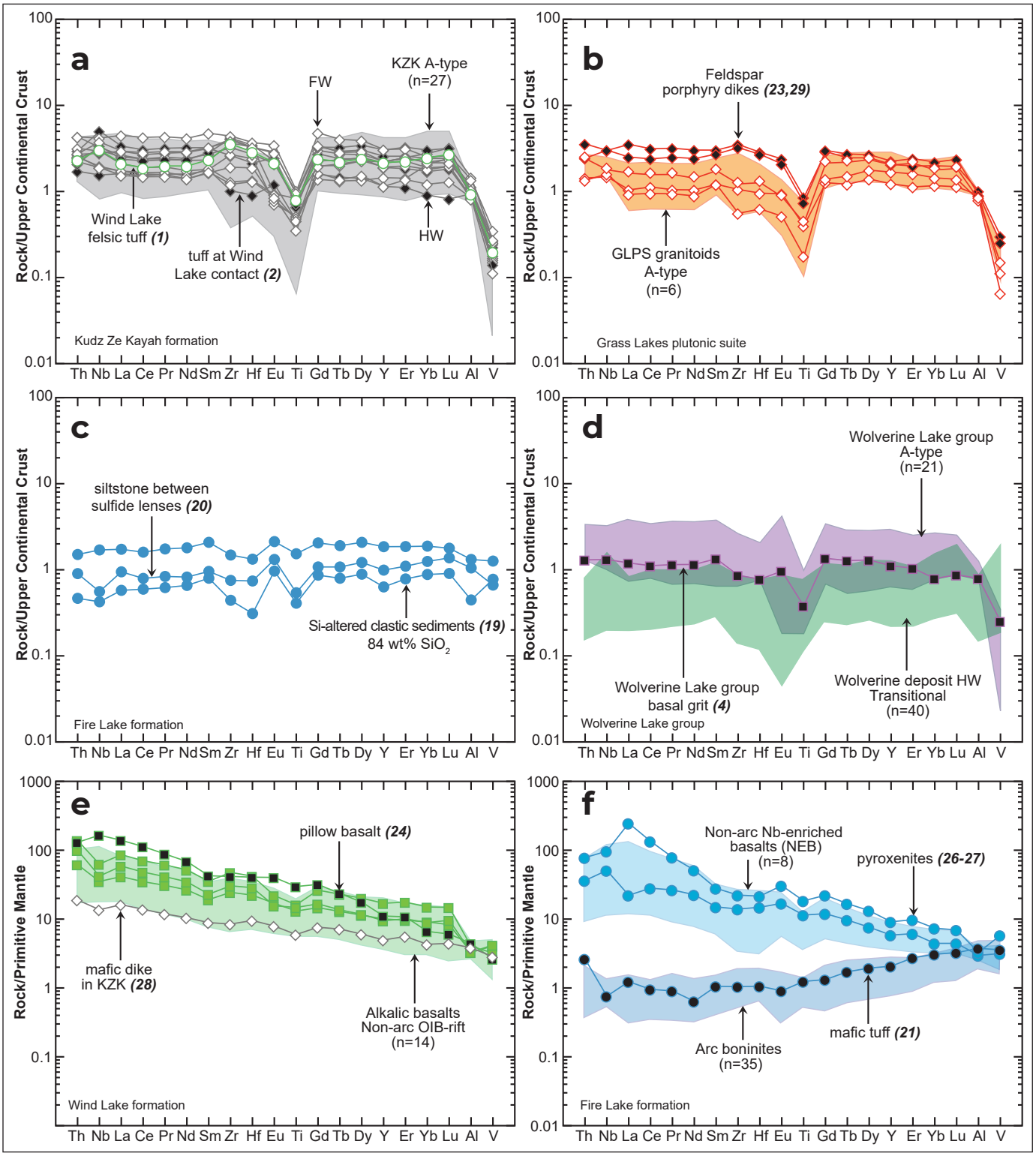

Figure 6. *Immobile trace element variations for felsic rock (***a–d***) and mafic rock (***e,f***) suites in the Finlayson Lake region. Results for felsic and mafic rocks are normalized to upper continental crust (McLennan, 2001) and primitive mantle (McDonough and Sun, 1995), respectively. Bold numbers in brackets correspond to sample numbers in Fig. 2 and Table 1. Shaded fields represent archival data with associated magmatic affinities (cf. references in Fig. 4). In panel* **(f)**, *only results with similar trace element patterns are shown as fields (boninites and Nb-enriched basalts, 43 of 76 total analyses for the Fire Lake formation).*

exhibits a relatively flat upper continental crust-normalized pattern with relatively more abundant LREE ($La/Sm_{UNC} = 0.89$) than HREE ($Gd/Lu_{UNC} = 1.5$; Fig. 6d). The immobile element concentrations overlap with other intraplate rocks of the Wolverine Lake group, primarily from the footwall of the Wolverine VMS deposits, and are distinctly more elevated compared to the hanging wall felsic rocks (Fig. 6d; Piercey *et al.*, 2001, 2008).

Discussion and Future Work

New lithogeochemical data from outcrop and drill core in the Finlayson Lake district overlap with existing data sets for rock units of the Grass Lakes and Wolverine Lake groups, despite a difference in the age of the data sets of 15+ years (Figs. 4–6). These data further support the interpretations of Piercey *et al.* (2001, 2002a) that these rocks formed during the evolution of a mid-Paleozoic convergent margin system on edge of western Laurentia, analogous to the development of the Japanese arcs, Sea of Japan, and Sino-Korean craton tectonic arrangement (Piercey *et al.*, 2006).

The Fire Lake formation represents the first stage of tholeiitic to boninitic arc to marginal-arc magmatism built atop a composite Yukon-Tanana basement (Grant, 1997; Piercey *et al.*, 2002b, 2004). Siltstones in the immediate hanging wall and those interbedded with Fyre Lake VMS mineralization have MORB to BAB MORB affinities that reflect erosion from source rocks formed during the onset of back-arc extension that led to separation of the Yukon-Tanana terrane from the western Laurentian continental margin (Figs. 4–6; Piercey *et al.*, 2002b, 2004). Ongoing spreading of the continental back-arc basin facilitated upwelling of asthenospheric mantle, partial melting, basaltic underplating, crustal melting and basalt–crustal melt mixing that led to calc-alkalic to alkalic, intraplate felsic volcanism associated with the Kudz Ze Kayah formation (Figs. 2, 4, and 5; Piercey *et al.*, 2001). The spatial and geochemical overlap between the Grass Lakes granite and porphyritic dikes and the Kudz Ze Kayah formation is shown in Figures 4 to 6 and supports the interpretation by Piercey *et al.* (2003) that the batholith may have been a staging chamber for extrusive volcanism. Overlying alkalic basalt from the Wind Lake formation, expressed as effusive and volcaniclastic eruptions or as deeper intrusive dikes, further corroborate the addition of high-temperature basaltic melts to the upper crust from ongoing back-arc extension and associated decompression melting of the mantle (*e.g.*, Piercey *et al.*, 2002a). Following a period of regional deformation and erosion between 361 and 358 Ma (Murphy *et al.*, 2002, 2006), basal quartzo-feldspathic grits of the Wolverine Lake group were deposited; their geochemical similarity to Kudz Ze Kayah volcanic rocks and Grass Lakes granitoid rocks indicate derivation from these or similar sources (Figs. 4–6; Piercey *et al.*, 2001).

Felsic rocks in the immediate hanging wall and footwall of the Kudz Ze Kayah VMS deposits have the highest Zr compositions (<830 ppm) and comparable HFSE and REE abundances ($Zr/Yb = 111–154$; $Nb/Y = 0.74–1.1$; $Zr/Y = 11.9–15.9$; $Nb/Ta = 15.1–17.2$; Figs. 4 and 5) of any published results from the Kudz Ze Kayah formation. Distal felsic volcanic rocks, however, show lower HFSE and REE ($Zr/Yb = 58–118$; $Nb/Y = 0.53–0.74$; $Zr/Y = 7.7–11.8$; $Nb/Ta = 11.8–12.4$). Variations in the Nb/Ta ratio (11.8–17.2, average = 14.8; n = 10) suggests mixing of crustal and mantle sources (*e.g.*, Piercey *et al.*, 2008). The elevated HFSE and REE concentrations in Kudz Ze Kayah felsic volcanic rocks have been attributed to high-temperature melting of continental crust and subsequent dissolution of HFSE-REE-rich accessory minerals (*e.g.*, zircon, monazite, apatite; Piercey *et al.*, 2001). This increased incompatible element budget has been shown to be associated with high temperature felsic melts in VMS belts worldwide, as in the VMS-hosting felsic rocks in the Abitibi greenstone belt (Barrie, 1995), the Iberian Pyrite Belt (Barrie *et al.*, 2002; Rosa *et al.*, 2009; Codeço *et al.*, 2018), and the Wolverine Lake group, Finlayson Lake district (Piercey *et al.*, 2008). Moreover, VMS deposits in crustal regimes are generally associated with thermally anomalous magmas and regional heat corridors that are conducive to the formation of VMS-related hydrothermal systems (Piercey, 2011).

Future work will investigate variations in the mineral-scale geochronological and geochemical characteristics of the felsic rocks throughout the Finlayson Lake district to assess their value as an indicator of prospectivity in mineral exploration and ancillary crustal evolution studies (*e.g.*, Piercey *et al.*, 2017; Manor and Piercey, 2018). High-precision chemical abrasion isotope dilution-thermal ionization mass spectrometry (CA-ID-TIMS) U-Pb zircon dating is underway to determine the temporal variations in VMS-related felsic volcanism throughout the Kudz Ze Kayah formation and the Wolverine Lake group. Whole-rock lithogeochemistry, Nd-Hf isotopic compositions, and *in situ* geochemical and isotopic analysis on mineral separates (zircon, monazite, and apatite) will be integrated in order to characterize the petrogenetic conditions and processes leading to magma genesis with potential links to VMS formation (*e.g.*, T, redox, metal and sulphur budgets, fluid compositions). These results will complement existing studies (*e.g.*, Piercey, 2001; Piercey *et al.*, 2002a, 2003, 2004, 2017) to further evaluate and test crustal evolution models for the northern Cordillera and also to test the role of asthenospheric mantle in the formation of the VMS-bearing and VMS-barren rock packages. The work will continue to refine existing models of VMS formation with respect to broad aspects of heat supply, fluid circulation, timing/episodicity of mineralizing events, and the interplay of tectonics, magmatism, and ore formation. Ultimately, this work will provide a unique integrated approach to magma prospectivity in an ancient, mid-Paleozoic felsic-hosted VMS terrane.

Conclusions

The new lithogeochemical results presented here support the current interpretations of an evolving, mid-Paleozoic (*ca.* 365-355 Ma) continental arc, marginal arc, and back-arc basin configuration at the western Laurentian margin. Results from strata immediately above and below the Kudz Ze Kayah VMS deposit place new constraints on the HFSE and REE end-member compositions (*e.g.*, Zr, Nb/Ta) and indicate a distinct period of high-temperature alkalic felsic volcanism within the Kudz Ze Kayah formation. Further work aims to identify mineral-scale and whole-rock geochemical characteristics of VMS-bearing stratigraphy to develop prospectivity criteria for future exploration in orogenic belts globally.

Acknowledgements

We acknowledge BMC Minerals for providing us the opportunity to study and sample drill core from the Kudz Ze Kayah, GP4F and Fyre Lake VMS deposits. Thanks to Robin Black, Neil Martin, and Darcy Baker for logistical and financial support while at KZK camp during the summer of 2017. Mark Baknes, Roger Hulstein, Ron Voordouw, Trent Newkirk, Dillon Hume, and other employees with BMC Minerals, Ltd. and Equity Exploration Consultants, Ltd., are also thanked for insightful discussions on the geology of KZK and the region. Flights to field sites would not have been possible without the excellent pilots from Trans North Helicopters. We thank Don Murphy for discussions and thorough reviews of this manuscript, and Karen MacFarlane for editorial support. Funding for this project was provided by BMC Minerals (No. 1) Ltd., Yukon Geological Survey, Targeted Geoscience Initiative 5 (TGI-5) program of the Geological Survey of Canada, and a NSERC Discovery Grant to Stephen Piercey.

Table 1. *Lithogeochemical results for felsic and mafic rocks in the Finlayson Lake region, Yukon.*

Sample	17MM-002	17MM-007	17MM-031	17MM-033	17MM-034	17MM-055*	17MM-066	17MM-074	17MM-075	17MM-077	17MM-001*	17MM-003*	17MM-038	17MM-040	17MM-054*
# on map[1]	2	6	10	11	12	25	31	32	33	34	1	3	16	17	24
Unit[2]	KZK - HW	KZK - HW	KZK - HW	KZK - FW	KZK - FW	KZK - HW	KZK - FW	KZK - FW	KZK - FW	KZK - FW	Wind Lake	Wind Lake	Wind Lake	Wind Lake	Wind Lake
UTME[3]	413907	415074	415049	415049	415049	366940	419500	419500	415122	415122	413749	412065	415397	415397	423699
UTMN[3]	6815182	6815570	6815467	6815467	6815467	6801900	6813355	6813355	6814798	6814798	6815933	6816318	6815422	6815422	6816422
Drillhole		K15-299	K15-301	K15-301	K15-301		K15-302	K15-302	K16-372	K16-372			K17-439	K17-439	
Depth (m)		66.35	30.13	118.37	128.51		46.71	175.31	62.22	401.11			23.61	70.50	
Lithology[4]	Felsic LT	Felsic LT	Felsic LT	Felsic LT	Felsic intrusive	Aphyric rhyolite	Felsic intrusive	Felsic CT	Felsic tuff	Felsic LT	Felsic tuff	Mafic tuff	Mafic intrusive	Mafic intrusive	Pillow basalt
Major elements (wt%)															
SiO_2	76	68.2	69.3	59.3	67.2	77.6	69.4	75.3	66.3	65.6	74	49.1	48.2	51.4	33.5
TiO_2	0.31	0.6	0.43	0.54	0.35	0.33	0.48	0.24	0.68	0.64	0.54	2.46	3.09	2.87	5.68
Al_2O_3	14	15	11.85	21	17.25	12.75	12.95	12.1	20.2	15.4	14	13.65	17.05	14.2	18.7
$Fe_2O_{3\ (T)}$	1.47	3.64	4.27	3.55	1.33	0.45	4.76	1.35	1.96	5.8	3.32	12.1	14.4	13.15	15.4
MnO	0.02	0.08	0.09	0.04	0.01	0.01	0.11	0.04	0.01	0.09	0.02	0.14	0.09	0.13	0.22
MgO	0.89	1.21	1.61	1.95	0.21	0.08	1.18	0.66	1.1	1.98	0.49	5.22	4.37	4.35	4.81
CaO	0.32	1.72	2.81	1.18	0.16	0.21	2.3	1.15	0.45	2.2	0.14	6.78	2.59	3.37	15.3
Na_2O	0.08	1.58	0.1	0.11	0.52	1.36	2.01	0.43	0.12	3.55	5.92	3.39	2.95	3.94	0.24
K_2O	5.04	4.29	3.83	8.02	12.45	8.1	4.99	7.38	7.26	2.39	1.17	0.2	1.48	2.49	0.11
Cr_2O_3	bdl	bdl	bdl	bdl	bdl	bdl	bdl	bdl	bdl	bdl	bdl	0.02	0.01	0.01	0.03
P_2O_5	0.15	0.17	0.18	0.07	0.05	0.04	0.06	0.07	0.21	0.2	0.08	0.41	0.88	0.54	1.06
SrO	bdl	bdl	bdl	bdl	0.02	bdl	0.02	0.01	bdl	bdl	bdl	0.01	bdl	0.01	0.14
BaO	0.28	0.22	0.11	0.4	1.37	0.12	0.24	0.09	0.31	0.26	0.08	<0.01	0.23	0.25	0.02
LOI	2.19	4.16	5.65	4.19	1.05	0.61	3.14	1.62	3.04	3.61	1.53	6.67	5.05	3.02	4
Total	100.75	100.87	100.23	100.35	101.97	101.66	101.64	100.44	101.64	101.72	101.29	100.15	100.39	99.73	99.21
Trace elements (ppm)															
Cs	2.19	2.17	1.78	3.37	2.13	1.54	2.15	4.48	3.39	1.46	1.85	0.43	0.86	9.14	0.18
Rb	180	135	130	349	283	240	104	162	203	71.1	43.9	10.6	40	98.4	3.6
Ba	2450	1905	981	3490	abl	1060	2190	806	2790	2290	661	40.5	2060	2180	149.5
Th	18.2	31.5	28.6	45.7	33.6	26.4	22.2	23.5	45.7	29.3	24.5	4.92	11.05	7.94	10.35
U	1.89	4.63	3.21	11.25	9.87	4.25	5.8	6.25	5.03	4.15	7.17	1.35	2.92	3.02	1.82
W	1	3	2	7	2	2	1	2	5	3	1	bdl	1	1	4
Nb	18.5	59.8	33.2	38.5	35	23.3	40.3	22.5	49.7	44.7	36.2	23.2	41.4	27.7	109
Ta	1.5	3.6	2	2.5	2.2	1.9	2.6	1.9	3.3	2.6	2.4	1.5	2.7	1.9	6.3
La	48	100	87.3	78.3	61.7	50.9	70.5	45.7	133.5	87.6	62.9	26.8	55.9	38.1	90.3
Ce	96.7	194	170	151.5	120.5	101.5	144	94.1	270	179.5	119	58.5	118	80.7	189.5
Pr	11.2	22.4	19.6	16.9	13.55	11.05	16.45	10.5	30.4	20.5	13.95	7.85	15.6	10.5	22.4
Sr	7.8	62.7	69.7	63.2	224	23.7	200	72.2	20.9	69.6	41	157.5	78.5	101	1150
Nd	41.1	83.1	73.5	59.2	44.9	36.1	60	36.1	107	74.5	51	33.2	64.6	43.5	85.8
Sm	7.85	14.4	14.1	10.35	8.08	7.35	12.7	7.5	21.2	14.5	10.45	7.79	14.4	9.35	17.3
Zr	192	765	491	686	505	361	784	228	828	727	673	257	500	319	437
Hf	5.2	18.7	12.3	18.8	13.8	10.8	19.8	7.5	21.3	18.7	16.5	6.3	11.9	8.1	11.5
Eu	1.05	2.5	2.15	0.82	0.62	0.68	1.95	0.74	3.02	2.43	1.87	2.61	3.38	2.4	6.2
Gd	6	12.5	10.3	7.5	5.21	6.14	12.35	7.38	18.05	12.85	9	7.97	14.3	9.04	17.35
Tb	0.93	1.86	1.52	1.27	0.84	0.87	2.06	1.33	2.56	1.8	1.4	1.28	2.27	1.35	2.33
Dy	4.92	10.5	8.3	7.9	4.68	5.3	11.95	7.89	13.55	10.05	8.32	7.69	13.55	7.89	11.9
Y	25	56	41.4	47.9	31.6	25	66.4	42	66.9	48.4	47.2	43.2	73	40.8	47.6
Ho	0.91	2.07	1.54	1.73	0.97	1.01	2.44	1.52	2.52	1.92	1.7	1.6	2.66	1.57	1.98
Er	2.53	5.86	4.2	5.68	3.25	3.13	7.45	4.52	7.13	5.62	5.11	4.21	7.73	4.41	4.73
Tm	0.36	0.81	0.59	0.84	0.61	0.4	1.09	0.66	0.91	0.73	0.83	0.66	1.04	0.63	0.57
Yb	1.98	5.28	3.72	6.03	4.51	2.65	6.6	3.93	5.47	4.72	5.36	4.02	6.61	3.92	2.92
Lu	0.26	0.77	0.58	1.02	0.77	0.41	1.01	0.62	0.83	0.68	0.86	0.56	1	0.65	0.41
Cr	20	20	20	20	30	20	10	10	20	20	10	130	50	70	220
V	24	26	19	28	18	17	15	12	37	29	21	333	264	345	216
Sn	6	5	4	17	9	7	7	7	6	4	3	3	2	2	6
Ga	20.7	26.7	19.6	37.4	22.9	20.6	23.6	18.6	35.4	23.5	21.2	22.2	27.2	21.3	39.7

*Outcrop samples
1 Number corresponds to sample locations on Figure 2
2 KZK = Kudz Ze Kayah formation; GLPS = Grass Lakes plutonic suite; HW = hanging wall; FW = footwall
3 Coordinates in NAD83 Zone 9N
4 LT = lapilli tuff; CT = crystal tuff; Fsp = feldspar; Qtz = quartz
bdl = below detection limit; abl = above detection limit

Table 1. *Lithogeochemical results for felsic and mafic rocks in the Finlayson Lake region, Yukon.*

Sample	17MM-060	17MM-043	17MM-047	17MM-049	17MM-050	17MM-056*	17MM-057*	17MM-004*	17MM-005*	17MM-051*	17MM-053*	17MM-061	17MM-062
# on map[1]	28	18	19	20	21	26	27	4	5	22	23	29	30
Unit[2]	Wind Lake?	Fire Lake - HW	Fire Lake - HW	Fire Lake - HW/FW	Fire Lake - FW	Fire Lake	Fire Lake	Wolverine Lake	GLPS	GLPS	GLPS	GLPS?	GLPS
UTME[3]	415122	419346	419346	419346	419346	411343	411789	429446	429291	409304	408605	415122	415122
UTMN[3]	6814798	6788812	6788812	6788812	6788812	6811450	6811402	6812106	6812095	6811726	6813581	6814798	6814798
Drillhole	K16-372	FL97-109	FL97-109	FL97-109	FL97-109							K16-372	K16-372
Depth (m)	27.14	87.40	203.94	265.54	352.44							103.45	585.00
Lithology[4]	Mafic intrusive	Siltstone	Si-altered clastic?	Siltstone	Mafic tuff/flow	Ultramafic	Ultramafic	Felsic grit	Granite	Granite	Fsp porphyry	Fsp-qtz porphyry	Granite
Major elements (wt. %)													
SiO_2	47.2	62	84.3	65.2	54.2	46.3	38.5	77.6	75.3	79.7	67.6	70.8	74.8
TiO_2	1.15	1.02	0.28	0.36	0.25	2.26	3.47	0.26	0.27	0.12	0.57	0.49	0.31
Al_2O_3	16.25	19.5	6.81	15.7	16.5	12.95	13.65	12.05	13.4	11.95	15	13.2	12.8
$Fe_2O_{3\,(T)}$	10.4	7.04	3.57	4.36	8.92	10.7	9.39	1.48	1.93	1.33	3.88	1.69	3.18
MnO	0.12	0.07	0.11	0.15	0.16	0.2	0.21	0.02	0.03	0.01	0.02	0.07	0.02
MgO	9.17	2.31	2.27	3.89	7.83	7.04	3.02	0.87	0.7	0.26	0.66	1.18	1.19
CaO	6.2	0.57	0.59	2.43	5.96	17.35	24.4	0.82	0.27	0.13	1.49	2.67	0.26
Na_2O	4.03	0.84	1.58	3.23	4.5	0.8	0.15	0.23	3.64	1.42	3.32	0.14	4.68
K_2O	0.78	3.75	0.74	2.37	0.48	0.12	0.1	6.06	3.2	5.16	5.78	6.67	2.33
Cr_2O_3	0.05	0.01	0.01	0.01	0.01	0.04	0.06	bdl	bdl	bdl	bdl	bdl	bdl
P_2O_5	0.14	0.16	0.04	0.05	0.02	0.29	0.74	0.15	0.15	0.08	0.15	0.15	0.08
SrO	0.01	0.02	bdl	0.04	0.01	0.07	0.12	bdl	bdl	bdl	0.02	bdl	bdl
BaO	0.03	0.09	0.2	0.61	0.09	0.01	0.02	0.13	0.08	0.03	0.18	0.16	0.06
LOI	5.1	3.88	1.4	2.27	1.94	1.71	6.38	2.05	1.24	1.29	0.76	3.66	0.88
Total	100.63	101.26	101.9	100.67	100.87	99.84	100.21	101.72	100.21	101.48	99.43	100.88	100.59
Trace elements (ppm)													
Cs	2.16	2.61	2.23	18.4	5.01	0.12	0.07	0.43	0.78	3.92	2.86	1.44	2.22
Rb	34.4	161.5	21.6	76.5	15	2.3	2.1	131	113.5	185.5	180	171	80.4
Ba	227	839	1820	5320	807	44.2	143	1105	750	298	1600	1450	509
Th	1.51	16.1	4.99	9.66	0.21	2.89	6.21	13.95	15.2	14.3	37.8	25.9	27.1
U	0.43	3.74	0.9	3.47	0.19	1.71	4.22	5.66	3.23	3.75	3.63	4.71	7.72
W	1	3	2	1	1	1	2	2	2	4	2	3	2
Nb	9	20.4	5.1	6.7	0.5	33.5	63.8	15.8	17.6	19	35.7	35.9	22.5
Ta	0.6	1.5	0.4	0.5	0.1	2.1	3.9	1.4	1.6	1.8	2.2	2.3	1.6
La	10.5	51.9	17.3	28.4	0.8	14.4	160	36	31.1	27.6	105	74.6	51.4
Ce	23.2	102.5	38.1	50.8	1.6	47.1	226	71.4	71.6	60.3	199	152	105.5
Pr	3.02	12.4	4.41	5.94	0.23	6.74	20.1	8.16	7.38	6.61	22.4	17.6	11.75
Sr	129.5	215	87.5	385	168.5	621	979	57.1	47.3	23.7	248	64.7	37
Nd	13.1	46.8	17.1	21.4	0.8	28.2	64.3	30	26.9	22.9	78.1	62.3	38.9
Sm	3.61	9.38	3.59	4.31	0.43	6.1	11.35	6.05	5.41	5.38	13.5	12.15	8.23
Zr	89	282	84	143	11	147	234	164	199	105	661	609	244
Hf	2.7	7.7	1.8	4.3	0.3	4.2	6.1	4.5	5.5	3.6	16.4	15.5	7.7
Eu	1.22	1.87	0.85	1.16	0.14	2.61	4.72	0.85	0.82	0.45	2.08	1.82	0.8
Gd	4.14	7.8	3.29	4.1	0.72	6.52	12.1	5.16	4.77	5.24	10.95	11.3	8.53
Tb	0.71	1.22	0.51	0.69	0.17	0.96	1.66	0.82	0.77	0.96	1.56	1.73	1.47
Dy	4.08	7.29	3.11	4.26	1.31	5.13	8.94	4.54	4.83	6.14	8.55	9.27	8.6
Y	21.4	40.8	13.9	21.8	8.9	25.2	39.3	24.5	26.8	36.6	44.9	49.1	47
Ho	0.87	1.44	0.62	0.86	0.33	1	1.7	0.84	1	1.24	1.63	1.91	1.76
Er	2.45	4.28	1.8	2.53	1.2	2.69	4.29	2.4	2.58	3.65	4.51	5.48	5.13
Tm	0.32	0.67	0.29	0.4	0.19	0.34	0.52	0.28	0.36	0.46	0.68	0.73	0.68
Yb	1.9	4.14	1.94	2.75	1.36	1.96	3.25	1.74	2.55	3.14	4.34	4.79	4.11
Lu	0.3	0.57	0.29	0.44	0.22	0.3	0.47	0.28	0.36	0.44	0.62	0.75	0.62
Cr	390	110	100	50	80	260	450	20	20	20	20	20	20
V	233	135	83	71	294	259	478	27	12	7	32	27	16
Sn	1	4	2	3	<1	3	4	6	4	7	4	4	4
Ga	18.1	26.9	11.9	19.7	14.4	20.2	22.9	19.1	19.1	19.5	24.6	24.7	21

*Outcrop samples
1 Number corresponds to sample locations on Figure 2
2 KZK = Kudz Ze Kayah formation; GLPS = Grass Lakes plutonic suite; HW = hanging wall; FW = footwall
3 Coordinates in NAD83 Zone 9N
4 LT = lapilli tuff; CT = crystal tuff; Fsp = feldspar; Qtz = quartz
bdl = below detection limit; abl = above detection limit

References

Barrie, C.T., 1995. Zircon thermometry of high temperature rhyolites near volcanic-associated massive sulfide deposits, Abitibi Province, Canada. Geology, vol. 23, p. 169–172. doi:10.1130/0091-7613(1995)023<0169.

Barrie, C.T., Amelin, Y. and Pascual, E., 2002. U-Pb geochronology of VMS mineralization in the Iberian Pyrite belt. Mineralium Deposita, vol. 37, p. 684–703. doi:10.1007/s00126-002-0302-7.

BMC Minerals Ltd., 2017. Kudz Ze Kayah Project, http://bmcminerals.com/projects/kudz-ze-kayah-project/, [accessed October 1, 2017].

Codeço, M.S., Mateus, A., Figueiras, J., Rodrigues, P. and Gonçalves, L., 2018. Development of the Ervidel-Roxo and Figueirinha-Albernoa volcanic sequences in the Iberian pyrite Belt, Portugal: Metallogenic and geodynamic implications. Ore Geology Reviews, vol. 98, p. 80–108. doi:10.1016/j.oregeorev.2018.05.009.

Bradshaw, G.D., Rowins, S.M., Peter, J.M. and Taylor, B.E., 2008. Genesis of the wolverine volcanic sediment-hosted massive sulfide deposit, Finlayson Lake District, Yukon, Canada: Mineralogical, mineral chemical, fluid inclusion, and sulfur isotope evidence. Economic Geology, vol. 103, p. 35–60. doi:10.2113/gsecongeo.103.1.35.

Colpron, M. and Nelson, J., 2011. A Digital Atlas of Terranes for the Northern Cordillera. Yukon Geological Survey, www.geology.gov.yk.ca.

Colpron, M., Nelson, J.L. and Murphy, D.C., 2006. A tectonostratigraphic framework for the pericratonic terranes of the northern Canadian Cordillera. *In*: Paleozoic Evolution and Metallogeny of Pericratonic Terranes at the Ancient Pacific Margin of North America, Canadian and Alaskan Cordillera, M. Colpron and J.L. Nelson (eds.), Geological Association of Canada, Special Paper 45, p. 1–23.

Gabrielse, H., Murphy, D.C. and Mortensen, J.K., 2006. Cretaceous and Cenozoic dextral orogen-parallel displacements, magmatism, and paleogeography, north-central Canadian Cordillera. *In*: Paleogeography of the North American Cordillera: Evidence For and Against Large-Scale Displacements, J.W. Haggart, R.J. Enkin, and J.W.H. Monger (eds.), Geological Association of Canada, Special Paper 46, p. 255–276.

Galley, A.G., Hannington, M.D. and Jonasson, I.R., 2007. Volcanogenic massive sulphide deposits. *In:* Mineral Deposits of Canada: A Synthesis of Major Deposit-Types, District Metallogeny, the Evolution of Geological Provinces, and Exploration Methods, W.D. Goodfellow (ed.), Geological Association of Canada, Mineral Deposits Division, Special Publication No. 5, p. 141–161.

Grant, S.L., 1997. Geochemical, radiogenic tracer isotopic, and U-Pb geochronological studies of Yukon-Tanana terrane rocks from the Money klippe, southeastern Yukon, Canada. Unpublished MSc thesis, University of Alberta, Edmonton, 177 p.

Ishikawa, Y., Sawaguchi, T., Iwaya, S. and Horiuchi, M., 1976. Delineation of prospecting targets for Kuroko deposits based on modes of volcanism of underlying dacite and alteration halos. Mining Geology, vol. 26, p. 105–117 (in Japanese with English abs.).

Large, R.R., Gemmell, J.B. and Paulick, H., 2001. The alternation box plot: A simple approach to understanding the relationship between alteration mineralogy and lithogeochemistry associated with volcanic-hosted massive sulfide deposits. Economic Geology, vol. 96, p. 957–971. doi:10.2113/gsecongeo.96.5.957.

Leat, P.T., Jackson, S.E., Thorpe, R.S. and Stillman, C.J., 1986. Geochemistry of bimodal basalt-subalkaline/peralkaline rhyolite provinces within the Southern British Caledonides. Journal of the Geological Society, vol. 143, p. 259–273. doi:10.1144/gsjgs.143.2.0259.

Lentz, D.R., 1998. Petrogenetic evolution of felsic volcanic sequences associated with Phanerozoic volcanic-hosted massive sulphide systems: the role of extensional geodynamics. Ore Geology Reviews, vol. 12, p. 289–327. doi:10.1016/S0169-1368(98)00005-5.

Lentz, D.R., 1999. Petrology, geochemistry, and oxygen isotope interpretation of felsic volcanic and related rocks hosting the Brunswick 6 and 12 massive sulfide deposits (Brunswick belt), Bathurst mining camp, New Brunswick, Canada. Economic Geology, vol. 94, p. 57–86. doi:10.2113/gsecongeo.94.1.57.

Manor, M.J. and Piercey, S.J., 2018. Re-evaluating the chronostratigraphic framework for felsic volcanic and intrusive rocks of the Finlayson Lake region, Yukon-Tanana terrane, Yukon. *In:* Yukon Exploration and Geology 2017, K. MacFarlane (ed.), Yukon Geological Survey, p. 111–128.

McDonough, W.F. and Sun, S.S., 1995. The composition of the Earth. Chemical Geology, vol. 2541, p. 223–253. doi:10.1016/0009-2541(94)00140-4.

McLennan, S.M., 2001. Relationships between the trace element composition of sedimentary rocks and upper continental crust. Geochemistry, Geophysics, Geosystems, vol. 2, p. 1–30. doi: 10.1029/2005GC001005.

Mortensen, J.K., 1992. Pre-Mid-Mesozoic tectonic evolution of the Yukon-Tanana Terrane, Yukon and Alaska. Tectonics, vol. 11, p. 836–853. doi: 10.1029/91TC01169.

Mortensen, J.K. and Jilson, G.A., 1985. Evolution of the Yukon-Tanana terrane: evidence from southeastern Yukon Territory. Geology, vol. 13, p. 806–810. doi:1130/0091-7613(1985)13<806:EOTYTE>2.0.CO;2.

Murphy, D.C., Colpron, M., Roots, C.F., Gordey, S.P. and Abbott, J.G., 2002. Finlayson Lake Targeted Geoscience Initiative (southeastern Yukon), Part 1: Bedrock geology. *In*: Yukon Exploration and Geology 2001, D.S. Emond, L.H. Weston and L.L. Lewis (eds.), Exploration and Geological Services Division, Yukon Region, Indian and Northern Affairs Canada, p. 189–207.

Murphy, D.C., Mortensen, J.K., Piercey, S.J., Orchard, M.J. and Gehrels, G.E., 2006. Mid-Paleozoic to early Mesozoic tectonostratigraphic evolution of Yukon-Tanana and Slide Mountain terranes and affiliated overlap assemblages, Finlayson Lake massive sulphide district, southeastern Yukon. *In*: Paleozoic Evolution and Metallogeny of Pericratonic Terranes at the Ancient Pacific Margin of North America, Canadian and Alaskan Cordillera, M. Colpron and J.L. Nelson (eds.), Geological Association of Canada, Special Paper 45, p. 75–106.

Pearce, J.A., Harris, N.B.W. and Tindle, A.G., 1984. Trace element distribution diagrams for the tectonic interpretation of granitic rocks. Journal of Petrology, vol. 25, p. 956–983.

Peter, J.M., Layton-Matthews, D., Piercey, S.J., Bradshaw, G.D., Paradis, S. and Bolton, A., 2007. Volcanic-hosted massive sulphide deposits of the Finlayson Lake District, Yukon. *In*: Mineral Deposits of Canada: A Synthesis of Major Deposit-Types, District Metallogeny, the Evolution of Geological Provinces, and Exploration Methods, W.D. Goodfellow (ed.), Geological Association of Canada, Mineral Deposits Division, Special Publication No. 5, p. 471–508.

Piercey, S.J., 2001. Petrology and tectonic setting of felsic and mafic volcanic and intrusive rocks in the Finlayson Lake volcanic-hosted massive sulphide (VHMS) district, Yukon, Canada: A record of mid-Paleozoic arc and back-arc magmatism and metallogeny. Unpublished PhD dissertation, University of British Columbia, Vancouver, Canada, 324 p.

Piercey, S.J., 2011. The setting, style, and role of magmatism in the formation of volcanogenic massive sulfide deposits. Mineralium Deposita, vol. 46, p. 449–471. doi:10.1007/s00126-011-0341-z.

Piercey, S.J. and Colpron, M., 2009. Composition and provenance of the Snowcap assemblage, basement to the Yukon-Tanana terrane, northern Cordillera: Implications for Cordilleran crustal growth. Geosphere, vol. 5, p. 439–464. doi:10.1130/GES00505.S3.

Piercey, S.J. and Murphy, D.C., 2000. Stratigraphy and regional implications of unstrained Devono-Mississippian volcanic rocks in the Money Creek thrust sheet, Yukon-Tanana Terrane, Southeastern Yukon. *In*: Yukon Exploration and Geology 1999, D.S. Emond and L.H. Weston (eds.), Exploration and Geological Services Division, Yukon Region, Indian and Northern Affairs Canada, p. 67–78.

Piercey, S.J., Paradis, S., Murphy, D.C. and Mortensen, J.K., 2001. Geochemistry and paleotectonic setting of felsic volcanic rocks in the Finlayson Lake volcanic-hosted massive sulfide district, Yukon, Canada. Economic Geology, vol. 96, p. 1877–1905. doi: 10.2113/gsecongeo.96.8.1877.

Piercey, S.J., Mortensen, J.K., Murphy, D.C., Paradis, S. and Creaser, R.A., 2002a. Geochemistry and tectonic significance of alkalic mafic magmatism in the Yukon-Tanana terrane, Finlayson Lake region, Yukon. Canadian Journal of Earth Sciences, vol. 39, p. 1729–1744. doi:10.1139/E02-090.

Piercey, S.J., Murphy, D.C., Mortensen, J.K. and Paradis, S., 2002b. Boninitic magmatism in a continental margin setting, Yukon-Tanana terrane, southeastern Yukon, Canada. Geology, vol. 29, p. 731–734. doi: 30/0091-7613(2001)029<0731:BMIACM>2.0.CO;2.

Piercey, S.J., Paradis, S.J., Peter, J.M. and Tucker, T.L., 2002c. Geochemistry of basalt from the Wolverine volcanic-hosted massive-sulphide deposit, Finlayson Lake district, Yukon Territory. Geological Survey of Canada, Current Research 2002-A3, 11 p.

Piercey, S.J., Mortensen, J.K. and Creaser, R.A, 2003. Neodymium isotope geochemistry of felsic volcanic and intrusive rocks from the Yukon-Tanana Terrane in the Finlayson Lake Region, Yukon, Canada. Canadian Journal of Earth Sciences, vol. 40, p. 77–97. doi: 10.1139/e02-094.

Piercey, S.J., Murphy, D.C., Mortensen, J.K. and Creaser, R.A., 2004. Mid-Paleozoic initiation of the northern Cordilleran marginal backarc basin: Geologic, geochemical, and neodymium isotope evidence from the oldest mafic magmatic rocks in the Yukon-Tanana terrane, Finlayson Lake district, southeast Yukon, Canada. Bulletin of the Geological Society of America, vol. 116, p. 1087–1106. doi:10.1130/B25162.1.

Piercey, S.J., Nelson, J.L., Colpron, M., Dusel-Bacon, C., Simard, R.-L. and Roots, C.F., 2006. Paleozoic magmatism and crustal recycling along the ancient Pacific margin of North America, northern Cordillera. *In*: Paleozoic Evolution and Metallogeny of Pericratonic Terranes at the Ancient Pacific Margin of North America, Canadian and Alaskan Cordillera, M. Colpron and J.L. Nelson (eds.), Geological Association of Canada, Special Paper 45, p. 281–322.

Piercey, S.J., Peter, J.M., Mortensen, J.K., Paradis, S., Murphy, D.C. and Tucker, T.L., 2008. Petrology and U-Pb geochronology of footwall porphyritic rhyolites from the wolverine volcanogenic massive sulfide deposit, Yukon, Canada: Implications for the genesis of massive sulfide deposits in continental margin environments. Economic Geology, vol. 103, p. 5–33. doi:10.2113/gsecongeo.103.1.5.

Piercey, S.J., Murphy, D.C. and Creaser, R.A., 2012. Lithosphere-asthenosphere mixing in a transform-dominated late Paleozoic backarc basin: Implications for northern Cordilleran crustal growth and assembly. Geosphere, vol. 8, p. 716–739. doi:10.1130/GES00757.1.

Piercey, S.J., Gibson, H.L., Tardif, N. and Kamber, B.S., 2016. Ambient redox and hydrothermal environment of the Wolverine volcanogenic massive sulfide deposit, Yukon: Insights from lithofacies and lithogeochemistry of Mississippian host shales. Economic Geology, vol. 111, p. 1439–1463. doi: 10.2113/econgeo.111.6.1439.

Piercey, S.J., Beranek, L.P. and Hanchar, J.M., 2017. Mapping magma prospectivity for Cordilleran volcanogenic massive sulphide (VMS) deposits using Nd-Hf isotopes: Preliminary results. *In*: Yukon Exploration and Geology 2016, K.E. MacFarlane and L.H. Weston, (eds.), Yukon Geological Survey, p. 197–205.

Rosa, D.R.N., Finch, A.A., Andersen, T. and Inverno, C.M.C., 2009. U-Pb geochronology and Hf isotope ratios of magmatic zircons from the Iberian Pyrite Belt. Mineralogy and Petrology, vol. 95, p. 47–69. doi: 10.1007/s00710-008-0022-5.

Ross, P.-S. and Bédard, J.H., 2009. Magmatic affinity of modern and ancient subalkaline volcanic rocks determined from trace-element discriminant diagrams. Canadian Journal of Earth Sciences, vol. 46, p. 823–839. doi:10.1139/E09-054.

Ross, P.-S., McNicoll, V.J., Debreil, J.A. and Carr, P., 2014. Precise U-Pb geochronology of the Matagami mining camp, Abitibi greenstone belt, Quebec: Stratigraphic constraints and implications for volcanogenic massive sulfide exploration. Economic Geology, vol. 109, p. 89–101. doi: 10.2113/econgeo.109.1.89.

Sebert, C., Hunt, J.A. and Foreman, I.J., 2004. Geology and lithogeochemistry of the Fyre Lake copper-cobalt-gold sulphide-magnetite deposit, southeastern Yukon. Yukon Geological Survey, Open File 2004-17, 46 p.

Shervais, J.W., 1982. Ti-V plots and the petrogenesis of modern and ophiolitic lavas. Earth and Planetary Science Letters, vol. 59, p. 101–118. doi: 10.1016/0012-821X(82)90120-0.

Tempelman-Kluit, D.J., 1979. Transported cataclasite, ophiolite and granodiorite in Yukon: Evidence of arc-continent collision. Geological Survey of Canada, Paper 79-1, 27 p.

Winchester, J.A. and Floyd, P.A., 1977. Geochemical discrimination of different magma series and their differentiation products using immobile elements. Chemical Geology, vol. 20, p. 325–343. doi: 10.1016/0009-2541(77)90057-2.

Yukon Geological Survey, 2018. Yukon Digital Bedrock Geology. Yukon Geological Survey, http://www.geology.gov.yk.ca/update_yukon_bedrock_geology_map.html [accessed 10 August 2018].

Appendix 1. *QA/QC results for ALS lithogeochemical analyses of the Finlayson Lake district, Yukon.*

	SLV-MC basalt							WP-1 Watts Point dacite (Coast Plutonic Complex)					17MM-031 KZK					17MM-062 Grass Lakes plutonic suite					17MM-066 KZK (GP4F)				
Sample	Q931840	Q931840 (ALS dup)	Q931840 (ALS dup)	Q931842	Mean	σ	% RSD	Q931841	Q931843	Mean	σ	% RSD	17MM-031	Q931876 (17MM-031)	Mean	σ	% RSD	17MM-062	Q931885 (17MM-062)	Mean	σ	% RSD	17MM-066	17MM-066	Mean	σ	% RSD
Rock Type	SLV-MC basalt	SLV-MC basalt	SLV-MC basalt	SLV-MC basalt				WP-1 dacite	WP-1 dacite				Felsic ash-lapilli tuff	Felsic ash-lapilli tuff				Qtz-Fsp porphyry	Qtz-Fsp porphyry				Int. intrusive	Int. intrusive			
Major elements (wt%)																											
SiO_2	49.8	49.8	49.8	50.3	49.93	0.25	0.50	65.6	65.3	65.45	0.21	0.32	69.3	65.1	67.20	2.97	4.42	74.8	75.8	75.30	0.71	0.94	69.4	68.2	68.80	0.85	1.23
Al_2O_3	15.6	15.6	15.6	15.65	15.61	0.03	0.16	16.75	16.45	16.60	0.21	1.28	11.85	12.1	11.98	0.18	1.48	12.8	13.05	12.93	0.18	1.37	12.95	12.7	12.83	0.18	1.38
Fe_2O_3	12.85	12.85	12.9	13.05	12.91	0.09	0.73	4.41	4.39	4.40	0.01	0.32	4.27	4.44	4.36	0.12	2.76	3.18	2.49	2.84	0.49	17.21	4.76	4.68	4.72	0.06	1.20
CaO	8.62	8.62	8.59	8.82	8.66	0.11	1.22	4.91	4.98	4.95	0.05	1.00	2.81	3.61	3.21	0.57	17.62	0.26	0.4	0.33	0.10	30.00	2.3	2.25	2.28	0.04	1.55
MgO	7.57	7.57	7.57	7.59	7.58	0.01	0.13	2.62	2.58	2.60	0.03	1.09	1.61	1.8	1.71	0.13	7.88	1.19	0.99	1.09	0.14	12.97	1.18	1.15	1.17	0.02	1.82
Na_2O	3.61	3.61	3.63	3.59	3.61	0.02	0.45	4.46	4.32	4.39	0.10	2.26	0.1	0.11	0.11	0.01	6.73	4.68	4.82	4.75	0.10	2.08	2.01	2.03	2.02	0.01	0.70
K_2O	0.54	0.54	0.55	0.53	0.54	0.01	1.51	1.64	1.63	1.64	0.01	0.43	3.83	4.05	3.94	0.16	3.95	2.33	2.27	2.30	0.04	1.84	4.99	4.91	4.95	0.06	1.14
Cr_2O_3	0.03	0.03	0.03	0.03	0.03	0.00	0.00	0.01	0.01	0.01	0.00	0.00	bdl	bdl				bdl	bdl				<0.01	bdl			
TiO_2	1.5	1.5	1.5	1.47	1.49	0.02	1.01	0.49	0.47	0.48	0.01	2.95	0.43	0.5	0.47	0.05	10.64	0.31	0.29	0.30	0.01	4.71	0.48	0.47	0.48	0.01	1.49
MnO	0.17	0.17	0.17	0.17	0.17	0.00	0.00	0.08	0.08	0.08	0.00	0.00	0.09	0.09	0.09	0.00	0.00	0.02	0.02	0.02	0.00	0.00	0.11	0.1	0.11	0.01	6.73
P_2O_5	0.25	0.25	0.25	0.24	0.25	0.01	2.02	0.17	0.17	0.17	0.00	0.00	0.18	0.19	0.19	0.01	3.82	0.08	0.08	0.08	0.00	0.00	0.06	0.06	0.06	0.00	0.00
SrO	0.05	0.05	0.05	0.05	0.05	0.00	0.00	0.09	0.08	0.09	0.01	8.32	bdl	bdl				bdl	bdl				0.02	0.02	0.02	0.00	0.00
BaO	0.02	0.02	0.02	0.02	0.02	0.00	0.00	0.07	0.07	0.07	0.00	0.00	0.11	0.1	0.11	0.01	6.73	0.06	0.06	0.06	0.00	0.00	0.24	0.23	0.24	0.01	3.01
LOI	-0.85			-0.72	-0.79	0.09	-11.71	0.2	0.17	0.19	0.02	11.47	5.65	6.5	6.08	0.60	9.89	0.88	0.95	0.92	0.05	5.41					
Total	99.76			100.79	100.28	0.73	0.73	101.5	100.7	101.10	0.57	0.56	100.23	98.59	99.41	1.16	1.17	100.59	101.22	100.91	0.45	0.44					
Trace elements (ppm)																											
Ba	165	165	163	156.5	162.38	4.03	2.48	645	613	629.00	22.63	3.60	981	927	954.00	38.18	4.00	509	521	515.00	8.49	1.65	2190	2130	2160.00	42.43	1.96
Ce	22.7	22.7	22.4	21.6	22.35	0.52	2.32	29.1	28.3	28.70	0.57	1.97	170	143.5	156.75	18.74	11.95	105.5	94.9	100.20	7.50	7.48	144	143	143.50	0.71	0.49
Cr	240	240	250	240	242.50	5.00	2.06	80	80	80.00	0.00	0.00	20	20	20.00	0.00	0.00	20	20	20.00	0.00	0.00	10	10	10.00	0.00	0.00
Cs	0.12	0.12	0.06	0.07	0.09	0.03	34.61	0.43	0.35	0.39	0.06	14.50	1.78	1.97	1.88	0.13	7.17	2.22	1.64	1.93	0.41	21.25	2.15	2.24	2.20	0.06	2.90
Dy	3.67	3.67	3.73	3.8	3.72	0.06	1.66	2.43	2.4	2.42	0.02	0.88	8.3	9	8.65	0.49	5.72	8.6	8.15	8.38	0.32	3.80	11.95	11.7	11.83	0.18	1.49
Er	1.86	1.86	1.84	1.89	1.86	0.02	1.11	1.39	1.49	1.44	0.07	4.91	4.2	5.3	4.75	0.78	16.38	5.13	5.04	5.09	0.06	1.25	7.45	7.21	7.33	0.17	2.32
Eu	1.45	1.45	1.44	1.43	1.44	0.01	0.66	0.93	0.92	0.93	0.01	0.76	2.15	1.94	2.05	0.15	7.26	0.8	0.7	0.75	0.07	9.43	1.95	1.92	1.94	0.02	1.10
Ga	22	22	21.1	21.6	21.68	0.43	1.97	19.3	19.8	19.55	0.35	1.81	19.6	20.4	20.00	0.57	2.83	21	20.1	20.55	0.64	3.10	23.6	23.1	23.35	0.35	1.51
Gd	3.88	3.88	4.14	4.18	4.02	0.16	4.04	2.78	2.79	2.79	0.01	0.25	10.3	9.78	10.04	0.37	3.66	8.53	7.5	8.02	0.73	9.09	12.35	12.5	12.43	0.11	0.85
Hf	2.6	2.6	2.7	2.8	2.68	0.10	3.58	3.5	3.3	3.40	0.14	4.16	12.3	14	13.15	1.20	9.14	7.7	6.6	7.15	0.78	10.88	19.8	19.6	19.70	0.14	0.72
Ho	0.7	0.7	0.71	0.68	0.70	0.01	1.80	0.48	0.48	0.48	0.00	0.00	1.54	1.89	1.72	0.25	14.43	1.76	1.71	1.74	0.04	2.04	2.44	2.4	2.42	0.03	1.17
La	10	10	10.3	9.3	9.90	0.42	4.29	14.4	13.3	13.85	0.78	5.62	87.3	74	80.65	9.40	11.66	51.4	46.6	49.00	3.39	6.93	70.5	70	70.25	0.35	0.50
Lu	0.24	0.24	0.23	0.21	0.23	0.01	6.15	0.21	0.2	0.21	0.01	3.45	0.58	0.75	0.67	0.12	18.08	0.62	0.61	0.62	0.01	1.15	1.01	1.05	1.03	0.03	2.75
Nb	8.9	8.9	8.5	8.5	8.70	0.23	2.65	3.6	3.5	3.55	0.07	1.99	33.2	35.5	34.35	1.63	4.73	22.5	22.6	22.55	0.07	0.31	40.3	40.7	40.50	0.28	0.70
Nd	14.8	14.8	14.5	13	14.28	0.86	6.04	15.7	14	14.85	1.20	8.09	73.5	63.1	68.30	7.35	10.77	38.9	36.1	37.50	1.98	5.28	60	58.9	59.45	0.78	1.31
Pr	3.2	3.2	3.16	2.94	3.13	0.12	3.99	3.85	3.62	3.74	0.16	4.35	19.6	16.75	18.18	2.02	11.09	11.75	10.75	11.25	0.71	6.29	16.45	16.6	16.53	0.11	0.64
Rb	6.1	6.1	6.2	5.5	5.98	0.32	5.36	23.7	22	22.85	1.20	5.26	130	143.5	136.75	9.55	6.98	80.4	69.4	74.90	7.78	10.38	104	102.5	103.25	1.06	1.03
Sm	4.02	4.02	3.87	3.8	3.93	0.11	2.82	3.03	2.98	3.01	0.04	1.18	14.1	11.75	12.93	1.66	12.86	8.23	7.76	8.00	0.33	4.16	12.7	12.85	12.78	0.11	0.83
Sn	2	2	2	2	2.00	0.00	0.00	2	2	2.00	0.00	0.00	4	4	4.00	0.00	0.00	4	4	4.00	0.00	0.00	7	7	7.00	0.00	0.00
Sr	497	497	505	478	494.25	11.47	2.32	789	743	766.00	32.53	4.25	69.7	88	78.85	12.94	16.41	37	39.9	38.45	2.05	5.33	200	199	199.50	0.71	0.35
Ta	0.6	0.6	0.5	0.5	0.55	0.06	10.50	0.3	0.2	0.25	0.07	28.28	2	2.1	2.05	0.07	3.45	1.6	1.9	1.75	0.21	12.12	2.6	2.7	2.65	0.07	2.67
Tb	0.64	0.64	0.63	0.66	0.64	0.01	1.96	0.41	0.43	0.42	0.01	3.37	1.52	1.67	1.60	0.11	6.65	1.47	1.36	1.42	0.08	5.50	2.06	1.97	2.02	0.06	3.16
Th	0.94	0.94	0.94	0.92	0.94	0.01	1.07	2.14	2.14	2.14	0.00	0.00	28.6	23.4	26.00	3.68	14.14	27.1	23.4	25.25	2.62	10.36	22.2	22	22.10	0.14	0.64
Tm	0.26	0.26	0.24	0.27	0.26	0.01	4.89	0.19	0.2	0.20	0.01	3.63	0.59	0.75	0.67	0.11	16.89	0.68	0.68	0.68	0.00	0.00	1.09	0.97	1.03	0.08	8.24
U	0.33	0.33	0.3	0.31	0.32	0.02	4.72	1.12	0.84	0.98	0.20	20.20	3.21	3.59	3.40	0.27	7.90	7.72	5.67	6.70	1.45	21.65	5.8	5.67	5.74	0.09	1.60
V	197	197	204	196	198.50	3.70	1.86	92	90	91.00	1.41	1.55	19	25	22.00	4.24	19.28	16	16	16.00	0.00	0.00	15	14	14.50	0.71	4.88
W	1	1	1	1	1.00	0.00	0.00	bdl	bdl				2	2	2.00	0.00	0.00	2	2	2.00	0.00	0.00	1	1	1.00	0.00	0.00
Y	18.2	18.2	18.2	17.3	17.98	0.45	2.50	13.7	12.8	13.25	0.64	4.80	41.4	50.6	46.00	6.51	14.14	47	46.1	46.55	0.64	1.37	66.4	64.3	65.35	1.48	2.27
Yb	1.6	1.6	1.44	1.48	1.53	0.08	5.39	1.26	1.29	1.28	0.02	1.66	3.72	4.51	4.12	0.56	13.58	4.11	4.09	4.10	0.01	0.34	6.6	6.57	6.59	0.02	0.32
Zr	104	104	105	95	102.00	4.69	4.60	133	119	126.00	9.90	7.86	491	595	543.00	73.54	13.54	244	206	225.00	26.87	11.94	784	775	779.50	6.36	0.82

Analyzing historic drilling data to investigate gold distribution on lower Hunker Creek and Klondike River

Sydney van Loon
Yukon Geological Survey

van Loon, S., 2019. Analyzing historic drilling data to investigate gold distribution on lower Hunker Creek and Klondike River. *In:* Yukon Exploration and Geology 2018, K.E. MacFarlane (ed.), Yukon Geological Survey, p. 111–126.

Abstract

The Yukon Consolidated Gold Corporation (YCGC) tested, mined, and documented placer gold resources in the Dawson region from 1923 to 1965. The company was established to acquire the holdings of other dredging operations and smaller companies in the Klondike, and during the time it was active in Yukon, YCGC produced a robust collection of maps and textual documents including drilling results, dredge reserves, thawing and stripping layouts, and dredging limits.

This paper uses historic YCGC data to summarize gold distribution characteristics in Hunker Creek and builds upon previously published summaries of YCGC data. Attributes of 1005 YCGC drill holes and shafts along lower Hunker Creek and a short section of the Klondike River were digitized, compiled, and analyzed in a Geographical Information System (GIS). A raster analysis of the digitized data allows for interpretation and examination of surficial material thicknesses and gold distribution in the project area and identifies potential prospects for further exploration.

* sydney.vanloon@gov.yk.ca

Introduction

Yukon Consolidated Gold Corporation (YCGC) operated in the Klondike for four decades (from 1923 to 1965) conducting mining operations and evaluating placer gold potential in many of the region's drainages. Technical staff at YCGC produced a robust collection of maps and textual documents including drilling results, dredging limits, dredge reserves, and thawing and stripping layouts during the time the company was active in Yukon. The exploration and mining data recorded by YCGC continues to assist modern mining activities in prominent gold-bearing drainages including Hunker, Bonanza, Quartz, Dominion and Sulphur creeks. Despite the vintage of these data, records from drilling conducted nearly one hundred years ago are thorough and a valuable tool for evaluating placer ground being mined today.

Bringing historic drill hole data and dredge limits into digital formats can assist the placer mining industry in unearthing new exploration targets. As shown in previous compilations (van Loon, 2016, 2017), translating paper records into a Geographical Information System (GIS) allows for a variety of spatial analyses that are difficult with paper maps and records. Placer potential can be identified through trends in gold distribution and surficial material thickness visible on raster maps that highlight tributary gold inputs, economic values in previously worked areas, and valley margins outside of dredge limits that may include unmined side pay and intermediate-level terraces.

Project Area

The project area (Fig. 1) is a 15 km-long stretch of valley bottom extending from the mouth of Colorado Creek, a left limit tributary of lower Hunker Creek, downstream to the mouth of Bear Creek in the Klondike River valley. Point and polygon data have been compiled from 31 historic YCGC maps dating from 1910 to 1958 (see references for YCGC file details); 1005 drill holes and shafts, and 25 km^2 of individual/isolated dredged area polygons have been digitized (Fig. 2). Of the 1005 drill holes and shafts, 83 are located on Dago and Paradise hills, which along with Australian Hill, are high-level White Channel benches perched above the modern Hunker Creek valley.

Hunker Creek has been a top producing placer creek since the discovery claim was first staked in 1897. Since then, the drainage has undergone extensive prospecting, drilling, dredging, cat mining and modern mining activities. More than 1.8 million crude ounces have been recovered from Hunker Creek and its respective tributaries since 1897. Dredge operations were active in the main stem of the drainage from 1908 to 1966 and produced more than 450,000 crude ounces.

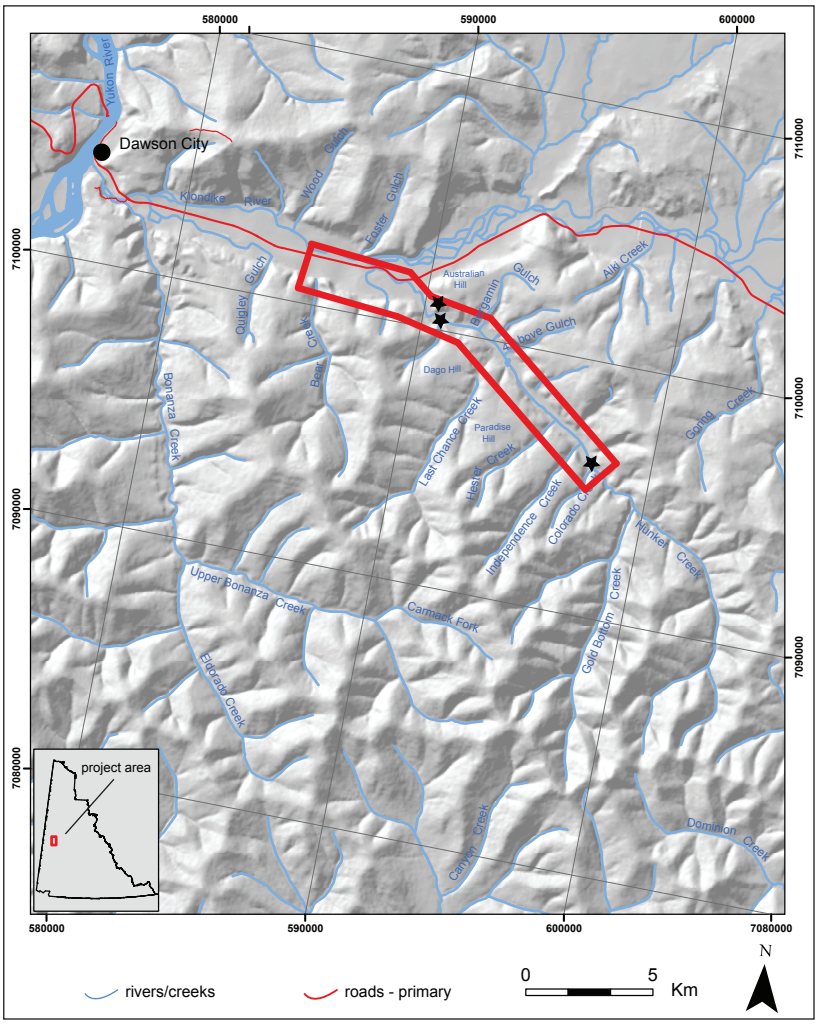

Figure 1. *Project area southeast of Dawson City on lower Hunker Creek and Klondike River valley; black stars indicate highest grades recovered from the YCGC drilling data set.*

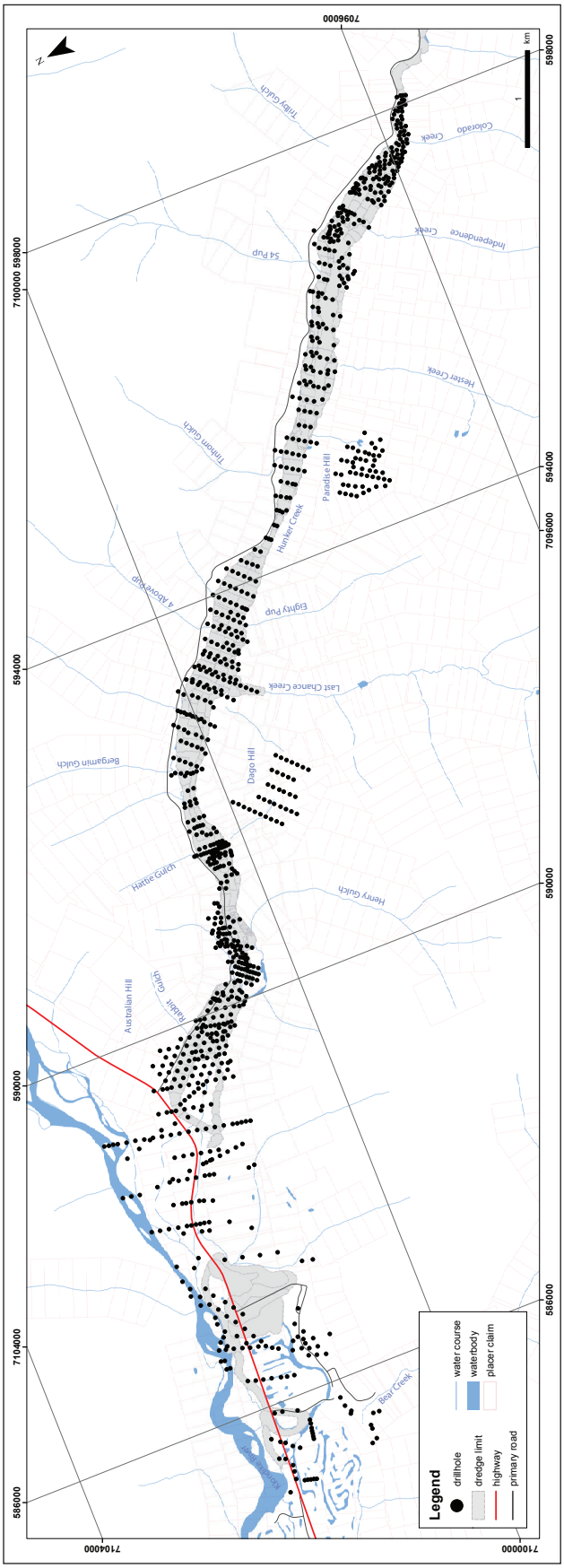

Figure 2. *Hunker Creek and Klondike River valley project area including YCGC drill holes and shafts (black dots) and dredge limits in grey.*

In 2018 a total of nine placer mines were sluicing in the project area, including operations in the modern valley, on intermediate-level terraces, in tributaries, and on high-level White Channel benches. The Hunker Creek drainage basin continues to be a significant gold producer in Yukon, with a total of 5,630 crude ounces reported in 2018 (as of December 12, 2018). The Klondike River has also undergone significant mining activities in the past, producing more than 275,000 crude ounces of gold since the 1930s (YGS, 2010).

Placer gold from Hunker Creek, and its principle tributaries Last Chance and Gold Bottom creeks, is variable in fineness and characteristics. Upper reaches of Hunker Creek range in fineness from 798 to 859, the middle reaches from 725 to 820, and the lower reaches from 701 to 726 (YGS, 2010). Benches in the lower reaches of the drainage also have variable fineness, with Australian Hill ranging from 850 to 860, Dago Hill from 798 to 859, and Paradise Hill from 735 to 802 (YGS, 2010). Gold characteristics in the drainage range from coarse to fine, with coarser components recovered from the major left limit tributaries of Hunker Creek.

Geologic Setting

The project area is primarily underlain by metamorphic rocks of the Yukon-Tanana terrane, largely Klondike schist, but also includes Finlayson assemblage metasedimentary rocks, Slide Mountain assemblage ultramafic rocks and Carmacks Group volcanic rocks (YGS, 2018). The Klondike schist is represented by quartzite, quartz-muscovite-chlorite schist, gneiss and amphibolite. The Finlayson assemblage consists of dark grey to black carbonaceous rocks including quartzite, graphitic quartzite and quartz-muscovite-chlorite schist. Slide Mountain assemblage structurally overlies the Klondike schist and comprises metamorphic igneous rocks which include dunite, peridotite and diabase. Volcanic rocks (andesite and porphyry) of the Carmacks Group are also present in outcrops along Last Chance Creek and on the right limit of Hunker Creek. The degree of bedrock weathering ranges from large blocky fragments to highly decomposed rock with pervasive clay alteration. Preserved mostly at high elevations in the Klondike, the White Channel gravel was deposited

at 2.6–3.3 Ma when a broad, meandering, gold-bearing paleo-Hunker River flowed up to 100 m above the modern Hunker Creek valley (Froese *et al.*, 2000; Westgate *et al.*, 2003).

A grey glacial outwash gravel known as the Klondike gravel occurs above, and is interbedded with the White Channel gravel in lower Bonanza, Hunker and Klondike valleys. Deposition of this gravel was *ca.* 2.6 Ma, when the most extensive advance of the Cordilleran Ice Sheet reached its maximum extent and initiated the establishment of the modern course of the Klondike and Yukon rivers (Hidy *et al.*, 2013). With the establishment of modern northward drainage, rapid incision occurred in Yukon River tributaries such as Bonanza and Hunker creeks (Lowey, 2004). The formerly broad and low-angled Hunker Creek drainage became increasingly incised into a narrow, bedrock entrenched valley, stranding high-level White Channel benches (Dago and Paradise hills) and establishing a number of intermediate-level benches above the modern valley floor.

Methods

Quality Assurance and Control (QA/QC)

As a large-scale enterprise scattered throughout the Klondike, YCGC collected vast amounts of geological information on a daily basis and there are many potential sources of error in these historic records. Transcription errors could have occurred from the field to the cartographer and resulted in incorrect values recorded on the original map. Additionally, the accuracy and reliability of location information is dependant on the accuracy of the data collector as well as the cartographer. When the historic data are brought into a modern GIS system, errors can be introduced both in geographical location information and raw data values that are manually entered into attribute tables. Once a series of drill holes and shafts have been digitized, QA/QC is required to identify any outlying locations or numbers that may represent errors in original documents or subsequent digitization. Outlying values and unrealistic calculations must be sensibly examined and should be removed from the data set to prevent skewing in raster analyses.

Conversions and Corrections

Calculations are required to convert this data set from imperial to metric, and to a modern grade that reflects the modern gold price. Overburden and dredge section thickness are converted from feet to metres, and modern grade is calculated based on today's average gold price of CDN$1,400. In addition to bulk unit conversions, other corrections and adjustments to the data set include:

- Gold distribution and surficial material thickness on high-level benches is calculated separately from the modern creek valley. Original YCGC records of drill holes and shafts located on high-level benches do not differentiate between overburden and dredge section thicknesses, therefore a 'total section thickness' is calculated for these records. As a result, data from the high-level benches are discussed separately from the modern valley.
- A drill hole with anomalously high gold values has been removed from the data set. Located at the mouth of Rabbit Gulch, on the right limit of Hunker Creek at the base of Australian Hill, the hole produced an historic grade of 3,360 cents/yd^3 (modern grade of $2,276/yd^3), which was 686% higher than the next highest value in the data set (490 cents/yd^3). As one of the richest holes drilled by YCGC, we consider its abnormally high value to be the result of the nugget effect.

Raster Analysis

A raster is a method used to display data where colours are used to represent information, such as gold grade. Raster surfaces are generated using a Spatial Analyst tool "Inverse Distance Weighting' (IDW) in ArcGIS. For this project area, two raster images were created from information associated with each drill hole; (1) grade raster and (2) surficial material thickness raster. High grades that form a continuous or semi-continuous linear feature are interpreted as pay channels representing the former thalweg of the stream. Using these linear features visible on the raster, pay channel characteristics, its location, and possibly gold contributors to the high-grade zones can be reconstructed.

Results

Modern gold grade calculated using the gold price of CDN$1,400/oz is displayed using raster data in Fig. 3, with red indicating areas of highest grade and green indicating lowest grade. The pay streak (in red) is disseminated and discontinuous throughout the modern valley bottom, and also occurs on the White Channel left limit benches. Increases in gold grade occur downstream of major tributaries including Hester, Independence and Last Chance creeks. The project area has been divided into three sections for ease of analyses: modern Hunker Creek valley, Klondike River valley, and left limit high-level benches on lower Hunker Creek.

Highest grades recovered from YCGC drill holes (indicated by black stars in Fig. 1) have been recovered at the mouth of Dago Gulch ($331/yd^3), the confluence of Colorado Creek and Hunker Creek ($322/yd^3), and the mouth of Rabbit Gulch on right limit Hunker Creek ($218/yd^3). Of the 1005 drill holes used in this study, 5% yielded grades greater than $50/yd^3. A significant number of drill holes (44%) resulted in grades ranging from $1 to $10/yd^3, and 10% of drill holes recovered grade between trace ($0.1) and less than $1/yd^3.

Modern Hunker Creek Valley

Concentration of the pay channel varies in the modern valley (Fig. 3), with high grades present at the mouth of most left limit tributaries. In the upper part of the study area, at the Colorado Creek confluence, the channel extends the width of the valley with a slight increase of grades on the left limit. Farther downstream, the broad pay streak narrows and remains in the centre of the valley bottom near the mouth of Independence Creek, and subsequently becomes disseminated and decreases in width as it remains pinned on the left limit of the valley. The pay channel remains intact on the high-level bench of Paradise Hill, approximately 85 m off the valley floor.

One of the areas of lowest grade in the project area is a 2.6 km-long section beginning 500 m downstream from the mouth of Hester Creek, to just upstream of the Last Chance Creek confluence, where grades range from $0 to $23/yd^3. Below Last Chance Creek the grades increase and the richest results were drilled at

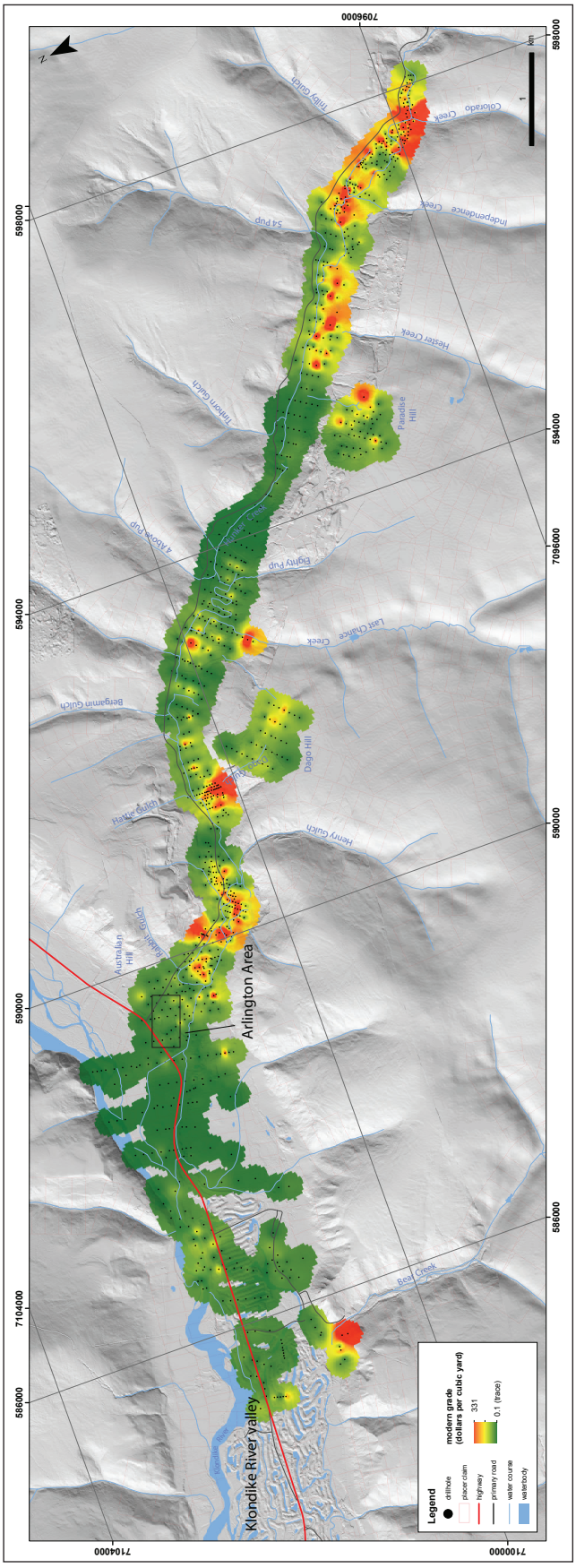

Figure 3. *Modern grade (calculated using the gold price at CDN$1,400/oz.); red colour indicates areas containing the highest gold value from drill hole results.*

the mouth of the left limit tributary, Dago Gulch. Farther downstream, the pay channel is well defined between Henry Gulch and Rabbit Gulch. The pay channel here appears to be up to 400 m in width, and to cross the valley in a diagonal direction from the left limit to the right limit.

No distinct pay channel is visible at the mouth of Hunker Creek where the drainage enters the broad Klondike River valley.

Klondike River Valley

Low gold grade values are present in the Klondike River valley (Fig. 4) where grades range from trace to $102/yd^3, with 86% of drill holes yielding between $0 and 10/yd^3. One hot spot is visible in lower Bear Creek, where values are as high as $102/yd^3. When grades were recalculated, assuming that most of the placer gold originated from a 1.8 m (6.0 ft) pay zone on the bedrock contact, areas of higher grade became apparent (Fig. 5). High-grade areas in this analysis include the mouth of Hunker Creek, on the north side of the Klondike River valley beside the modern river channel, and upstream from Bear Creek closer to the right limit of the Klondike River valley. Drill holes with no associated surficial material thickness were excluded from the recalculation (including the previous high visible at Bear Creek in Fig. 4).

High-Level Benches

Drilling occurred on the high-level benches on lower Hunker Creek in 1941 (Dago Hill) and 1916 (Paradise Hill). A total of 83 holes were analyzed, with drill hole

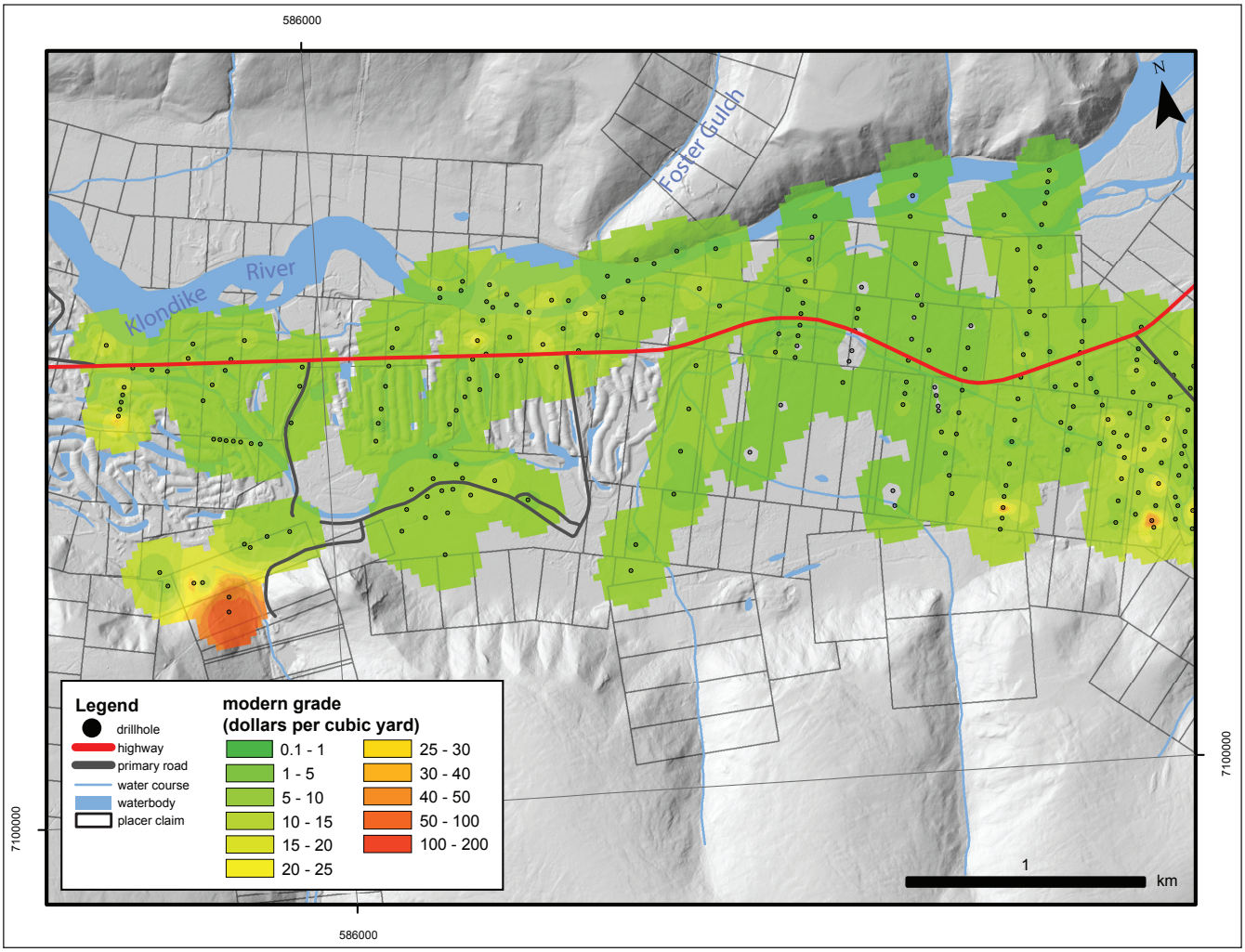

Figure 4. *Modern grade raster in the Klondike River valley; red colour indicates areas containing the highest gold value from drill hole results.*

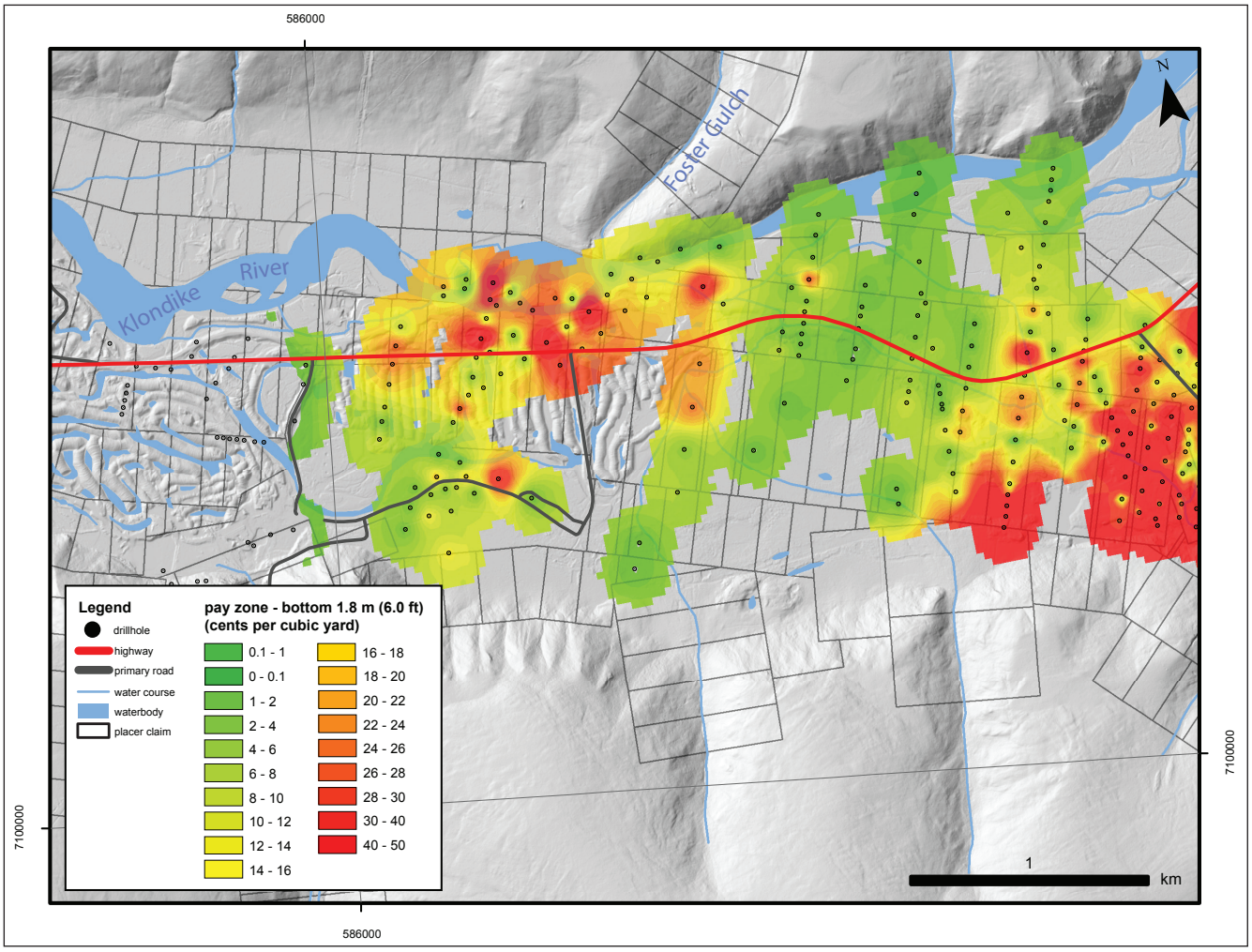

Figure 5. *Pay zone (bottom 1.8 m (6.0 ft) of dredge section) in the Klondike River valley illustrating the increase in gold grade values after accounting for the dilution factor.*

data consisting of total section thickness and grade. A total section thickness was derived from the benches because legends were not included on the maps and it was not possible to differentiate between the surficial material (overburden or gravel) values on the map. Total section thickness varies from 8–44 m (26–155 feet), with the thickness increasing laterally to the south, as you move from the rim toward the south margin of the valley (Fig. 6).

Similar to the Klondike River valley, grades on Dago and Paradise hills were recalculated to adjust for a concentrated (1.8 m-thick) pay zone located on the bedrock surface and to account for grade dilution if the total section thickness is used to calculate grade. Figure 7 displays the new "pay zone" grade for the high-level benches and interpreted margins of a reconstructed channel is represented by dashed lines. Derived from the GIS data, the maximum width of the channel is 400 m, and grades range from $50 to $165/yd^3 (Fig. 7). The Dago Hill paystreak was documented by McConnell (1907) to be 1128 m in length and range from 91 to 152 m in width; his calculations use the highest grade zone and did not include the medium-grade gravel bordering the pay channel.

Figure 6. *Satellite image of Dago Hill and Paradise Hill on lower left limit Hunker Creek, overlain by a raster image of total section thickness (gravel and overburden).*

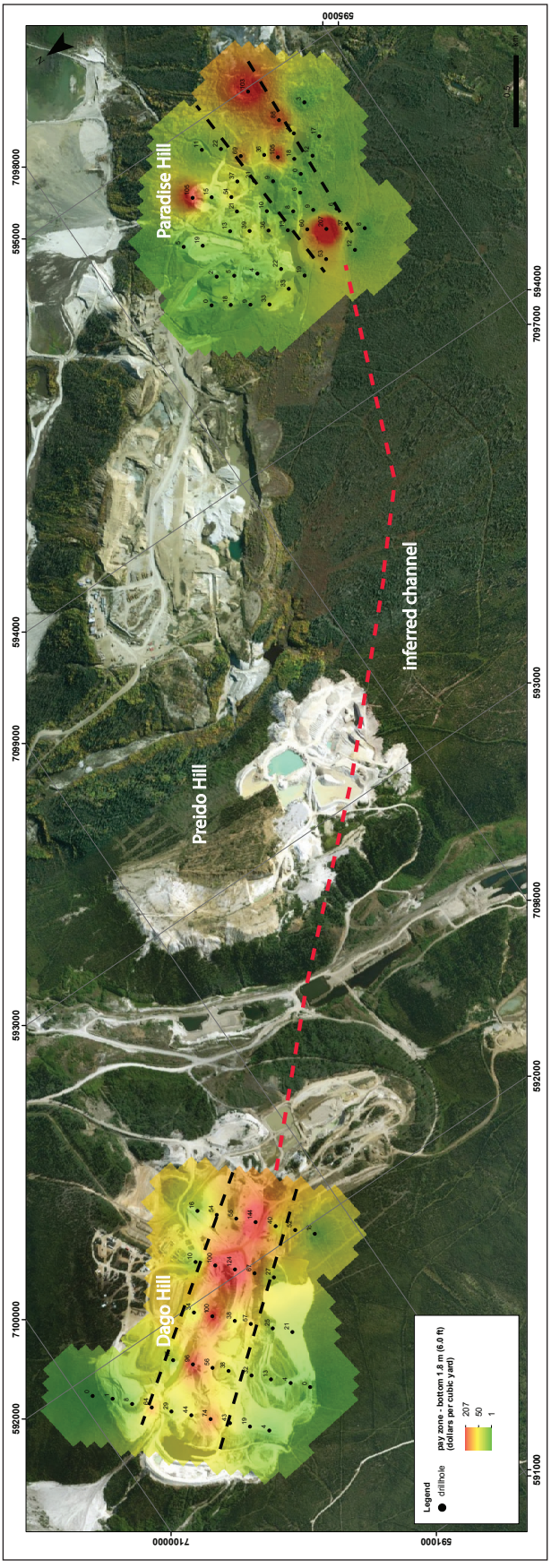

Figure 7. *Satellite image of Dago Hill and Paradise Hill on lower left limit Hunker Creek, overlain by pay zone raster. The reconstructed high-grade channel on the hills is represented by a black dashed line; red dashed line in the inferred pay channel that once connected both hills.*

Discussion

A pay streak in the upper reach of the project area is clearly visible from Colorado Creek to below Hester Creek (Fig. 3). This pay streak is interpreted to represent the concentrated equivalent of the former high-level pay streak that lowered vertically during base-level adjustment. Topography of the valley also influences the concentration of gold around Independence Creek due to the widening on the valley, which causes the stream hydraulics to decrease and enhance the deposition of gold. Vertical lowering of the pay channel is also visible in lower Hunker Creek, where the richest hot spot in the drainage is present at the mouth of the left limit tributary of Dago Gulch and directly across on the right limit, at the mouth of Rabbit Gulch. The accumulation of gold at the mouth of both gulches is contributed to the fluvial fan derived from their headwaters, which is reworking the paleo-Hunker Creek pay channel.

Low grades between Hester and Last Chance creeks are interpreted to be the result of the pay streak being "hung-up" on left limit high-level benches. These intact pay channels are visible on Dago and Paradise hills (Figs. 3 and 7) and are original channel deposits from the paleo-Hunker system. When the pay channel becomes constrained on high-level benches, grades in the modern valley become insignificant, highlighting the importance of reworked Pliocene gold within the modern channels. The inconsistent pattern of the pay streak within modern Hunker Creek is therefore directly attributed to variable reworking of the high-level pay streak. McConnell (1907) concluded that the richest sections of the modern valley are contributed to "the paystreak of the old valley [that] has been almost entirely destroyed and the gold contents washed down to the level of the present valley" (p. 24). Another large factor influencing gold distribution is the lithology and competency of the underlying bedrock, as noted by McConnell (1907). When he reported gold enrichment on the left limit hills of lower Hunker Creek, he attributed the enrichment to the decomposed nature of the bedrock, which contributed clay to the system and acted as a false-bedrock.

Where the high-level pay streak has been reworked by tributary streams, enrichment can be seen at the stream's confluence with Hunker Creek. The sharp spike in pay at the mouth of Hester Creek suggests Hester Creek eroded and reworked the heavy pay channel situated on the high-level benches, enriching the pay streak and transporting it into the Hunker Creek valley. A similar pattern is present at the mouth of Colorado Creek.

Farther downstream, where Hunker Creek valley enters the Klondike River valley, the prominent pay channel disappears. The White Channel deposit is traceable beyond Dago Hill and crosses the modern valley to Australian Hill. White Channel gravel is overlain by Klondike River gravel and extensive prospecting and sampling on the hill failed to produce a pay streak with similar grades and extent as preserved on Paradise and Dago hills (McConnell, 1907). Additional samples on the rim carried only minimal values, which could direct present day exploration to lower reconcentrated bench deposits some 10–50 m off the modern valley. The channel could be preserved on the lower right limit of Australian Hill, or on an intermediate-terrace on the left limit which has been concealed by glacial outwash and loess. Elimination of the channel could also be due to vigorous erosion by glacial fluvial action during glaciation. Evidence from McConnell's work in 1907 supports the reworking of the paystreak in the Klondike valley, as he believed the Hunker Creek high-level White Channel gravel extended for considerable distance into the Klondike River valley, but was destroyed during the deposition of the Klondike River and therefore scattered the gold throughout the valley.

Despite the absence of a continuous Hunker Creek pay streak in the Klondike valley, areas of enriched gold values are present (Fig. 5) and interpreted to be related to two possible sources of gold. Areas of enrichment are situated on the right limit of the broad valley, slightly downstream from the mouth of Foster Gulch, at the mouth of Bear Creek, and on the far left limit valley margin downstream from the Hunker Creek valley.

The first source is the paleo-Hunker channel that was once flowing on the far left limit of the drainage, and remains inconsistently preserved on high-level benches.

It is possible this pay streak extended into the Klondike valley where it has been reworked into modern Klondike valley gravel. The enriched paleo-Hunker pay streak may be visible in a series of small partially connected lenses in the Klondike valley rather than a continuous streak, and becomes destroyed farther downstream as it meanders its way to the Yukon River.

A second possible source for the enriched gold values is from bedrock sources in the Klondike River itself. Recent mining along the Klondike River has recovered small angular nuggets of gold, which suggests a local source.

The richest pay zone in the project area is situated in the uppermost 1.2 m (3.9 ft) of bedrock and within the lower 0.6 m (2.0 ft) of gravel on the bedrock surface (Daily, 1940). It is noted in the YCGC Report of Drilling Operations and Shaft work (1909) that the pay channel became richer in areas where "hard bedrock appears and forms a riffle." One of these riffles was present 100 m downstream from the mouth of Hester Creek, where a hot spot is present, and the miner reportedly recovered significant coarse gold (YCGC, 1909). The Hunker Creek pay channel was likely enriched by contributions from Hester Creek, and the trend was further enhanced by the riffle, which trapped the coarse gold derived from the main stem and the tributary.

Arlington – Predicted and Actual Dredge Recoveries

In the early 1930s the Arlington area at the confluence of Hunker Creek and the Klondike valley (Figs. 8 and 9) was divided into three blocks (A, B and C) and extensively drilled to determine the economics of the ground. This grade evaluation included the tailings from Yukon Gold Dredge No. 5, which was active in the Block C area in 1909. Favourable results were obtained by

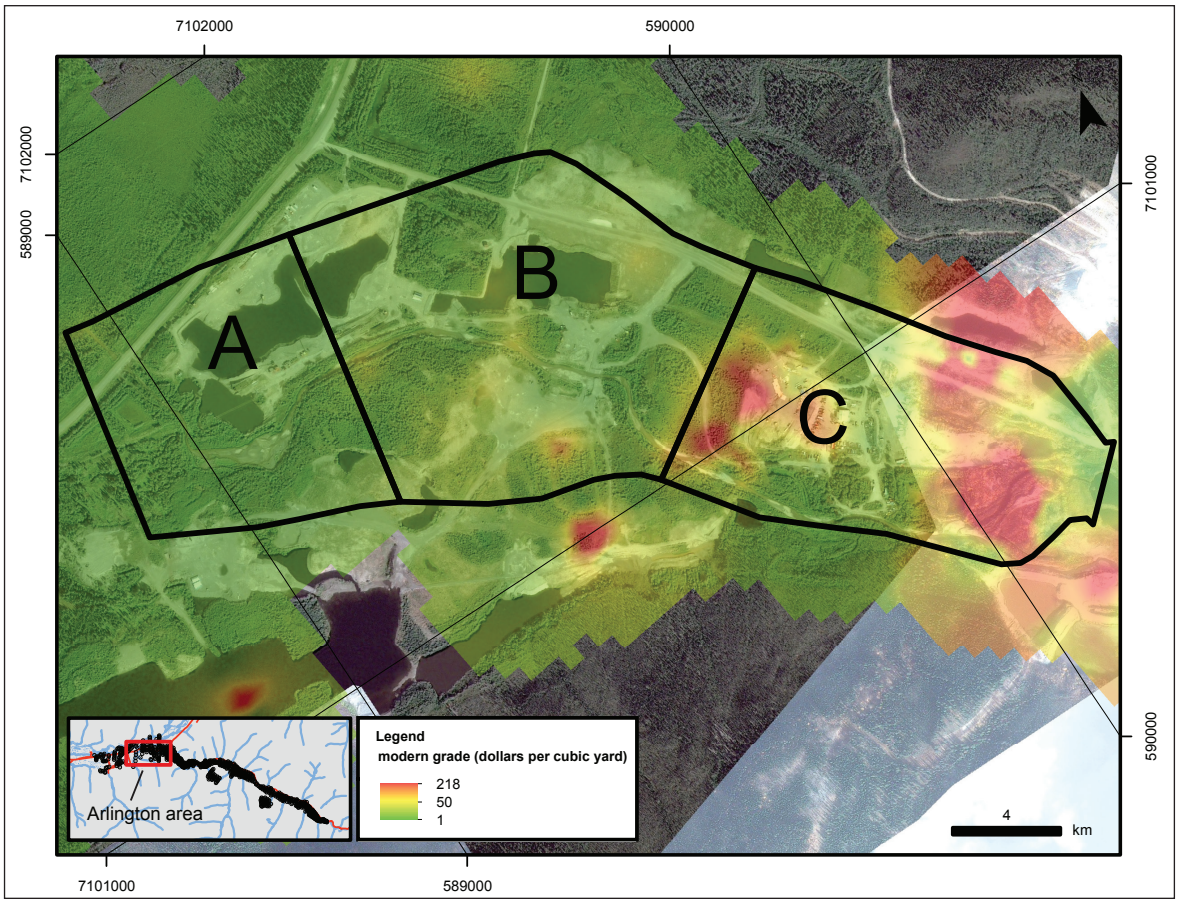

Figure 8. *Satellite image of the Arlington area at the mouth of Hunker Creek overlain by a raster image of recalculated pay zone (bottom 1.8 m) grade; black lines indicate the three blocks discussed in analyzing estimate verse actual production values.*

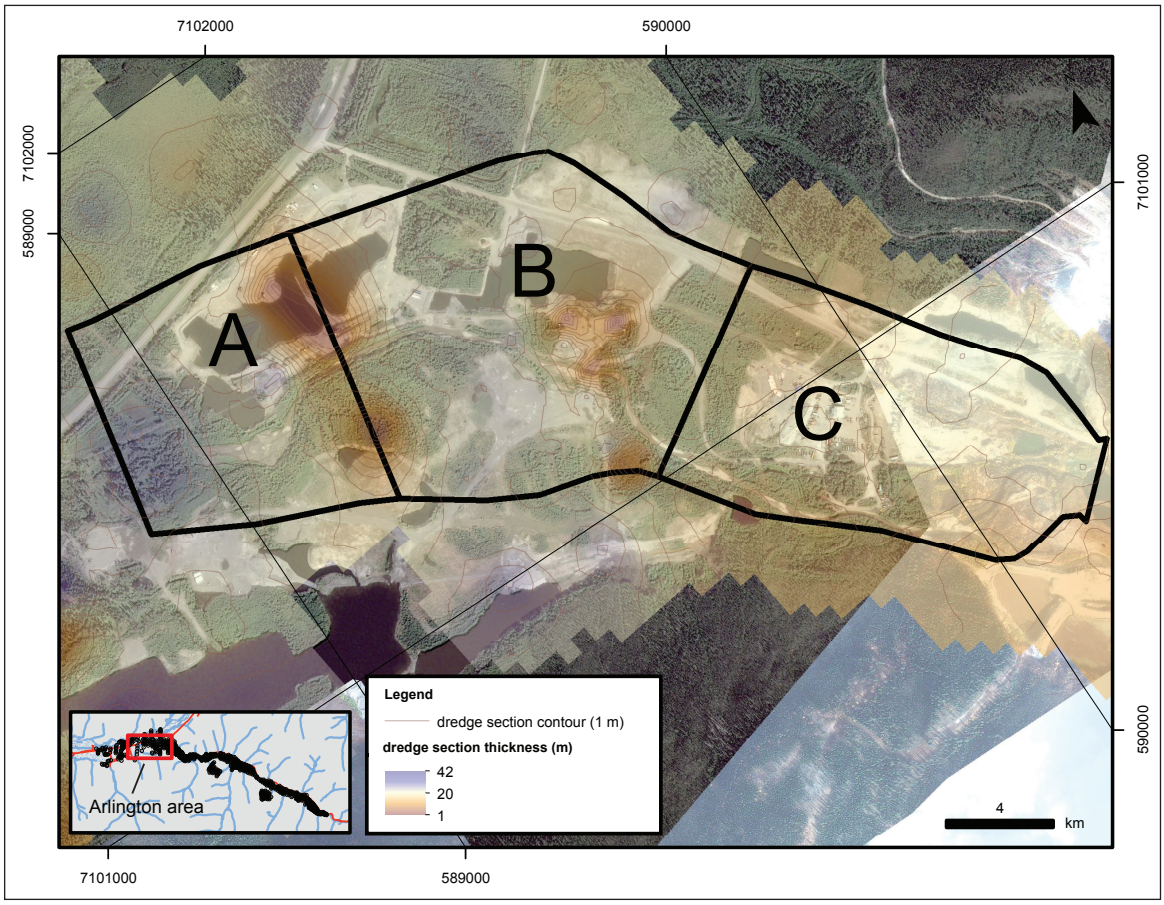

Figure 9. *Satellite image of the Arlington area at the mouth of Hunker Creek overlain by a raster image of dredge section thickness; black lines indicate the three blocks discussed in analyzing estimate verse actual production values.*

the drilling evaluation, and the company dredged the ground in 1940 with Dredge #4 (Daily, 1940). Table 1 compares estimates of volume, grade and depth based on drilling with actual recovered values during the dredging program.

Block A is the smallest of the blocks, contained the lowest average grade at 6.9 cents/yd^3, and had production values that were over-estimated by 23.3%. Block B is the largest block of the three, contained average grades of 19.5 cents/yd^3, and had production values that were over-estimated by 2.2%, and therefore contained the most reliable drilling data. Farthest upstream on lower Hunker Creek, Block C was the most productive area despite having already been dredged (Daily, 1940). Average recovered grades in Block C were 52.5 cents/yd^3 and the average production value was over-estimated by 22.6%.

Comparing the Arlington blocks estimate and actual values can help put drilling reliability into perspective. When the geology of a particular location and/or drainage is well understood, drilling data can more reliably predict the economics; whereas when pay channel characteristics are unknown or hypothesized, there is potential for a large discrepancy in production values. In van Loon (2016), the reliability of drilling accuracy was analyzed for mid-Dominion Creek, suggesting an average under-estimation of gold recovery by 8%. For the Arlington area the drilling accuracy shows a higher degree of discrepancy. This was determined by standardizing the depth in order to compare the grade predicted by the drilling to the actual grade derived from dredging results. In Table 1, the standardized depth results highlight that both block A and C over-estimated the drilling by ~20%, whereas

Table 1. *Comparison of estimate and actual data by Block A, B, and C of Arlington on lower Hunker Creek (Daily, 1940).*

	Block A		Block B		Block C	
	Estimate	*Actual*	Estimate	*Actual*	Estimate	*Actual*
Area (ft^2)	390,158	320,234	2,706,905	1,489,049	2,313,120	2,391,476
Average depth (ft)	33.5	39.8	32.0	37.2	26.1	29.1
yd^3 dredged	422,565	472,471	2,802,737	2,049,958	1,946,932	2,578,284
Recalculated yardage dredged (actual area x estimate depth = X; X/27)		397,327		1,764,799		2,311,760
Average dredge section value (cents/yd^3)	10.7	6.9	23.1	19.5	75.7	52.5
Recalculated average value of dredge section (standardized depth)		8.2		22.6		58.6
% difference between estimated value and recalculated value		23.3		2.2		22.6
Gross (dollars)	45,114	32,514	648,666	399,575	1,472,043	1,355,879

in Block B grade was over-estimated by 2.2% from the actual recovery. A summary of the dredging operation at Arlington by A.F. Daily (1940) concluded that:

- Block A was nearly all frozen except a strip on the left limit of the block. It was deemed difficult to thaw the Klondike River gravel in this block because it was a challenge to sink the hand-driven thawing points in such dense, coarse material. In order to reach the more profitable ground in Block B, dredging operations were limited to a narrow strip along the left limit edge of block A; enabling the company to reach higher grade ground quicker in the season. Coarse gravel that was difficult to thaw could be a significant factor in the 23% lower than expected gold recovery for Block A.
- Block B was also predominately frozen, with an excessive amount of sand encountered during dredging in the upper part of the block. Grades picked up as the dredge migrated towards Block C, where they started to process less Klondike River gravel. Drilling likely accurately predicted grades in this block due to the consistency of grade in Hunker Creek gravel, the pay zones tight association with the bedrock contact, and the frozen ground conditions that did not accentuate the grade when drilled.
- Block C had extensive drifts and a portion of its area on the left limit was worked by Dredge #5 in 1909. Gravel was largely frozen, but had thawed tailings that were determined economic to re-dredge. A significant contributor to the lower than expected grades recovered is the excess sand the dredge encountered, which was broadly distributed throughout the block. Massive sand in the project area is likely due to a technogenic source; historic dredge slickens, and/or fines, as a result from old-timer workings. The sand decreased the actual dredging rate, as well as hindered operations due to managing the fine-grained material that carried little to no values. Less gold was recovered from Block C than estimated, likely due to encountering the thick deposit of sand and the extensive old-timer workings that are hard to delineate (and account for) through drilling.

In contrast to the variability of the geological setting in Blocks A and B, Block C of the Arlington concession is characterized by a narrow, well-defined pay channel of very high grade (Fig. 8). Thinner surficial material thicknesses, and in particular, thinner muck thicknesses, contribute to more efficient and economical recoveries (Fig. 9).

Several variables can affect the reliability of drilling data. In the Klondike one of the most significant factors is the percentage of high-grade material that was excavated by old-timers (as in Block C), which is challenging to account for unless drill hole spacing was greatly reduced to several metres. Gravel characteristics can impact the ability to effectively thaw a column/section (as in Block A), and if blocks of frozen gravel are dredged, gold could remain inaccessible, still in section, and/or preserved, during the dredging process. The nugget effect could also contribute to inconsistent recovery, as likely occurred in the high-grade gravel of Block C.

Dredge recovery problems may also have contributed to the poor accuracy of the Arlington area estimates. Potential inefficiencies in dredging allow for remnants of *in situ* gravel to remain on the bedrock contact. The ability of dredges to recover gold can be affected by a few different factors:

1. thickness of surficial materials - if a gravel package was too thick, it presented a challenge for the dredge to reach the bedrock surface;
2. coarseness of surficial materials - if a gravel was too coarse and boulder enriched, it could impact the capacity on the bucket line; and
3. variability in bedrock lithology and topography; specifically its competency, degree of weathering, how it fractures and bedrock highs that make dredging challenging.

Exploration

A number of under-explored targets exist in the lower part of Hunker Creek and consist of hidden/buried channels and benches. As Hunker Creek incised below the original White Channel surface, gold is concentrated and vertically lowered to be preserved on intermediate-level terraces as well as the modern creek bottom. Because lateral movement of gold is difficult, there is potential for economic gravel deposits on the rim slopes, and at the base of the high-level terraces on intermediate and low-level terraces on the left limit. At the mouth of Dago Gulch, an intermediate-level terrace has been recently excavated and proven to contain economic grades ~10 m above the modern valley bottom. Enrichment in this location is likely attributed to reworking and re-concentrating of the heavy pay channel off the bench by Dago Gulch, and contributions from colluviation of Dago Hill rim material. Surface expression of these intermediate benches is limited due to their narrow width and thick packages of overburden (muck) concealing the landform. Drilling and geophysics are the most practical methods of locating these targets. Exploration for these narrow intermediate-level benches on the inside of the bends within the incised valley is recommended. For example, the northeasterly facing rim slope of Dago Hill is on an inside bend of Hunker Creek, and similarly, the slope between Hattie and Rabbit Gulch is an inside bend.

Using extrapolated grade information to direct bench exploration to areas with high grade, two areas of interest identified are (1) immediately downstream of Last Chance Creek on the left limit, and (2) a 1 km-long section between Henry Gulch and the next tributary downstream (unnamed left limit tributary). Formed during the deepening of the valley, these benches are likely to be small deposits with irregular distribution and could occur at various elevations from the valley floor to the high-level terrace (McConnell, 1904).

Another exploration target within the project area is side pay on the valley margins that is preserved beneath thick and often frozen overburden. Using grade data, and observing the absence of high grades both in the valley bottom and on the bench, we are able to determine locations where gold concentrations have the potential to be hung up on low-level terraces, or on the valley margins. An area that is identified as prospective due to high grades and potential for bench preservation is an 800 m-long section between Dago Gulch and Henry Gulch, on the left limit of Hunker Creek.

Potential also remains in secondary tributaries of Last Chance Creek and Hester Creek, as well as the headwaters of Hester and Colorado creeks, all of which appear to be contributing gold to the Hunker Creek valley. Lastly, continued exploration of the Hunker Creek pay channel and its disseminated nature in the Klondike River valley has potential to support large open pit mining operations that can target economic gravel on the bedrock contact. Additional exploration is warranted along the left limit of the Klondike River valley, both in the valley bottom and within a high-level terrace deposit.

Conclusion

Activity has occurred in the Hunker Creek and Klondike River valleys without pause for more than one hundred years. Initial activities of shafting, hand mining and hydraulic operations transformed into dredging operations, cat mining, and finally, modern day mechanized mining where operators process material more efficiently, operate within lower margins, and excavate thicker deposits.

Placer deposits in the modern valley were the initial target for miners exploring the Klondike, but with further exploration and drilling, additional targets including intermediate and high-level benches were discovered. Following a heavy pay steak that was continuous farther upstream and decreased to nearly absent downstream, the miners were able to adjust their focus and interpret the way the landscape may have looked before the last glacial influence. Using historic drilling data we are able to reconstruct gold distribution and confirm a pay channel trajectory on the high-level benches of the left limit of Hunker Creek, which can further enhance the knowledge of placer deposits for modern miners.

In summary, three prominent gold distribution patterns are present in the project area: (1) a heavy pay channel was present prior to the first glaciation, when the Hunker Creek channel was more than twice its current width, and after erosional down cutting the pay channel was variably reworked either into the modern channel, remained intact within the high-level deposits or was partially reworked; (2) reworking of the Pliocene pay streak into the modern channel appears to have left a disseminated or irregular gold distribution that may be caused by bedrock bed roughness; and (3) principal tributaries (Last Chance Creek) are contributing to the gold population, with secondary tributaries (Colorado Creek) also potential sources of input.

This compilation resulted in the identification of prospective targets in intermediate-level benches on the lower section of Hunker Creek where high grades in the valley margins can be extrapolated from drill data.

Three additional exploration ideas derived from the modeling exercise include (1) inefficient dredging due to frozen ground, particularly in coarse gravel where hand-drive points were unable to penetrate sufficiently; (2) areas where potential for a rich rim has been reworked into low-level terraces and/or the valley bottom (base of Australian Hill; base of upstream portion of Dago Hill); and (3) in secondary tributaries in the headwaters of Colorado, Hester, and Independence creeks are also encouraging areas to conduct future examinations.

Acknowledgments

Many thanks are owed to the Technical Services unit at YGS, especially to Brett Elliot for creating a web-based map to display and make the YCGC data searchable. Additional thanks are owed to our digitizing contractor Laura Grieve, to Karen MacFarlane, Kristen Kennedy and Jeff Bond for the contributions and edits to this project, and lastly to the placer industry for ground-truthing the value in this historic data set.

References

Daily, A.F., 1940. The Yukon Consolidated Gold Corporation, Limited Report on Arlington Area Operations 1935 to 1940. Energy, Mines and Resources Property File Collection; Archives Canada file MG 28 Series 111-43.

Froese, D.G., Barendregt, R.W., Enkin, R.J. and Baker, J., 2000. Paleomagnetic evidence for multiple Late Pliocene – Early Pleistocene glaciations in the Klondike area, Yukon Territory. Canadian Journal of Earth Science vol. 37, p. 863–877.

Green, L., 1977. The Gold Hustlers. Alaska Northwest Publishing Company, Anchorage, AK, 339 p.

Hidy, A.J., Gosse, J.C., Froese, D.G., Bond, J.D. and Rood, D.H., 2013. A latest Pliocene age for the earliest and most extensive Cordilleran Ice Sheet in northwestern Canada. Quaternary Science Reviews, vol. 61, p. 77–84.

Lowey, G.W., 2004. Placer geology of the Stewart River (115N&O) and part of the Dawson (116B&C) map areas, west-central Yukon, Canada. Yukon Geological Survey, Bulletin 14, 275 p.

McConnell, R.G., 1905. Report on the Klondike gold fields. Geological Survey of Canada, Annual Report, part B, vol. 14, p. 1–71.

McConnell, R.G., 1907. Report on gold values in the Klondike high level gravels. Geological Survey of Canada, Report No. 979, 34 p.

van Loon, S., 2016. Digitizing and spatially analyzing historic YCGC drill data from Dominion Creek: A pilot project. *In:* Yukon Exploration and Geology 2015, K.E. MacFarlane and M.G. Nordling (eds.), Yukon Geological Survey, p. 253–280, including appendices.

van Loon, S., 2017. Digital analysis of historic drilling data to reconstruct the placer gold distribution in Sulphur Creek and lower Dominion Creek, central Yukon. *In:* Yukon Exploration and Geology 2016, K.E. MacFarlane and L.H. Weston (eds.), Yukon Geological Survey, p. 225–242.

Westgate, J.A., Sandhu, A.S., Preece, S.J. and Froese, D.G., 2003. Age of the gold-bearing White Channel Gravel, Klondike district, Yukon. *In:* Yukon Exploration and Geology 2002, D.S. Emond and L.L. Lewis (eds.), Exploration and Geological Services Division, Yukon Region, Indian and Northern Affairs Canada, p. 241–250.

Yukon Consolidated Gold Corp. Mid Hunker drilling. Energy, Mines and Resources Property File Collection, YCGC26442.

Yukon Consolidated Gold Corp. Difference in elevation between X25 and Hunker Flat above Narrows. Energy, Mines and Resources Property File Collection, YCGC26434.

Yukon Consolidated Gold Corp. Plan of placer mining claims below discovery on Hunker Creek. Energy, Mines and Resources Property File Collection, YCGC25160.

Yukon Consolidated Gold Corp. Plan of Placer Mining Claims from No. 39 Below Discovery to No. 65 Below Discovery on Hunker Creek - Plan No. 5037. Energy, Mines and Resources Property File Collection, YCGC25100

Yukon Consolidated Gold Co., Report of drilling operations and shaft work for the examination of claims between #50 and #63 below Hunker Creek. Energy, Mines and Resources Property File Collection.

Yukon Consolidated Gold Co., 1909. Report of Hunker development company's properties. Energy, Mines and Resources Property File Collection.

Yukon Consolidated Gold Corp., 1910. Dredge No. 4 Workings. Energy, Mines and Resources Property File Collection, YCGC26287.

Yukon Consolidated Gold Corp., 1911. Sketch plan showing McDonnell and Barrett Lays, 1911, Plan no. 5036. Energy, Mines and Resources Property File Collection, YCGC26451.

Yukon Consolidated Gold Corp., 1913. Plan of portion of Klondike Valley ahead of dredges Canadian No. 2 and 4. Energy, Mines and Resources Property File Collection, YCGC25164.

Yukon Consolidated Gold Corp., 1915. Dredge No. 4 Workings. Energy, Mines and Resources Property File Collection, YCGC26288.

Yukon Consolidated Gold Corp., 1915. Map accompanying report for Yukon Gold Company. Energy, Mines and Resources Property File Collection, YCGC25158.

Yukon Consolidated Gold Corp., 1916. Blueprint: Examination of Paradise Hill, Shafts and Drill Holes. Energy, Mines and Resources Property File Collection, YCGC26566.

Yukon Consolidated Gold Corp., 1917. Plan of Klondike valley portion of Hydraulic Mining Lease No. 18. Energy, Mines and Resources Property File Collection, YCGC26528.

Yukon Consolidated Gold Corp., 1923. Plan showing Drilling results and area dredged in portion of Klondike valley, 1923, by Dredges Canadian 2 to 4 - Plan no. 289. Energy, Mines and Resources Property File Collection, YCGC26526.

Yukon Consolidated Gold Corp., 1933. Anderson Concession, Drilling and Plan. Energy, Mines and Resources Property File Collection, YCGC 26356.

Yukon Consolidated Gold Corp., 1933. Anderson Concession, Hunker Drilling. Energy, Mines and Resources Property File Collection, YCGC26435.

Yukon Consolidated Gold Corp., 1934. Arlington project - General map showing examination results and proposed method of working to accompany a report by R.E. Franklin. Energy, Mines and Resources Property File Collection, YCGC 25159.

Yukon Consolidated Gold Corp., 1934. Arlington Project General Map showing results and proposed method of working to accompany report by R.E. Franklin. Energy, Mines and Resources Property File Collection, YCGC 26468.

Yukon Consolidated Gold Corp., 1937. Dredge No. 4 Progress Map, Arlington Area - Plan No. 2. Energy, Mines and Resources Property File Collection, YCGC26358.

Yukon Consolidated Gold Corp., 1941. Dago Hill Examination. Energy, Mines and Resources Property File Collection, YCGC25180.

Yukon Consolidated Gold Corp., 1943. No. 11 Stripping Layout. Energy, Mines and Resources Property File Collection, YCGC 26410.

Yukon Consolidated Gold Corp., 1946. No. 11 Stripping Layout. Energy, Mines and Resources Property File Collection, YCGC26403.

Yukon Consolidated Gold Corp., 1947. No. 11 Stripping Layout. Energy, Mines and Resources Property File Collection, YCGC 26397.

Yukon Consolidated Gold Corp., 1948. No. 11 Stripping Layout. Energy, Mines and Resources Property File Collection, YCGC 26411.

Yukon Consolidated Gold Corp., 1949. No. 11 Stripping Layout. Energy, Mines and Resources Property File Collection, YCGC 26399.

Yukon Consolidated Gold Corp., 1949. No. 11 Stripping Layout. Energy, Mines and Resources Property File Collection, YCGC 26412.

Yukon Consolidated Gold Corp., 1951. No. 11 Stripping Layout. Energy, Mines and Resources Property File Collection, YCGC 26400.

Yukon Consolidated Gold Corp., 1952. No. 11 Stripping Layout. Energy, Mines and Resources Property File Collection, YCGC 26452.

Yukon Consolidated Gold Corp., 1953. No. 11 Stripping Layout. Energy, Mines and Resources Property File Collection, YCGC 26409.

Yukon Consolidated Gold Corp., 1957. Paradise Hill layout. Energy, Mines and Resources Property File Collection, YCGC25118.

Yukon Consolidated Gold Corp., 1958. Last Chance Drill Hole Layout. Energy, Mines and Resources Property File Collection, YCGC26534.

Yukon Consolidated Gold Corp., 1958. No. 11 Thaw Layout. Energy, Mines and Resources Property File Collection, YCGC 26454.

Yukon Consolidated Gold Corp., 1958. Paradise Hill hydraulic cut. Energy, Mines and Resources Property File Collection, YCGC25117.

Yukon Geological Survey, 2010. Yukon Placer Database – Geology and mining activity of placer occurrences. Yukon Geological Survey, CD-ROM.

Yukon Geological Survey, 2018. Yukon Digital Bedrock Geology. Yukon Geological Survey, http://www.geology.gov.yk.ca/update_yukon_bedrock_geology_map.html, [accessed December, 2018].

Stratigraphy of the Faro Peak formation, central Yukon: New field observations of Jurassic synorogenic sedimentation along the Yukon-Tanana–Slide Mountain terrane boundary

A.C. Wiest* and L.P. Beranek**
Department of Earth Sciences, Memorial University of Newfoundland

Wiest, A.C. and Beranek, L.P., 2019. Stratigraphy of the Faro Peak formation, central Yukon: New field observations of Jurassic synorogenic sedimentation along the Yukon-Tanana–Slide Mountain terrane boundary. *In:* Yukon Exploration and Geology 2018, K.E. MacFarlane (ed.), Yukon Geological Survey, p. 127–142.

Abstract

The Faro Peak formation is a Lower Jurassic(?) unit assigned to the Yukon-Tanana terrane in the southern Tay River map area (NTS 105K). A two-year project was initiated in 2018 to investigate the Faro Peak formation and constrain its stratigraphy, age, and significance to Cordilleran tectonic evolution. The exposed base of the Faro Peak formation includes argillite and organized to disorganized sandstone units that crop out southwest of the Yukon-Tanana–Slide Mountain terrane boundary near Faro. Lower Faro Peak formation units have mafic-intermediate volcanic provenance and were deposited by concentrated density flows or turbidity currents. The upper Faro Peak formation contains massive, disorganized conglomerate and sandstone units that were sourced from the Yukon-Tanana and Slide Mountain terranes and deposited by non-turbulent debris or density flows. The Faro Peak formation is likely the remnant of a synorogenic basin that formed as a result of Intermontane belt exhumation in central Yukon.

* acwiest@mun.ca
** lberanek@mun.ca

Introduction

Late Triassic–Early Jurassic plate convergence and collision along the northern Cordilleran margin resulted in the exhumation of the Intermontane terranes—Yukon-Tanana, Slide Mountain, Stikinia, Quesnellia, and Cache Creek—and subsequent generation of overlapping synorogenic basins (Mihalynuk *et al.*, 1994; Johnston *et al.*, 1996; Evenchick *et al.*, 2007; Knight *et al.*, 2013; Nelson *et al.*, 2013). In central Yukon, synorogenic Lower to Middle Jurassic strata assigned to the Laberge Group record the timing and spatial extent of Intermontane belt exhumation and represent a regional basin known as the Whitehorse trough (Fig. 1; e.g., Tempelman-Kluit, 1984; Dickie and Hein, 1995; Hart *et al.*, 1995; Colpron *et al.*, 2015; van Drecht and Beranek, 2018). Colpron *et al.* (2015) recently proposed that Laberge Group deposition was coincident with the onset of foreland basin subsidence in southern Canadian Rockies (see Fernie Formation in Fig. 1), suggesting that the Whitehorse trough and related synorogenic basins in Yukon and northern British Columbia are critical to understanding the early growth of the Cordilleran orogen.

Isolated occurrences of Lower Jurassic(?) strata known informally as the Faro Peak formation crop out near the Yukon-Tanana–Slide Mountain terrane boundary in the Faro region of central Yukon and are presumably correlative with synorogenic rock units of the Whitehorse trough (Fig. 1; e.g., Pigage, 2004; Colpron *et al.*, 2015). A two-year project was initiated to test this hypothesis and constrain the role of Intermontane belt tectonics on Faro Peak formation deposition. In this article, we summarize the field geology of Faro Peak formation outcrops visited during summer 2018. These field observations will be integrated with future detrital zircon U-Pb-Hf studies to confirm the depositional age and provenance of Faro Peak formation rock units and determine the spatial extent of Jurassic exhumation and synorogenic sedimentation in the northern Cordillera.

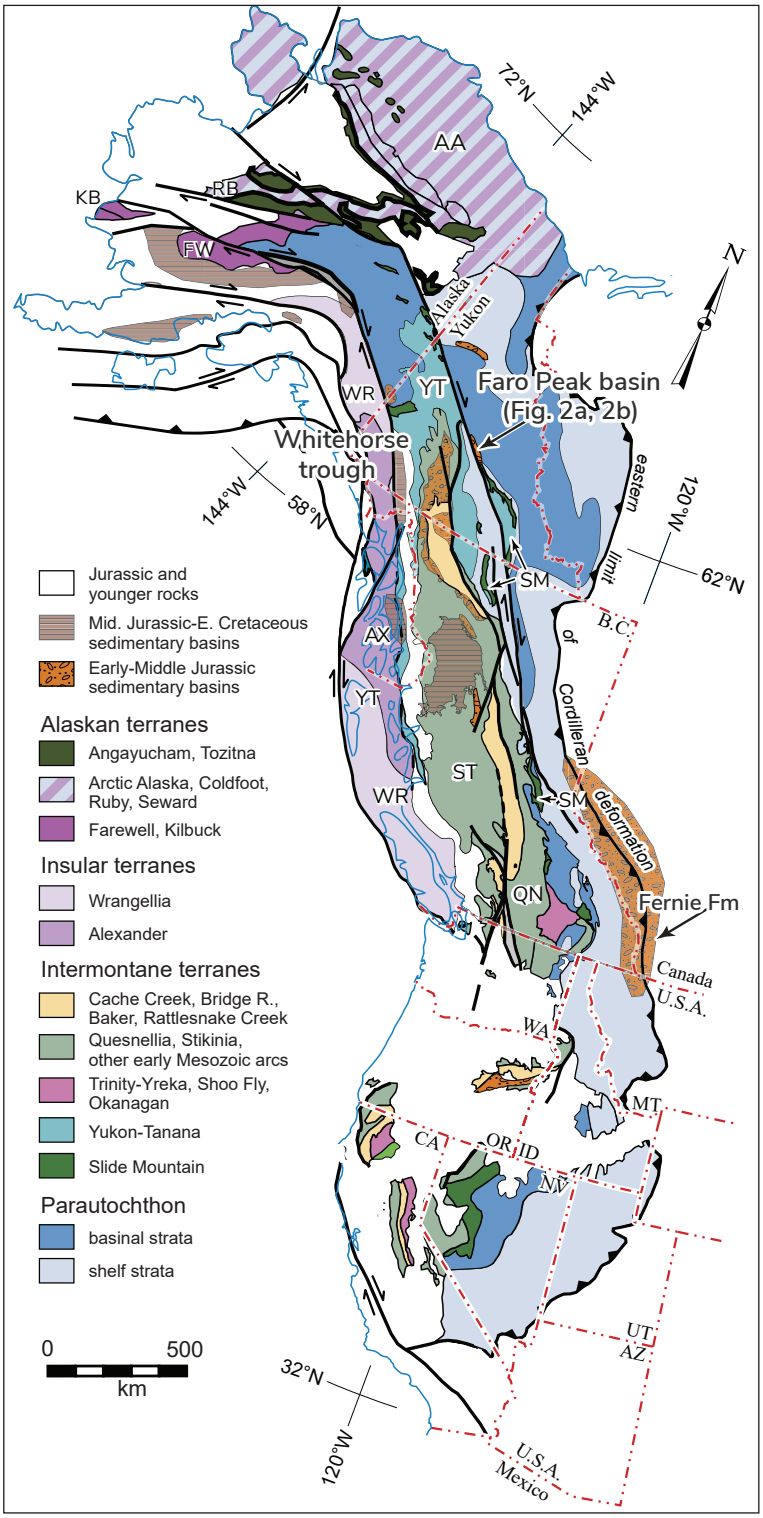

Figure 1. *Paleozoic to early Mesozoic terrane map of the North American Cordillera and associated Jurassic basins modified from Colpron et al. (2015). Terrane abbreviations: AA–Arctic Alaska; AX–Alexander; FW–Farewell; KB–Kilbuck; QN–Quesnellia; RB–Ruby; SM–Slide Mountain; ST–Stikinia; WR–Wrangellia; YT–Yukon-Tanana.*

Geological Background

The Faro townsite is located along the eastern edge of the Intermontane belt in the southern Tay River map area (NTS 105K). In this region, the Intermontane terranes are juxtaposed against North American continental margin strata of Selwyn basin along the Inconnu thrust to the northeast and Cassiar terrane across the Tintina fault to the southwest (Fig. 2a; Pigage, 2004). The Yukon-Tanana and Slide Mountain terranes are separated by the northwest-trending Vangorda fault in the Faro region (Fig. 2b). Pigage (2004) concluded that the Vangorda fault had normal displacement, whereas Colpron et *al.* (2015) interpreted a strike-slip history based on its correlation with the Jules Creek fault (Murphy et *al.*, 2006) in southeastern Yukon.

The Faro Peak formation sits unconformably on quartzite, schist, and other metasedimentary rock units of the pre-Late Devonian Snowcap assemblage, which forms the exposed base of the Yukon-Tanana terrane in central Yukon (Fig. 2b; Colpron et *al.*, 2006). Rocks that comprise the Faro Peak formation were first described by Tempelman-Kluit (1972, 1979) and informally named by Pigage (2004). The Faro Peak formation is generally divided into two members (e.g., Pigage, 2004): a lower member of interbedded basalt, argillite, chert, greywacke, limestone, and conglomerate, and an upper member of massive, polymictic conglomerate with pebble to boulder-sized clasts that are dominated by local Yukon-Tanana and Slide Mountain rocks. The Faro Peak formation has an erosional top and maximum thickness estimates range from >560 m (Pigage, 2004) to >840 m (Tempelman-Kluit, 1979).

Pigage (2004) assigned a Late Triassic depositional age to the Faro Peak formation based on Carnian to Rhaetian conodont elements retrieved from limestone clasts and beds in the lower and upper members. Beranek (2009) collected samples of upper member sandstone at two fossil localities and reported 220–190 Ma detrital zircon populations that instead support an Early Jurassic maximum depositional age for the upper Faro Peak formation. Analogous detrital zircon populations have been recognized in Laberge Group strata of the Whitehorse trough (Colpron et *al.*, 2015;

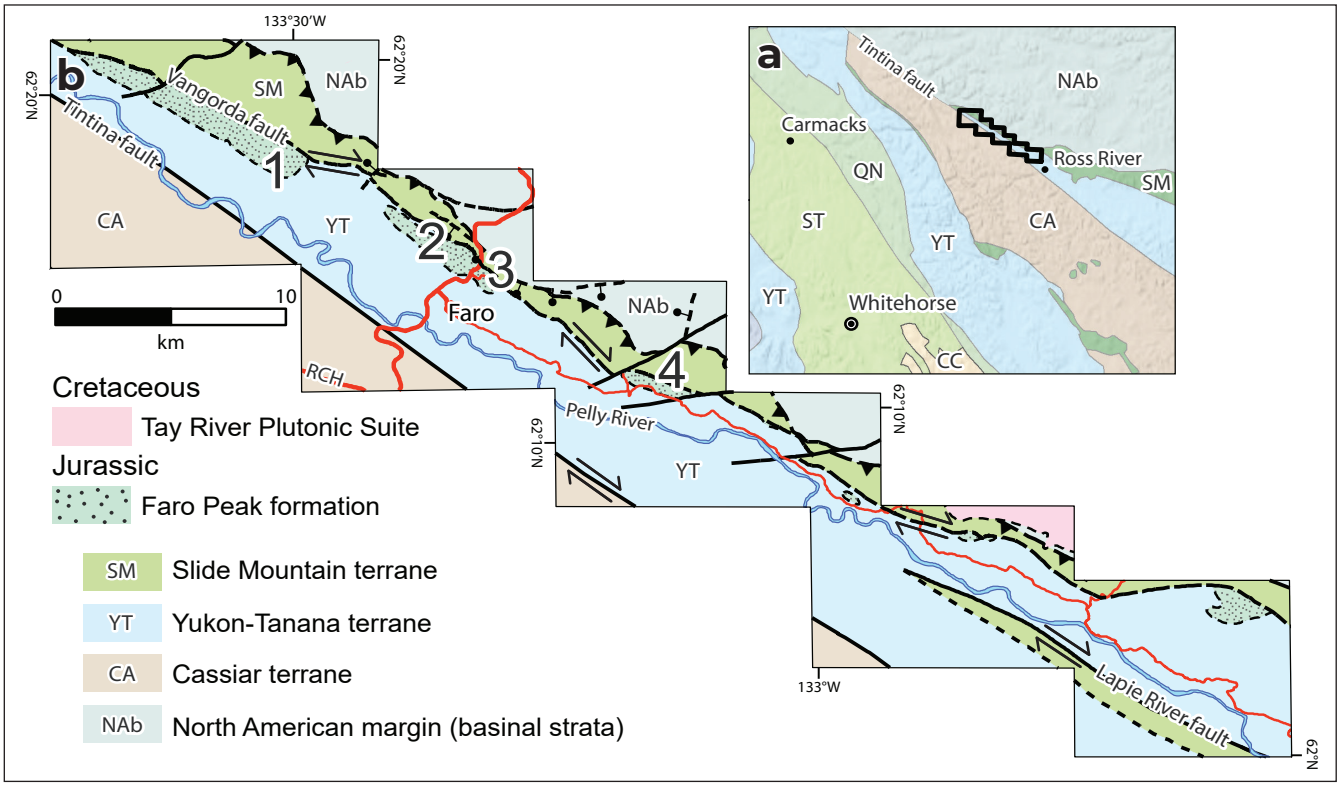

Figure 2. (a) *Terrane map of central Yukon modified from Yukon Geological Survey (2018).* ***(b)*** *Simplified bedrock geology of the southern Tay River map area modified from Pigage (2004). The numbers 1–4 denote the field localities described in this article.*

van Drecht and Beranek, 2017), suggesting that the Faro Peak formation comprises the remnants of a much larger synorogenic basin system related to Jurassic exhumation across central and southern Yukon.

2018 Field Studies

Locality 1–Faro Peak

Faro Peak and adjacent alpine ridges ~15 km northwest of Faro likely represent the thickest exposures of the Faro Peak formation (locality 1 in Fig. 2b). Lower member rock units observed during summer 2018 crop out along the northeastern flank of Faro Peak (Fig. 3), immediately southwest of the Vangorda fault, and comprise poorly exposed sections of argillite, siltstone, and fine-grained micaceous lithic arenite (Fig. 4a). Pigage (2004) reported that potentially correlative basalt and fine-grained siliciclastic rocks are exposed in the lower Faro Peak formation south and west of Rose Mountain, ~3 km northwest of Faro Peak (Fig. 3). If correct, these lower Faro Peak formation rocks may be coeval with Permian basalt and chert northeast of the Vangorda fault (Campbell Range formation) and represent an overlap assemblage that covers the Yukon-Tanana and Slide Mountain terranes. However, it is possible that these basalt and siliciclastic rock units are instead part of the Slide Mountain terrane and not Faro Peak formation, which may call for a reassessment of the Vangorda fault and location of the Yukon-Tanana–Slide Mountain terrane boundary in this region.

The upper member of the Faro Peak formation near Faro Peak mostly consists of brown weathering, granule to cobble, matrix to clast-supported, polymictic conglomerate intercalated with feldspathic lithic to lithic arenite (Fig. 4b,c). The gravelly and sandy lithofacies are generally massive and lack sedimentary structures, which make stratigraphic younging and bedding determinations difficult. Clast types in the gravelly lithofacies are dominated by quartzite and mica schist with subordinate populations of limestone, grey

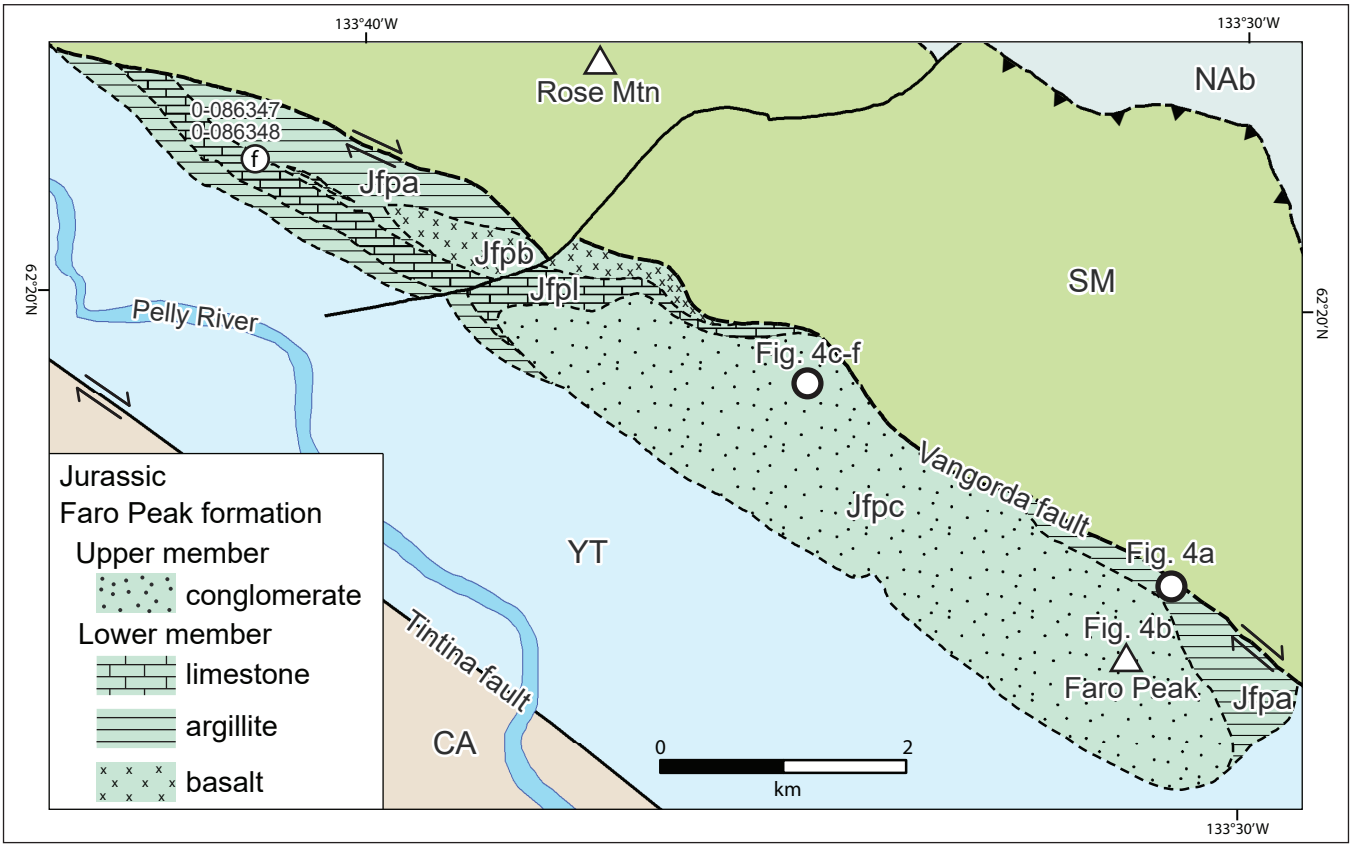

Figure 3. *Simplified bedrock geology of the Faro Peak area (locality 1) modified from Pigage (2004). Faro Peak formation units: Jfpc–upper member conglomerate and sandstone; Jfpl–lower member limestone; Jfpa–lower member argillite, chert, siltstone, and sandstone; Jfpb–lower member basalt. Terrane abbreviations as in Fig. 2b.*

Figure 4. *Field photographs of the Faro Peak area (locality 1).* ***(a)*** *Lower member argillite, siltstone, and fine-grained micaceous lithic arenite along northeastern flank of Faro Peak;* ***(b)*** *upper member lithic sandstone at Faro Peak;* ***(c)*** *upper member clast-supported polymictic conglomerate;* ***(d)*** *upper member grey chert clast;* ***(e)*** *upper member quartz-feldspar porphyry clast; and* ***(f)*** *upper member felsic intrusive clast. Scale bar has 1 cm solid divisions.*

to green to pink chert (Fig. 4d), argillite, and aphanitic to porphyritic basalt. Vein quartz, quartz-feldspar porphyry (Fig. 4e), and felsic intrusive rocks (Fig. 4f) occur as minor clast components.

Abundant quartzite and schist rock fragments in the Faro Peak area successions imply provenance from the underlying Snowcap assemblage, which suggests that gravel and coarse-grained sand deposition were coincident with the exhumation of Yukon-Tanana basement. Subordinate basalt, chert, and argillite clasts are furthermore consistent with derivation from the adjacent Campbell Range formation and older rock units of the Slide Mountain terrane near Rose Mountain. Limestone and intermediate-felsic intrusive rocks have uncertain provenance, but our working hypothesis calls for these clasts to have origins from Yukon-Tanana and/or Stikinia rock assemblages that similarly flank the Whitehorse trough in the Carmacks area of central Yukon (e.g., Colpron et *al*., 2015).

Locality 2–Whiskey Mountain

The Faro Peak formation underlies the region ~3 km north of Faro, including Whiskey Mountain to the west of the Faro Mine Access Road (locality 2 in Fig. 2b; Figs. 5 and 6a). Some of the oldest lower member strata in this region, <500 m south of the Vangorda fault, consist of grey to green, fine to medium-grained, feldspathic lithic arenite (Fig. 6b). Preliminary petrographic observations show evidence of angular plagioclase crystals and volcanic rock fragments that

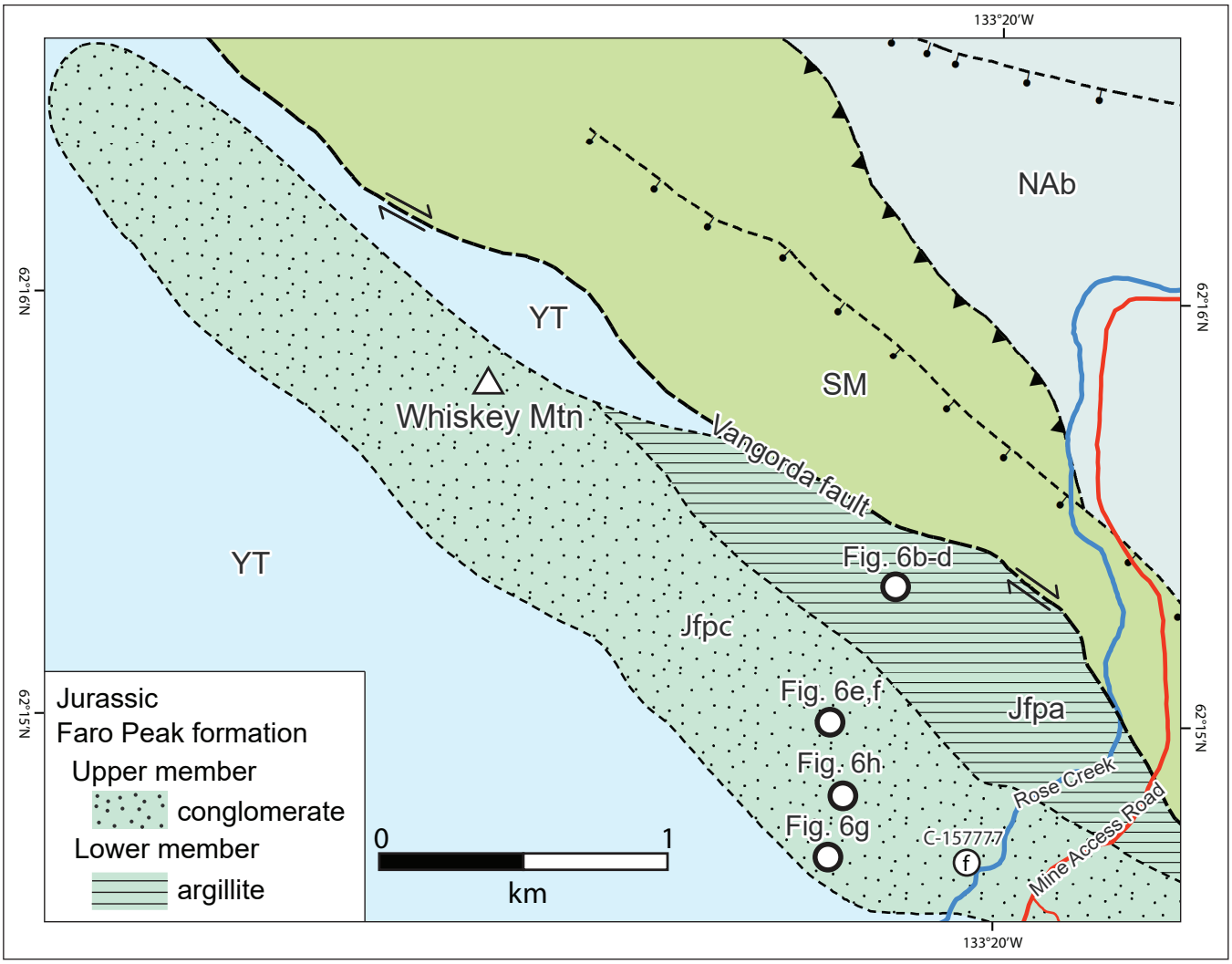

Figure 5. *Simplified bedrock geology of the Whiskey Mountain area (locality 2) modified from Pigage (2004). Faro Peak formation units: Jfpc–upper member conglomerate and sandstone; Jfpa–lower member argillite, siltstone, and sandstone. Terrane abbreviations as in Fig. 2b.*

suggest a proximal igneous source (Fig. 6c). Mud–sand couplets affected by isoclinal folding (Fig. 6d), interpreted in the field as convolute bedding, overlie these strata. Massive, tabular beds of coarse to very coarse grained feldspathic arenite units occur stratigraphically above the convolute beds.

The depositional contact between the lower and upper members is not well exposed in the Whiskey Mountain area. Near the cliffs along Rose Creek, immediately west of the Faro Mine Access Road, this contact may be evident where interbeds of argillite and sandstone of the lower member are overlain by sandstone and conglomerate of the upper member. More broadly, our field observations indicate that interfingered relationships may occur between some lower and upper member rock units. At other Whiskey Mountain locations, upper member rock units show both lateral and vertical fining trends, which may also indicate that sandstone layers form erosional channels within conglomerate units rather than the two having conformable, interbedded relationships. Graded bedding and channelized sandstone features are rarely observed because of vegetation and massive nature of the outcrop, but evident within some of the lower parts of the upper member at Whiskey Mountain (Fig. 6e,f). Regionally, upper member conglomerate

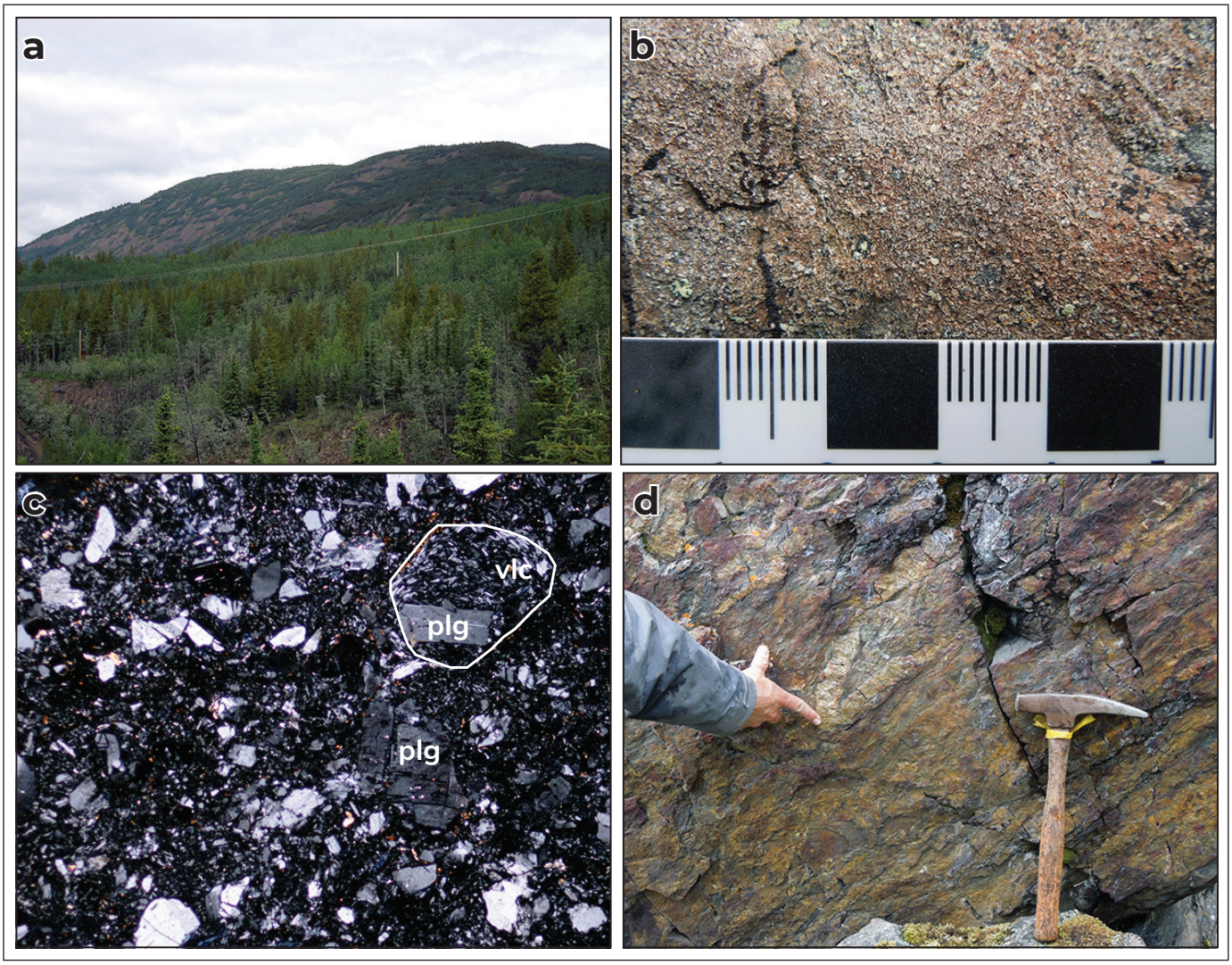

Figure 6. *Field photographs of the Whiskey Mountain area (locality 2).* ***(a)*** *North-directed view of Whiskey Mountain area and Faro Peak formation exposures from Faro townsite;* ***(b)*** *lower member feldspathic lithic arenite;* ***(c)*** *photomicrograph of lower member feldspathic lithic arenite showing angular plagioclase (plag), quartz, and volcanic lithic fragments (vlc) at 4x magnification;* ***(d)*** *isoclinal fold in convoluted beds of lower member;* ***(e)*** *through* ***(h)*** *on next page.*

units are recognized to directly overlie Snowcap assemblage basement (Pigage, 2004), suggesting that the lower member was completely removed by erosion in some areas.

Upper member units in the Whiskey Mountain area generally consist of massive, brown weathering, granule to boulder, clast-supported, polymictic conglomerate and interbedded micaceous feldspathic lithic arenite (Fig. 6g). The dominant clast types are micaceous quartzite, mica schist, chert, and limestone with Carnian conodont elements (C-157777; Pigage, 2004). Some of the micaceous quartzite and mica schist clasts are up to 50 cm in size, suggesting local derivation from the underlying Snowcap assemblage. Other clast types include basalt, argillite, vein quartz, quartz-feldspar porphyry, hornblende granodiorite, and augite-phyric basalt (Fig. 6h). Upper member sandstone adjacent to the Carnian fossil collection at Whiskey Mountain correspondingly shows a mixture of detrital zircon U-Pb ages that indicate recycled Precambrian contributions from Snowcap assemblage quartzite and schist and Late Triassic–Early Jurassic contributions presumably from igneous sources (Colpron *et al.*, 2015).

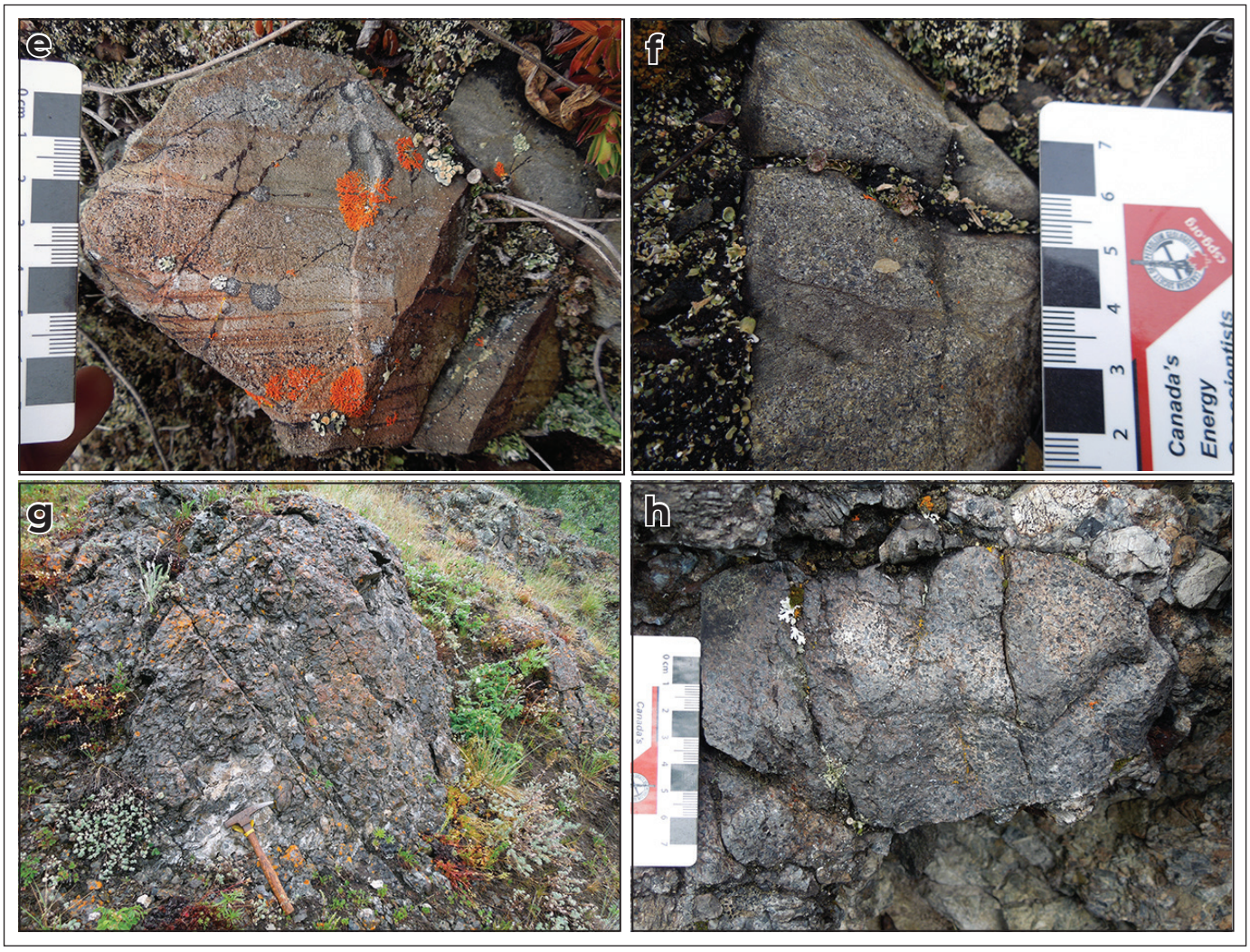

***Figure 6** continued. **(e)** graded bedding in upper member sandstone; **(f)** channelized sandstone lens in upper member conglomerate; **(g)** upper member clast-supported conglomerate; and **(h)** upper member augite-phyric basalt clast.*

Locality 3–Repeater Hill

Lower and upper member exposures of the Faro Peak formation crop out along the access road and flanks of the informally named Repeater Hill (site of the NorthwesTel repeater), ~2.5 km northeast of the Faro townsite (locality 3 in Fig. 2b; Fig. 7). The contact between lower and upper members is observed along the southeastern flank of Repeater Hill where dark grey, fine to medium-grained micaceous sandstone interfingers with, or pinches out, into matrix-supported conglomerate with pebble-sized clasts of schist, chert, argillite, micaceous quartzite, and limestone (Fig. 8a–c). This section reappears on the west side of Repeater Hill and may be analogous to the interfingered relationships observed in the adjacent Whiskey Mountain area. Grey limestone to silty limestone subcrop exposures at the top of Repeater Hill (Fig. 8d) contain early Carnian conodont elements (C-304121; Pigage, 2004) and have unclear contact relationships with upper member conglomerate.

Upper member rock units that are exposed along Repeater Road are dominated by massive, brown to grey weathering, matrix to clast-supported, pebble to cobble conglomerate (Fig. 8e) and lithic feldspathic arenite (Fig. 8f). Most clast types along the road consist of quartzite, mica schist (Fig. 8g), limestone, and chert; clasts of quartz-feldspar porphyry and other igneous rocks were observed along southwestern flank of Repeater Hill.

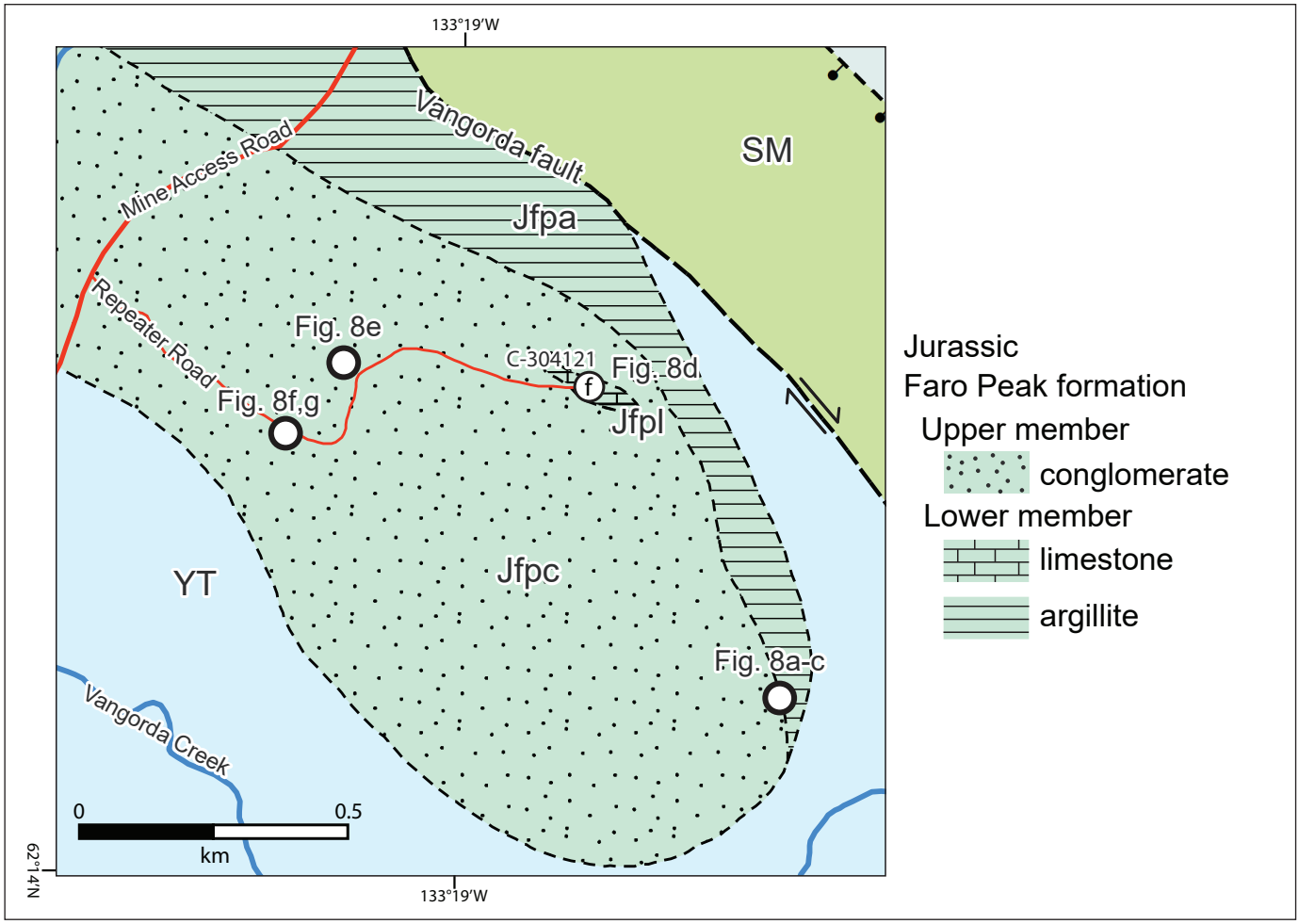

Figure 7. *Simplified bedrock geology map of the Repeater Hill area (locality 3) modified from Pigage (2004). Faro Peak formation units: Jfpc–upper member conglomerate and sandstone; Jfpl–lower member limestone; Jfpa–lower member argillite, chert, siltstone, and sandstone. Terrane abbreviations as in Fig. 2b.*

Figure 8. *Field photographs Repeater Hill area (locality 3).* ***(a)*** *Contact between lower and upper members along southeastern flank of Repeater Hill;* ***(b)*** *upper member basal conglomerate;* ***(c)*** *top of lower member argillite unit;* ***(d)*** *lower member limestone to silty limestone near repeater;* ***(e)*** *upper member matrix to clast-supported conglomerate on Repeater Road;* ***(f)*** *and* ***(g)*** *on next page.*

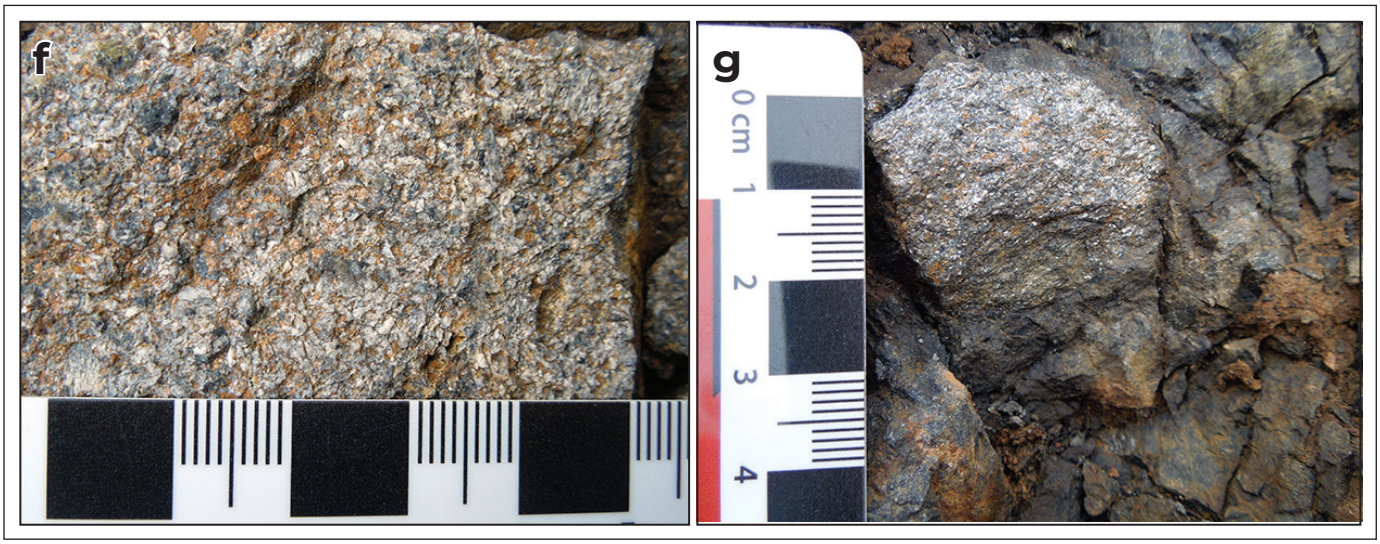

***Figure 8** continued. **(f)** upper member lithic feldspathic sandstone; and **(g)** upper member mica schist clast.*

Locality 4–Blind Creek Road and Dena Cho Trail

Upper member strata were accessed by foot traverse along the Blind Creek Road and western end of the Deno Cho Trail ~11 km east of Faro (locality 4 in Fig. 2b; Fig. 9). Near Blind Creek, Faro Peak formation outcrops mostly consist of massive, matrix to clast-supported, granule to pebble conglomerate units with quartzite, schist, chert, limestone, and minor felsic igneous and basalt clasts that resemble other upper member exposures across the southern Tay River map area (Fig. 10a–c). Sandstone matrix from a Blind Creek conglomerate layer with late Carnian limestone clasts (C-103825; Pigage, 2004) yielded Late Triassic–Early Jurassic and older detrital zircon populations that suggest mixed Mesozoic igneous and Snowcap assemblage provenance (Colpron *et al.*, 2015).

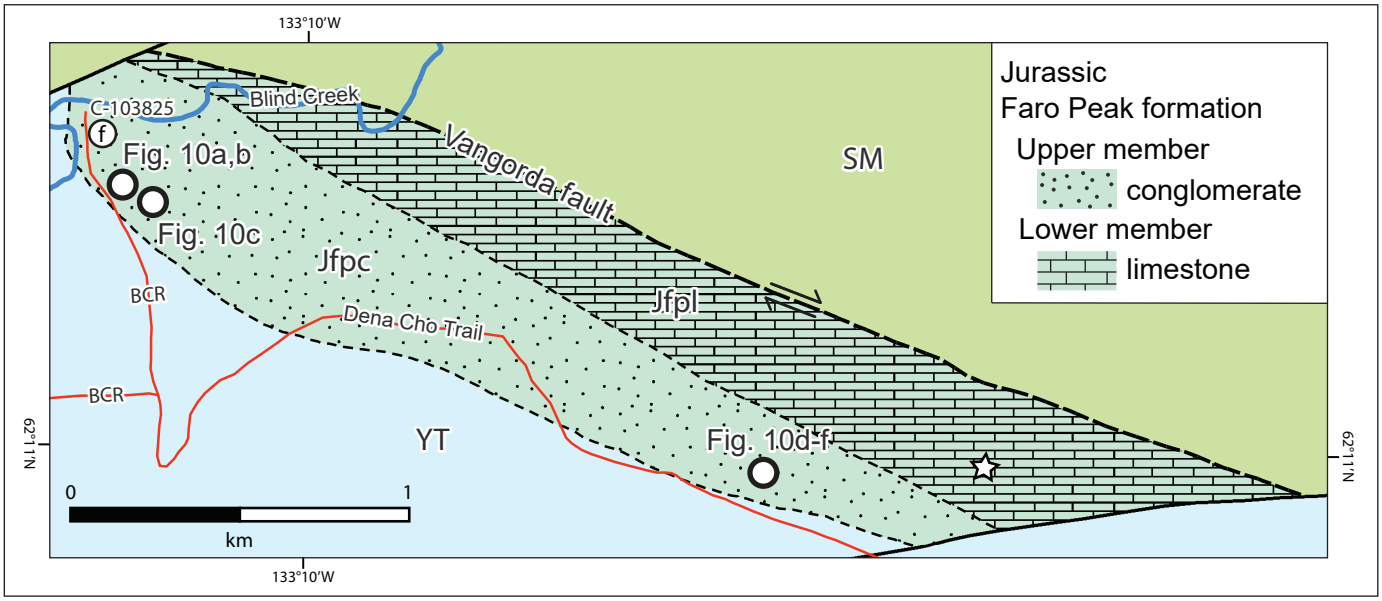

***Figure 9.** Simplified bedrock geology of the Blind Creek Road and western Dena Cho Trail areas (locality 4). Star denotes location of chloritized basalt outcrop with possible Slide Mountain terrane (Campbell Range formation) affinities. Faro Peak formation units: Jfpc–upper member conglomerate and sandstone; Jfpl–lower member limestone. BCR–Blind Creek Road. Terrane abbreviations as in Fig. 2b.*

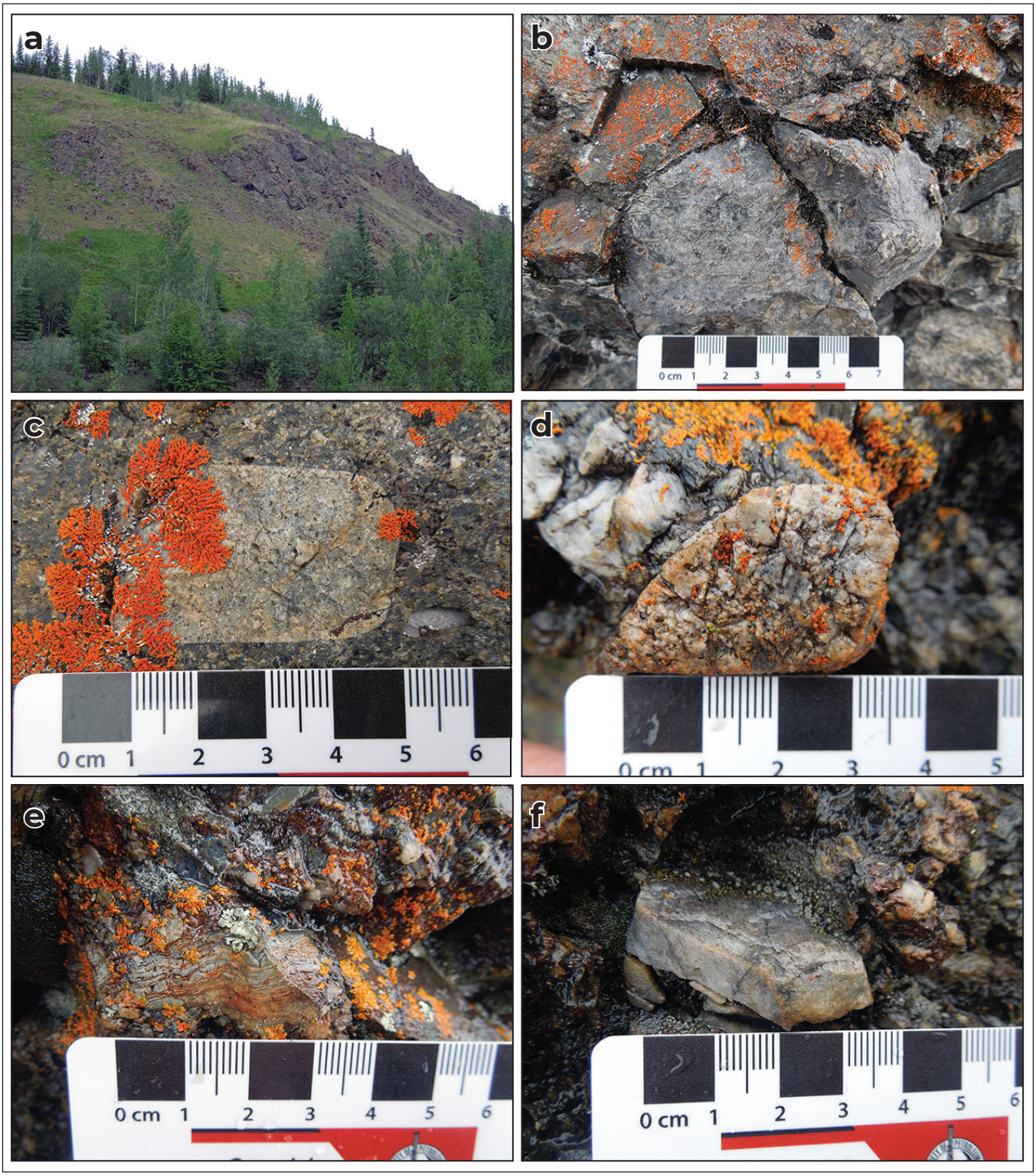

Figure 10. *Field photographs of Blind Creek Road and western Dena Cho Trail areas (locality 4).* ***(a)*** *Northeast-directed view of upper member conglomerate outcrops east of Blind Creek;* ***(b)*** *upper member limestone clast;* ***(c)*** *upper member quartz porphyry clast;* ***(d)*** *upper member felsic intrusive clast;* ***(e)*** *upper member bedded chert clast; and* ***(f)*** *upper member quartzite clast.*

Rounded and discontinuous exposures of the upper member occur along the Dena Cho Trail to the southeast of Blind Creek (Fig. 9) and generally comprise pebble to cobble conglomerate with interlayers of coarse-grained to pebbly sandstone. Clasts consist of quartzite, bedded chert, limestone, and schist with minor amounts of quartz-feldspar porphyry and felsic intrusive rocks (Fig. 10d–f). At one location along the Dena Cho Trail, a brown weathering outcrop assigned to the Faro Peak formation consists of chloritized basalt that resembles the adjacent Campbell Range formation (see Fig. 9). This outcrop is either an unmapped basalt unit within the Faro Peak formation or represents an outlier or fault sliver of Slide Mountain terrane.

Preliminary Conclusions and Future Research

The Faro Peak formation is characterized by an upper member of massive, disorganized conglomerate and sandstone units and a lower member of argillite, siltstone, and sandstone units that contain massive to graded to convolute bedding features. The depositional setting and emplacement mechanisms of these Faro Peak formation facies are the topics of current research and will continue to be a focus during the second field season in summer 2019. Tempelman-Kluit (1972) interpreted the massive and coarse-grained nature of the upper member conglomerate to indicate deposition adjacent to a fault scarp complex, presumably linked to displacement along the Vangorda fault or its predecessor. The lower member contains feldspathic and volcanic lithic sandstone strata, which further implies proximity to a mafic-intermediate igneous source. Our working hypothesis calls for massive clast to matrix-supported conglomerate and sandstone units of the upper member to represent non-turbulent, concentrated debris or density flow deposits that most likely accumulated in a subaqueous environment. Stratigraphic features in some lower member units include disorganized sand, organized sand–mud couplets, and graded bedding, which are generally consistent with concentrated density flow or turbidity current deposition.

The abundance of coarse-grained (up to boulder-sized) rock fragments in the upper member, including those derived from Yukon-Tanana basement, suggests that Faro Peak formation deposition was coincident with regional exhumation and tectonic erosion. For example, Knight *et al*. (2013) concluded that Early Jurassic extension along the Willow Lake fault of central Yukon resulted in the exhumation of Yukon-Tanana basement rocks from mid-crustal depths during the time of Faro Peak formation deposition. The recent plate tectonic model for the Whitehorse trough by Colpron *et al*. (2015) is broadly compatible with a strike-slip/transtensional setting for the Faro Peak basin along the Intermontane belt–ancient North American margin boundary. It follows that crustal-scale faults in the Faro region could have accommodated regional exhumation of Yukon-Tanana basement and adjacent Slide Mountain terrane. Although the Faro Peak formation was deposited along a convergent margin, we are investigating transtensional origins for the Faro Peak basin, including modern analogues in southern California (e.g., Ridge basin; Link, 2003) and Jamaica (e.g., Wagwater basin; Wescott and Etheridge, 1983).

Faro Peak formation rock units were sampled for petrographic and detrital zircon U-Pb-Hf studies at more than 20 locations during summer 2018. Petrographic data will constrain the framework composition of lower and upper member strata and document lateral or vertical changes in provenance. The youngest population of detrital zircon U-Pb ages will be used to constrain the maximum depositional age of lower and upper member rock units (e.g., Dickinson and Gehrels, 2009), whereas combined U-Pb-Hf data will identify specific provenance areas and regional crustal evolution of the Intermontane terranes. These results will be integrated with existing (Colpron *et al*., 2015) and forthcoming (e.g., van Drecht and Beranek, 2017) detrital zircon U-Pb(± Hf) data from Lower to Middle Jurassic strata of the Whitehorse trough and Lower Jurassic foreland basin strata in the southern Canadian Rockies (Pană *et al*., 2018) to better constrain Cordilleran tectonic evolution.

Field studies in summer 2019 will focus on the northwestern and southeastern extents of the Faro Peak formation in the southern Tay River map area.

Near Rose Mountain, we will investigate the contact relationships and stratigraphic architecture of lower member units that include basalt, chert, and mafic greywacke adjacent to the Vangorda fault (Fig. 3). The goal of this research is to ascertain if the lower Faro Peak formation in this location: (1) represents a Permian overlap assemblage between Yukon-Tanana and Slide Mountain terranes; (2) represents a fault sliver of Slide Mountain terrane (Campbell Range formation); or (3) represents a Late Triassic–Early Jurassic succession of basalt and related sedimentary rocks assigned to Yukon-Tanana terrane. Three isolated occurrences of Faro Peak formation occur in proximity to the Deno Cho Trail ~25, 30, and 45 km to the southeast of Faro (Fig. 2b), respectively, and include chert, mafic greywacke, and other rock units that may be similar to lower member strata near Rose Mountain. Field studies of these Faro Peak formation strata will therefore provide information about the timing and nature of stratigraphic units along the length of the Vangorda fault and their significance to understanding the Yukon-Tanana–Slide Mountain terrane boundary.

Acknowledgements

This is a product of the Geo-mapping for Energy and Minerals (GEM) program at Natural Resources Canada. The Yukon Geological Survey supported field logistics and helicopter transport to alpine exposures. Maurice Colpron provided helpful field discussions about Yukon-Tanana rock units and regional geology. Reviewer Lee Pigage provided thoughtful and constructive comments that improved this manuscript.

References

Beranek, L.P., 2009. Provenance and paleotectonic setting of North American Triassic strata in Yukon: the sedimentary record of pericratonic terrane accretion in the northern Canadian Cordillera. Unpublished PhD thesis, University of British Columbia, British Columbia, Canada, 324 p.

Colpron, M., Crowley, J.L., Gehrels, G.E., Long, D.G.F., Murphy, D.C., Beranek, L.P. and Bickerton, L., 2015. Birth of the northern Cordilleran orogen, as recorded by detrital zircons in Jurassic synorogenic strata and regional exhumation in Yukon. Lithosphere, vol. 7, p. 541–562.

Colpron, M., Nelson, J.L. and Murphy, D.C., 2006. A tectonostratigraphic framework for the pericratonic terranes of the northern Canadian Cordillera. *In*: Paleozoic Evolution and Metallogeny of Pericratonic Terranes at the Ancient Pacific Margin of North America, Canadian and Alaskan Cordillera, M. Colpron and J.L. Nelson (eds.), Geological Association of Canada Special Paper 45, p. 1–23.

Dickie, J.R. and Hein, F.J., 1995. Conglomeratic fan deltas and submarine fans of the Jurassic Laberge Group, Whitehorse Trough, Yukon Territory, Canada: fore-arc sedimentation and unroofing of a volcanic island arc complex. Sedimentary Geology, vol. 98, p. 263–282.

Dickinson, W.R. and Gehrels, G.E., 2009. Use of U-Pb ages of detrital zircons to infer maximum depositional ages of strata: A test against a Colorado Plateau Mesozoic database. Earth and Planetary Science Letters, vol. 288, p. 115–125.

Evenchick, C.A., McMechan, M.E., McNicoll, V.J. and Carr, S.D., 2007. A synthesis of the Jurassic-Cretaceous tectonic evolution of the central and southeastern Canadian Cordillera: Exploring links across the orogeny. *In*: Whence the Mountains? Inquiries into the Evolution of Orogenic Systems: A Volume in Honor of Raymond A. Price, J.W. Sears, T.A. Harms, and C.A. Evenchick (eds.), Geological Society of America Special Paper 433, p. 117–145.

Hart, C.J.R., Dickie, J.R., Ghosh, D.K. and Armstrong, R.L., 1995. Provenance constraints for Whitehorse Trough conglomerate: U-Pb zircon dates and initial Sr ratios of granitic clasts in Jurassic Laberge Group, Yukon Territory. *In*: Jurassic Magmatism and Tectonics of the North American Cordillera, D.M Miller and C. Busby (eds.), Geological Society of America Special Paper 299, p. 47–63.

Johnston, S.T., Mortensen, J.K. and Erdmer, P., 1996. Igneous and metaigneous age constraints for the Aishihik metamorphic suite, southwest Yukon. Canadian Journal of Earth Sciences, vol. 33, p. 1543–1555.

Knight, E., Schneider, D.A. and Ryan, J.J., 2013. Thermochronology of the Yukon-Tanana terrane, west-central Yukon: Evidence for Jurassic extension and exhumation in the northern Canadian Cordillera. Journal of Geology, vol. 121, p. 371–400.

Link, M.H., 2003. Depositional systems and sedimentary facies of the Miocene-Pliocene Ridge basin, southern California. *In*: Evolution of Ridge basin, southern California: An interplay of sedimentation and tectonics, J.C. Crowell (ed.), Geological Society of America Special Paper 367, p. 17–87.

Mihalynuk, M.G., Nelson, J.A. and Diakow, L.J., 1994. Cache Creek terrane entrapment: Oroclinal paradox within the Canadian Cordillera. Tectonics, vol. 13, p. 575–595.

Murphy, D.C., Mortensen, J.K., Piercey, S.J., Orchard, M.J. and Gehrels, G.E., 2006. Mid-Paleozoic to early Mesozoic tectonostratigraphic evolution of the Yukon-Tanana and Slide Mountain terranes and affiliated overlap assemblages, Finlayson Lake massive sulphide district, southeastern Yukon. *In*: Paleozoic Evolution and Metallogeny of Pericratonic Terranes at the Ancient Pacific Margin of North America, Canadian and Alaskan Cordillera, M. Colpron and J.L. Nelson (eds.), Geological Association of Canada Special Paper 45, p. 75–105.

Nelson, J.L., Colpron, M. and Israel, S. 2013. The Cordillera of British Columbia, Yukon, and Alaska: Tectonics and Metallogeny. *In*: Tectonics, Metallogeny and Discovery: The North American Cordillera and Similar Accretionary Settings, M. Colpron, T. Bissig, B.G. Rusk and J.F.H. Thompson (eds.), Society of Economic Geologists, Special Publication 17, p. 53–109.

Pană, D.I., Poulton, T.P. and DuFrane, S.A., 2018 (*in press*). U-Pb detrital zircon dating supports Early Jurassic initiation of the Cordilleran foreland basin in southwestern Canada. Geological Society of America Bulletin, doi:10.1130/B31862.1.

Pigage, L.C., 2004. Bedrock geology compilation of the Anvil District (parts of NTS 105K/2, 3, 5, 6, 7, and 11), central Yukon. Yukon Geological Survey, Bulletin 15, 103 p.

Tempelman-Kluit, D.J., 1972. Geology and origin of the Faro, Vangorda, and Swim concordant zinc-lead deposits, central Yukon Territory. Geological Survey of Canada, Bulletin 208, 73 p.

Tempelman-Kluit, D.J., 1979. Five occurrences of transported synorogenic clastic rocks in Yukon Territory. Geological Survey of Canada, Paper 79-1A, p. 1–12.

Tempelman-Kluit, D.J., 1984. Geology, Laberge (105E) and Carmacks (115I), Yukon Territory. Geological Survey of Canada, Open File 1101, 10 p.

van Drecht, L.H. and Beranek, L.P., 2017. Jurassic stratigraphy and tectonic evolution of the Whitehorse trough, central Yukon: new insights from laser ablation split stream (LASS) detrital zircon U-Pb geochronology and Hf isotope geochemistry. Geological Society of America, Abstracts with Programs, vol. 49, no. 6.

van Drecht, L.H. and Beranek, L.P., 2018. New investigations of basal Laberge Group stratigraphy, Whitehorse trough, central Yukon. *In*: Yukon Exploration and Geology 2017, K.E. MacFarlane (ed.), Yukon Geological Survey, p. 151–163.

Wescott, W.A. and Ethridge, F.G., 1983. Eocene fan delta/submarine fan deposition in the Wagwater Trough, east-central Jamaica. Sedimentology, vol. 30, p. 235–247.

Yukon Geological Survey, 2018. Yukon Digital Bedrock Geology. Yukon Geological Survey, http://www.geology.gov.yk.ca/update_yukon_bedrock_geology_map.html [accessed November, 2018].